AIR Earthquake Model for Canada

AIR WORLDWIDE

Contact Information

AIR is headquartered in Boston with additional offices in North America, Europe, and Asia. For information on our office locations, visit http://www.air-worldwide.com/About-AIR/Offices/.

AIR welcomes feedback on its documentation. To contact us regarding this document please email us at: ModelDocumentationFeedback@air-worldwide.com.

Revision History

Date	Description
June 15, 2017	Document release

Table of Contents

List of Figures

List of Tables

1 Facts at a Glance

1.1 Model Facts

Model Name: AIR Earthquake Model for Canada

Release Date: June 2017

Software Systems: CATRADER 19.0 and Touchstone 5.0

Modeled Country: Canada

Modeled Perils: Ground shaking from earthquakes, as well as liquefaction, tsunami, landslides, and fire following earthquake.

Model Abstract: The AIR Earthquake Model for Canada is an event-based model that captures the effects of earthquake-induced ground shaking, liquefaction, tsunami, landslide, and fires following earthquakes on properties and infrastructure in Canada. The model captures the complex seismicity of the region by generating events along subduction zones (including both interface and in-slab events), active crustal faults, and within 82 seismic source zones through smoothed background seismicity. The earthquake generation process determines the magnitude, location, rupture length and width, depth, and fault orientation and mechanism. By including separate stochastic catalogs to represent time-dependent and time-independent seismicity, the model presents a comprehensive view of earthquake risk in Canada. Empirical attenuation relationships, faulting mechanisms, and local site conditions that affect the site-amplification factors are considered in the local ground shaking intensity calculations. The engineering component of the model has been extensively validated against published research and observed damage data from historical earthquakes. Overall model performance has been validated against the historical loss data that is available for Canada, as well as data from other regions. The AIR Earthquake Model for Canada has been developed to meet the wide spectrum of earthquake risk management needs of all stakeholders, including the insurance and reinsurance industry and accounts for policy conditions specific to Canada.

Model Limitations and Assumptions: The AIR Earthquake Model for Canada uses geological, seismic, and geodetic data collected from a wide variety of reports, including the recently released historical earthquake catalog from the Geological Survey of Canada (GSC). AIR's modeled seismicity rate and event location data depends largely on the accuracy of this historical catalog. In addition, it is important to recognize that *except* for the Cascadia subduction zone, the AIR model is time-independent; thus, the probability of earthquake occurrence at any location or along any segment of a fault follows a Poissonian model. For a full description of these and other key assumptions and limitations of the AIR Earthquake Model for Canada, see the document *Interim Guidance on Solvency II Compliance: Model Assumptions and Limitations* available on the Client Portal of the AIR website www.air-worldwide.com.

1.2 Canada – Country Facts

Figure 1 shows the CRESTA zones of Canada.

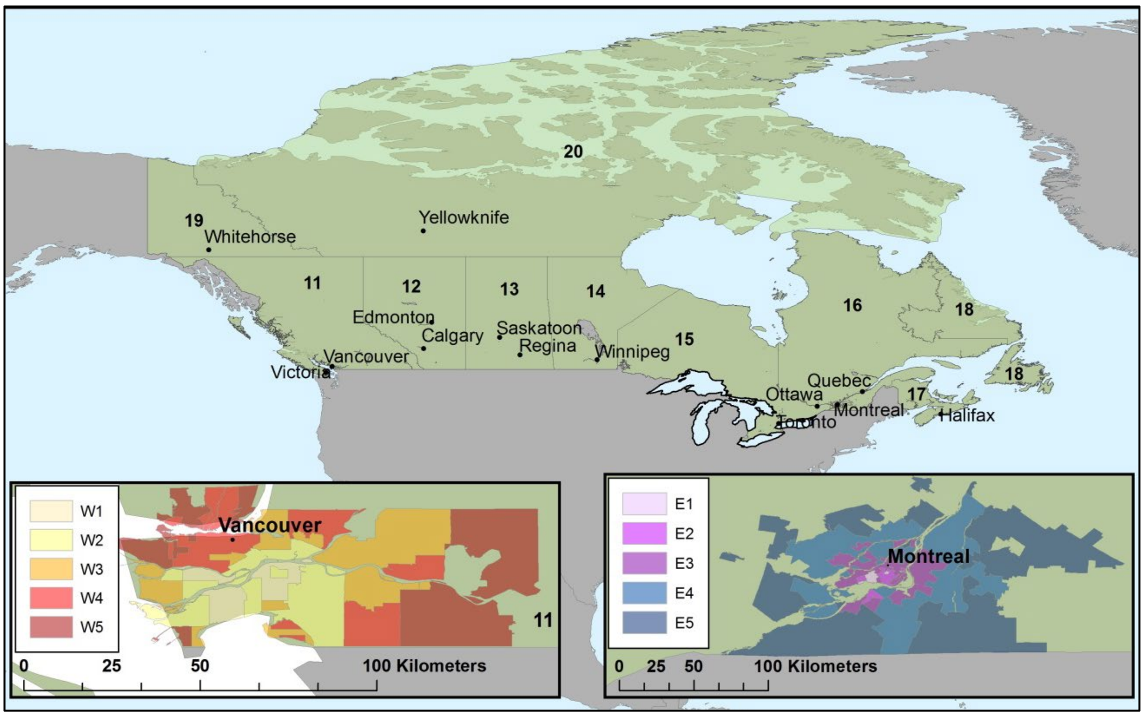

Figure 1. CRESTA Zones of Canada

Table 1 lists and describes the CRESTA zones shown in Figure 1.

Table 1. CRESTA Zones of Canada

Zone	Name
Z11	West, Very Low (British Columbia, excluding Zones W1-W5)
Z12	Alberta
Z13	Saskatchewan
Z14	Manitoba
Z15	Ontario Very Low
Z16	Quebec Very Low (excluding Zones E1-E5)
Z17	Maritime Provinces
Z18	Newfoundland
Z19	Yukon Territories
Z20	Northwest Territories and Nunavut

Zone	Name
ZE1	East Extreme
ZE2	East Very High
ZE3	East High
ZE4	East Moderate
ZE5	East Low
ZW1	West Extreme
ZW2	West Very High
ZW3	West High
ZW4	West Moderate
ZW5	West Low

Canada includes ten provinces and three territories, as shown in Figure 2.

Figure 2. Provinces and territories of Canada

The FSA regions of Canada are shown in Figure 3.

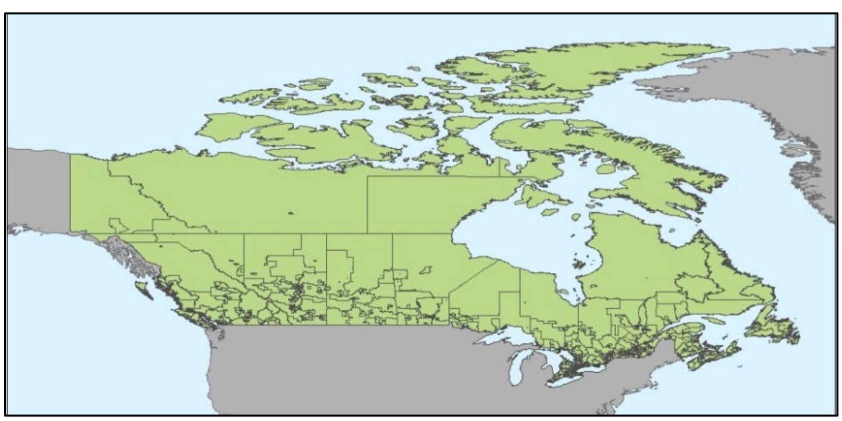

Figure 3. FSA regions of Canada

1.3 Data Sources

Key data sources used in the development of the AIR Earthquake Model for Canada are described below, for each major component and peril of the model.

Event Generation: Data used to generate the model's stochastic catalogs were obtained from several sources, including the following: the Geological Survey of Canada (GSC) Seismic Model (Halchuck, et al., 2014); publications from the GSC (for example, Adams and Halchuk, 2003); the 2014 U.S. National Seismic Hazard Model (Peterson et al. 2014) the USGS significant earthquake database (for events occurring between 1900 and 1973); the USGS Preliminary Determination of Epicenter (PDE) data (for events occurring between 1973 and 2012); publications of the USGS (including Wesson et al. 2007 and Petersen et al. 2008; Special edition of Earthquake Spectra, vol. 31, No. S1); information from the Division of Geological and Geophysical Surveys of Alaska (Koehler et al. 2012); the Canadian Base Network (see Craymer et al. 2011); and several other literature resources, including Elliott et al. (2010), Leonard et al. (2007, 2008), Mazzotti et al. (2011), and McCaffrey et al. (2013).

Local Intensity Calculation: Several sources, including the following, were used to estimate the ground shaking intensity associated with each event of the stochastic catalog: Natural Resources Canada geological maps including Fulton (1996), Klassen et al. (1992), and Prest and Hode-Keyser (1975); as well as the multiple literature sources from which the model's ground motion prediction equations (GMPEs) were obtained, including Atkinson and Goda (2011), Abrahamson and Silva (2008), Boore and Atkinson (2008), Campbell and Bozorgnia (2008), Chiou and Youngs (2008), Chouinard and Rosset (2007, 2011), Motazedian et al. (2011), Hunter et al. (2010), Ventura et al. (2004), and Monahan et al. (2000).

Damage Estimation: Data sources used to formulate the model's vulnerability component include the following: National Building Code of Canada (1953-2015); International Building Code (IBC) 2000-2015; claims data from the 1994 Northridge earthquake, obtained from the California Department of Insurance (DOI) and private insurers; damage reports from the 1989 Loma Prieta earthquake, the 2003 San Simeon earthquake, and the 2008 Chino Hills earthquake, obtained from the Office of Emergency Services (OES) in California; damage to unreinforced masonry (URM) buildings from earthquakes in Italy since 1975, obtained from the Italian Department of Civil Protection; data from historical earthquakes in Canada, obtained from Natural Resources Canada (EQCAN); the well-accepted FEMA HAZUS methodology (FEMA 2003); and AIR damage surveys following the 2011 Tohoku, Japan, earthquake, as well as the

2010 and 2011 earthquakes in Christchurch, New Zealand. Tsunami damage data from 2011 Tohoku earthquake, provided by MLIT Japan, were also used.

Liquefaction: The model's liquefaction component – which covers six regions of Canada, namely the Lower Mainland, Metro Victoria area, Greater Toronto area, National Capital Region, Greater Montreal Areas, and Quebec City – was developed using groundwater depth data obtained from the Groundwater Information Network and from local (provincial) government agencies in Canada, along with surficial soil information from Natural Resources Canada. The liquefaction component of the model follows methods summarized by Idriss and Boulanger (2008) and Andrus and Stokoe (2000).

Landslide: The landslide component of the AIR model relies on high resolution Digital Elevation Model (DEM) data, surficial and bedrock geological maps, and seasonal precipitation data. The DEM data were obtained from GeoBase, a Canadian government initiative that provides Canadian Digital Elevation Data (CDED) at scales of 1:50,000 and 1:250,000, and the Shuttle Radar Topography Mission (SRTM), an international research effort that has made DEM data available on a near-global scale from 56° S to 60° N, at a resolution of 3 arc seconds for Canada. For six highly populated urban areas of Canada (the Lower Mainland, Metro Victoria area, Greater Toronto area, National Capital Region, Greater Montreal Areas, and Quebec City), CDED is used at 1:50,000 scale. Seasonal precipitation data were obtained from a Canadian government website (http://climate.weather.gc.ca/). The landslide component also employs information from literature resources, including Newmark (1965), Wilson and Keefer (1985), Jibson et al. (2000), and Arias (1970).

Tsunami: The AIR model employs high resolution bathymetry, elevation, land use/land cover (LULC), and levee location and height data to estimate the intensity of tsunamis resulting from events of the stochastic catalog. High resolution bathymetry data were obtained from the National Geophysical Data Center (NGDC) (ETOPO1, a 1 arc-minute global relief dataset), the Southern Alaska Coastal Relief Model (a 24 arc-second dataset of relief data for the Gulf of Alaska, Bering Sea, and the Aleutian Islands), the NOAA Center for Tsunami Research digital elevation model for the Strait of Juan de Fuca (available on a 5 arc-second grid), and the NOAA Center for Tsunami Research digital elevation model for Northern California (available on a 36 arc-second grid. High resolution elevation data were obtained from the United States Geological Survey (data available on a 30-meter grid) and from GeoBase Canada (23-meter grid). Land use land cover (LULC) data (vintage: 2005) were obtained from the Commission for Environmental Cooperation North American Environmental Atlas. To determine the location of levees in the modeled region, AIR researchers digitized levee data provided by the British Columbia Ministry of Forests, Lands, and Natural Resource Operations. Levee locations were also determined from aerial imagery, including Google Streetview. Because levee height data was not available, a levee height of 2 meters was assumed.

Industry Exposure Database: The AIR industry exposure database for Canada contains detailed data on risk counts, replacement values, and building construction and occupancy characteristics obtained from the most recent available census data, business directories, construction manuals, and other reports. For example, risk and attribute data were obtained from Statistics Canada, Natural Resources Canada, and the Canada Mortgage and Housing Corporation, among other sources. Land use and elevation data are obtained from various regional and global data sets, including the U.S. National Aeronautics and Space Administration (NASA) and the North American Land Change Monitoring System. For a full description of the industry exposure database and the sources used to develop it, see the document *AIR Industry Exposure Database for Canada*, which is available on the Client Portal of the AIR website (www.air-worldwide.com).

1.4 Historical Catalog

AIR's historical catalog for Canada includes 50,088 earthquakes of magnitude 2.0 and greater, occurring between 1638 and 2012. The majority of this historical catalog was obtained from the Geological Survey of Canada (J. Adams, personal communication, 2012). With both instrumentally-recorded events and historical records of pre-instrumentally-recorded events, this historical earthquake catalog represents the most up-to-date understanding of the location and magnitude of past earthquakes occurring in and near Canada. All earthquake magnitudes in this catalog were converted to moment magnitudes by the GSC. In addition, AIR added historical events in the vicinity of Canada, including the northern portion of the 48 contiguous United States as well as Alaska, to aid in modeling seismicity near the borders between the U.S. and Canada. The primary source of these additional historical events is the United States Geological Survey (USGS) National Earthquake Information Center.

1.5 Stochastic Catalog

The AIR Earthquake Model for Canada incorporates two 10,000-year catalogs of simulated earthquakes: a time-dependent (TD) catalog with 22,880 events that can potentially cause a loss at locations in Canada, of which 8,112 cause loss to the industry exposure for Canada; and a time-independent (TID) catalog. Stochastic events included in the model are of magnitude 5.0 and greater.

In the model, the time-dependent (TD) catalog is the standard (recommended, and therefore default) catalog. Unless otherwise specified, the exhibits in this document refer to the time-dependent catalog. For information about how the time-dependent catalog was generated, see Section 3.2, subsection "Time Dependency and the Model's Stochastic Catalogs."

Table 2 shows the magnitude distributions of all simulated events in the time-dependent catalog, both loss-causing and those that do not cause loss to the current distribution of industry exposure for Canada.

Table 2. Magnitude distribution of simulated events that can potentially cause a loss in the modeled region (standard time-dependent catalog)

Magnitude	≥ 8.0	7.5 to 8.0	7.0 to 7.5	6.5 to 7.0	6.0 to 6.5	5.5 to 6.0	5.0 to 5.5	Total
Event Count	334	559	1,574	1,211	2,448	5,254	11,500	22,880
Percentage	1.46%	2.44%	6.88%	5.29%	10.70%	22.96%	50.26%	100%

Note: Each band in this table and those that follow include the number of events with a magnitude (rounded to one decimal place) greater than or equal to the lower value and less than the higher value. So the 7.5 to 8.0 bin includes all events with a magnitude greater than or equal to 7.5 and less than 8.0.

Table 3 shows the distribution of unique loss-causing simulated events (that is, those that cause losses to the current distribution of the industry exposures of Canada), by magnitude, for the modeled region.

Table 3. Magnitude distribution of simulated loss-causing events in the modeled region (time-dependent catalog)

Magnitude	≥ 8.0	7.5 to 8.0	7.0 to 7.5	6.5 to 7.0	6.0 to 6.5	5.5 to 6.0	5.0 to 5.5	Total
Event Count	288	192	428	785	1,200	1943	3,276	8,112
Percentage	3.55%	2.37%	5.28%	9.68%	14.79%	23.95%	40.38%	100%

1.6 Catalog Optimization

The low rate of seismicity in central and eastern Canada suggests that a 10,000-year simulated catalog may not be long enough to obtain a stable exceedance probability curve for CRESTA zones and other small regions within these portions of the country. For this reason, a 100,000-year catalog was first produced during model development. A multivariate optimization procedure was then applied to this 100,000-year catalog to create a final 10,000-year catalog whose loss exceedance probability curve in each CRESTA zone, and magnitude-frequency rate in each seismic source zone, are consistent with those of the original 100,000-year catalog.

Figure 4, Figure 5, and Figure 6 show the impact of this optimization procedure on loss estimates for CRESTA Zones E1-E5 (which contain Montreal), CRESTA

Zones W1-W5 (which contain Vancouver), and for all of Canada, respectively. In each plot, the blue curve represents the losses derived from the 100,000-year catalog, the green curve represents the losses derived from the optimized 10,000-year catalog, and the ten red curves represent the losses derived from each of the ten 10,000-year subsets of the original 100,000-year catalog (i.e., the subsets consisting of years 1-10,000, 10,001-20,000, 20,001-30,000, and so on). In each plot, note the good agreement between the loss estimates for the optimized 10,000-year catalog and the original 100,000-year catalog.

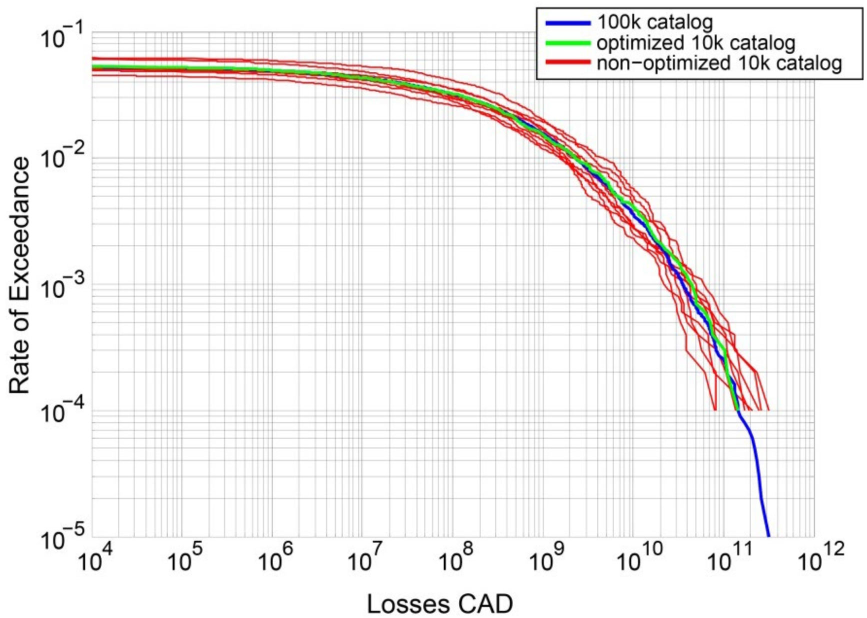

Figure 4. Loss exceedance probability curves of the 100,000-year catalog, optimized 10,000-year catalog, and each 10,000-year subset of the 100,000-year catalog for CRESTA Zones in Montreal

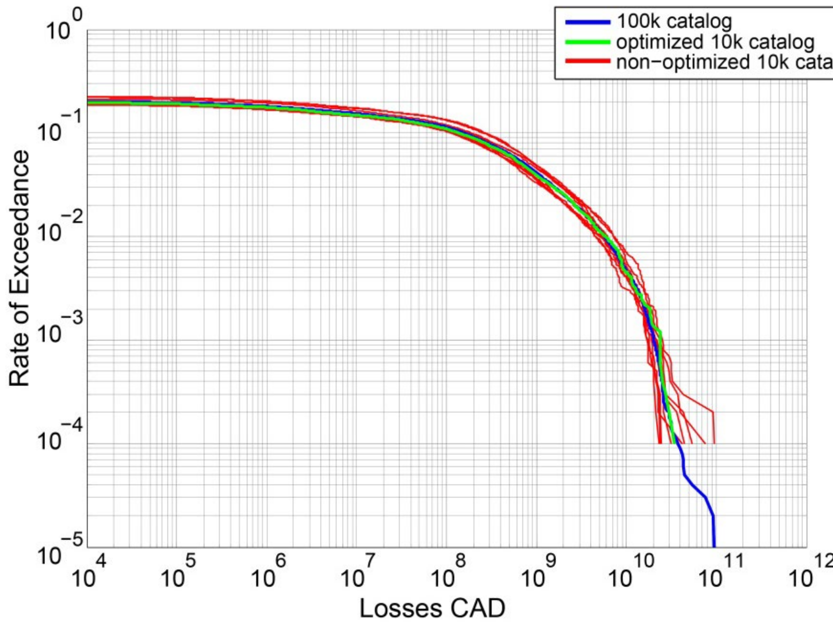

Figure 5. Loss exceedance probability curves of the 100,000-year catalog, optimized 10,000-year catalog, and each 10,000-year subset of the 100,000-year catalog for CRESTA Zones in Vancouver

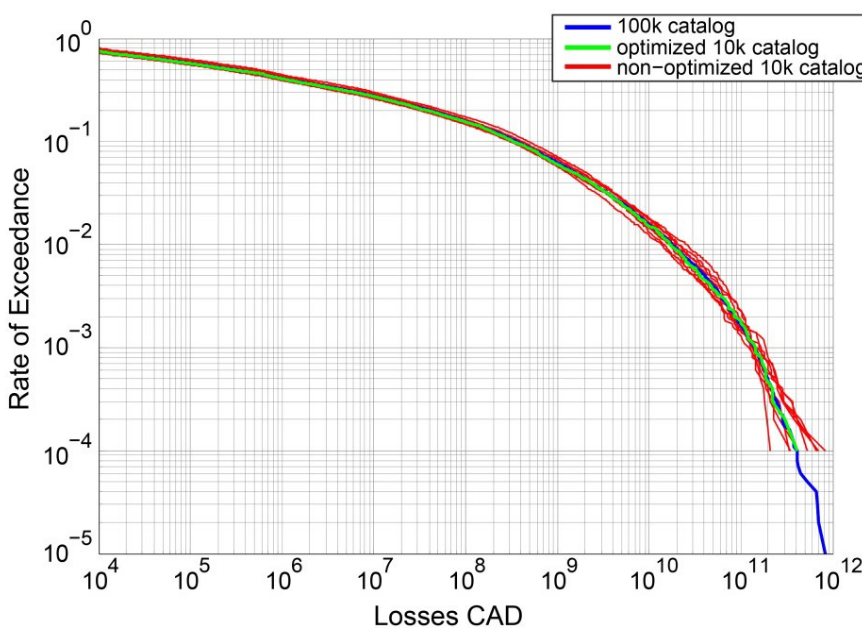

Figure 6. Loss exceedance probability curves of the 100,000-year catalog, optimized 10,000-year catalog, and each 10,000-year subset of the 100,000-year catalog for all of Canada

Figure 7 and Figure 8 show the impact of the optimization process on the frequency-magnitude distributions of earthquakes produced within 200 km of Montreal, and within 200 km of Vancouver. In each plot, the red dots represent the annual rate of earthquakes of magnitude greater than or equal to each magnitude based on the 100,000-year catalog, and the blue dots represent the same based on the optimized 10,000-year catalog. For each plot, note the good agreement between the frequency-magnitude distributions for the optimized 10,000-year catalog and the original 100,000-year catalog.

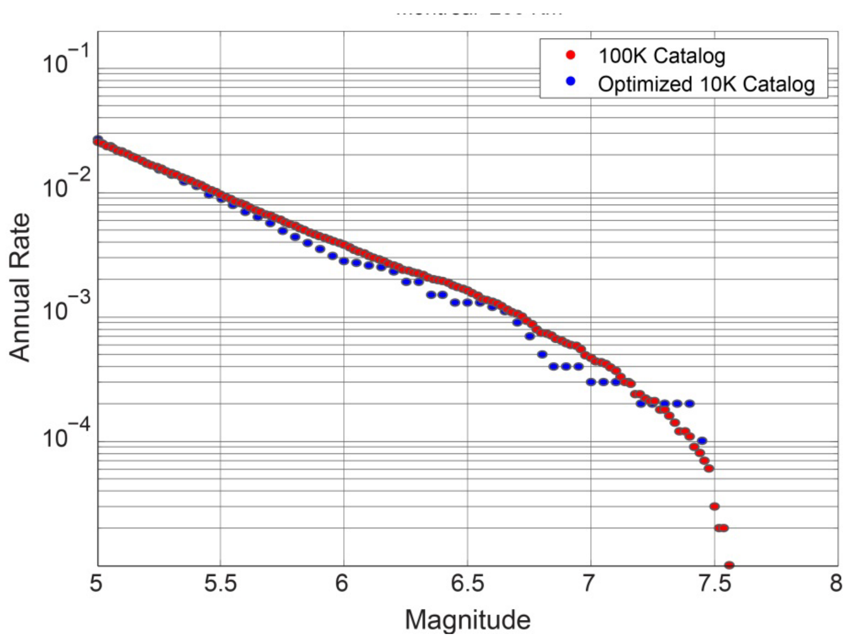

Figure 7. Frequency-magnitude distributions based on the 100,000-year catalog and the optimized 10,000-year catalog for earthquakes within a 200km radius of the city of Montreal

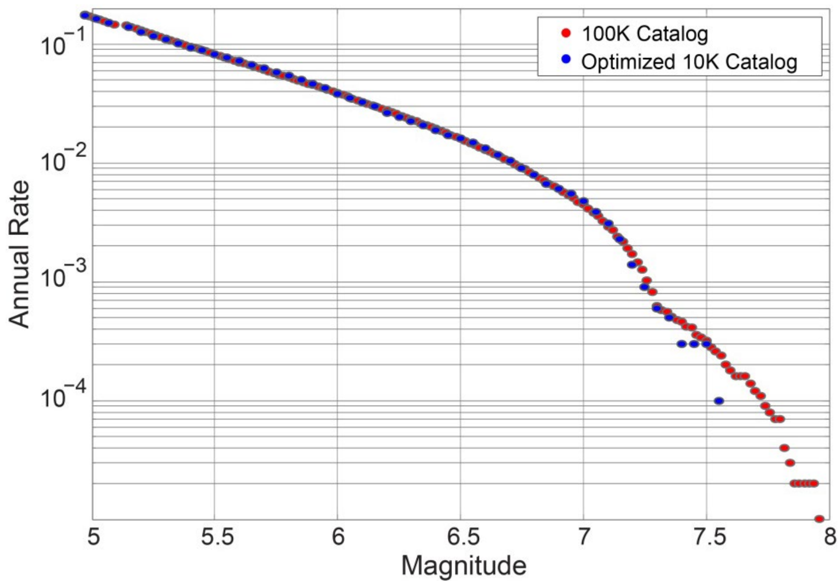

Figure 8. Frequency-magnitude distributions based on the 100,000-year catalog and the optimized 10,000-year catalog for earthquakes within a 200km radius of the city of Vancouver

1.7 Model Resolution

Several surficial geological maps of different resolution, covering different regions of Canada, were used to classify site conditions and estimate ground shaking intensity. A 90 arc-second (~2,000 m) base soil map covering all of Canada was developed from geological data obtained from the Geological Survey of Canada. Provincial-level soil maps, with a resolution of 9 to 18 arc-second (~250-500 m), provide a second layer of coverage for Quebec, British Columbia, and Ontario. Regions of high exposure concentration, including Montreal, Vancouver, Victoria, and Quebec City, are covered by a third, high-resolution map layer (0.9-1.8 arc-second; ~25-50 m).

In Touchstone, users may input risk at the level of CRESTA zones, FSA, LDU (postal codes), and street address. CATRADER industry loss files are developed using 1-km grid industry exposures. CATRADER users may input risk at the level of CRESTA zones, provinces, and FSA; losses are reported at the country, province, and FSA level.

1.8 Modeled Lines of Business

The lines of business included in the AIR Earthquake Model for Canada in CATRADER are residential (single-family homes), mobile home, commercial/industrial, and automobile. Touchstone also supports large industrial facilities. For details on how these lines are modeled in CATRADER and Touchstone, see Section 7 and 8, respectively.

1.9 Construction and Occupancy Classes

Number of Supported Construction Classes: 75

Number of Supported Occupancy Classes: 110 (includes 62 classes for large industrial facilities).

Please refer to Section 8 for details on supported construction and occupancy classes in Touchstone.

1.10 Modeled Industry Losses

It is important to distinguish between insurable and insured losses when modeling the industry exposure. To that end, some definitions are in order:

Insurable exposure: Total replacement value and number of properties (risk count) that are eligible for insurance. Certain building types are extremely vulnerable to natural perils and consequently are unlikely to be insured. Such properties are identified in each modeled region and are excluded from the industry database of insurable properties.

Insured exposure: Although eligible for insurance, "take-up" or purchase of insurance coverage for eligible properties varies by peril and region. For example, coverage for some natural perils may be mandatory in a region, and consequently the insurance take-up rate would be 100%. For other natural perils, insurance may be voluntary and take-up may be in single-digit percentage values. Based on available information, AIR provides estimates of take-up rates for each modeled region and simulated peril. Insured exposure is calculated by multiplying the take-up rate by the insurable risk count and replacement values.

Insurable loss: Estimated losses to insurable exposure (as though the take-up rate is 100%).

Insured loss: Estimated losses to insured exposure.

Note that both insurable and insured loss account for policy terms (deductibles and limits).

Modeled occurrence loss estimates are provided below, for selected annual exceedance probabilities. Modeled aggregate loss estimates for Canada as a whole and for selected provinces are also provided. Please note that the losses *do not* include demand surge.

In addition, note that modeled losses due to fire following earthquake perils can be obtained separately from losses due to other perils in the AIR software. In contrast, tsunami, liquefaction and landslide losses are not separable from shake losses in the software.

Finally, note that these losses are calculated using late 2012 industry exposures.

Modeled Insured Occurrence Losses

	All Perils (Shake, Fire Following, Liquefaction, Tsunami, and Landslide):	Shake, Liquefaction, Landslide, and Tsunami:	Fire Following Only:
Canada			
1% Exceedance Probability (100-year):	CAD 4,766.2 million	CAD 4,474.1 million	CAD 297.6 million
0.4% Exceedance Probability (250-year):	CAD 17,428.8 million	CAD 16,415.3 million	CAD 1,403.6 million
Quebec			
1% Exceedance Probability (100-year):	CAD 1,311.6 million	CAD 1,242.6 million	CAD 77.6 million
0.4% Exceedance Probability (250-year):	CAD 4,766.1 million	CAD 4,474.1 million	CAD 323.7 million
Ontario			
1% Exceedance Probability (100-year):	CAD 32.0 million	CAD 30.3 million	CAD 1.2 million
0.4% Exceedance Probability (250-year):	CAD 453.0 million	CAD 437.2 million	CAD 21.6 million
British Columbia			
1% Exceedance Probability (100-year):	CAD 1,605.3 million	CAD 1,490.7 million	CAD 97.2 million
0.4% Exceedance Probability (250-year):	CAD 7,951.7 million	CAD 6,770.0 million	CAD 428.2 million

Modeled Insurable Occurrence Losses

	All Perils (Shake, Fire Following, Liquefaction, Tsunami, and Landslide):	Shake, Liquefaction, Landslide, and Tsunami:	Fire Following Only:
Canada			
1% Exceedance Probability (100-year):	CAD 9,494.3 million	CAD 9,110.4 million	CAD 297.6 million
0.4% Exceedance Probability (250-year):	CAD 26,881.2 million	CAD 25,565.3 million	CAD 1,403.6 million
Quebec			
1% Exceedance Probability (100-year):	CAD 3,413.4 million	CAD 3,162.0 million	CAD 77.6 million
0.4% Exceedance Probability (250-year):	CAD 13,263.1 million	CAD 12,695.7 million	CAD 323.7 million

Ontario

1% Exceedance Probability (100-year):	CAD 91.7 million	CAD 91.7 million	CAD 1.2 million
0.4% Exceedance Probability (250-year):	CAD 1,486.8 million	CAD 1,483.0 million	CAD 21.6 million

British Columbia

1% Exceedance Probability (100-year):	CAD 2,183.7 million	CAD 2,077.7 million	CAD 97.2 million
0.4% Exceedance Probability (250-year):	CAD 9,763.5 million	CAD 9,027.03 million	CAD 428.2 million

Modeled Insured Aggregate Losses

Average annual aggregate *insured* losses (all perils) are shown in Figure 9 for Canada as a whole and for the five provinces with the highest average annual aggregate insured loss.

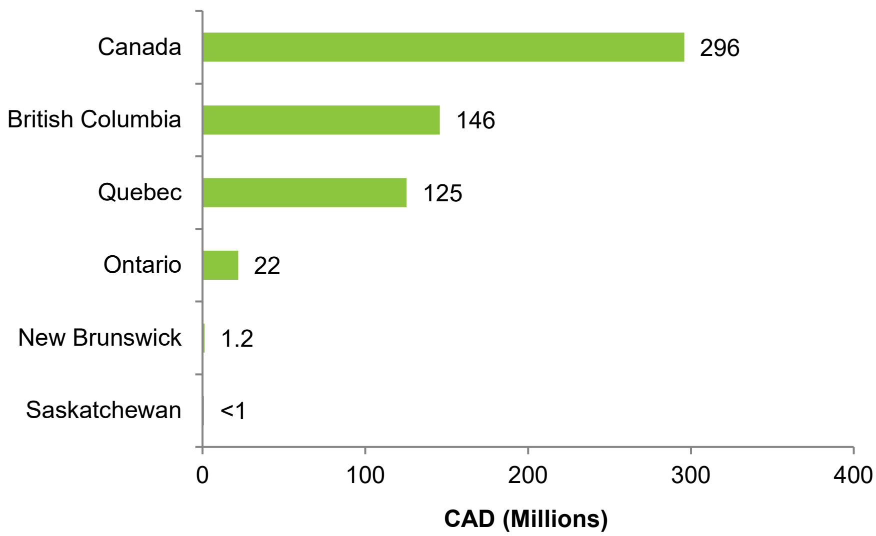

Figure 9. Insured aggregate average annual loss (CAD)

Modeled Insurable Aggregate Losses

Average annual aggregate *insurable* losses (all perils) are shown in Figure 10 for Canada as a whole and for the five provinces with the highest average annual aggregate insurable loss.

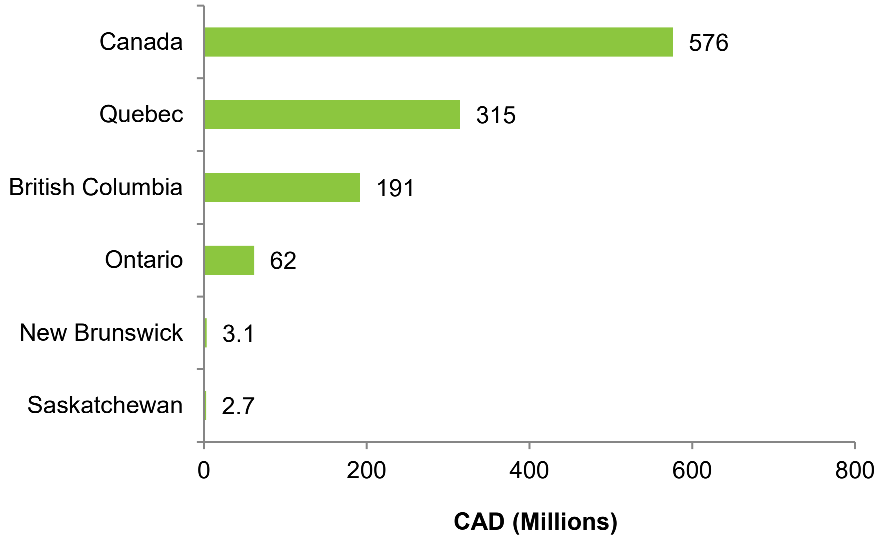

Figure 10. Insurable aggregate average annual loss (CAD)

A loss cost map for all perils—ground shaking, liquefaction, landslide, tsunami, and fire following—is shown in Figure 11. This map depicts the average annual loss to Coverage A (buildings) of a uniform exposure type (construction class 100, occupancy class 301, unknown building height and age) with a uniform exposure value, calculated at a 1 kilometer grid resolution. Note that Average Properties was turned on, but demand surge was *not* included, in this calculation.

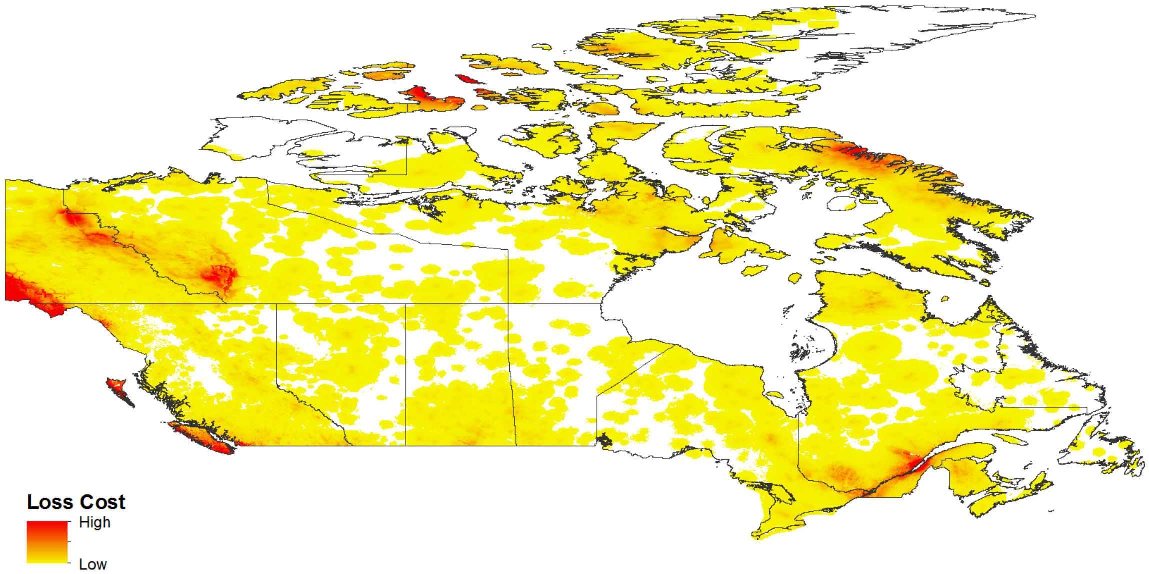

Figure 11. Loss cost map for Canada earthquake (all perils)

1.11 Modeled Losses for Historical Earthquakes

Table 4 and Table 5 list the modeled insurable and insured loss estimates for significant historical earthquakes affecting Canada, respectively. These modeled losses include loss to property and contents, business interruption, and additional living expenses in Canada. (Losses to exposures in the United States are not included in the table; however, historical events that are estimated to inflict losses within the United States, in addition to losses in Canada, are indicated in the far right column). These losses were calculated using 2012 industry exposures. Note that these losses do not include demand surge. For information about these historical earthquakes, please refer to Section 2.3.

Table 4. Modeled insurable industry loss estimates for historical earthquakes in Canada (CAD), based on 2012 industry exposures

Year	Event	Residential	Mobile Home	Commercial/ Industrial	Auto	Total	U.S. Loss?
1663	Charlevoix-Kamouraska region QC - Scenario 1	5,669,212,682	26,085,374	6,810,408,159	69,525,852	12,575,232,067	Y
1663	Charlevoix-Kamouraska region QC - Scenario 2	3,298,867,085	18,319,403	3,924,820,158	46,553,887	7,288,560,533	Y
1663	Charlevoix-Kamouraska region QC - Scenario 3	8,195,140,129	38,095,072	10,612,821,777	102,607,808	18,948,664,785	Y
1700	Cascadia Subduction Zone Offshore of BC	7,346,964,794	67,660,407	15,498,353,290	163,431,115	23,076,409,606	Y
1732	Montreal region QC - Scenario 1	106,089,784,394	137,558,283	262,388,968,738	1,702,404,749	370,318,716,164	Y
1732	Montreal region QC - Scenario 2	43,476,924,197	80,097,272	117,913,409,928	763,700,490	162,234,131,887	Y
1732	Montreal region QC - Scenario 3	27,499,843,846	85,747,186	73,893,933,843	492,113,587	101,971,638,461	Y
1791	Charlevoix-Kamouraska region QC	198,935,200	1,008,145	209,936,283	4,165,469	414,045,097	N
1860	Charlevoix-Kamouraska region QC	527,316,461	5,098,274	786,423,183	9,345,447	1,328,183,367	N
1870	Charlevoix-Kamouraska region QC	2,783,442,892	12,833,110	2,944,341,304	34,627,395	5,775,244,702	Y
1899	Yakutat Bay AK	331,310	11,888	401,515	964	745,678	N
1904	Passamaquoddy Bay NB	20,312,341	3,071,737	44,700,717	1,406,552	69,491,346	Y
1918	Vancouver Island BC	22,340,513	342,882	51,887,404	151,948	74,722,745	N
1920	Gulf Islands BC	238,043	3,386	278,569	0	519,999	Y
1925	Charlevoix-Kamouraska region QC	599,497,932	4,888,231	1,450,444,211	8,274,046	2,063,104,420	N
1929	Laurentian Slope Offshore of NS and NL	9,362	39	43,484	0	52,886	N
1933	Baffin Bay NU	11,921	0	33,736	0	45,657	N
1935	Témiscaming region QC	209,452,522	481,734	969,636,981	2,693,591	1,182,264,827	N
1944	Between Massena NY and Cornwall ON	580,815,646	1,743,193	618,442,729	13,492,490	1,214,494,058	Y
1946	Vancouver Island BC	2,144,601,499	19,967,515	1,931,115,709	16,526,231	4,112,210,954	N
1949	Offshore of Haida Gwaii/Queen Charlotte Islands BC	8,548,964	36,023	31,574,308	87,807	40,247,102	N
1958	Lituya Bay AK	628,099	13,180	1,173,204	309	1,814,791	N
1964	Prince William Sound AK	0	0	70,035,780	10,232,785	80,268,565	N
1970	Offshore of Haida Gwaii/Queen Charlotte Islands BC	171,425	28	306,945	922	479,320	N
1979	Southern Yukon region YT	6,617	154	36,331	0	43,103	N
1982	Miramichi Highlands NB	675,376	13,245	436,505	18,091	1,143,216	N
1985	North Nahanni River NT	11,859	0	7,867	0	19,725	N
1988	Saguenay region QC	24,008,055	458,030	75,333,923	193,933	99,993,941	N
2001	Nisqually WA	30,860	89	64,060	0	95,009	Y
2002	Denali AK	139,172	10,180	342,383	627	492,360	N
2010	Val-des-Bois QC	10,487,747	717,525	1,082,142	591,764	12,879,180	N
2011	Vancouver Island BC	15,797	513	161,365	8	177,681	N
2012	Haida Gwaii/Queen Charlotte Islands BC	3,309,377	12,633	11,995,369	27,934	15,345,313	N

Modeled losses include loss to property and contents, business interruption, and additional living expenses. Losses do not include demand surge.

Table 5. Modeled insured industry loss estimates for historical earthquakes in Canada (CAD), based on 2012 industry exposures

Year	Event	Residential	Mobile Home	Commercial/ Industrial	Auto	Total	U.S. Loss?
1663	Charlevoix-Kamouraska region QC - Scenario 1	208,976,275	953,049	4,150,891,754	69,525,852	4,430,346,930	Y
1663	Charlevoix-Kamouraska region QC - Scenario 2	124,319,957	668,684	2,400,271,438	46,553,887	2,571,813,965	Y
1663	Charlevoix-Kamouraska region QC - Scenario 3	340,062,800	1,600,153	6,464,386,946	102,607,808	6,908,657,705	Y
1700	Cascadia Subduction Zone Offshore of BC	4,212,156,453	33,294,597	13,220,043,069	163,431,115	17,628,925,234	Y
1732	Montreal region QC - Scenario 1	17,185,154,511	11,404,926	169,101,684,056	1,702,404,749	188,000,648,243	Y
1732	Montreal region QC - Scenario 2	6,581,938,894	5,112,676	75,582,654,107	763,700,490	82,933,406,166	Y
1732	Montreal region QC - Scenario 3	3,412,024,351	6,061,519	46,820,302,379	492,113,587	50,730,501,836	Y
1791	Charlevoix-Kamouraska region QC	12,831,297	22,988	128,246,601	4,165,469	145,266,353	N
1860	Charlevoix-Kamouraska region QC	16,316,495	113,774	484,754,532	9,345,447	510,530,250	N
1870	Charlevoix-Kamouraska region QC	113,046,831	271,264	1,796,653,577	34,627,395	1,944,599,067	Y
1899	Yakutat Bay AK	29,758	594	203,146	964	234,462	N
1904	Passamaquoddy Bay NB	398,903	30,717	22,472,517	1,406,552	24,308,690	Y
1918	Vancouver Island BC	9,047,108	137,153	44,122,795	151,948	53,459,005	N
1920	Gulf Islands BC	166,149	2,327	236,784	0	405,259	Y
1925	Charlevoix-Kamouraska region QC	33,497,363	106,222	893,130,167	8,274,046	935,007,797	N
1929	Laurentian Slope Offshore of NS and NL	93	0	22,710	0	22,805	N
1933	Baffin Bay NU	119	0	15,181	0	15,300	N
1935	Témiscaming region QC	14,659,467	11,926	621,208,091	2,693,591	638,573,074	N
1944	Between Massena NY and Cornwall ON	65,862,430	61,780	385,190,814	13,492,490	464,607,513	Y
1946	Vancouver Island BC	895,738,473	8,087,806	1,644,907,184	16,526,231	2,565,259,694	N
1949	Offshore of Haida Gwaii/Queen Charlotte Islands BC	3,422,576	14,409	27,547,417	87,807	31,072,209	N
1958	Lituya Bay AK	55,085	659	597,807	309	653,858	N
1964	Prince William Sound AK	0	0	59,530,413	10,232,785	69,763,198	N
1970	Offshore of Haida Gwaii/Queen Charlotte Islands BC	68,570	12	260,903	922	330,406	N
1979	Southern Yukon region YT	330	8	18,166	0	18,504	N
1982	Miramichi Highlands NB	6,754	133	218,252	18,091	243,230	N
1985	North Nahanni River NT	119	0	3,540	0	3,658	N
1988	Saguenay region QC	1,561,744	9,161	45,944,037	193,933	47,708,872	N
2001	Nisqually WA	21,601	62	54,451	0	76,115	Y
2002	Denali AK	6,958	509	171,191	627	179,285	N
2010	Val-des-Bois QC	210,183	14,351	649,285	591,764	1,465,584	N
2011	Vancouver Island BC	6,318	206	137,160	8	143,692	N
2012	Haida Gwaii/Queen Charlotte Islands BC	1,323,751	5,053	10,547,693	27,934	11,904,431	N

Modeled losses include loss to property and contents, business interruption, and additional living expenses. Losses do not include demand surge.

1.12 Navigating the Document

Figure 12 illustrates the components of the AIR Earthquake Model for Canada. Section 2 provides a brief overview of earthquakes and earthquake risk in Canada. Section 3 details the generation of simulated events that populate the stochastic catalog, and Section 4 describes how the intensity of ground shaking, liquefaction, landslide, and tsunami is modeled at each site. Section 5 discusses the model's damage functions for each peril, details the model's fire following earthquake component, and includes information on estimating damage to industrial facilities. Section 6 provides a discussion of the financial module.

For details on the implementation of the AIR Earthquake Model for Canada in CATRADER and Touchstone, please refer to Section 7 and Section 8, respectively. Section 9 offers selected references and Section 10 provides an overview of AIR Worldwide.

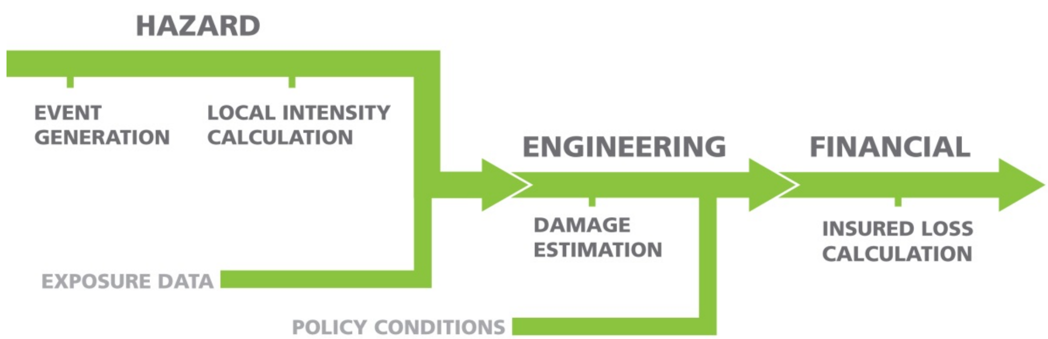

Figure 12. Components of the AIR Earthquake Model for Canada

2 Earthquakes in Canada

2.1 Earthquakes: An Overview

An earthquake results from a sudden displacement of rock along a fault. It accompanies a rapid release of energy in the form of seismic waves, which propagate outward from a focus.

The process begins when rocks that experience stress along faults begin to deform as the strain builds within them. When the stress exceeds the strength of the rock and overcomes the friction that resists the relative movement of opposite sides of the fault, the fault ruptures and releases energy. Some of the energy released dissipates as friction along the fault; the rest is transferred as seismic waves that radiate from the initial point of rupture and cause ground motion at the earth's surface.

Faults are rarely found in isolation; instead, they tend to form zones of related fault traces. Long faults may be segmented, with each segment having an individual rupture history and mechanism. Ruptures during a weak to moderate earthquake are believed to be contained within one segment of a fault, but more powerful earthquakes may manifest themselves along multiple segments. Fault zones vary in depth, width, and orientation.

A fault plane can be vertical or sloping in relation to the earth's surface. In sloping faults, the rock volume above the fault plane is known as the hanging wall, and the rock volume below the fault plane is the footwall. One type of earthquake faulting mechanism is dip-slip, which can be subclassified as either normal or reverse faulting. Normal faulting occurs when the hanging wall slips down relative to the footwall, resulting in an extension of crustal matter. Reverse faulting occurs when the hanging wall lifts relative to the footwall, which causes a shortening of the crustal material. Strike-slip faults have a nearly vertical surface; their movement is horizontal, parallel to the strike of the fault surface. Oblique-slip faulting is a combination of strike-slip and normal or reverse faulting.

While faults may form a visible trace on the earth's surface, some remain buried within the earth. These blind faults represent a significant seismic hazard, as they are often difficult to detect prior to rupture. Hazard assessment of blind faults is challenging and often plagued with uncertainty.

Generally, active faults are those which have demonstrated activity during the last 10,000 years, or during the Holocene period. Potentially active faults are those that have demonstrated activity during the last 1.65 million years, or during the Quaternary period.

Plate Tectonics

The theory of plate tectonics was developed to explain the evidence for large-scale motion of the earth's continents. The crust and upper mantle form the rigid, strong lithosphere, which is divided into large plates that move relative to one another. The largest plates are the Pacific, North American, South American, Eurasian, African, and Australian plates.

These lithospheric plates move over the asthenosphere, a hot, viscous layer of weak solid rock that is continuously moving and transferring heat from the interior to the surface of the earth. The boundaries between plates are where most earthquake and volcanic activity occurs.

There are several types of boundaries between neighboring plates. Convergent boundaries occur where two plates move towards one another; if one of these plates sinks, or subducts, beneath the edge of the other plate, a subduction zone is formed (Figure 13). Seismic activity may be particularly rampant in subduction zones.

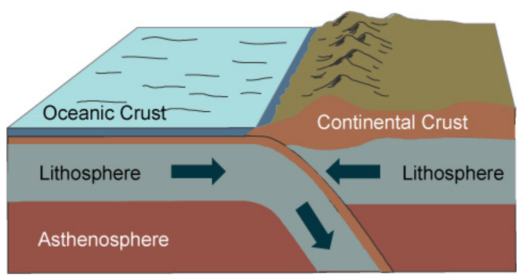

Figure 13. The earth's layers at a subduction zone

Continental-collision boundaries occur where two low-density plate edges move towards one another; this process may result in crustal rock being thrust upward, which is how linear mountain systems are formed. Divergent boundaries occur where plates move away from one another, which allows for the formation of new crustal material.

Transform boundaries occur where one plate moves past another. Due to massive amounts of friction, however, the plates do not simply glide past each other. Rather, stress builds up in the rocks along the fault until the strain is too great. At that point, the potential energy is released in the form of an earthquake.

While the majority of earthquakes do occur at plate boundaries, intraplate earthquakes can occur along fault zones in the interior of a plate. A large intraplate earthquake usually has a long recurrence time, which makes it difficult to estimate the associated risk.

Seismic Waves

Seismic waves transmit tectonic energy through the earth at speeds of up to several miles per second. Seismic waves produce ground motion on the earth's surface that may damage buildings, trees, cars, roads, and other structures. Soil properties, local geological features, and other factors play a role in attenuating or amplifying seismic waves at a given location.

There are several types of seismic waves. Body waves travel through the earth, while surface waves travel along its surface. The two types of body waves that are generated by an earthquake are primary and secondary waves, also known as P and S waves, respectively. P waves are faster and capable of traveling through both solids and liquids. These waves exhibit an alternating compression-dilatation motion in the direction of wave propagation. S waves are slower and travel only through solid material. These waves produce a sideways-shearing motion perpendicular to the direction of wave propagation.

Surface waves, which are responsible for the majority of earthquake damage, include Love waves and Rayleigh waves. Love waves move horizontally, perpendicular to the direction of wave propagation. Rayleigh waves are slow waves that move in an elliptical, or rolling, motion. Note that seismic-wave amplitude, which is the height of an individual wave cycle, or the maximum displacement, decreases with increasing depth in the earth for these surface waves. The amplitude of a seismic wave is one measure of its destructive potential.

In addition to amplitude, there are several ways to mathematically describe wave activity. The wave frequency is the number of wave cycles per second that pass a reference point. A wave's period is the elapsed time, in seconds, between peaks, or the time it takes one complete cycle of the wave to pass a reference point. The wavelength is the distance between repeating units of a propagating wave of a given frequency, at some instant in time.

Measuring Earthquake Magnitude and Intensity

The severity of an earthquake can be measured by the damage it inflicts on structures at the earth's surface or by the energy released at its focus, which is where the rupture originates. Earthquake magnitude characterizes the total energy released by an earthquake, while earthquake intensity refers to the resulting level of ground shaking at a particular location and the observed effects of an earthquake on people, buildings, and other features. While the magnitude of an earthquake is a characteristic of the earthquake as a whole, intensity varies from place to place within an affected region.

An earthquake's intensity at different locations can be described semiquantitatively using the Modified Mercalli Intensity (MMI) scale[1], which was developed in its original form in 1902 and is based on observations of shaking severity and its effects at different locations. The MMI at a particular location is based on human judgment and the observed post-event damage. Today, ground-motion intensity can be directly measured using strong-motion seismographs. The characteristics of ground-motion intensity can be quantified by physical parameters such as peak ground acceleration (PGA) and spectral acceleration (Sa). Shaking intensity at a particular location depends not only on earthquake magnitude, but on the local surface geology and the proximity of the location to the earthquake source.

Magnitude is a measure of an earthquake's size. There are several types of earthquake magnitude, including moment magnitude (M_W), Richter magnitude (M_L), body-wave magnitude (M_b), and surface-wave magnitude (M_s). Magnitude scales are generally logarithmic in nature; that is, an increase of one point on a magnitude scale represents approximately a ten-fold increase in wave amplitude and a thirtyfold increase in the amount of energy released during the earthquake. AIR models utilize the moment-magnitude scale, which is based on seismic moment. The seismic moment is defined as:

$M_o = \mu AD$

where

μ = the shear modulus of elasticity of the rupturing material

A = the rupture area

D = the average slip over the rupture area

The moment magnitude is considered superior to other magnitude scales because it is based on earthquake source parameters, rather than on a particular type of seismic wave, like the surface-wave or body-wave magnitude scales, or a particular type of instrument, such as the Richter magnitude scale. The type and amplitude of the seismic waves that reach an instrument and are recorded depend on earthquake magnitude, the radiation pattern of seismic waves, which depends on the rupture mechanism, and the complex structures along the wave propagation path between the source and the seismic stations. Different earthquakes can generate different types of seismic waves. Small earthquakes

[1] Please see http://earthquake.usgs.gov/learning/topics/mercalli.php for a more detailed description of this intensity scale.

generate seismic waves with short periods, while larger earthquakes can generate seismic waves with long to very long periods.

Most seismic waves will saturate beyond a certain magnitude; that is, wave amplitude will not increase beyond that magnitude. Therefore magnitude scales based on the amplitude of a particular type of seismic wave will also experience saturation. Moment magnitude does not have such a limitation.

Paleoseismic and Geodetic Data

The modeling of earthquakes requires historical data. For large earthquakes, the catalog is complete further back in time because such events are more likely to have been observed and documented than smaller events. However, improvements in instrument sensitivity and coverage have led to increased recordings of smaller events. The completeness of a historical catalog is therefore a function of time and magnitude.

Paleoseismology and geodetic data are often used to augment instrumentally recorded earthquake catalogs in order to estimate current seismic hazard. Paleoseismology is the study of the location, timing, and size of prehistoric earthquakes. Prehistoric earthquakes are evidenced by offsets in geologic formations found in exhumed fault zones, signs of rapid uplift or subsidence near coastal areas, laterally offset stream valleys, and liquefaction artifacts, such as sand boils.

The geodetic measurement of fault slip rate is another source of information that is used to supplement historical data. The Global Positioning System (GPS) is now the most widely used technology for measuring crustal deformations in a region. The observed crustal deformation represents elastic strain accumulation in the crust. By calculating the rate at which elastic strain accumulates along a fault or seismic zone, estimates can be made as to how often large earthquakes may occur.

Paleoseismic and geodetic data assist in estimating the frequency of large-magnitude earthquakes; for smaller events, the historical earthquake data tends to be more complete. For earthquakes above some magnitude, which is region-dependent, geodetic and paleoseismic data become more reliable compared to historical earthquake data, as Figure 14 illustrates.

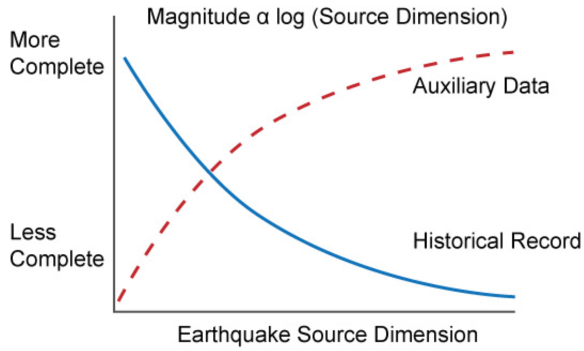

Figure 14. Data completeness as function of earthquake source dimension

The Gutenberg-Richter Relationship

The Gutenberg-Richter relationship expresses the association between magnitude and the earthquake occurrence rate on a fault or in a given area, at or above each magnitude. The relationship can be used to provide a more complete picture of seismicity in regions where historical data is lacking, as it holds over a wide variety of magnitudes and locations.

The Gutenberg-Richter relationship is parameterized by the a-value, which is the logarithm of the earthquake occurrence rate above some reference magnitude, and the b-value, which is the rate at which the logarithm of the cumulative annual frequency decreases as the magnitude increases. Scientists usually truncate this relationship at a limiting magnitude above which the probability of an earthquake's occurrence is zero (Figure 15).

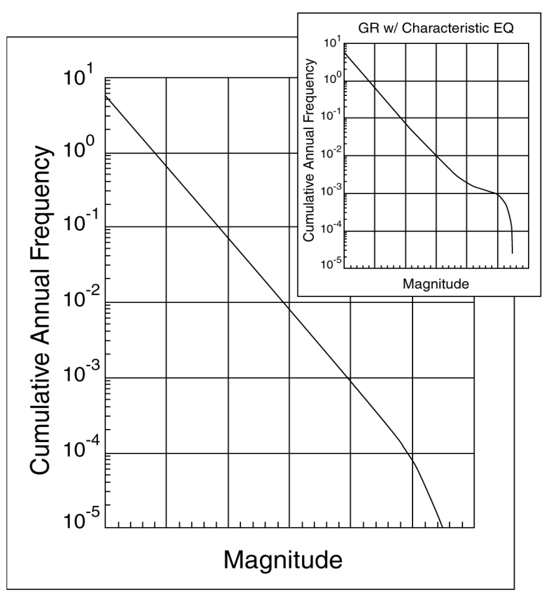

Figure 15. A sample Gutenberg-Richter distribution

Note that the a-value is the logarithm of the y-intercept of the distribution, and the b-value represents the slope of the graph away from the characteristic earthquake or limiting magnitudes. The presence of large-magnitude characteristic earthquakes increases the frequency at these magnitudes.

Historical seismicity data, paleoseismic data, and geodetic slip-rate data are used to estimate the upper-bound magnitude of the Gutenberg-Richter distribution.

Characteristic Earthquakes

The characteristic-earthquake theory states that active faults tend to generate earthquakes of about the same magnitude at regular time intervals. This concept is used to simulate seismic activity along active faults. In order to model characteristic earthquakes, the earthquake magnitude and return period must be specified. Magnitude can be estimated from historical data, paleoseismological data, and fault length. The return period is estimated from paleoseismological data, fault slip rates, or seismic-moment rates as estimated from fault slip rates.

Tsunami Formation

A tsunami is not a tidal wave; rather, it is a series of waves with very long wavelengths that form when a large amount of water is displaced by a release of energy in the ocean. While most tsunamis are associated with earthquakes, some are caused by landslides or volcanic eruptions that occur under the ocean.

When an earthquake occurs under the ocean, the released energy that deforms the ocean floor is transferred to the water above causing a rise in the water column that lies over the part of the floor that is thrust upwards. If enough energy is released, the displacement of the water can reach the surface and produce a tsunami. Tsunamis that are generated by earthquakes move outwards in all directions from the earthquake's epicenter. A tsunami moving through the deep ocean resembles a rise in the water level rather than a large sea wave. At that point, a tsunami is generally no higher than about half a meter, has a very long wavelength (typically greater than 100 km), and moves at tremendously high speeds. At an ocean depth of 4 km, tsunamis typically move at speeds of around 800 km/h.

A tsunami tends to become amplified as it approaches the shore, particularly if it enters bays or inlets. The reason is that at shallower depths and the friction at the sea floor slow the forward speed of the wave allowing the back of the wave to move towards the front, horizontally compressing the wave and thus making it taller. At a water depth of 50m, a tsunami typically moves at a speed of around 90 km/h with a wavelength of 23 km. At a depth of 10 m, the same tsunami slows to

45 km/h and its wavelength shortens to 11 km. Once the wave starts to move over land it continues to slow down due to friction but does not build up. The changes in the wave speed as the tsunami approaches the shoreline is a crucial aspect of a tsunami model. In the deep ocean, the tsunami moves at the speed of a jet airplane; however, because of the small amplitude and long wavelength it could pass under a boat without incident. Towards the shore however, the higher amplitude and shorter wavelength yield a more pronounced waveform that is more likely to carry a boat forward.

Figure 16 illustrates the generation and movement of a tsunami. Panel (a) shows a subduction earthquake beneath the ocean floor displacing the water above. Panel (b) shows the resulting tsunami traveling over the open ocean. Panel (c) shows the tsunami wavelength shortening and the wave growing taller as it enters shallower water near the shoreline and is slowed by friction. Panel (d) shows the tsunami after it reaches the shoreline and moves over land.

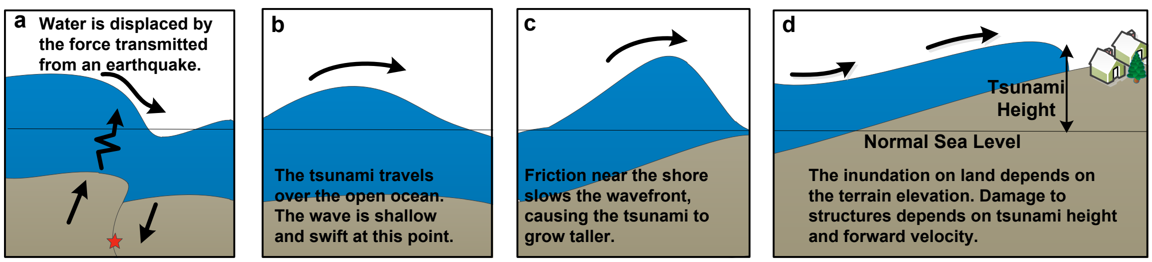

Figure 16. Generation and movement of a tsunami from an earthquake

2.2 Canada Earthquake Risk

The Hazard

Earthquake hazard in Canada is largely due to seismic zones along the country's western Pacific coast, including the offshore seismic zone near Haida Gwaii/Queen Charlotte Islands, the Cascadia subduction zone, and the St. Elias region of British Columbia and the Yukon. In fact, the Geological Survey of Canada reports more than 1000 earthquakes in western Canada each year. As a part of the Pacific "Ring of Fire", the Canadian west coast is one of the few regions of the world to exhibit all three of the major types of plate motion – divergence, convergence, and strike-slip – that cause significant seismic activity. Figure 17 shows the tectonic context of Canada, including these plate boundaries. The historical seismicity of Canada (all earthquakes of magnitude ≥ 5.0 since 1700) is shown in Figure 18.

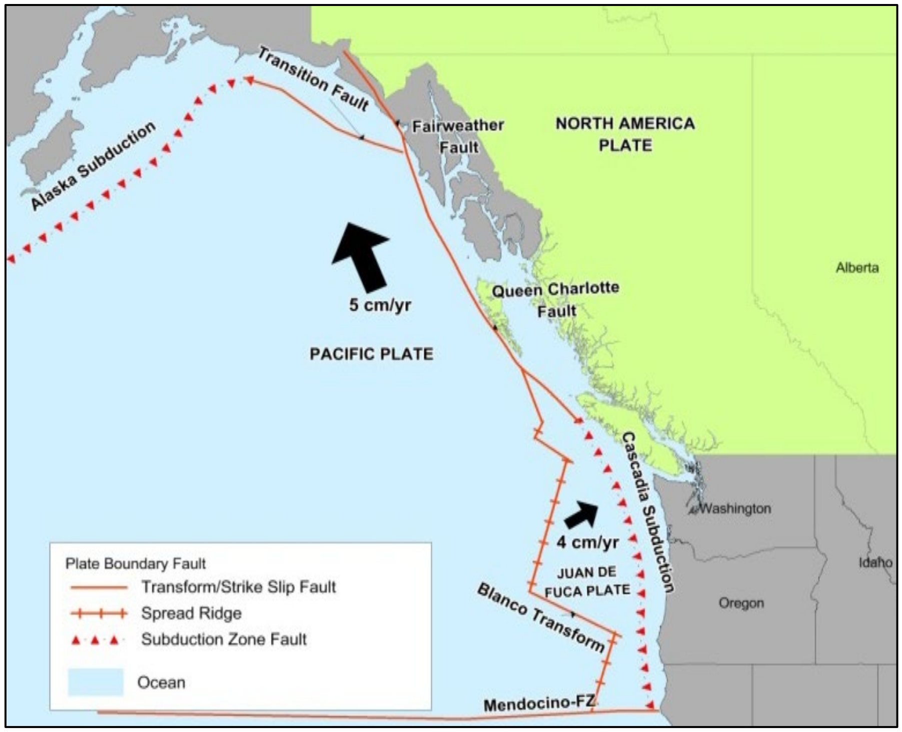

Figure 17. Tectonic context of Canada (the large arrows show plate motion relative to the North American plate)

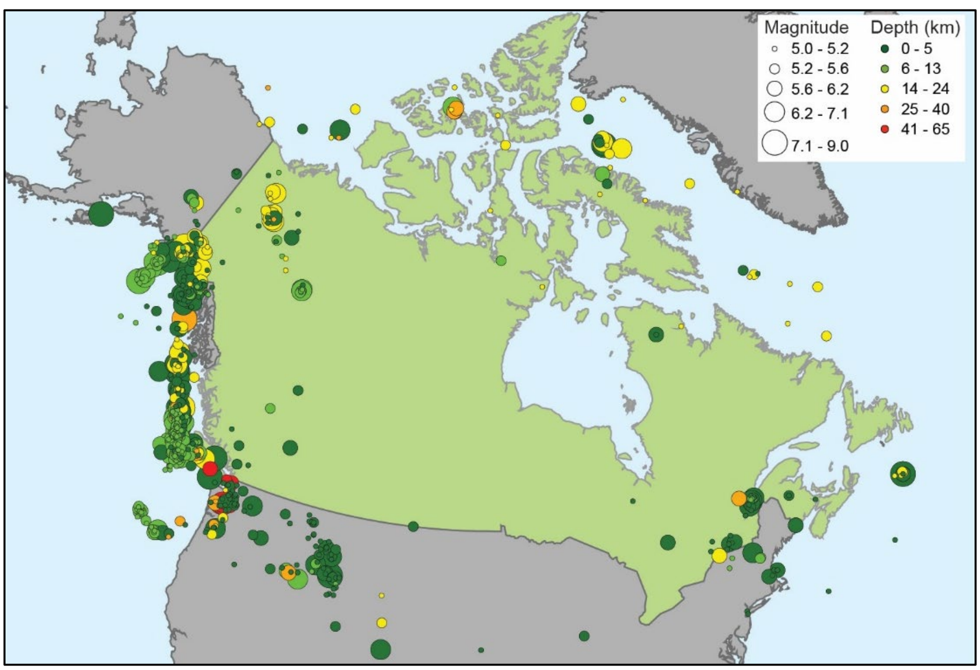

Figure 18. Historical seismicity in Canada since 1700 (M ≥ 5.0)

Moving inland from the Pacific coast, earthquakes become much less frequent and smaller in magnitude. However, pockets of increased seismicity do exist in the tectonically stable regions of central and eastern Canada. In eastern Canada, damaging earthquakes have been produced by ancient faults in seismic zones such as the Charlevoix-Kamouraska seismic zone and the Laurentian Slope seismic zone.

The Exposure

In Canada, earthquake risk is the highest in Vancouver, Victoria, Montreal, Ottawa, and Québec City. Cumulatively, these cities house 26% of Canada's population, and all are important economic and cultural centers. However, by some estimates, fully 40% of Canadians live and work in regions of moderate-to-high seismic risk. Comparing the spatial distribution of Canada's population (Figure 19) and historical seismicity in Canada (Figure 18) underscores this fact.

Figure 19. Population density of Canada

Regions of elevated seismic risk in Canada, and the most significant exposures located within them, are described below.

Offshore of Haida Gwaii/Queen Charlotte Islands

The Queen Charlotte Fault is a part of the fault system that forms the strike-slip interface between the Pacific plate to the west and the North American plate to the east. As these two plates slide past one another, very large earthquakes can result from the buildup of stresses within the fault zone. In the past century, four major earthquakes ($M \geq 7.0$) have been linked to this fault system. In 1949, the largest earthquake recorded in Canada (magnitude 8.1) was spawned by a 500-kilometer rupture along the Queen Charlotte Fault.

Many cities in British Columbia, including Vancouver and Victoria, are vulnerable to earthquakes caused by the Queen Charlotte fault system. Throughout its central business district, Vancouver's above-ground electrical system renders the city especially vulnerable to earthquake damage. In addition, nearly half of the city of Victoria is underlain by soft sediments that would likely become unstable during strong ground shaking. North of Vancouver, the Seymour Falls Dam does not meet current seismic standards. Improvements are underway to strengthen this critical component of the Vancouver water network.

Cascadia Subduction Zone

West of Vancouver Island, the Cascadia subduction zone extends south towards California, forming the junction between the Juan de Fuca plate to the west and the North American plate to the east (Figure 17). Over time, tectonic forces push the Juan de Fuca plate under the North American plate. However, for the past three centuries, these plates have been locked together, generating enormous stresses within the Cascada subduction zone. When these stresses are released, powerful earthquakes occur, such as the formidable 9.0 M event that struck the region in January of 1700. According to geological evidence, the Cascadia subduction zone gives rise to a similar megathrust earthquake every 300-800 years.

A megathrust earthquake within the Cascadia subduction zone would likely devastate Victoria and Vancouver in British Columbia, and seriously damage cities in the northwestern United States including Seattle and Portland. Such an earthquake might also generate a powerful tsunami that could inundate shorelines along the west coast of North America and cause damage in countries across the Pacific Ocean, such as Japan.

St. Elias Region and the Southwest Yukon Territory

The St. Elias region, formed by adjacent sections of the southwest Yukon Territory, northwest British Columbia, and southeast Alaska, is distinguished by rapid uplift (30 mm/yr, on average) and high levels of seismicity. Both are caused by the interaction of the Pacific plate and the North American plate, which slide past one another to the south but collide to the northwest, subducting the Pacific plate under the North American plate near the Aleutian Islands. Although the St. Elias region of Canada is sparsely populated, minimizing risk to people and property, earthquakes there would likely affect Anchorage, which is the most populous city in Alaska.

Cordillera Region

High seismicity rates in the northern Canadian Rocky Mountains have yielded notable earthquakes, such as the magnitude 6.5 event that struck the Mackenzie Mountains in the Northwest Territories in 1985. At latitudes lower than 60° North, the seismicity of the Cordillera region rapidly decreases. On the whole, the low population density of the Canadian Cordillera minimizes its seismic risk.

Western Quebec Seismic Zone

This enormous seismic zone stretches from the Ottawa Valley to Eastern Ontario, housing the urban areas of Montreal, Ottawa-Hull, and Cornwall. Seismological and geological records reveal that three significant earthquakes have occurred in this zone. For example, in 1732 a magnitude 5.8 event caused serious damage to the city of Montreal. In addition, a magnitude 6.2 earthquake shook the Témiscaming area in 1935. On average, the Western Quebec seismic zone gives rise to one small earthquake ($M \leq 3.0$) every five days.

Home to over 2.8 million people, Montreal is the most populated city in Québec and a major economic hub of eastern Canada. Unfortunately, Montreal is highly vulnerable to earthquakes because many of its older buildings are unreinforced masonry structures. In addition, some parts of the city are built on soft clay layers that are up to 50 feet thick, which would dangerously amplify ground shaking during an earthquake.

Ottawa, Canada's capital city and its fourth largest metropolitan area, is also located within the Western Quebec Seismic Zone where it stretches into eastern Ontario. Much of Ottawa is built on fine-grained post-glacial sediments – specifically, sand, silt, and clay – with high pore water content. This combination of small grain size and significant pore water results in "sensitive soils" that are susceptible to landslides triggered by earthquakes, heavy rains, or other factors.

Charlevoix-Kamouraska Seismic Zone

Unlike the seismic zones of western Canada, the Charlevoix-Kamouraska seismic zone is located far from any plate boundary. Thus, its earthquake activity is not directly associated with specific plate motions, and is less well understood. However, Charlevoix-Kamouraska is the most seismically active region in eastern Canada. According to historical records, five earthquakes of magnitude 6 or larger have occurred in the region since 1600.

The moderate earthquake potential of the Charlevoix-Kamouraska seismic zone increases the seismic vulnerability of nearby cities, such as Quebec City (located just 100 km from the zone). Much of Quebec City near the shores of the St.

Charles River is underlain by thick alluvial deposits. During an earthquake, these soft soils would amplify ground shaking, thus greatly increasing damage. In addition, many buildings in Quebec City are constructed of unreinforced masonry, which is extremely vulnerable to earthquake vibrations.

Lower St. Lawrence Seismic Zone

Each year, about 60 small-to-moderate earthquakes occur in the Lower St. Lawrence Seismic Zone, though most are too small to be felt ($M \leq 2.5$). With their epicenters beneath the St. Lawrence River, these earthquakes are thought to result from slip along paleo-rift faults in the earth's crust.

Although the Lower St. Lawrence Seismic Zone is located nearly 400 kilometers downstream from Québec City, future earthquakes produced in this zone would likely affect this city and surrounding communities.

Laurentian Slope Seismic Zone

Located offshore of Canada's southeast Atlantic coast, the Laurentian Slope Seismic Zone produced a large 7.2 M earthquake in 1929. This earthquake triggered small onshore landslides, but more significantly, a large submarine slump that generated a tsunami. As the tsunami swept the shores of the Burin Peninsula of Newfoundland, 27 people were drowned and many homes and businesses were destroyed.

Geological evidence suggests that submarine slides similar to the 1929 event are extremely rare on the Laurentian slope. Earthquakes too small to be felt are not uncommon here, however, which underscores the enhanced seismic risk of the Canadian maritime provinces.

2.3 Significant Historical Canada Earthquakes

Eighteen of the more significant earthquakes in Canadian history are described in this section. They are notable in terms of their effects on the surrounding region and the damage incurred. In addition, historical and paleoseismic information about these earthquakes was used to inform the development of the AIR Earthquake Model for Canada. These eighteen events, along with an additional 15 earthquakes, comprise the marquee event set of 33 earthquakes included with the model in the AIR software. The epicentral locations of these 33 earthquakes are shown in Figure 20. (Modeled losses for these events are provided in Section 1.11.) Several of these events also impact the U.S. Please note, the losses presented herein are for Canada only.

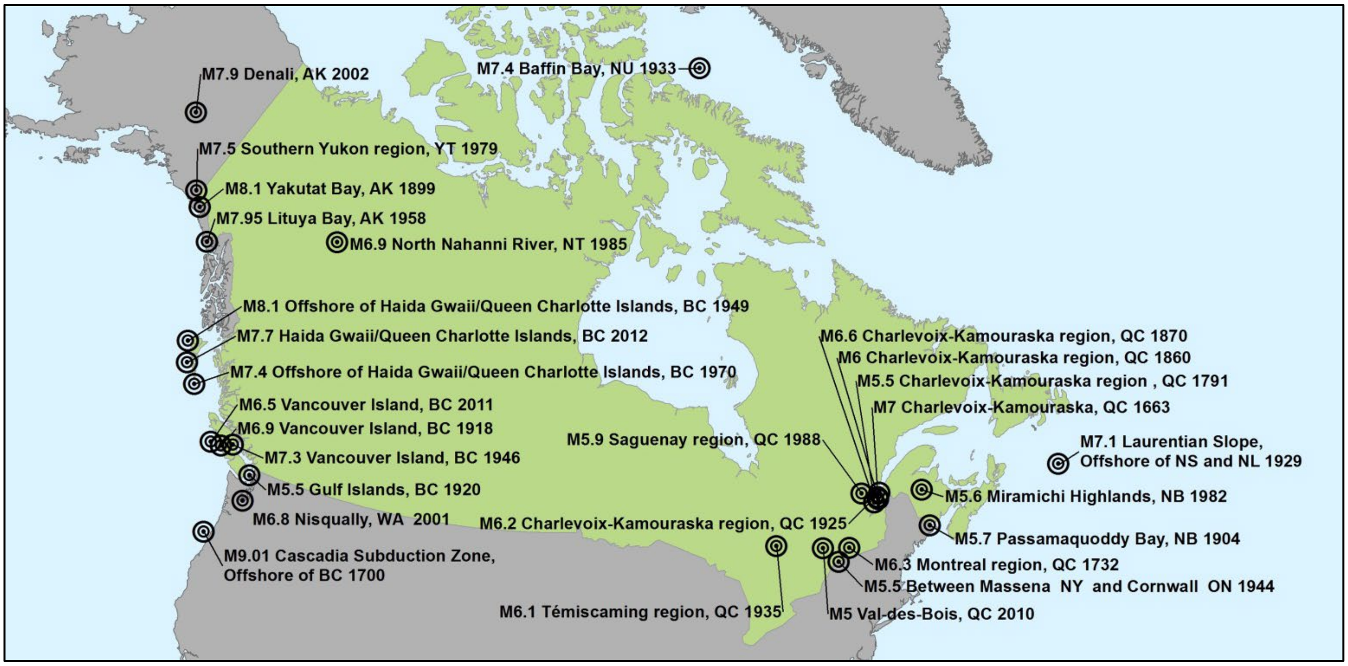

Figure 20. Epicentral locations of significant historical earthquakes in Canada

1663 Charlevoix-Kamouraska, Quebec, M7.0

Historical records indicate that a powerful earthquake occurred in the Charlevoix-Kamouraska region on February 5, 1663, which was felt widely across eastern North America, a region about 750,000 square miles in size. According to contemporary reports, the earthquake damaged masonry walls, cracked chimneys, and threw objects from shelves. This earthquake also caused extensive landslides along the St. Lawrence River, as well as large rockfalls in the vicinity of Trois-Rivières, Quebec. Although there is much uncertainty associated with the earthquake's parameters, analysis of the available geological and paleoseismological data suggests that this event exhibited a magnitude of 7.0.

If the 1663 Charlevoix-Kamouraska earthquake were to occur today, AIR estimates that it would cause insurable losses ranging between CAD 7.2 billion and CAD 18.9 billion, and insured losses ranging from CAD 2.6 billion and CAD 6.9 billion[2]. (A loss range is provided here to reflect the large uncertainty associated with this earthquake's parameters.)

[2] Note that this loss estimate and all other loss estimates provided in this section are for damage to exposures in Canada only. These estimates do not include losses to exposures in the United States.

1700 Cascadia Subduction Zone, British Columbia, M9.0

On January 26, 1700, a 1000-kilometer section of the Cascadia megathrust ruptured, producing one of the largest earthquakes the world has experienced. This event caused dramatic and prolonged ground shaking, and gave rise to a tsunami in the Pacific Ocean that destroyed several coastal buildings in Japan and wiped out the winter village of the Pachena Bay people of Vancouver Island. Geological evidence suggests that 13 earthquakes of this size have occurred along the Cascadia subduction zone in the last 6000 years.

If the 1700 M9.0 Cascadia subduction zone earthquake were to occur today, AIR estimates that this event would cause insurable losses of more than CAD 23.1 billion, and insured losses of CAD 17.6 billion.

1732 Near Montreal, Quebec, M6.3

On September 16, 1732, a strong earthquake shook eastern Canada. With its epicenter near Montreal, the earthquake damaged hundreds of houses in that city. According to contemporary accounts, the event cracked masonry walls and felled chimneys in Montreal. Although the earthquake's exact magnitude, depth, and other parameters are difficult to constrain using the available geological and paleoseismological data, contemporary observations of the event's intensity suggest that the earthquake was a magnitude 6.3 event.

Reflecting the uncertainty in the source parameters of the 1732 M6.3 event near Montreal, AIR estimates that this earthquake would cause insurable losses ranging from CAD 102.0 billion to CAD 370.3 billion if it were to occur today. Insured losses from this event occurring today are estimated to range from CAD 50.7 billion to CAD 188.0 billion.

1918 Vancouver Island, British Columbia, M6.9

This large seismic event occurred just after midnight on December 6, 1918. Although the exact epicentral location of this event is not known, this powerful earthquake caused strong ground shaking on Nootka Island, due west of Vancouver Island. The earthquake awakened people throughout the greater Vancouver region, and was felt as far south as Washington State, U.S., and as far east as central British Columbia. However, only limited damage to the Estevan Point lighthouse and the Ucluelet wharf, both located on Vancouver Island, was reported.

If the 1918 M6.9 Vancouver Island earthquake were to occur today, AIR estimates that this event would cause insurable losses of CAD 74.7 million, and insured losses of more than CAD 53.5 million.

1925 Charlevoix-Kamouraska, Quebec, M6.2

The significant March 1, 1925 Charlevoix-Kamouraska event was caused by slip within the Charlevoix-Kamouraska Seismic Zone, the most seismically active region in eastern Canada. The large magnitude and shallow depth (about 10 km) of the Charlevoix-Kamouraska event, along with the widespread use of unreinforced masonry for structures in the region, made this event notably damaging. The earthquake fractured chimneys and other unreinforced masonry structures in Quebec City and the nearby community of Shawinigan.

If the 1925 M6.2 Charlevoix-Kamouraska earthquake were to occur today, AIR estimates that this event would cause more than CAD 2.0 billion in insurable losses, and over CAD 935 million in insured losses.

1929 Laurentian Slope Offshore of Nova Scotia and Newfoundland, M7.2

On November 18, 1929, a powerful earthquake occurred about 250 kilometers south of Newfoundland, along the Grand Banks. Although this earthquake was felt on the continent as far as Montreal and New York City, relatively little damage was reported on land, and that was confined to cracked chimneys and small landslides on Cape Breton Island, Nova Scotia. The most significant effects of this event were a submarine slump that ruptured several trans-atlantic cables, and a giant tsunami that killed 28 people and destroyed many homes, ships, and businesses. The 1929 Laurentian Slope earthquake thus caused the largest documented loss of life associated with an earthquake in Canada.

If the 1929 Laurentian Slope M7.2 earthquake were to occur today, AIR estimates that this event would result in only very minor insurable losses and insured losses. Damages due to submarine slump were not accounted for in the estimated losses.

1933 Baffin Bay, Nunavut, M7.3

The strong 1933 Baffin Bay temblor did not cause any damage due to the remote offshore location of its epicenter. Ground shaking was reported in Upernavik, Greenland, but no records of ground shaking have emerged for Northern Canada from this event. This earthquake is notable for being the largest seismic event recorded instrumentally along the passive margin of North America, as well as the largest earthquake ever detected above the Arctic Circle.

AIR estimates that if the 1933 Baffin Bay M7.3 earthquake were to occur today, this event would cause insignificant insurable or insured losses.

1935 Témiscaming, Quebec, M6.2

On November 1, 1935, a significant earthquake struck Quebec approximately 10 kilometers east of the town of Témiscaming. Ground shaking was felt as far west as Thunder Bay, Ontario, and as far east as the Bay of Fundy. In Témiscaming, about 80% of all chimneys in the town were damaged and some brick walls were cracked. Near the epicenter, small rock falls were also observed. In addition, the earthquake triggered a 30-meter slide of railroad embankment near Parent, Quebec, about 300 kilometers northeast of Témiscaming.

AIR estimates that if the 1935 Témiscaming M6.2 earthquake were to occur today, this event would result in insurable losses of more than CAD 1.2 billion, and insured losses exceeding CAD 639 million.

1944 Between Massena, New York, and Cornwall, Ontario, M5.6

In spite of its moderate magnitude, this earthquake caused considerable damage to both Cornwall, Ontario, and Massena, New York State. Most of the damage took the form of fallen masonry, with the worst damage occurring in both communities where structures were underlain by the Leda clay. In both Cornwall and Massena, about 90% of the chimneys were damaged. The Collegiate and Vocational School in Cornwall was particularly heavily damaged, with its brick walls cracked and its gym roof broken by fallen masonry.

AIR estimates that if the 1944 Massena-Cornwall M5.6 earthquake were to occur today, it would cause insurable losses of more than CAD 1.2 billion, and insured losses of more than CAD 464 million.

1946 Vancouver Island, British Columbia, M7.3

With its epicenter on central Vancouver Island, this earthquake was the largest onshore seismic event observed in Canada. Although ground shaking was reported as far away as Portland, Oregon, and Prince Rupert, British Columbia, most of the damage was confined to Vancouver Island. Unreinforced masonry structures, especially chimneys, were damaged by the earthquake’s vibrations. In communities closest to the epicenter, such as Cumberland, Union Bay, and Courtenay, up to 75% of the chimneys were toppled.

If the 1946 Vancouver Island M7.3 earthquake were to occur today, AIR estimates that this event would result in more than CAD 4.1 billion in insurable loss, and insured losses of nearly CAD 2.6 billion.

1949 Offshore of Haida Gwaii/Queen Charlotte Islands, British Columbia M8.1

Widely felt across much of western North America, this magnitude 8.1 earthquake was the largest seismic event in Canada to be recorded by a seismograph. With its epicenter just offshore of Haida Gwaii (the Queen Charlotte Islands), ground shaking on those islands was so severe that cows were knocked off their feet. However, reported damage on Haida Gwaii and the mainland was confined to fallen chimneys and shattered windows.

If the 1949 offshore of Haida Gwaii/Queen Charlotte Islands M8.1 earthquake were to occur today, AIR estimates that this event would result in insurable losses of CAD 40.2 million, and insured losses of CAD 31.0 million.

1958 Lituya Bay, Alaska, M7.95

Due to the remoteness of its epicenter, this large earthquake that struck on July 9, 1958 caused only moderate damage to buildings and other structures. For example, submarine cables, oil lines, and bridges were damaged. However, five lives were lost due to ground shaking, slumping, and a rockslide-generated gravity wave that swept out of Lituya Bay.

If the 1958 Lituya Bay, Alaska M7.95 earthquake were to occur today, AIR estimates that the insurable or insured losses would be insignificant.

1985 North Nahanni River, Northwest Territories, M6.9

Between 1985 and 1988, an unusual burst of crustal seismicity gave rise to a series of three fairly large earthquakes (M6.6, M6.9, and M6.2) in the Nahanni Range of the Northwest Territories. The M6.9 1985 North Nahanni River earthquake was the largest event of this sequence; this earthquake was also distinguished by its relatively shallow focal depth of 6.5 kilometers. Due to the remote location of its epicenter– nearly 100 kilometers from the nearest communities – this earthquake did not cause significant damage. In fact, damage reports from this event stated that objects were shaken from cupboards and furniture was shifted, but no structural damage occurred.

If the 1985 North Nahanni River M6.9 earthquake were to occur today, AIR estimates that it would cause insiginificant insurable or insured losses.

1988 Saguenay region, Quebec, M5.9

On November 25, 1988, Quebec and much of eastern Canada was shaken by a magnitude 5.9 earthquake. The epicenter of the earthquake was located near Saguenay, Québec, about 75 kilometers north of the Charlevoix-Kamouraska

Seismic Zone. Although this event was felt over a 1000-kilometer radius around Saguenay, no structural damage was reported. Within the sparsely-populated epicentral region, ground shaking of intensities up to MMI VII was observed. However, damage near the epicenter was limited to cracked masonry walls and minor landslides.

If the 1988 Saguenay M5.9 earthquake were to occur today, AIR estimates that this event would cause insurable losses approaching CAD 100 million, and insured losses of CAD 47.7 million.

2001 Nisqually, Washington, M6.8

On February 28, 2001, a strong earthquake shook the Pacific Northwest. While the earthquake was felt across a wide region stretching from northern Oregon to southern British Columbia and eastward into Montana, its relatively deep focal depth (52 km) resulted in less ground shaking than would be expected for a M6.8 event. While serious building damage—largely collapsed walls from unreinforced masonry buildings, fallen chimneys, and damage to under-reinforced bridges—from the 2001 Nisqually earthquake was confined to the Seattle, Washington (U.S.) region, this event caused minor damage such as broken windows, pipes, water mains, and sewer pipes, in Victoria, British Columbia.

If the 2001 Nisqually, Washington M6.8 earthquake were to occur today, AIR estimates that the insurable or insured losses would be insignificant.

2002 Denali, Alaska, M7.9

In this very strong seismic event, three separate faults ruptured on November 2, 2002, resulting in a total rupture length of about 330 kilometers. This powerful earthquake caused significant damage to transportation systems in central Alaska and minor damage to the Trans-Alaska Pipeline. However, due to the strict engineering requirements imposed during construction of the pipeline in the 1970s, this vital component of Alaska's oil and gas industry escaped major damage. Multiple avalanches and rockslides in the Alaska Range were reported as well. Fortunately, the 2002 Denali earthquake caused comparatively little structural damage, and no deaths were reported, due to the geographical remoteness of its epicenter.

If the 2002 Denali, Alaska, M7.9 earthquake were to occur today, AIR estimates that this event would cause insignificant insurable or insured losses.

2010 Val-des-Bois, Quebec, M5.0

On June 23, 2010, Ontario and Quebec were shaken by a moderate M5.0 earthquake that occurred 55 km northeast of Ontario at a focal depth of 22 km, which was also felt as far south in the United States as Kentucky. While the earthquake produced the strongest ground shaking ever felt in Ottawa, damage in the epicentral region was largely confined to non-structural elements such as chimneys and cracked masonry. However, near the epicenter, a section of highway Route 307 was blocked by a landslide, and a bridge partially collapsed.

If the 2010 Val-des-Bois, Quebec, M5.0 earthquake were to occur today, AIR estimates that this event would cause insurable losses approaching CAD 12.9 million, and the insured losses would be insignificant.

2012 Haida Gwaii/Queen Charlotte Islands, British Columbia, M7.7

With its epicenter located just offshore of Graham Island (one of the largest of the Haida Gwaii/Queen Charlotte Islands) and a focal depth of 20.1 km, the magnitude 7.7 earthquake that struck on October 28, 2012, was widely felt across British Columbia. The West Coast and Alaska Tsunami Warning Center issued a tsunami warning for coastal regions of British Columbia in response to this event, which was shortly lifted.

If the 2012 Haida Gwaii/Queen Charlotte Islands M7.7 earthquake were to occur today, AIR estimates that this event would cause insurable losses of CAD 15.3 million, and insured losses of CAD 11.9 million.

3 Event Generation

The AIR Earthquake Model for Canada explicitly models the effects of ground shaking, liquefaction, landslide, fire damage, and tsunami inundation on insured properties in Canada. The model domain is shown in Figure 21. Although the model captures the effects of earthquakes that occur anywhere within the model domain, the model only reports losses inflicted within Canada.

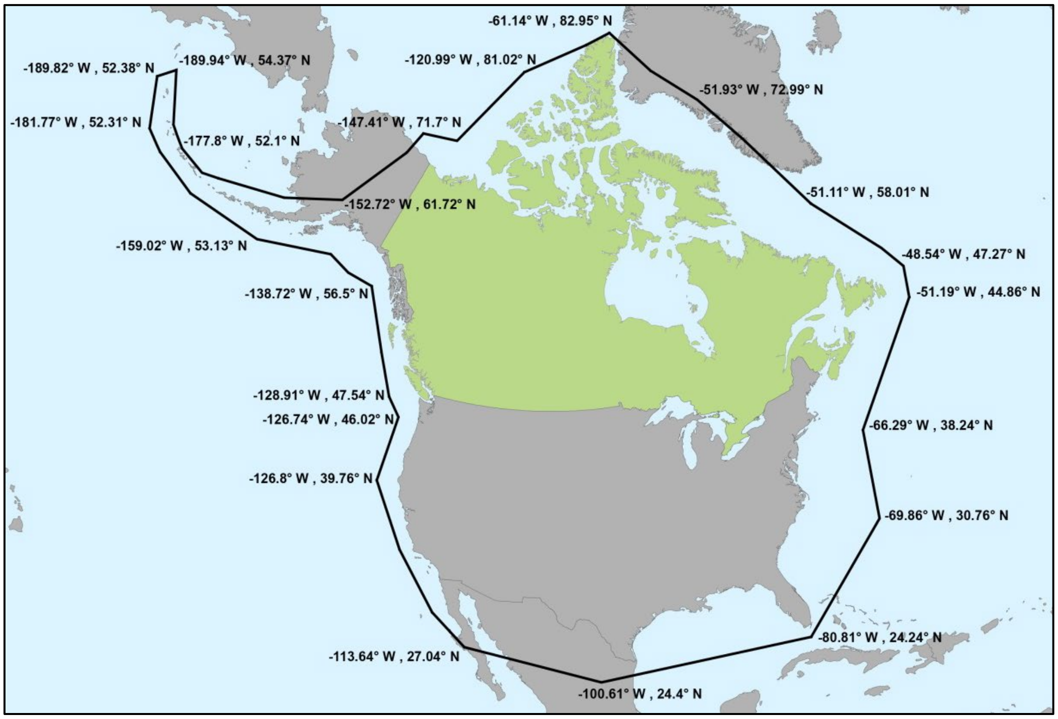

Figure 21. Model domain of the AIR Earthquake Model for Canada

To capture the complex nature of earthquakes in Canada, earthquake hazard is modeled using a combination of the characteristic earthquake approach and the distributed earthquake method. Large earthquakes, which can be associated with subduction zones or active crustal faults, are modeled as characteristic events (accounting for magnitude uncertainties). Smaller magnitude earthquakes produced by these subduction zones and by active faults are modeled as distributed earthquakes within each rupture area. Background seismicity is used to address earthquake hazard in Canadian regions that do not exhibit these geological features. This background seismicity model accounts for the small-to-moderate earthquakes that occur on as-yet-unknown (or unmapped) faults. In the AIR model, distributed earthquakes and background seismicity are modeled using the Gutenberg-Richter magnitude-rate relationship. Finally, while the seismicity of most regions of Canada is modeled using a time independent method, a time dependent method is employed to model earthquake occurrence in the Cascadia subduction zone. These techniques are used to generate a 10,000-year stochastic catalog of simulated earthquake events. Each event in the model's stochastic catalog is associated with an epicenter, magnitude, rupture length and width, azimuth, dip, dip azimuth, depth, and rupture mechanism.

Details on the data and methodology used to construct the model's stochastic catalog are provided below.

3.1 Data Sources

Historical Earthquake Data

The historical catalog (i.e., compilation of data on past earthquakes) used to construct the stochastic catalog was obtained from the Geological Survey of Canada (GSC) (J. Adams, personal communication, 2015). With both instrumentally-recorded events and historical records of pre-instrumentally-recorded events dating back to 1638, including earthquakes with magnitudes as low as 2.0, this historical earthquake catalog represents the most up-to-date understanding of the location and magnitude of past earthquakes occurring in and near Canada. All earthquake magnitudes in this catalog were converted to moment magnitudes by the GSC.

Additional historical events in the vicinity of Canada, including the northern portion of the 48 contiguous United States, as well as Alaska, were added in order to model seismicity in zones near the borders between the U.S. and Canada. The primary source of these additional historical data is the United States Geological Survey (USGS) National Earthquake Information Center. Specifically, the model uses information from the USGS Significant Earthquake Database (http://earthquake.usgs.gov/earthquakes/eqarchives/epic/) for historical events between 1900 and 1973, and the USGS Preliminary Determination of Epicenters (PDE) Database for historical events between 1973 and 2012.

Data on Active Crustal Faults

The historical catalog described above is supplemented with data on active faults in Alaska and the northwest contiguous United States, which pose seismic hazard to Canada. Most known active faults that can potentially affect Canada are located in the western coastal and offshore regions of Canada and the United States, including Southern Alaska. Several of these active faults are shown in Figure 22 below. Data on active faults, including slip rates and information about characteristic earthquakes, were collected from the United States Geological Survey (USGS) (Wesson et al. 2007) and the Division of Geological and Geophysical Surveys of Alaska (Koehler et al. 2012). Note that the rupture model for the Cascadia subduction zone follows the implementation of paleotsunami and geodetic results by the USGS (Petersen et al. 2015).

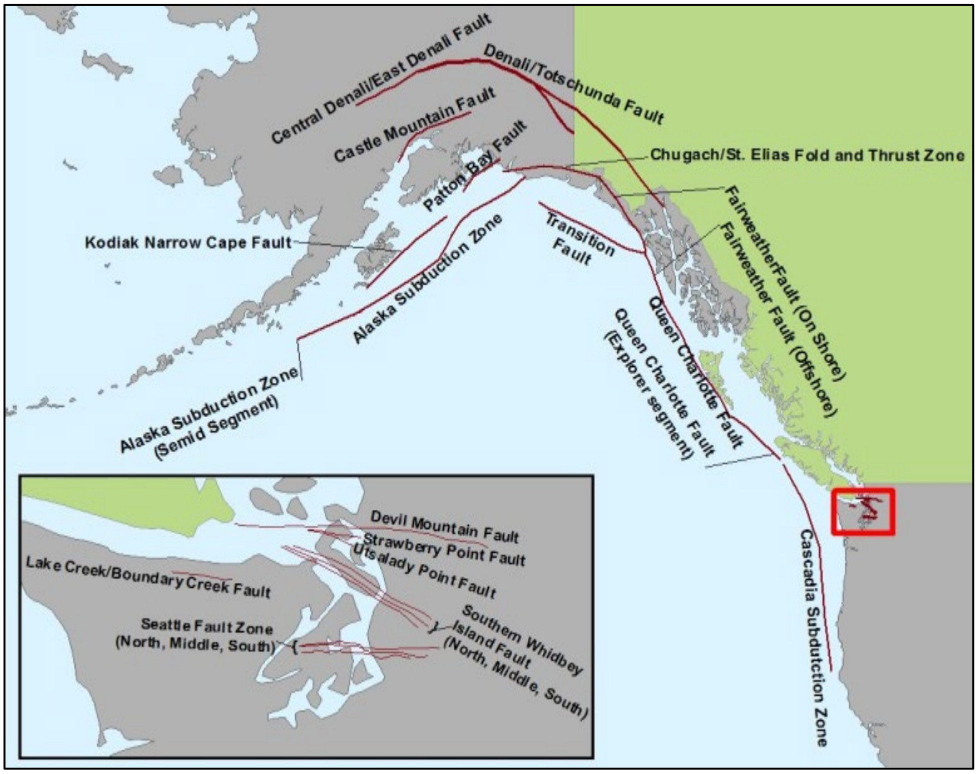

Figure 22. Major active faults in the western coastal and offshore region of Canada, Alaska, and the contiguous United States (inset map: faults in Washington State, U.S.)

Geodetic Data

Geodetic data consisting of over 1,000 GPS observations, 587 leveling observations, and 24 tidal gauge observations, as well as slip rates and slip vector azimuths, were obtained from the following sources:

- McCaffrey et al. (2013): GPS observations, slip rates and slip azimuths of the U.S. Pacific Northwest and Western Canada;
- Mazzotti et al. (2011, 2003): GPS observations of Canada and the U.S. Pacific Northwest;
- Elliott et al. (2010): GPS observations of the Southeastern Alaska region;
- Leonard et al. (2007, 2008): GPS observations of the East Alaska-NW Canada Region;

- Burgette et al. (2009): Uplift from leveling and tide gauge data, Cascadia region;
- Mazzotti et al. (2007): Uplift from tide gauge data;
- Dragert et al. (1994): Uplift from tide gauge data;
- Mitchell et al. (1994): Uplift from tide gauge data;
- Savage and Lisowski (1991): Uplift from tide gauge data; and
- Global CMT Catalog: Focal mechanism slip vector azimuths and slip rates from various studies.

These data were used to assess the deformation rate and state of non-transient crustal strain in western Canada. The results of this kinematic study were then incorporated into the development of the seismicity model (details about this process are provided in the section that follows).

3.2 Modeling Regional Seismicity

In the AIR model, regional seismicity is assessed source zone by source zone. The model domain is first divided into several seismic source zones based on historical seismic activity, the distribution of active faults, and deformation styles as revealed by geological, seismological, and GPS data. For each source zone, seismicity is then modeled using a combination of one or more data sets, including historical earthquake information, active fault data, plate tectonic information, and GPS-derived strain rates. For areas with active fault data and/or GPS information, the rate of seismic moment accumulation is also estimated based on kinematic modeling. The estimated rate of seismic moment accumulation is used to constrain the rate of seismicity in the source zones, especially for magnitude ranges for which historical data is not sufficient to derive the magnitude-frequency distribution for the region.

The characteristic earthquake approach is used for modeling large magnitude events in subduction zones and crustal faults, for which there is sufficient geological and seismological information to create a characteristic earthquake model. Smoothed background seismicity is used for small-to-moderate magnitude events associated with subduction zones and active crustal faults, as well as small-to-moderate magnitude events that occur on as-yet-unknown (or unmapped) faults.

To generate the stochastic catalog, earthquakes are simulated source zone by source zone, with earthquake occurrence determined by a stationary Poisson (time independent) process, and earthquake magnitude and frequency distribution determined by the Gutenberg-Richter law. The spatial distribution of stochastically simulated earthquakes within each source zone is modeled using several factors, including historical seismicity.

However, for the Cascadia subduction zone, a time-dependent process is used to model earthquake occurrence, reflecting the good availability of historical rupture data for this seismic source. The results of this time-dependent process are then integrated with the time-independent seismicity probabilities.

Each step of this process is described in more detail below.

Seismic Source Zones

The AIR Earthquake Model for Canada uses 82 seismic source zones, as shown in Figure 23.

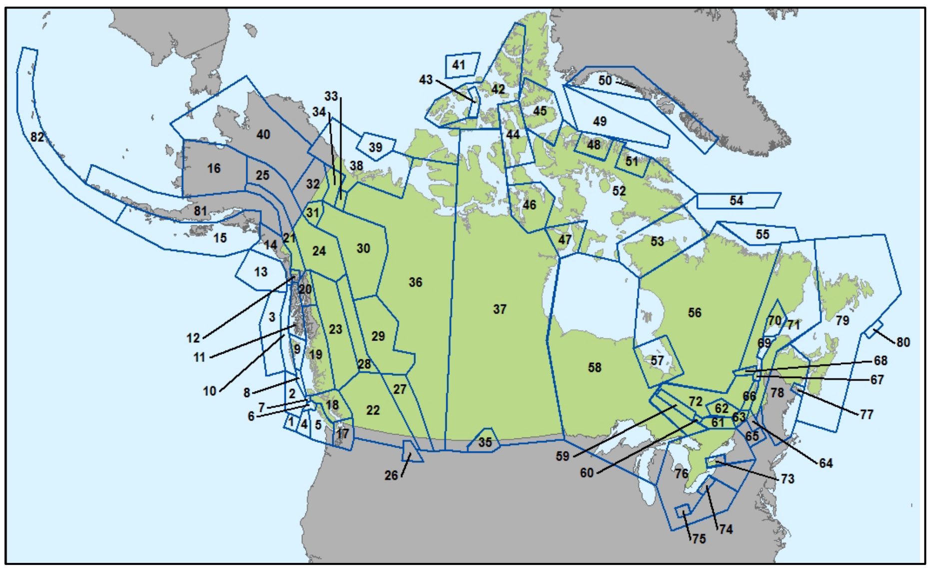

Figure 23. The distribution of seismic source zones used in the AIR model

The seismic source zones used in the AIR model follow those proposed by the Geological Survey of Canada (GSC) in Adams and Halchuk (2003). To create a country-wide seismic hazard map in 2005, the GSC used two seismic source models, H and R, to assess regional seismicity. The H model reflects the distribution of earthquake clusters, while the R model reflects large-scale seismotectonic structures.

In 2015, the GSC updated this seismic source zone model, slightly modifying the H and R models. The R model is designed mainly to account for the fact that large magnitude earthquakes in eastern Canada may occur outside of the earthquake clusters that define the H model source zones. This is because these earthquake clusters may be a continued local response to past large magnitude earthquakes.

However, the next large magnitude earthquake may not necessarily happen at, or very near, the location of past large earthquakes. Therefore, the AIR Earthquake Model for Canada uses the R model, as well as the H model, to determine the distribution of large magnitude earthquakes in eastern Canada as needed. For example, in the St. Lawrence Valley – the most seismically active portion of eastern Canada – a combination of the H and R models is used to capture seismicity, as shown in Figure 24.

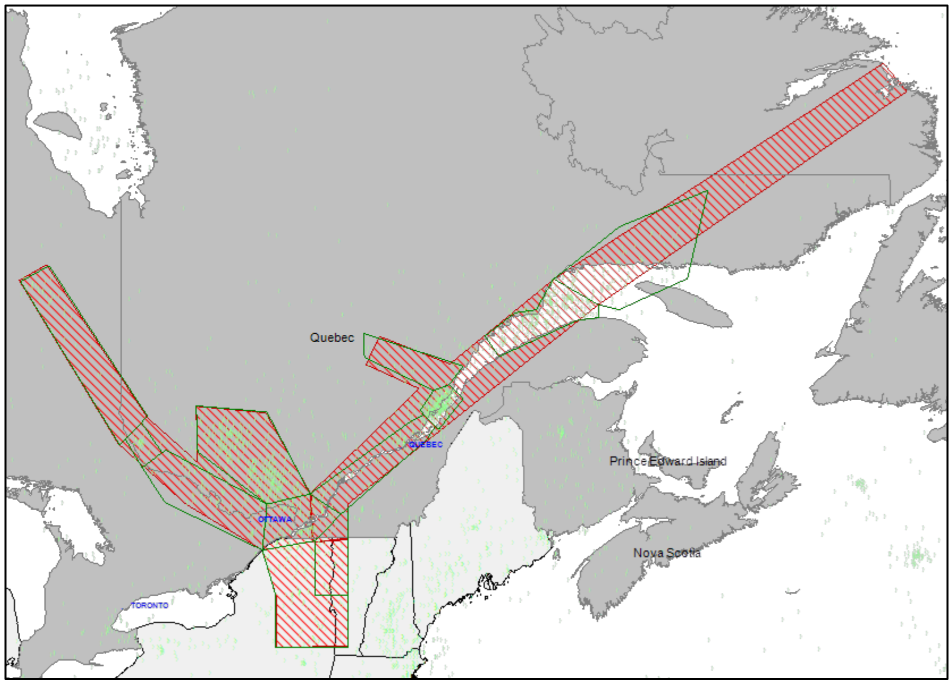

Figure 24. Modified R-model source zones (red) and H-model source zones (green) used to model the distribution of large magnitude earthquakes in the St. Lawrence Valley. The light green circles show historical seismicity in the region.

Completeness Time

Seismicity parameters a- and b- cannot be estimated for seismic source zones unless the historical seismicity catalog for that zone can be considered complete, given a certain magnitude threshold. Hence, the AIR model determines the completeness time interval of the historical catalog for each source zone, as described below.

To determine the completeness time interval of the historical catalog for each seismic source zone, many local factors must be considered, including the history of seismic monitoring stations, and the timing and magnitude distributions of past earthquakes. Thus, different completeness time intervals are expected for different regions of a country. For example, completeness times for Southeastern

Canada are shown in Table 6 (obtained via private communication from the GSC). For other zones, completeness times used in the GSC (2003) seismic hazard map were adopted.

Table 6. Completeness times used for zones in Southeastern Canada in the AIR model

Magnitude	Completeness Time
2.35	1975
2.75	1963
3.25	1938
3.75	1928
4.75	1900
5.95	1850

Active Crustal Faults

In western Canada, both crustal faults and subduction zones are drivers of seismic hazard, giving this region a unique seismic setting in comparison to the rest of the country (see Figure 22 for the location of these faults). Table 7 lists the major active crustal faults used in the AIR Earthquake Model for Canada.

Table 7. Active faults used in the AIR model

Fault Name	Fault Name
Alaska Subduction zone - Semid segment	Seattle fault zone - middle branch
Alaska Subduction zone – Kodiak PW	Seattle fault zone - northern branch
Cascadia Subduction Fault	Seattle fault zone - southern branch
Central Denali - East Denali Fault	Southern Whidbey Island fault - central
Central Denali - East Denali Fault, main branch	Southern Whidbey Island fault - north
Central Denali - Totschunda Fault, main branch	Southern Whidbey Island fault - south
Denali - Totschunda Fault, minor branch	Strawberry Point Fault
Chugach St. Elias fold and Thrust belt	Utsalady Point Fault
Queen Charlotte Fault	Lake Creek-Boundary Creek fault
Fairweather Fault - offshore	Transition Fault
Fairweather Fault - on shore	Kodiak Narrow Cape Fault
Patton Bay Fault	Devil Mountain Fault
Castle Mountain	Cascadia Subduction zone

The seismicity of these faults was constructed based on the estimated magnitudes and recurrence intervals of their characteristic earthquakes. Note that, generally, the annual rate of occurrence of a characteristic event on a fault can be estimated either from paleoseismological data or from the fault slip rate. If paleoseismological data are unavailable, the recurrence rate of characteristic events can be estimated based on the relationship between the total seismic moment accumulation rate of the fault and the seismic moment of the characteristic earthquake. (See Section 2.1 for a discussion of seismic moment.) The total seismic moment accumulation rate of the fault is a simple function of fault slip rate and fault slip area. Because these characteristic earthquake magnitudes have inherent uncertainties, AIR seismologists have applied a Gaussian distribution around the characteristic magnitude for each fault that employs a characteristic earthquake model, to account for the uncertainty in the estimated characteristic magnitude while the moment rate is kept balanced.

The magnitude and recurrent rate model for the Cascadia subduction zone is based on the USGS 2014 national seismic hazard model. The rupture model for the Cascadia Subduction Zone is constrained by about 5,000 years of paleoseismic evidence of coastal subsidence and tsunami (e.g. Kelsey et al 2002; 2005; Nelson et al 2006), a 10,000 year record of turbidites in ocean sediment cores (Goldfinger et al 2012), inland tsunami deposits in southwestern Oregon, and evidence of deep non-volcanic tremors.

Evidence of prehistorical earthquakes suggests that not only does the full Cascadia Subduction Zone rupture with a Mw 8.6-9.3 recurring about every 500 years, as in the 1700 Mw 9.0 megathrust earthquake, the subduction zone also has a history of partial ruptures. Some partial rupture models for rupture of the southern portion of the subduction zone include magnitudes Mw 8.1 – 9.1 and relatively longer return periods than full ruptures – on the order of 1,000 – 2,5000 years.

The Cascadia Subduction Zone is modeled with a logic tree approach including branches for magnitude, different down-dip geometries, and rupture areas and recurrence periods. The down-dip edge (or deepest possible bottom rupture edge of the subducting slab) can have a substantial impact on distance to surface and hazard for certain inland areas. The location of the down-dip edge is constrained by geodetic models of subduction coupling (i.e. where the plate is locked and builds stress) (McCaffrey et al., 2012 and Schmidt et al., 2012), thermal models of the elastic and transitional zones in earth’s crust, and the top of the region of observed non-volcanic tremor – or slow slipping earthquakes. The AIR model adopts the complex geometries for the Cascadia Subduction Zone by implementing different scenarios developed by the USGS. Although events are represented in the stochastic catalog as a single set of parameters, they are modeled with 3D gridded geometries in depth and slip surface for the calculation of ground motion and tsunamigenic potential, respectively.

Geodetic Data and Kinematic Modeling

The crustal areas of western Canada and the northwestern U.S. are experiencing strain due to the interaction between the Pacific and North American plates within the Cascadia subduction zone. However, a large component of this crustal strain is transient, reflecting the strain that will be relieved when the Cascadia subduction zone ruptures in a large characteristic earthquake. In the AIR model, GPS data are used to estimate locking along the Cascadia subduction zone, as well as crustal deformation rates in western Canada.

To understand the rate of seismic energy accumulation along major active faults and within the crustal areas of western Canada, AIR compiled over 1,000 GPS, leveling, and tide gauge data (see Figure 25). The geodetic data were used to develop kinematic models to estimate the rate of slip accumulation along the Cascadia subduction zone and moment rates in the seismic source zones along the western coast of British Columbia. Specifically, the transient component representing the locking state of the Cascadia subduction zone was calculated and removed from the total moment rate determined from geodetic data and kinematic modeling results. The remaining residual strains were translated into crustal seismic moment rates and were used, along with other information, to constrain the frequency of large earthquakes. The results of this kinematic model also provide the distribution of the seismic slip accumulation rate along the Cascadia subduction zone. This information was used to formulate the slip distribution for Cascadia interface earthquakes, which is needed for the tsunami simulation component of the AIR model.

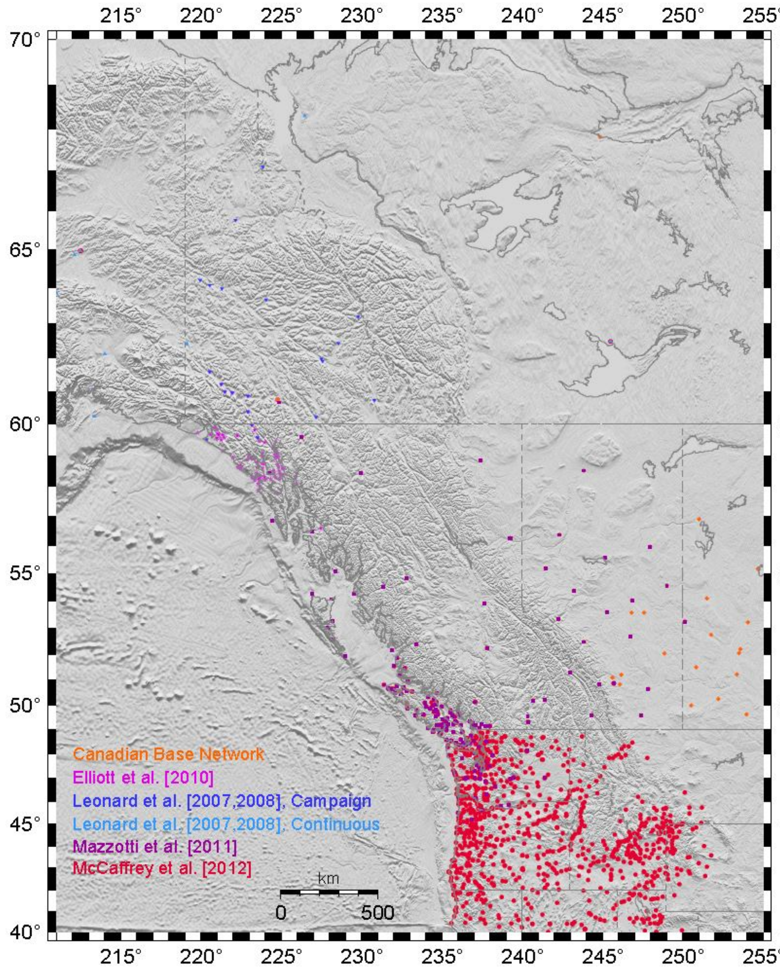

Figure 25. Geodetic data compiled and used in the AIR model

Time Dependency and the Model's Stochastic Catalogs

Except for the Cascadia subduction zone, the AIR Earthquake Model for Canada is a *time independent* model. That is, the probability of earthquake occurrence at any location or along any segment of a fault follows a Poissonian model, and is thus independent of past earthquake occurrences. The long rupture history for the Cascadia subduction zone that has been established from paleoseismological studies makes it possible to develop a time dependent seismicity model for this plate boundary.

However, it is important to note that the AIR Earthquake Model for Canada includes *two* stochastic catalogs: a time-independent (TID) catalog and a time-dependent (TD) catalog (with the TD catalog considered as the "standard" in the model). The TD catalog is constructed by calculating time dependent rupture probabilities for the Cascadia subduction zone, translating them into equivalent long term Poissonian time independent rates, and then integrating these resultant values with other time independent seismicity probabilities. Further details about the TID and TD approaches and this integration process are provided below.

The general concept of the time dependent model follows the methodology presented in *USGS Open-File Report 99-517*. However, AIR seismologists have reformulated this methodology to include various types of model and parametric uncertainty into the time dependent analysis. Time-dependent rupture probability can be meaningfully estimated only for characteristic earthquakes on faults with a long history of past earthquakes, usually obtained from catalogs of historical seismicity and paleoseismic data.

Historically, the estimation of the probability of earthquake occurrence has been based on Poissonian models in which the rate of occurrence for a given seismic source is assumed to be constant over time. This is a "memoryless" (time-independent) model; that is, the probability of occurrence does not depend on when the last similar earthquake occurred.

However, the likelihood of a major earthquake on a fault depends on many things, including the distribution of stresses in the fault region, the structure of the fault itself, and the frictional forces that act to resist rupture. To predict the occurrence of characteristic earthquakes on faults, these physical processes need to be understood. While the knowledge and understanding of fault rupture phenomena for purposes of prediction is still limited, there has been progress in formulating the probability of occurrence beyond the purely Poissonian (TID) model.

While the results of many studies show that Poissonian (TID) models are adequate for estimating the probability of occurrence of earthquakes over a large region, data suggest that, for individual faults, the occurrences of large earthquakes are, in fact, time dependent (TD). Earthquakes occur as the result of the slow accumulation of strain within the earth. Different time-dependent models for the occurrences of earthquakes on faults have been developed based on this concept and are being used for earthquake hazard analysis today. The most notable TD model in practice is the renewal model.

The renewal model assumes that the probability of occurrence of a characteristic earthquake on a fault increases with the time elapsed since the occurrence of the previous such earthquake. The conditional probability of occurrence is generated from probability distribution functions that are developed based on statistical information regarding the recurrence of regional earthquakes, as well as information on a specific fault, such as the mean recurrence interval and the elapsed time since the last occurrence. Different probability distributions have been used for such analyses, most commonly the lognormal and the Brownian Passage Time (BPT) (Matthews, 2002) distributions.

AIR's time dependent fault rupture model for the Cascadia subduction zone follows the Uniform California Earthquake Rupture Forecast Version 3 (UCERF3) fault-specific time dependent model for active faults in California. The UCERF3 uses the Brownian Passage Time (BPT) renewal model to estimate the time-dependent probabilities for characteristic earthquakes on faults. Following the recommendation of the USGS rupture model for the Cascadia subduciton zone, the time-depedent probability of each type of characteristic earthquakes in the subduction zone is calculated with the last rupture time set at 1700.

Generating the Stochastic Catalog (Time-Independent Method)

The AIR Earthquake Model for Canada simulates earthquakes by source zone. For each source zone, the minimum set of parameters that must be determined include the upper bound earthquake magnitude, the occurrence rates of earthquakes above the minimum magnitude (M≥5.0), and the a-value and the b-value of the Gutenberg-Richter magnitude-frequency empirical relationship (the GR relationship). The method used to estimate each parameter is dependent on the available data in the zone. For zones where the historical earthquake catalog is the only data type available, AIR uses the historical earthquake data to estimate the a- and b- values of the GR relationship. The upper bound magnitude used in the GSC hazard model (Adams and Halchuk, 2003) is generally adopted for the GR relationship for these zones.

For zones that have active fault data and/or moment rates estimated from geodetic and fault data in western Canada, AIR uses a combined approach of the characteristic earthquake model and a smoothed seismicity model to simulate earthquakes. The seismic moment accumulation rate in the zone is first determined from geological, seismological, and geodetic data using a complex regional kinematic model. The total seismic moment rate in the zone is partitioned between earthquakes simulated using a characteristic earthquake model for faults, and earthquakes simulated using the smoothed seismicity approach. This partition is accomplished through seismic moment budget balancing. Because the rate of moderate-to-small magnitude events is relatively high, their occurrence can be reasonably constrained by the historical earthquake data and modeled by the Gutenberg-Richter (GR) magnitude rate distribution. The rate of large magnitude earthquakes is constrained by both the historical seismicity data and the moment accumulation rate through the balancing of the total moment rate in the zone.

This process was employed somewhat differently by AIR for Eastern, Central, and Western Canada. Region-specific details of the stochastic catalog generation process are provided below.

Central and Eastern Canada

Much of central and eastern Canada is located in a stable continental environment; thus, the seismicity rate in this part of Canada is low to moderate. There are no known active faults for which a characteristic model can be used to model the seismicity.

Therefore, for central and eastern Canada, AIR employs a traditional hazard modeling approach that uses historical earthquake data to determine the empirical GR relationship for each seismic source zone and estimate the rate of earthquakes of different magnitudes. AIR also adopted both the H- and R- seismic source zone delineation schemes used by the GSC in its 2005 hazard report (as stated in the preceding subsection). The H zones are primarily delineated based on earthquake clusters, whereas the R zones are drawn based on both regional seismicity and regional geological or tectonic information. AIR modified the R zones defined by the GSC by merging smaller R zones in similar tectonic settings into larger zones, because the R zones were used by AIR in a different way than they were used by GSC. Specifically, instead of using a logic tree approach to integrate the two seismicity models based on the H and R zones, AIR uses the simplified R zones to redistribute larger magnitude events simulated in the H zones that are enclosed by the R zone. This approach was used for the following two reasons.

First, earthquake clustering is characteristic of seismic activity in a stable continental environment. Indeed, clustered earthquake activity can span decades in many stable continental regions in the world. Therefore, H zones may better characterize seismic risk in these stable regions. In contrast, the R zone model may overestimate the seismic rate in areas outside the H zones to a degree that would significantly contradict historical data (e.g. overestimating the rate of magnitude 5.0 - 6.0 earthquakes that can cause significant damage).

Second, many seismologists have suggested that clustered seismic activity in stable continental regions is a response to larger historical earthquake ruptures (e.g. Adams 2011), and many of these clustered earthquakes are in fact aftershocks of large historical events. These larger events are not necessarily correlated with or controlled by previous large earthquakes, i.e. they are independent events. In such cases, the H model may not fully capture regional seismic risk. The R zones, on the other hand, encompass a region of similar tectonic or geological setting, and large events similar to one another may thus occur in these zones. In addition, the H zones found within a single R zone would be expected to resemble each other in seismicity. Redistribution of larger earthquakes simulated in the H zones to the larger R zone around them allows the model to accommodate the intended purposes of both the H and R models. This redistribution technique also addresses the concern that the R zone model may overestimate the risk of small to moderate earthquakes outside of the H zones.

The parts of central and eastern Canada that fall outside of both the H and R zones are highly stable and thus exhibit a very low seismicity rate. A minimum occurrence rate and a regional b-value were set by AIR for these areas, following an approach similar to that used by the GSC for their F model (see Adams and Halchuk, 2003). In setting the minimum rate, the GSC used a global rate derived from selected continental shields (Fenton et al., 2006), along with rates estimated using data from the Canadian shield and the broader North American shield. The global rate determined from the selected continental shields is much higher than the rate in the Canadian shield and the North America shield. It is, however, debatable whether the rate estimated from other continental shields – which may lie in a very different tectonic environment (e.g. Atkinson and Martens, 2007) – can be applied to Canada. For this reason, and the fact that the hazard models developed by the GSC and by Fenton et al. (2006) were meant to be conservative as they were designed to inform building codes and the design of critical facilities, AIR uses data from the Canadian shield to estimate the rate of seismicity in highly stable portions of eastern and central Canada. The definition of the Canadian shield boundary is similar to the North American shield boundary defined by Fenton et al. (2006); however, in the AIR model, the Canadian shield extends south only to 45° North latitude.

Western Canada

For seismic source zones in western Canada (shown in Figure 26), regional seismicity is assessed by integrating the results of the kinematic model, the characteristic earthquake model, and the GR model.

The kinematic model developed by AIR for western Canada uses GPS and other geodetic data, fault slip rates, and plate motion velocities to calculate a continuous strain and moment rate field for the entire region. AIR uses a regional fault block model and a continuous kinematic model to remove the transient strain rate due to the locking of fault slip along the Cascadia subduction zone. The strain rate and moment rate thus estimated represent the long-term rate of seismic energy accumulation within the crust.

After the total seismic moment has been determined for a source zone, the a- and b- values of the GR relationship for that zone are then estimated from the historical catalog. Next, the upper bound magnitude of the GR relationship is initially set to the value recommended by Adams and Halchuk (2003). Finally, this upper bound magnitude is adjusted so that, within each seismic zone, the moment from the integration of the truncated GR distribution and the moment from characteristic earthquakes along active faults equals the total seismic moment estimated for the zone.

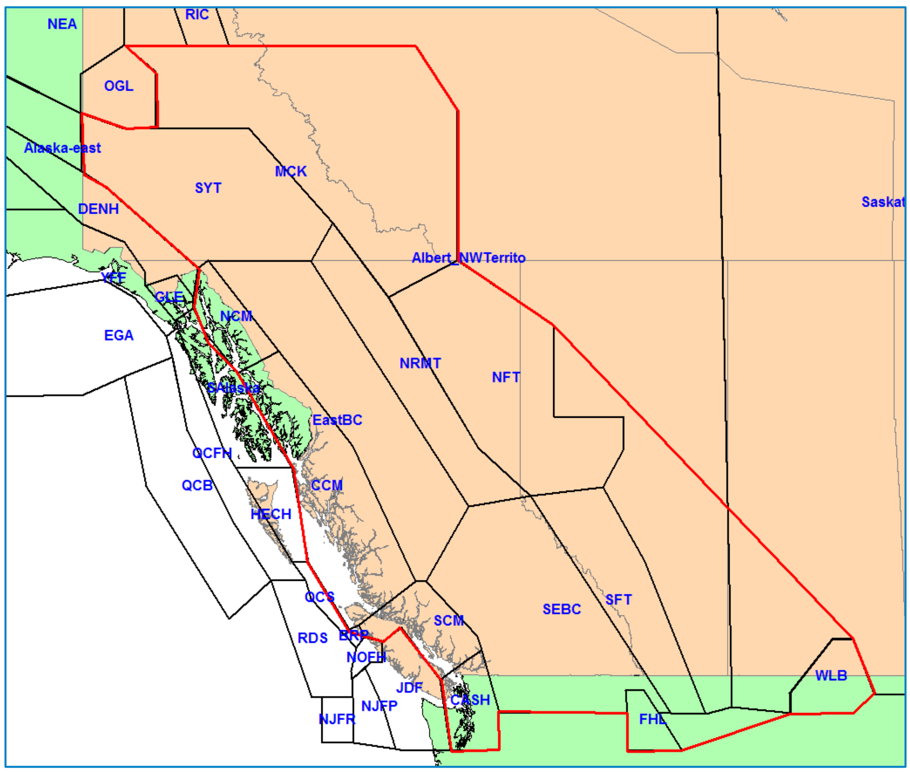

Figure 26. Seismic source zones in western Canada

Comparing the GR distribution obtained using moment rate constraints to that obtained without moment rate constraints (the blue data points and the black data points in Figure 27, respectively) reveals that, when moment rate constraints are used, the upper bound magnitude of the GR distribution is larger. This result agrees well with published studies demonstrating that the moment from kinematic models is larger than that calculated from historical earthquakes in the region (e.g. Mazzotti et al. 2005, 2011). This magnitude difference is most pronounced for events with an exceedance probability of ≤ 0.04% (corresponding to events of ≥M7.5). Although it is still unclear whether crustal regions near the major active faults that threaten Western Canada could produce such large earthquakes, the historical data do not allow this possibility to be ruled out.

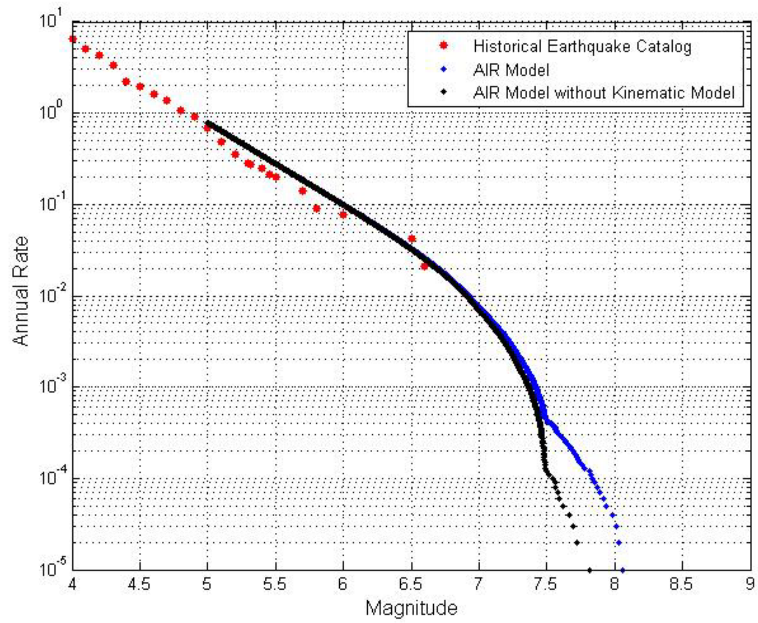

Figure 27. Magnitude-rate distribution for seismic source zones in Western Canada (within the red polygon in the previous figure), with (light blue) and without (black) moment constraints from the kinematic model

In two seismic source zones (Zones 17 and 18) of the Georgia Strait-Puget Sound region, deep events are modeled separately because historical deep events have caused considerable damage here in the past. Figure 28 shows the magnitude distribution used for modeling deep events (with depth > 30km) in Zone 17 of the AIR model.

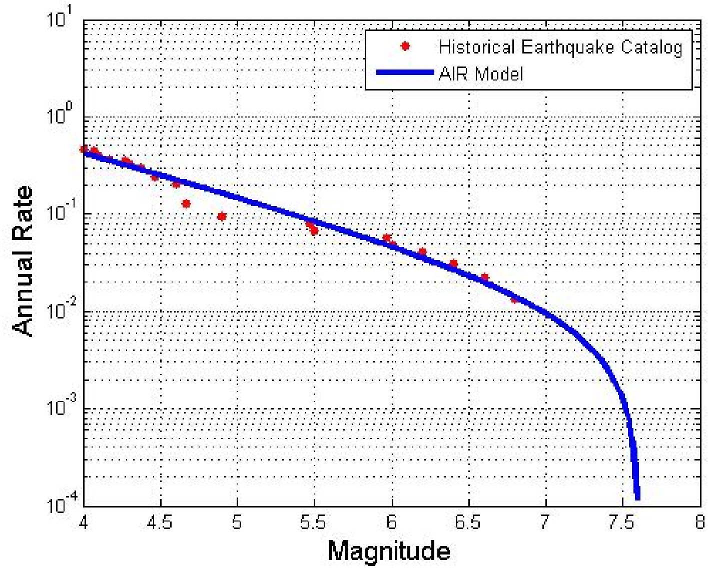

Figure 28. Historical and modeled magnitude-rate distributions for deep earthquakes in Zone 17

3.3 Modeled Earthquake Variables

Epicenter

The epicenter of an earthquake is the location on the earth's surface directly above the point of initial rupture. For modern earthquakes, epicenters can be determined by gathering information from a network of local, regional, or global seismometers. For pre-instrumental earthquakes, the determination of earthquake-epicenter locations is greatly facilitated when the faults are visible on the surface. In the case of blind faults, epicenter locations must be inferred from the seismic activity of the area, macroseismic intensity surveys, or by subsurface-sounding techniques. Many faults remain undiscovered, however.

Magnitude

Magnitude, a measure of the energy released during an earthquake, provides a useful way to compare seismic events. As described in Section 2.1, a variety of magnitude scales have been used to describe earthquakes. The AIR Earthquake Model for Canada uses the moment-magnitude scale (M_w), which is considered to be superior to other magnitude scales because it is based on the physical properties of the earthquake source and is more accurate for large earthquakes. Moment magnitude is applicable over a wider range of rupture sizes than the Richter magnitude scale.

The reported magnitudes of historic earthquakes typically are rouned to one decimal point. This rounding reflects the limited precision in the reported magnitudes and magnitude uncertainty. The AIR earthquake models generally use three decimal points for stochastically simulated events. Three digits were used mainly for the convenience of simulation and insurance of smoothness in the magnitude frequency distribution. In the updated model, we use two decimal points for magnitude measures of the stochastic events to be closer to the reported magnitude measures. This change does not impact the model results significantly.

Focal Depth

The focal depth is the vertical distance between the point where the fault rupture originates and the earth's surface (Figure 29). Most earthquakes that take place outside of subduction zones occur within the top 20 km of the crust. Earthquakes that occur deeper than 30 km are usually associated with subduction zones. However, the focal depth of earthquakes in subduction zones can range from a few kilometers to 700 km. Focal depth is an important parameter because seismic waves are attenuated as they travel through the earth, away from their source, and deeper earthquakes of a given magnitude typically cause less damage than those at shallower depths. Therefore crustal events, in general, may cause more damage than deeper events not only because they often occur within land areas but also because they are shallower and thus closer to the earth’s surface.

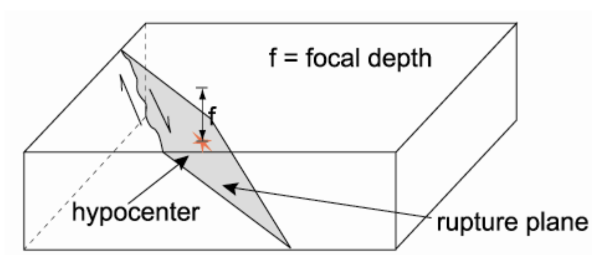

Figure 29. Focal Depth

Focal depth is modeled both by a statistical approach based on historical earthquakes and by a physical approach using tectonic characteristics, as discussed earlier in the section on gridded seismicity.

Rupture Length

Rupture length is the span of the fault that ruptures during an earthquake. In the AIR Earthquake Model for Canada, rupture length is modeled as a function of the magnitude of the event, with the relationships between rupture length and magnitude determined through empirical regression analysis. The rupture lengths of different types of earthquakes are determined using different magnitude-rupture length relationships appropriate for a particular type of earthquake.

Rupture Azimuth and Dip Angle

The rupture azimuth and dip angle are parameters that define the orientation of a fault. The rupture azimuth is the angle between true north and the line of intersection between the rupture plane and the surface of the earth, measured clockwise from north as viewed from above. In the AIR model, the rupture plane is aligned with the principal faulting orientations for the region. For simulated earthquakes based on the characteristic earthquake model, azimuths are aligned with fault orientations based on historical geological fault maps and recent earthquake fault plane azimuths.

The dip azimuth is the angle between true north and the direction in which the rupture plane dips. By convention, the dip azimuth is 90 degrees clockwise from the rupture azimuth. The dip angle is the angle between the horizontal and rupture plane. In the model, dip angles are estimated based on seismotectonic data, the rupture parameters of historical earthquakes, and published research. Since energy is distributed across the rupture plane, a fault's spatial orientation is important for estimating damage.

Fault Rupture Mechanism

See Section 2.1 for a description of the rupture mechanisms of faults. In this model, the fault rupture mechanisms for earthquakes are based on historical and seismic-survey data.

3.4 Stochastic Catalog Summary Statistics

The AIR Earthquake Model for Canada incorporates a "standard" time-dependent 10,000-year stochastic catalog, as well as a time-independent 10,000-year stochastic catalog. The standard time-dependent 10,000-year stochastic catalog contains 22,880 simulated events, of which 8,112 cause loss to the industry exposure in Canada. Stochastic events included in the model are of magnitude 5.0 and greater.

3.5 World Scenarios Event Set

As a supplement to the AIR Earthquake Model for the United States, AIR is releasing extreme disaster scenarios (EDS) and realistic disaster scenarios (RDS). EDS and RDS events are meant to provide clients with additional touch points to assist in assessing large loss potential. While they represent low probability—and in some cases very low probability—scenarios, they are nevertheless scientifically plausible.

The included EDS events are probabilistic scenarios; note, however, that these EDS events are not included in the model's time-dependent (standard) 10,000-year stochastic catalog. Rather, the EDS events in the AIR Earthquake Model are included in the World Scenarios event set in Touchstone and CATRADER. Brief descriptions of the EDS and RDS events that would cause significant loss in Canada are provided below. Modeled losses for these events can be found in Sections 8 and 9.

Realistic Disaster Scenarios

RDS ERRO British Columbia Earthquake (100-year)

The 100-year return period event is a M6.5 reverse faulting rupture in the crust with a focal depth of 12 km. It is on an unknown fault at the southern point of Vancouver Island at Metchosin, on the Strait of Juan de Fuca, south of Victoria. Damages in British Columbia are largely attributed to ground shaking, with minor contribution to damage from fire following earthquake.

RDS ERRO British Columbia Earthquake (250-year)

The 250-year return period event is a M6.5 deep earthquake beneath the border with Birch Bay, Washington. The focal depth is 67 km. Damages in British Columbia are largely attributed to ground shaking and liquefaction, along with some minor contribution to damage from fire following earthquake.

RDS ERRO British Columbia Earthquake (500-year)

The 500-year return period event is a M6.8 deep earthquake beneath the Strait of Juan de Fuca. Ground shaking impacts range from Vancouver Island to Washington State. The focal depth of the event is 61 km. Damages in British Columbia are largely attributed to ground shaking and liquefaction, along with some minor contribution to damage from fire following earthquake.

RDS ERRO Quebec Earthquake (100-year)

The 100-year return period event is a M6.3 reverse faulting crustal earthquake with a focal depth of 20 km. The rupture occurs on an unknown fault in the Charlevoix seismic zone in the Saint Laurence River Valley.

RDS ERRO Quebec Earthquake (250-year)

The 250-year return period event is a M6.7 reverse faulting crustal earthquake with a focal depth of 18 km. The rupture occurs on an unknown fault north of Montreal.

RDS ERRO Quebec Earthquake (500-year)

The 500-year return period event is a M6.2 reverse faulting crustal earthquake with a focal depth of 11 km. The rupture occurs on an unknown fault near Montreal, where most exposure at risk is located.

Extreme Disaster Scenarios

With this model release, AIR is introducing several EDS events for the AIR Earthquake Model for Canada, with events located in eastern Canada, western Canada, and the United States. EDS events are meant to provide clients with additional touch points to assist in assessing large loss potential. While they represent unlikely—and in some cases extremely unlikely—scenarios, they are nevertheless scientifically plausible.

Note that while some of these EDS events are fully probabilistic scenarios that are included in the model's time-dependent (standard) 10,000-year stochastic catalog, others were created using a deterministic process and therefore have not been assigned a probability of occurrence or return period. Deterministic methods were used to generate events that are scientifically plausible, yet unlikely to be captured via standard stochastic modeling techniques due to the relative scarcity of historical data or a lack of a full scientific consensus as to their likelihood.

The EDS events in the AIR Earthquake Model for Canada are included in the World Scenarios event set in Touchstone® and CATRADER®.

Brief descriptions of the EDS events are provided below.

IBC Eastern Scenario

With its epicenter beneath the St. Lawrence River about 100 km northeast of Quebec City, and a shallow focal depth of just 10 km, this M7.1 earthquake is powerful enough to be felt throughout much of Quebec, New Brunswick, Nova Scotia, and parts of the United States. Although this event results from slip within a seismic zone that is located beneath the St. Lawrence River, no tsunami is triggered by this earthquake.

This event was generated by AIR using a fully probabilistic technique, and represents a 0.2% exceedance probability (500-year return period). This event is available in the model's standard time-dependent 10,000-year stochastic catalog.

EDS Quebec City Earthquake

This M7.4 earthquake occurs at a shallow depth (16 km), with its epicenter located 50 kilometers north of Quebec City (where most of the exposure at risk in the region is located). Due to its high magnitude and relatively shallow focal depth, the event is felt over much of Quebec, New Brunswick, Nova Scotia, and parts of the United States.

This event was generated by AIR using a fully probabilistic technique. This EDS event is *not* available in the model's standard (time-dependent) 10,000-year stochastic catalog.

EDS Ottawa Earthquake

With a magnitude of 6.6 and a focal depth of 19 km, this moderately powerful earthquake epicentered 25 kilometers west of Ottawa causes ground shaking that can be felt over much of Ontario, southern Quebec, and New York State and other parts of the U.S. However, the majority of exposure at risk from this event is located in the metropolitan Ottawa region.

This event was generated by AIR using a fully probabilistic technique. This EDS event is *not* available in the model's standard (time-dependent) 10,000-year stochastic catalog.

EDS Toronto Earthquake

The moderately powerful (M6.6) Toronto scenario is comprised of an earthquake that strikes about 6 km to the west of Lake Ontario and 8 km south of Toronto, with a shallow focal depth of just 8 km. Ground shaking is felt across Ontario, southern Quebec, and parts of the northern U.S. (including New York State). The highest concentration of exposures at risk from this event is located in the metropolitan Toronto region.

This event was generated by AIR using a fully probabilistic technique. This EDS event is *not* available in the model's standard (time-dependent) 10,000-year stochastic catalog.

EDS Montreal Earthquake

With a magnitude of 6.8 and a focal depth of 19km, this moderately powerful earthquake causes ground shaking in most of Ontario, southern Quebec, New York State (U.S.), and other parts of the United States. The epicenter of this earthquake is located 8 km west of Montreal, between the Ottawa River and the Saint Lawrence River. Most exposures at risk are located in the Greater Montreal metropolitan area.

This event was generated by AIR using a fully probabilistic technique, and is available in the standard time-dependent 10,000-year stochastic catalog.

The location of these five EDS events of eastern Canada is shown in Figure 30.

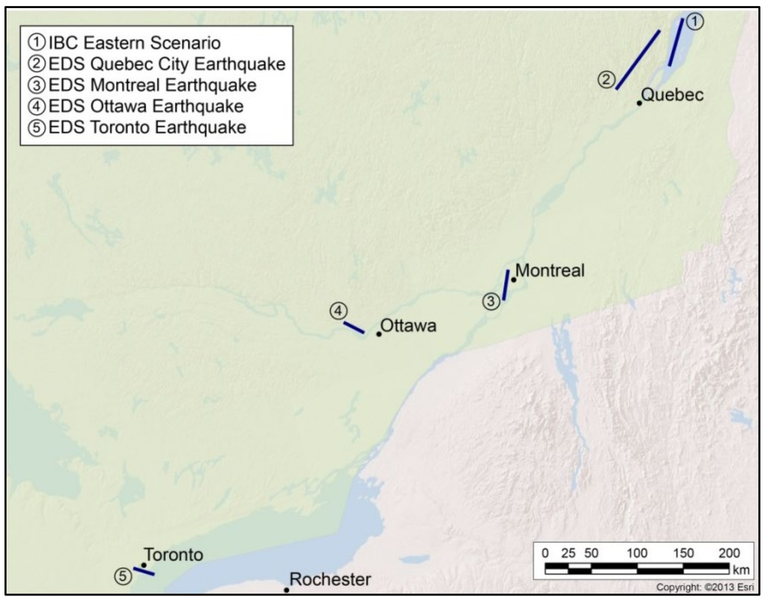

Figure 30. Fault traces of the five EDS events of eastern Canada (Canada = green; United States = grey)

EDS British Columbia Earthquake

At M9.2 and a rupture depth of 14 km, this extremely powerful earthquake is produced by slip within the Cascadia subduction zone, with its epicenter located approximately 250 km from downtown Vancouver. The nature, size, and location of this event enable it to generate a tsunami. Due to its very large magnitude and relatively shallow focal depth, this earthquake can be felt over much of British Columbia and the United States Pacific Northwest. While properties on Vancouver Island – including the provincial capital city of Victoria – would experience the strongest ground shaking, much of the island outside of Victoria contains comparatively little insured exposures. Therefore, the greatest concentration of exposures at risk from this powerful earthquake is considered to be in the metropolitan Vancouver region.

Because this EDS event was created deterministically, it is not available in the model's stochastic catalogs.

IBC Western Scenario

The IBC Western Scenario is a very strong M9.0 earthquake with a shallow focal depth (11 km) that occurs within the Cascadia subduction zone. With its epicenter located about 75 km off the coast of Vancouver Island (approximately 300 km from downtown Vancouver), the earthquake produces a tsunami. While this powerful earthquake causes strong ground shaking over much of Vancouver Island and the nearby Canadian mainland, including Vancouver city, the most significant insured losses from this event would be confined to Victoria and the greater Vancouver metropolitan region. However, this event would be readily felt across British Columbia and the Northwest Pacific United States (including Washington and Oregon states).

This event was generated by AIR using a fully probabilistic technique, and represents a 0.2% exceedance probability (500-year return period). This EDS event is *not* available in the model's standard (time-dependent) 10,000-year stochastic catalog.

The location of the two EDS events of western Canada is shown in Figure 31.

Figure 31. Fault traces of the two EDS events of western Canada (Canada = green; United States = grey)

EDS Pacific Northwest Earthquake M9.4 Cascadia Earthquake

In this extreme scenario, a M9.4 earthquake ruptures the full length of the Cascadia Subduction Zone along the Pacific Northwest and northern California. A tsunami wave inundates the coast with wave heights over 20 m at sites along the Washington and Oregon coast, and Crescent City, CA. Damage from shake, tsunami, fire, and all other subperils is widespread. Compared to magnitudes of observed global earthquakes, this scenario is second only to the 1965 M9.5 Validivia earthquake in Chile.

Additional EDS Events

There are additional EDS Events that originate in the U.S., but impact Canada. These events occur in Maine, Michigan, New Hampshire, Ohio, and Vermont.

These events were generated by AIR using a fully probabilistic technique. These EDS evenst are *not* available in the model's standard (time-dependent) 10,000-year stochastic catalog.

3.6 Historical Earthquake Scenarios: Accounting for Uncertainty in Source Parameters

A historical event set for the AIR Earthquake Model for Canada is included in CATRADER and Touchstone. However, in some cases, AIR provides alternate views of a historical event's source parameters, reflecting the uncertainty associated with the values for these parameters that are available in the literature and other data sources. This process is described in more detail below.

AIR examined the source parameters for 39 historical earthquake events affecting Canada from 1700 to 2012. The degree of uncertainty associated with source parameter hypocenters, magnitudes, and mechanisms is generally a function of the time of the earthquake occurrence and the quality of recording of the earthquake. In terms of source parameter reconstruction, events occurring prior to about 1900 – that is, before the installation of seismic instruments – exhibit the greatest levels of uncertainty. Source parameter uncertainty is greatly reduced for earthquake events between 1900 and 1976, as analog seismic instrumentation was becoming available during that time period. Uncertainty in source parameter reconstruction is even smaller after 1976 (and reduction in uncertainty continues to the present day), as seismic events in this time frame have routinely been recorded using digital seismometers.

To accommodate this observed uncertainty in source parameters for historical events, the AIR Earthquake Model for Canada provides three alternate scenarios for the historical earthquakes of 1732 and 1663. The rationale for providing alternate scenarios for these two events is described in further detail below.

Large uncertainty is associated with all aspects of the 1663 earthquake in eastern Canada due mainly to the lack of settlers in the vicinity of the rupture. In fact, to this day no surface rupture has been associated with this event. Therefore, source parameterization can be constrained only by piecing together reports of damage gathered around the time of the event. Several source parameterization models can match some of the anecdotal information associated with this notable event. For example, the limited information available for this event allows its epicenter to be located to a resolution of 0.1 decimal degrees in latitude and longitude, and its depth to be constrained to the upper crust. However, a wide range of magnitudes have been reported for this event. With this overall lack of precision in mind, AIR assumes a few tens of kilometers of uncertainty in locating the epicenter of 1663 earthquake.

A very high degree uncertainty is also associated with all aspects of the 1732 earthquake that ruptured in eastern Canada. As is the case for the 1663 earthquake, source parameterization can be reconstructed only by carefully considering reports of damage gathered at the time of the event. Several source parameterization models are available, but, at best, the limited information for this earthquake can only loosely locate its epicenter in the vicinity of Montreal, constrain its depth to the upper crust, and suggest a wide range of possible earthquake magnitudes. Given the overall lack of precision, AIR assumes several tens of kilometers of uncertainty in locating the epicenter of 1732 earthquake.

3.7 Validating Stochastic Event Generation

The AIR Earthquake Model for Canada has been extensively validated, with each component of the model carefully verified against historical data. This section provides a few exhibits that validate the stochastic event generation procedure.

Validating Frequency

The AIR Earthquake Model for Canada uses historical earthquake data to validate the magnitude frequency distribution of the optimized 10,000-year earthquake catalog. Figure 32 and Figure 33 compare the magnitude frequency distributions derived from the 100,000-year stochastic catalog to the magnitude frequency distributions made from the historical catalog, for regions within a 200-km radius of selected major Canadian cities. In each graph, the blue dots show the historical data, while the green lines represent the magnitude frequency distributions derived from the 10,000-year stochastic catalog. Note that the magnitude frequency distribution of the optimized 10,000-year stochastic catalog is consistent with the historical seismicity in each region.

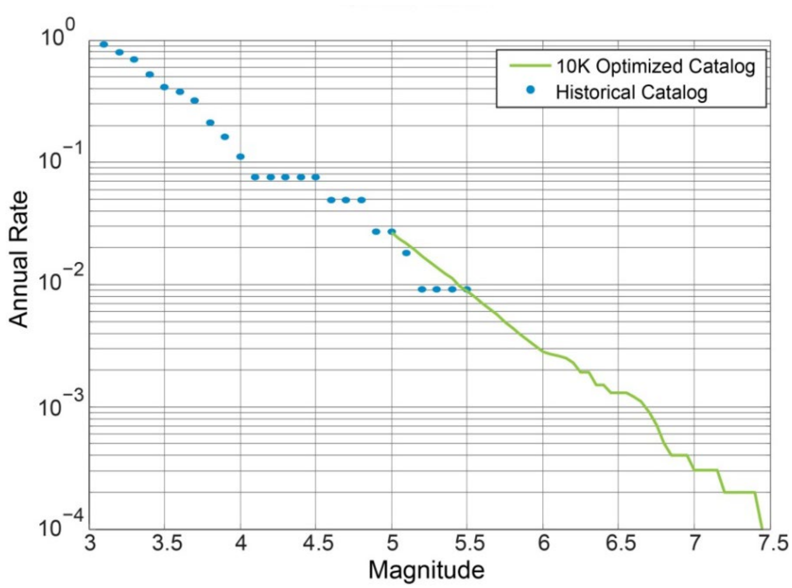

Figure 32. Comparison of historical and simulated magnitude-frequency distributions for Montreal and the surrounding 200 kilometers

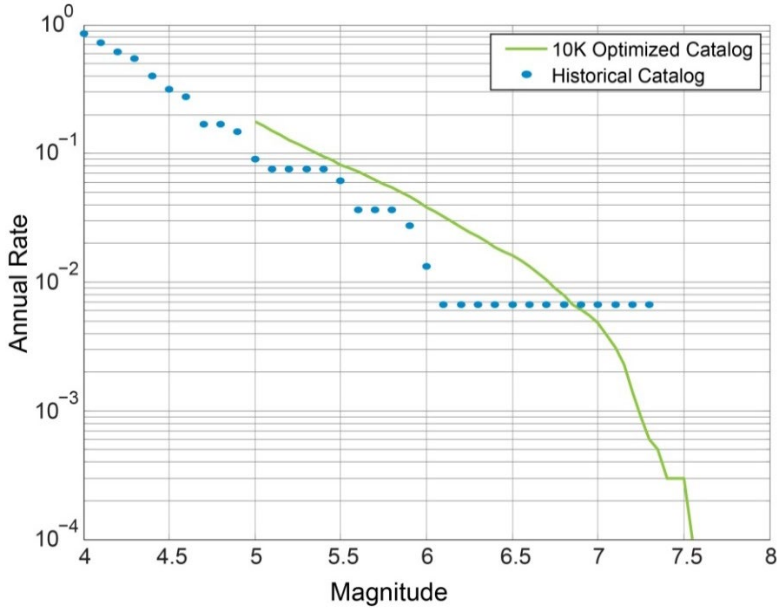

Figure 33. Comparison of historical and simulated magnitude-frequency distributions for Vancouver and the surrounding 200 kilometers

Validating Modeled Focal Depth

Figure 34 compares the focal depths of earthquakes in the stochastic catalog to the focal depths of historical earthquakes in Canada. Note the good agreement between the modeled and historical focal depths, in most depth bins for which historical data are available.

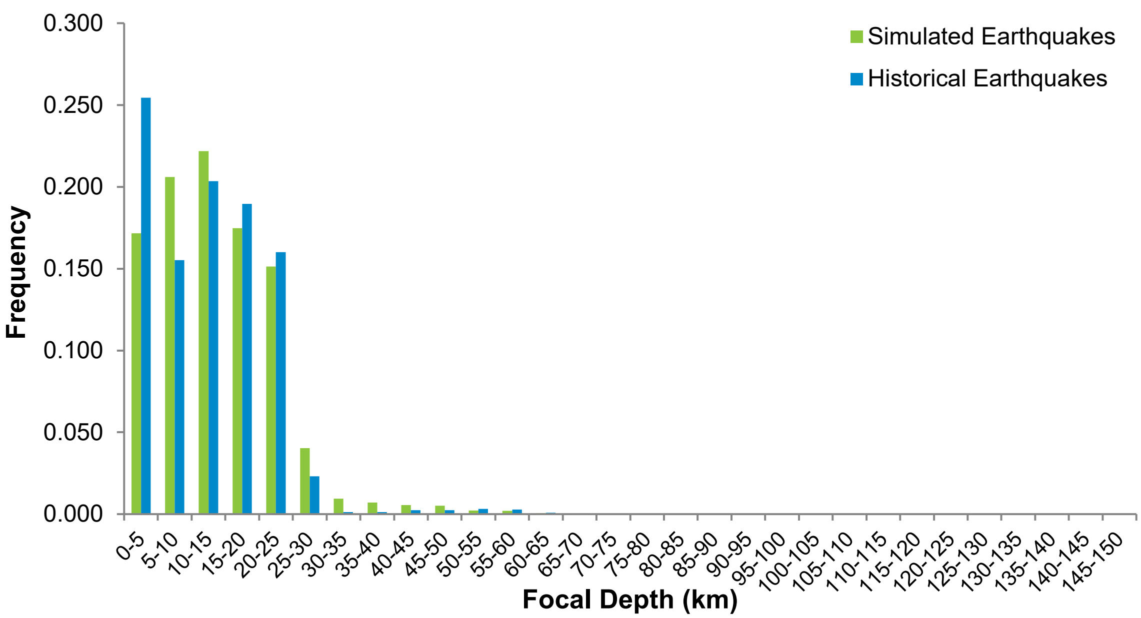

Figure 34. Modeled (green) and historical (blue) focal depths for earthquakes in Canada

3.8 Generating Simulated Tsunamis

Regions along the Canadian west coast – particularly those in close proximity to the Cascadia subduction zone – are at risk from tsunamis triggered by undersea earthquakes. The AIR Earthquake Model for Canada therefore includes a fully probabilistic tsunami module in which the origin, propagation, and inundation of tsunamis are modeled throughout their lifespan, allowing their impact on exposures in Canada to be assessed.

It is important to note, however, that only stochastic events produced by seismic sources offshore of western North America – particularly the Cascadia subduction zone and the Alaska-Aleutian subduction zone – are considered to pose tsunami risk to Canada in the AIR model. There is no modeled tsunami risk for eastern Canada.

The following section discusses the method used to determine which of the catalog's simulated earthquakes would generate a tsunami. The characteristics and occurrence probability of these tsunamis are based on the parameters and location of the generating earthquakes. Subsequent sections discuss the propagation of these tsunamis and how their effective inundation depth (that is, local intensity) is calculated (Section 4.4). The method used to estimate damage inflicted by the tsunamis is discussed in Section 5.9.

Tsunami Model Domain

In the AIR Earthquake Model for Canada, tsunami hazard and intensity are estimated within a nested model domain, as shown in Figure 35.

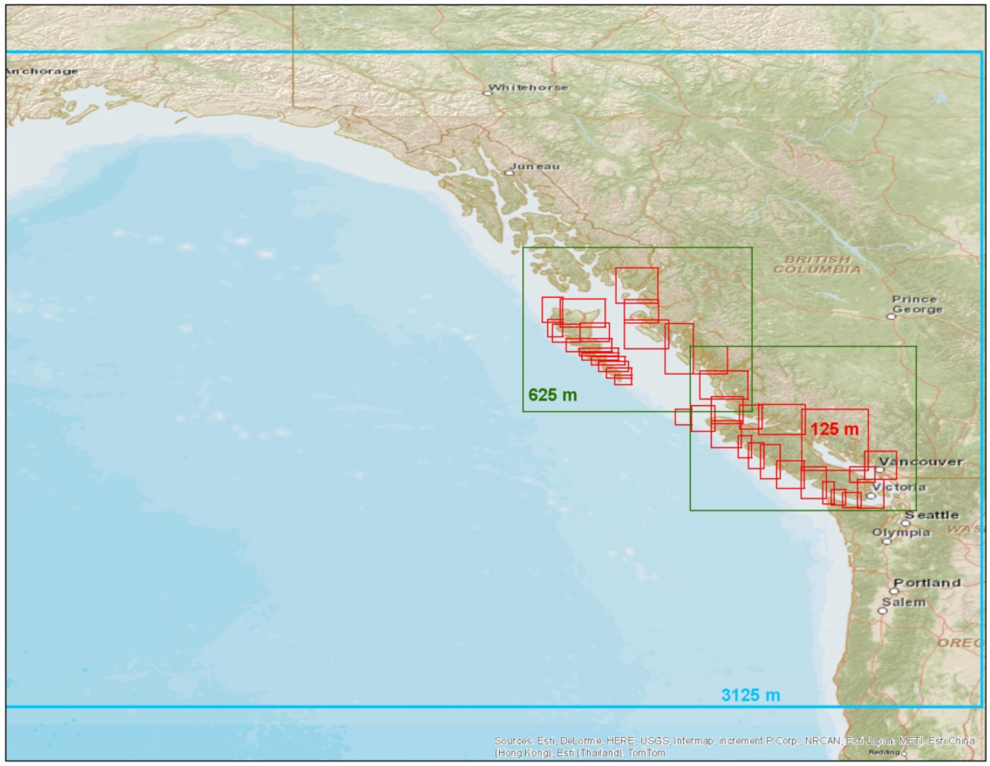

Figure 35. The model domain for tsunami in the AIR Earthquake Model for Canada consists of three nested domains with different resolutions

This nested domain approach is used to maximize the model's efficiency and reduce computation time. The tsunami simulations are conducted within 125-meter resolution domains over land (shown in red in Figure 35), a 625-meter resolution domain in near-shore regions (shown in green), and a 3125-meter resolution domain in the open ocean (shown in blue). Note that the 3125-meter resolution domain extends west as far as the International Date Line.

Determining Tsunamigenic Events

The size and impact of a tsunami are determined by several factors, beginning with the characteristics of the fault and its subsequent rupture. These characteristics also determine the volume of water that is displaced vertically during a rupture, creating the potential for a tsunami.

To identify tsunamigenic events in the catalog, AIR researchers first determined which stochastic earthquake events were capable of producing a tsunami. For stochastic events produced by the Cascadia subduction zone or the Alaska-Aleutian subduction zone with magnitudes of M7.0 or higher, AIR scientists examined the earthquake locations, geometry (length and width of the fault plane, dip angle, and focal depth), and faulting mechanisms to determine if the event would cause significant vertical offset of the ocean floor. If an event in the stochastic catalog would result in significant vertical offset of the ocean floor, it is considered tsunamigenic.

For events that were determined to be potentially tsunamigenic, AIR scientists then estimated the slip distribution of the rupture plane. The amount of vertical displacement an earthquake can cause at the ocean floor depends not only on the fault parameters used in the ground motion intensity calculation (e.g., strike, dip, fault length, fault width, etc.), but also on the amount of fault slip and the slip direction (which are not required to calculate ground motion intensity). Fault slip along an earthquake rupture is generally larger for larger magnitude earthquakes; however, for large earthquakes fault slip along the entire earthquake rupture plane is typically not uniform. Therefore, to create realistic rupture scenarios for tsunami modeling, AIR seismologists determined the coseismic fault slip along the rupture plane for tsunamigenic events according the following procedure.

First, the mean fault slip on the entire rupture plane was estimated using the relationship between the seismic moment of the event, the rupture area, and the mean coseismic slip. Then, based on the statistics of coseismic distributions of recent historical earthquakes, a range of ratios between maximum slip and mean slip were identified and used to constrain the distribution of seismic slip along the simulated fault ruptures. Next, using a widely adopted fault block model, and recent GPS and other geodetic data, AIR seismologists determined the distribution of fault coupling (that is, fault slip accumulation rate) along the subduction zone faults considered in the tsunami model. An example for the Cascadia subduction zone is shown below in Figure 36.

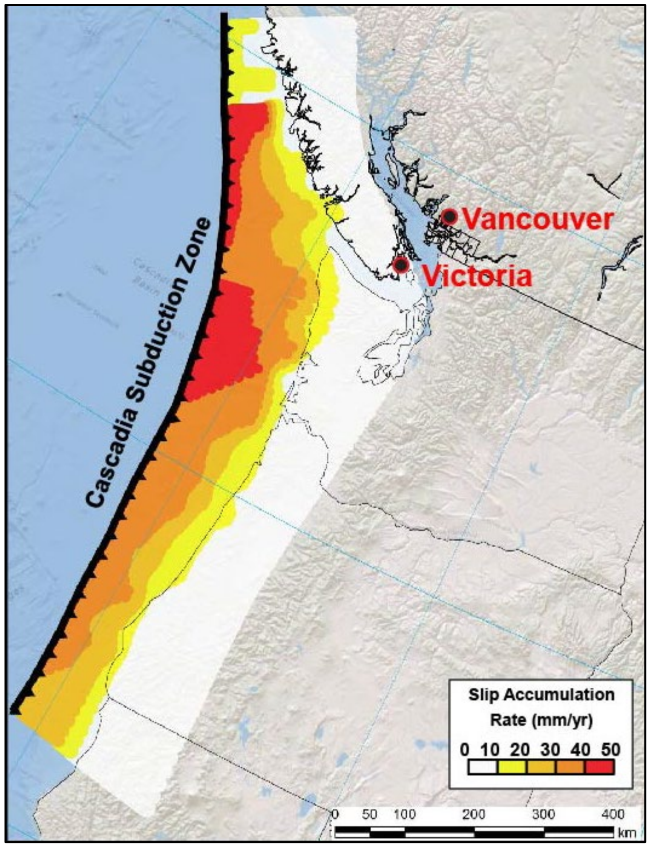

Figure 36. Distribution of slip accumulation along the Cascadia subduction zone, which was determined from the fault block model and GPS data

Fault coupling represents how fast seismic energy is accumulating along different parts of a fault during an interseismic period. For the Cascadia subduction zone, which last ruptured during the 1700 megathrust earthquake (see Section 2.3 for a description of this event), fault coupling may also represent the distribution of total seismic energy accumulation along this subduction zone fault. In fact, geodetic data in Japan and Chile obtained before the recent Tohoku and Maule earthquakes show that the rate of slip accumulation before these large events was closely correlated with the fault slip that occurred during the earthquake rupture. That is, larger fault slip patches were correlated with areas of faster slip accumulation (or stronger fault coupling). Therefore, the distribution of fault coupling obtained from the fault block model was used by AIR to constrain the distribution of fault slip for stochastically simulated earthquake ruptures.

Finally, to stochastically simulate the slip along different parts of each tsunamigenic fault rupture, the mean fault slip, the ratio of maximum fault slip to mean fault slip (and its variation), and the distribution of fault coupling along the subduction zones was integrated. In this integration process, the sum of the seismic moments of all of the subfaults that exhibit different slips was kept consistent with the total seismic moment of the event (which corresponds to the earthquake magnitude). The probability of a fault segment being assigned a larger than mean slip increases with the interseismic fault slip accumulation rate of the fault segment.

After the slip was determined for each subsegment of the earthquake rupture, the vertical displacement field of the ocean floor was then calculated. This calculation was based on the fault geometry and fault slip using the elastic dislocation model. This vertical displacement field initiates the tsunami wave in the open ocean.

Once a tsunami wave is generated, the model mathematically simulates its evolution and development from its inception to its farthest inland extent. These characteristics of the tsunami depend on several parameters including the height and speed of the tsunami, as well as topography. For further information about how the AIR model simulates tsunami propagation after a stochastic event has initiated a tsunami, see Section 4.4.

4 Local Intensity Calculation

After stochastic events have been generated, their effects at a particular location must be calculated. Surface geology, attenuation, and site amplification factors must be considered in this component of the model. In addition to these, the type of ground soil and the amount of water are included to determine the soil effects on shaking intensity and the probability of liquefaction.

The effects of an earthquake at a given site are often the result of multiple earthquake-related perils. While the initial shock affects the generation and many of the characteristics of these perils, their intensity at a site often depends on factors that are unrelated to the magnitude of the earthquake.

In addition to shaking intensity, liquefaction, and landslide, the probability of fire breakouts following an earthquake at any given location must also be considered. This depends not only on the type of exposure and its density but also on wind speed and direction, which affect the number and intensity of fires. If the event generates a tsunami, then coastal bathymetry and local topography are also taken into consideration to determine the effective tsunami depth.

4.1 Ground Shaking Intensity

In order to analyze damage and loss for each simulated earthquake, the ground motion intensity at each affected surface location must be calculated. This ground motion can range from barely perceptible trembling to violent shaking, depending not only on the magnitude of the event, but also on the distance from the rupture to the affected site, the geological characteristics of the region, and local site conditions.

Ground shaking intensity is commonly measured in term of peak ground acceleration (PGA) and spectral acceleration (Sa). The peak ground acceleration is the maximum value of the ground acceleration and is typically referred to as motion in the horizontal direction. Spectral acceleration is the maximum response of a simple building, with a single natural frequency of vibration, to earthquake ground motions. Sa approximates what a building experiences as modeled by a particle mass on a massless vertical rod having the same natural period of vibration as the building.

Different buildings respond differently to the ground motion that occurs during a particular earthquake. A building will be most sensitive to ground motion components that are close to its natural frequency of vibration. Thus, while PGA is the maximum acceleration experienced at a free ground surface, spectral acceleration is more relevant for estimating building damage.

Stochastic and Correlated Ground Motion Fields

The vulnerability module was calibrated against historical earthquake damage and loss information. For this reason, it is necessary to reconstruct the ground motion fields for selected historical events to make the modeled ground motion field as consistent with the observed intensity data as possible. This is a challenge, as the actual ground motion data for these events are often limited to: (1) a handful of recordings at different sites and; (2) a regional MMI intensity map. In every case, insufficient information exists to construct unique regional ground motion fields for the selected historical earthquakes.

To address this challenge, a series of stochastic ground motion fields were simulated using regional ground motion prediction equations and available ground motion information for each event. These stochastic ground motion fields were then used to calibrate the vulnerability module.

These simulations consider site-to-site ground motion correlated effects (Mahdyiar et al. 2010) as described below.

The assessment of ground motion intensity has traditionally been based on an approach that used event magnitude, the source-to-site distance, and the local soil conditions. These calculations also accounted for variability in the ground motion, based on observed deviations during historical earthquakes. The variable ground motion intensities were included in the equations by means of a lognormally-distributed error term, also known as a “residual."

Recent studies of these ground motion residuals show that, rather than being randomly distributed through an area during an earthquake, there is a distinct correlation between residuals at one site and residuals at nearby sites. That is, observations have shown that if the ground motion is higher than expected at a particular site, it is more likely that a nearby site will also experience higher-than-expected ground motion.

For hazard and risk analysis, it is common practice to estimate the ground motion at sites using regional GMPEs. GMPEs provide estimates of the *median ground motion* as a function of magnitude, distance, and source mechanisms, and provide an estimate of uncertainty in ground motion due to source radiation, path, and local site effects. A typical GMPE often is formulated as:

$$\ln(Y) = \ln(\overline{Y}) + \varepsilon_{Inter} + \varepsilon_{Intra}$$

where Y is the logarithm of the point estimate of the GM, $\overline{Y}$ is the median of the logarithm of the point estimate of GM, and ε_{inter} and ε_{intra} are the inter- and intra-event random errors that reflect the source and path and site related uncertainties, respectively. ε_{inter} and ε_{intra} and are assumed to be independent. The inter-event component leads to an overall regional spatial correlation for any two sites:

$$\rho_{GM} = \frac{\sigma^2_{Inter}}{\sigma^2_{Inter} + \sigma^2_{Intra}}$$

However, studies on the similarities in ground motion for different events, after removing the estimated median of the ground motion values, indicate that the ground motion correlation for sites close to one another is statistically larger than that predicted by the equation above. This intra-site correlation, which is distance dependent, can have a large impact on the regional loss distribution, making the damage from some earthquakes very costly (Bazzurro and Park 2007). The overall ground motion correlation, including intra-site correlation, can be formulated as:

$$\rho_T = \frac{\sigma^2_{Inter} + \rho(d) * \sigma^2_{Intra}}{\sigma^2_{Inter} + \sigma^2_{Intra}}$$

where $\rho(d)$ is the intra-site correlation, with d representing the distance between stations (Boore et al. 2003, Park et al. 2007).

Estimating the expected losses for each calibrating earthquake requires simulating sets of stochastic ground motion fields that reflect the inter-event and intra-site spatial correlation constrained by observed ground motion data, when available. That is, when ground motion recordings are available, the information can be used to constrain the simulation at sites near the recording stations. For earthquakes with only MMI data or contour maps, the intensity information can be translated into ground motion values that are again used to constrain the simulation, while taking into consideration uncertainty in the intensity-to-ground-motion conversion. Thus the approach taken by AIR explicitly takes into account the quality of the available data.

In summary, it is important to formulate a stochastic ground motion simulation procedure that is: (1) based on the regional attenuation equations; (2) captures the stochastic nature of the ground motion and the intra-site correlation effects, and; (3) incorporates the constraints imposed by different kinds of observations.

A practical approach is to simulate a set of stochastic ground motion residuals, with respect to the median ground motion, at sites of interest that conform to the imposed ground motion constraints. The many sets of residual fields capture the regional inter-event, intra-event, and intra-site correlation effects. Given that the residuals are simulated for the reference site conditions, the regional footprint can be constructed using information about the shallow soil site conditions.

By adding stochastically simulated residuals to the median ground motion and applying the shallow site response, different realizations of the ground motion footprint for an earthquake are created.

Ground Motion Prediction Equations

Empirical ground motion prediction equations, or GMPEs, are practical tools used to estimate earthquake ground motion intensity as a function of the magnitude, distance, and rupture mechanism of an earthquake. These equations, which were more commonly termed attenuation relationships in the past, describe how the intensity of certain ground-motion parameters at the surface vary as the seismic waves propagate outward from the rupture source. Typically, ground motion decreases with distance due to geometric spreading and the absorption and scattering of energy as the waves travel through the earth. However, particular complex phenomena can sometime significantly amplify ground motions even at great distances from the rupture; for instance, deep alluvium basins can amplify long period ground motions, and soft, shallow soils over bedrock or stiff soil formations can amplify ground motions at a variety of seismic wave frequencies.

It is important to note that in many regions of high seismicity, GMPEs are based on a large amount of ground motion recordings from historical earthquakes, especially for small and moderate magnitude events (magnitudes 5.5-7.0) and moderate-to-large distances (greater than 10-20 km). Hence, ground motion prediction for such events and distance ranges is robust, while for larger magnitude events and shorter distances there exists more uncertainty. In areas of low seismicity far from the tectonic plate boundaries, however, GMPEs rely much more on physical models because the scarce empirical recordings are only available for small local earthquakes, or are borrowed from other areas of the world where rare, large magnitude events of similar tectonics have been observed and recorded. Therefore, GMPEs for these low-seismicity regions are generally associated with a higher degree of uncertainty than the GMPEs for more seismically active regions.

The general form of the GMPEs used in the AIR Earthquake Model for Canada is as follows:

$$Sa = f(M, D, d, C, F, T)$$

where

Sa = spectral acceleration or peak ground acceleration (m/s^2)

M = earthquake magnitude

D = distance from rupture plane (km)

d = focal depth (km)

C = site condition

F = faulting mechanism

T = period (inverse of frequency) (s)

The AIR model uses a different suite of GMPEs for Eastern Canada, Western Canada, and the Cascadia subduction zone, in accordance with Atkinson and Boore's (2011) proposed interim updated seismic hazard model for Canada, and in accordance with the latest set of GMPEs recommended by the United States Geological Survey (USGS). Indeed, the GMPEs recommended for regions of Canada by Atkinson and Boore (2011) are very similar to those used in the USGS 2008 update to the United States seismic hazard map (although a few of the GMPEs for Eastern North America or Western North America have since been updated).

To appropriately capture epistemic uncertainty in the calculated ground motion, a logic tree approach is used, with weighting factors assigned to each GMPE. Peak ground acceleration and different spectral acceleration values are used to formulate the earthquake building response. AIR chose to use the same (or very similar) weighting factors assigned to GMPEs in the 2008 USGS national seismic hazard map update, as these factors were selected following an extensive peer review process. However, the AIR logic tree approach also acknowledges new and updated GMPEs and associated weighting factors recommended by local experts such as Atkinson and Boore (2011). Further details of this process, as implemented for each region of Canada, are provided below.

Eastern Canada: Stable Continental Region

Nearly all GMPEs for eastern Canada are based on physical/stochastic and ground motion simulation models. This is because empirical recordings of ground motion are scarce for eastern Canada; in fact, such recordings are only available for small local earthquakes. Empirical ground motion recordings are also "borrowed" from rare, large magnitude events of similar tectonics observed and recorded in other areas of the world. Therefore, GMPEs for these low seismicity regions are generally associated with a higher degree of uncertainty than the GMPEs for more seismically active regions. To address epistemic uncertainty associated with GMPEs, it is common practice to integrate different sets of GMPEs using a logic tree approach. Therefore, AIR uses the most recent set of GMPEs developed for stable continental regions, and incorporates the GMPEs recommended for Eastern Canada by Atkinson and Goda (2011). The GMPEs and weighting factors applied to each equation that AIR used for eastern Canada are listed in Table 8 below.

Table 8: GMPEs and weighting factors used in eastern Canada (stable continental region)

Attenuation Equations	Weighting Factor
Atkinson, 2008 (revised by Atkinson and Boore, 2011)	0.1
Atkinson and Boore, 2006 (revised by Atkinson and Boore, 2011)	0.1
Frankel et al.,1996	0.1
Campbell, 2003	0.1
Silva et al., 2002	0.1
Somerville, 2001	0.2
Toro et al., 2002	0.2
Tavakoli and Pezeshk, 2005	0.1

Western Canada: Active Region

One of the most important components of the 2008 USGS National Seismic Hazard Maps was the incorporation of the Next Generation GMPEs for shallow crustal faults in the western United States. This had a significant impact on the estimation of ground motion intensity of large magnitude crustal earthquakes. Because of the scarcity of near field ground motion data for large magnitude earthquakes, the near field GMPEs for these earthquakes was previously heavily guided by expert opinion. Since the mid-1990s, however, the number of strong motion stations deployed around the globe has multiplied and these stations have recorded several large magnitude earthquakes. To exploit this infusion of new data—more than three times the amount previously available—a multidisciplinary research effort was initiated in 2003 by the Pacific Earthquake Engineering Research Center (PEER). The effort, which concluded in 2007, was called the Next Generation of Ground Motion Attenuation Models (NGA) Project. It focused on predicting ground motion from shallow crustal earthquakes in the western United States, but also looked more widely at similar tectonic regions.

The result of the NGA project is a set of GMPE equations that is more reliable and scientifically defensible than any previously produced. Because they use a higher quantity and quality of ground motion data, the NGA equations provide a more realistic (i.e., data-driven) estimate of ground motion in terms of the source scaling for large magnitude events, faulting mechanisms, focal depth, site location relative to the hanging wall, basin depth, and site conditions.

For shallow crustal earthquakes in western Canada, AIR uses the four NGA attenuation equations for active crust with equal weighting, as per USGS recommendation; however, AIR incorporates the 2011 revision to the Boore and Atkinson (2008) GMPE that has been recommended by Atkinson and Goda (2011) (see Table 9).

Table 9. GMPEs and weighting factors used in western Canada (active region)

Attenuation Equation	Weighting Factor
Abrahamson and Silva, 2008	0.25
Boore and Atkinson, 2008 (revised by Atkinson and Boore, 2011)	0.25
Campbell and Bozorgnia, 2008	0.25
Chiou and Youngs, 2008	0.25

Cascadia Subduction Zone (Interface and In-slab Earthquakes)

For subduction interface and in-slab deep earthquakes in the Cascadia subduction zone, different sets of GMPEs are used in the AIR model, as shown in Table 10 below. Note that this suite of GMPEs, which is broadly consistent with the GMPEs used in the USGS update to the U.S. seismic hazard map in 2008, has been recommended by others for possible consideration in the 2015 Canadian seismic hazard map (see Atkinson and Goda 2011).

Table 10. GMPEs and weighting factors used for subduction zones

	Attenuation Equation	Weighting Factor
Subduction Events	Atkinson and Boore, 2003	0.2
	Youngs et al., 1997	0.2
	Zhao et al., 2006a	0.4
	Gregor et al., 2002	0.1
	Atkinson and Macias, 2009	0.1
In-slab (deep) Events	Atkinson and Boore, 2003	0.45
	Youngs et al., 1997	0.45
	Zhao et al., 2006a	0.05
	Goda and Atkinson, 2009	0.05

Note that two of these GMPEs – Zhao et al. (2006a) and Goda and Atkinson (2009) – are empirically derived from strong-motion recordings from interface and in-slab earthquakes in Japan. Similarly, the Atkinson and Boore (2003) GMPE is developed using a worldwide ground motion dataset, which is adjusted for the Cascadia subduction zone. It should also be noted that the Atkinson and Macias (2009) equation, and the Gregor et al. 2002 equation, are developed based on finite-fault stochastic simulations, and assess the possible effects of megathrust Cascadia earthquakes (a necessary step, as there are no ground motion records from such an event in that region).

With hundreds of detailed, excellent quality strong-motion records from the M9.0 2011 Tohoku event in Japan now available, AIR explored whether these data can shed light on ground motion behavior and magnitude scaling law for Cascadia megathrust earthquakes. Whether the Tohoku data can be generalized and used for the Cascadia region is a point of debate, because the Tohoku data represent strong site amplification at high frequencies and large distances, due to thin layers of soft sediment atop bedrock in the affected region, which is very different from the site conditions in the Cascadia region. Selected studies that explore the application of Tohoku data to the Cascadia region are described below.

For example, Zhao and Xu (2012) demonstrate that the Gregor et al. (2002) GMPE shows a low magnitude scaling rate compared to the strong motion observations from the Tohoku event. But, the magnitude scaling rate of the Gregor et al. (2002) GMPE for a megathrust event, which has been validated against two M8.0 earthquakes (the 1985 Michoacan, Mexico, and the 1985 Valpariso, Chile, events) performs better for megathrust events (such as Tohoku) than GMPEs derived empirically without the benefit of observations from M9.0 events. In addition, as a part of a seismic hazard study for BC Hydro, Abrahamson (2012) has developed subduction zone GMPEs that have been adjusted using data from the Tohoku, Japan (2011) and Maule, Chile (2010) subduction zone events; however, these GMPEs poorly match the Tohoku ground motion data (see Abrahamson 2012). In contrast, Atkinson (2012) finds that the Tohoku ground motion data applied to site conditions for British Columbia show a reasonable fit to the stochastic GMPE derived by Atkinson and Macias (2009) for the Cascadia region.

Because research is still ongoing regarding magnitude scaling for megathrust earthquakes in light of the Tohoku event, AIR uses the GMPEs recommended by Atkinson and Goda (2011) for the Cascadia subduction zone, with appropriate weighting factors, as shown in Table 10 above.

Site Classifications and Ground Motion Amplification

As seismic waves travel through the earth from the rupture source to the earth's surface, ground motion intensity may be amplified or de-amplified due to local site conditions. The degree of amplification depends on the level of ground motion, the material properties of the site, and the frequency or period composition of the arriving waves.

If the arriving seismic waves are of low to moderate intensity, a site with a soft surface geology may experience significantly higher levels of ground motion than a rock site, especially for low frequency seismic waves, which are most damaging to mid- and high-rise buildings. However, if the ground motion is of a high intensity, a site with soft soils may experience lower ground motion than one of firm soil or rock due to the nonlinear behavior of soil.

Soil behaves in a linear fashion when seismic waves are weak. That is, the wave amplitudes increase as seismic stress increases. However, at a certain level of seismic stress, wave amplitudes no longer increase as quickly as stress increases. Such conditions are easily reached for loose, porous soils. Site conditions may be classified based on the physical properties of the surface geological materials.

The expanded National Earthquake Hazard Reduction Program (NEHRP) soil types are defined in Table 11 below, which also lists the average shear-wave velocities for each soil class. Note that intermediate soil types are expressed as a combination of two classes. The average shear-wave velocity for a given soil type is determined from the shear-wave velocities observed at locations identified with that soil type.

Table 11: Soil Classifications and Average Shear-Wave Velocities

Soil Class	Description	Average Shear Wave Velocity (m/s)
A	Very hard rock (crystalline rock with few fractures)	1620
AB	Hard rock	1150
B	Firm to hard rock	1050
BC	Firm rock	760
C	Soft to firm rock (gravelly soil and soft rock)	540
CD	Soft rock (gravelly and stiff soil)	360
D	Stiff clay and sandy soil	270
DE	Soft soil to firm soil (silty clay and sand)	185
E	Soft soil (includes mud)	150

These soil classifications account for variations in ground motion amplification, since the amplification factors are calculated directly from the mean shear-wave velocities.

Soil Maps

The AIR Earthquake Model for Canada uses surficial or Quaternary geological maps and available shear wave measurement data to develop soil classification maps at various scales. In Canada, the main geologic formations are pre-Tertiary bedrock and Quaternary glacial tills, or till veneer on top of the bedrock. These formations do not tend to amplify ground motion. The main units that constitute soft soil layers in Canada are the Champlain Sea marine clay/silt deposits in the east, the Fraser river fluvial deltaic delta deposits in the west, various postglacial deposits (alluvium, bog deposits, flood plain deposits, and so on), and some glaciolacustrine and glaciomarine units. The Champlain Sea marine clay/silt deposits and Fraser river deltaic deposits can be over 100 meters thick; therefore, these units can be major contributors to ground motion amplification. The thickness of the post-glacial deposits generally varies significantly over short distances; therefore, any correlation established between site class and post-glacial deposits may have large uncertainties. For this reason, AIR used thickness information wherever possible to constrain the mapping between individual geological units and site classes.

In addition, microzonation studies in Montreal (e.g. Chouinard and Rosset, 2007; 2011), Ottawa (Motazedian et al., 2011; Hunter et al., 2010), Vancouver and Victoria of British Columbia (Ventura et al., 2004; Monahan et al., 2000) were used to obtain shear wave velocity measurements for various types of sediments. These data were used to calculate the average shear wave velocity in the top 30 meters of soil (Vs 30) and predominant periods of site response in Montreal and Ottawa in microzonation studies (e.g. Chouinard and Rosset, 2007; 2011; Motazedian et al., 2011).

Several data sources were used to establish the mapping between geological units and site classes, to develop regional and local soil maps for Canada. Table 12 below shows the spatial coverage, data type, resolution, and sources of the soil maps implemented in the model. The highest spatial resolution of maps in major urban areas is about 25 to 50 meters. Figure 37 and Figure 38 below show the distribution of different resolution maps in eastern and western Canada. It should be noted that most large, densely populated cities are covered by high resolution soil maps (at 50 meter resolution), as shown in Figure 37.

Because of limited availability of sediment thickness data and the uncertainty associated with mapping between geological units and Vs 30, AIR has adopted the site classification maps from microzonation studies in Montreal and Victoria. The microzonation study results in downtown Ottawa and Vancouver have also been used in combination with surficial geological maps to create the soil maps covering larger areas in and around Ottawa and Vancouver.

When calculating the level of ground motion amplification at a site, only the top (higher-resolution) layer soil map was used. That is, if a region was covered by two or more layers of maps, only the higher-resolution map was used. In metropolitan areas that were covered by two or three layers of maps, such as Vancouver, Ottawa, Montreal, Quebec City and Toronto, the higher resolution soil condition map was used.

Table 12: Soil map data and references

Regions Covered	Data type and scale	Model Resolution	Data Source
Entire Canada	Geologic map 1:5,000,000	0.025 arc degree, About 2,000 meters.	Fulton, R.J., Compiler, 1996, Surficial materials of Canada, Geological Survey of Canada, Map 1880A, scale 1:5 000 000.
East Quebec Province	Glacial landform and deposits 1:1,000,000	0.005 arc-degree about 500 meters	Klassen, R.A., Paradis, S. Bolduc, A.M., and Thomas, R.D., 1992: Glacial landforms and deposits, Labrador, Newfoundland and eastern Quebec, Geological Survey of Canada, Map 1814A, scale 1:1,000,000.
West Quebec Province	Surficial geology 1:1,000,000	0.005 arc-degree about 500 meters	1:1,000,000 Surficial Geological Map, Urban and Environmental Geology of St. Lawrence Valley, Natural Resources Canada, Government of Canada, 2004 - 2010
Montreal, Quebec	Surficial Geology 1:50,000 Geotechnical 1:50,000	0.0005 arc-degree, 50m	Prest, V.K., and J. Hode-Keyser, Surficial Geology, Montreal Island, 1975. Chouinard Luc and Rosset Philippe, Microzonation of Montreal, variability in soil classification, 4th IASPEI/IAEE International Symposium, August 2011
St. Lawrence Valley, Quebec, including Quebec city	Surficial Geology 1:50,000	0.0005 arc degree about 50 meters	Urban and Environmental geology of the St. Lawrence Valley, Surficial Geology, Government of Canada, Earth Sciences Sector of Natural Resources Canada, 2010
Halifax	Surficial geology 1:50,000	0.0005 arc degree about 50 meters	Utting, D.J., B.E. Fisher, A.L. Ehler, Digital geological data generated as part of the surficial mapping project of the Halifax metropolitan and surrounding areas, Halifax and Hants countries, Nova Scotia, 2011.
Southern Ontario	Quaternary Geology and Surficial Geology 1:50,000	0.0005 arc degree about 50 meters	Ontario Geological Survey and Geological Survey of Canada, 2003, Surficial geology of Southern Ontario.

Regions Covered	Data type and scale	Model Resolution	Data Source
Ontario Province	1:1,000,000	0.005 arc degree about 500 meters	Ontario Geological Survey, 1997, Quaternary geology of Ontario-seamless coverage of the province of Ontario: Ontario Geological Survey, ERLIS Data Set 14.
Victoria, BC	Quaternary Geology and Geotechnical 1:25,000	0.00025 arc degree About 25 meters	Relative Amplification of Ground Motion Hazard Map of Metro Victoria, Patrick A. Monahan, Victor M. Levson, Paul Henderson, and Alax Sy, scale 1:25,000, 2000. Quaternary geological map of Metro Victoria, Patrick A. Monahan and Victor M. Levson, scale 1:25,000, 2000.
Vancouver (including New Westminster, Mission, Chilliwack, Coquiltam, and Vancouver)	Surficial Geology 1:50,000	0.0005 arc degree about 50 meters	Geological Survey of Canada, 1980, Surficial geology, New Westminster, British Columbia, scale 1:50,000. Geological Survey of Canada, 1979, Surficial geology, Vancouver, British Columbia, scale 1:50,000. Geological Survey of Canada, 1980, Surficial geology, Mission, British Columbia, scale 1:50,000. Geological Survey of Canada, 1980, Surficial geology, Chilliwack, British Columbia, scale 1:50,000.
British Columbia	Geology and Surficial Geology 1:250,000	0.0025 arc degree about 250 meters	Massey, N.W.D., MacIntyre, D.G. Desjardins, P.J. and Conet, R.T., 2005, Digital Geology Map of British Columbia, B.C. Ministry of Energy and Mines, Open File 2005-2, scale1:250,000.

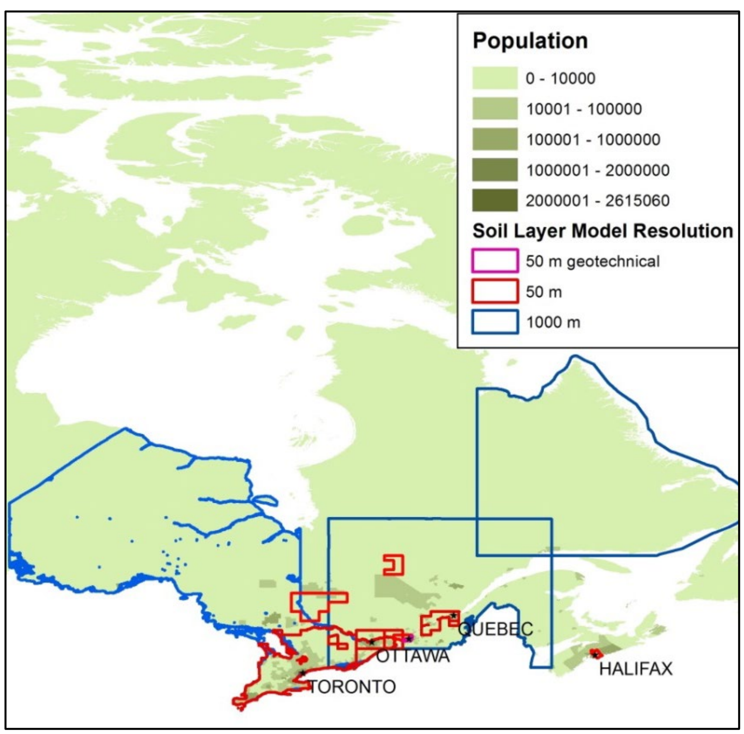

Figure 37. Soil map coverage in eastern Canada. Background color represents population distribution.

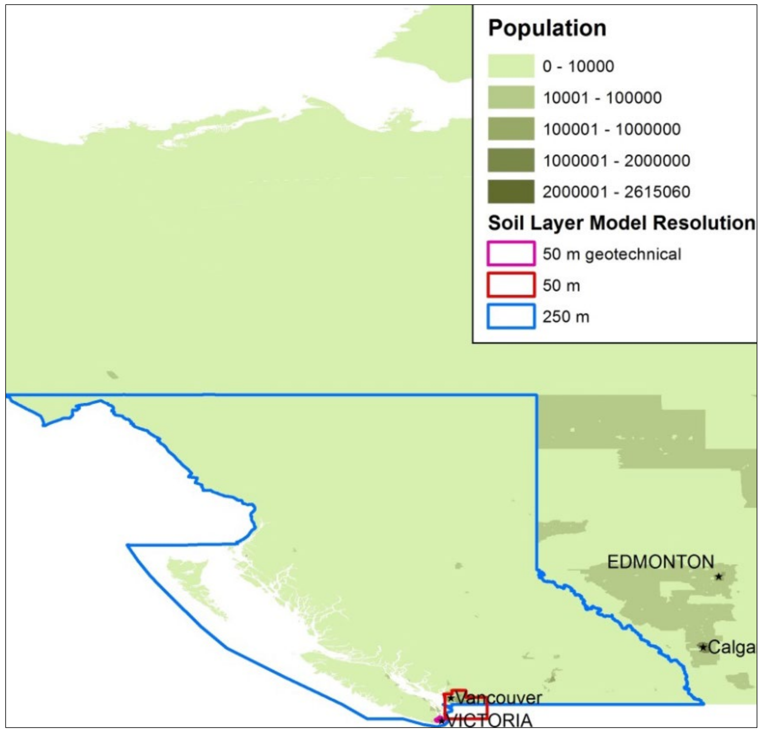

Figure 38. Soil map coverage in western Canada. Background color represents population distribution

Validating the Site Classification Maps

Site classification maps are best validated using shear wave velocity measurements in the top 30 meters of soil (Vs30). However, shear wave velocity measurements are expensive, and such data are usually limited in coverage. In the absence of direct Vs30 measurements, validation must be achieved indirectly, by comparing site classification maps developed by different researchers or using different methods.

In Canada, microzonation studies in several metropolitan cities, including Ottawa, Montreal, and Vancouver have been carried out in recent years (e.g. Chouinard and Rosset, 2007; 2011; Motazedian et al., 2011; Monahan et al., 2000). Site classification maps based on Vs30 measurements in Montreal and Victoria have been directly adopted. In Ottawa, this microzonation study was conducted in the downtown area. Using this information, AIR created a site classification map based on the surficial geological map in the greater Ottawa region. Figure 39 compares this site classification map with soil types estimated from over 2000 Vs30 measurements in the Ottawa region. Note the good agreement between the site classification map in this region and the measured Vs30 data.

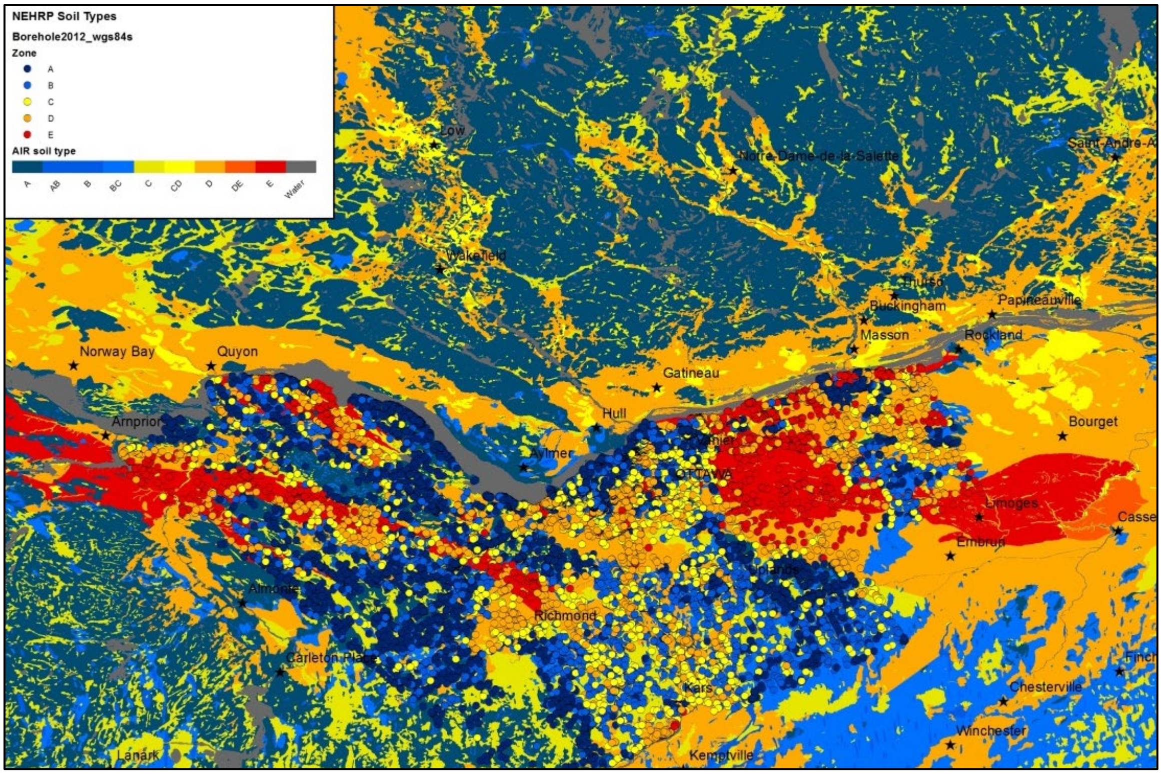

Figure 39. Comparison of AIR soil map (inferred from surficial geology) and soil types estimated from Vs30 measurements in boreholes (yellow dots) (Note that the AIR soil types correspond to the expanded NEHRP soil types)

In Vancouver, most survey work for microzonation studies has been carried out in the downtown area. Figure 40 below shows the distribution of borehole data where shear wave velocity measurements are available. Most of the survey sites in the downtown area can be classified as DE or E in the expanded NEHRP site classes. The soil map developed from large scale geologic maps in the Vancouver area compares reasonably well with the measured Vs30 data (see Figure 40 below).

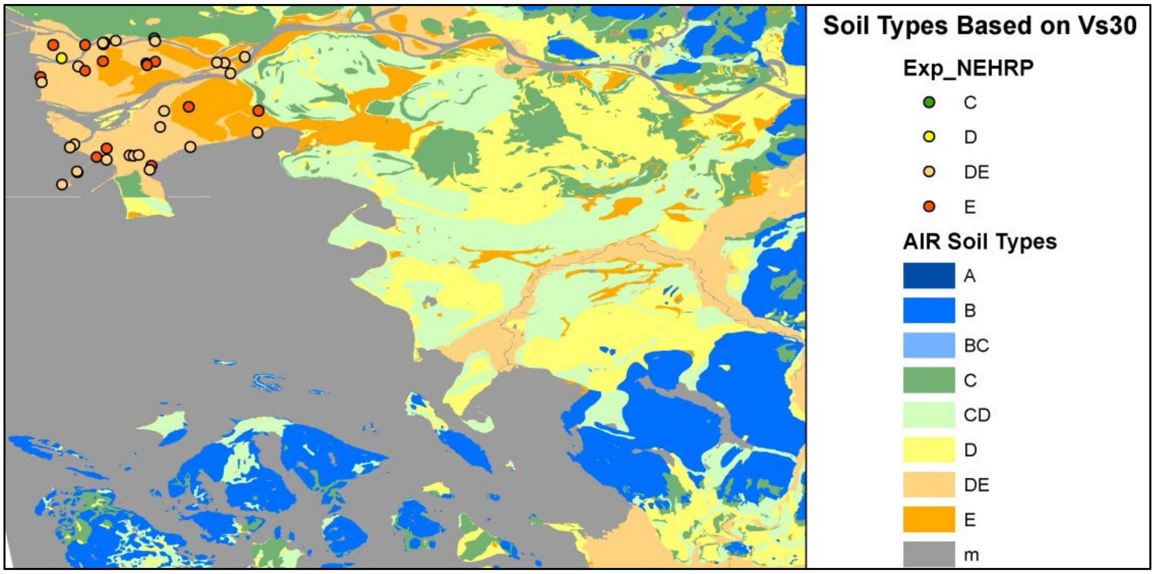

Figure 40. Comparison of AIR soil map inferred from surficial geology and soil types estimated based on Vs 30 measurements in boreholes (dots). The AIR soil type is the expanded NEHRP soil classification.

NGA Local Site Amplification

In the AIR Earthquake Model for Canada, local site amplification is calculated using an empirical algorithm that relates the Vs30[3] of a site (which is inferred from local site condition maps) to its amplification factor. The algorithm used in the AIR model was developed as a part of the 2008 Next Generation Attenuations (NGA) project (Power et al. 2008). In this project, researchers developed analytical and parametric site response relationships to explore the non-linear and linear responses of shallow soil layers to ground shaking (Walling et al. 2008).

Prior to the development of the NGA site amplification algorithm, the National Earthquake Hazard Reduction Program (NEHRP) site conditions were used to calculate earthquake wave amplification or de-amplification at different locations. Although both methods (NGA and NEHRP) use Vs30 values to quantify local site amplification, there are two primary advantages to using the NGA algorithm:

- In the NGA database, Vs30 values are assigned to each strong motion recording station based on borehole and site observations, age and other geological and technical information. Thus, the NGA database contains a comprehensive set of Vs30 measurements for quantifying ground motion amplification. In contrast, the NEHRP database contains relatively few observations of amplified ground shaking at soft soil sites, and the

[3] Vs30 = the average shear wave velocities for the top 30 meters of the earth's surface.

majority of these observations come from just two earthquakes (the 1989 Loma Prieta and the 1994 Northridge earthquakes).

- Use of the rich NGA project database has allowed several studies to better quantify the non-linear behavior of upper soft ground layers during different levels of ground shaking (Power et al. 2008).

Thus, use of the NGA equations has significantly improved our understanding of site responses to different levels of ground shaking, and these equations are used to calculate local site amplification in the AIR model. For comparison, however, amplification factors yielded by the NGA and the NEHRP methods (for a reference engineering site condition with Vs30 of 760 m/s) are provided below (Figure 41).

Note that for soil classes B (firm to hard rock) and C (soft to firm rock), there is good agreement between the amplification of ground shaking predicted by these two methods for all levels of ground motion (Figure 41). For soft soil classes D and E, however, the NGA and NEHRP methods predict different amplification factors when the level of ground motion is low. As highlighted above, this difference is due to the improved understanding and modeling of shallow site responses to ground shaking that is facilitated by the NGA database.

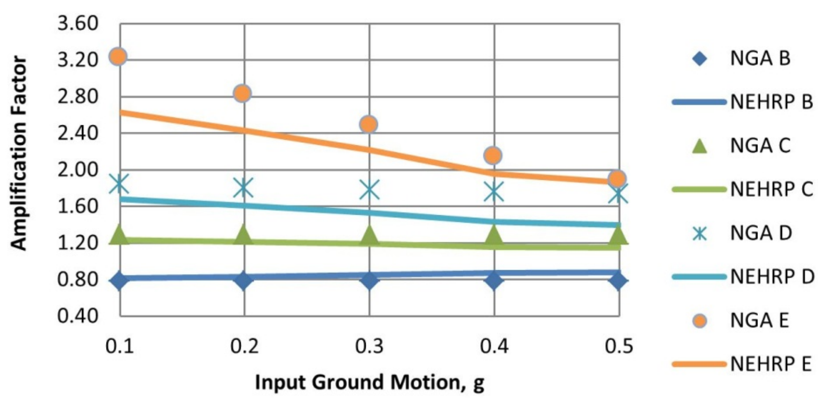

Figure 41. Comparison of NGA and NEHRP Site Amplification Factors with Respect to a Reference Engineering Rock Site for Long Period Waves

Alluvial Basin Effects

The ground motion on deep alluvial basins can be further amplified above and beyond what would be expected using the near-surface soil stiffness parameter only. If the basin depth is provided for an area, the NGA equations can account for its effect on ground motion (Campbell and Bozorgnia, 2007).

The Georgia Basin is an overlap of two sedimentary basins lying beneath the 220 km long Strait of Georgia between Vancouver Island and the mainland of British Columbia. The Georgia Basin is located within one of the most seismically active zones and most populated coastal areas in Canada. The Fraser River Delta in Greater Vancouver is of particular concern, because it hosts much of the population of Greater Vancouver and serves as a transport, utility, and communications corridor to Vancouver Island.

The geometry of the basin has been studied extensively in the last decade through geophysical surveys (e.g., bathymetric swath-mapping, seismic reflection and refraction, gravity) in the Strait of Georgia (Barrie et al., 2005; Lowe et al., 2003; Ramachandran et al., 2004, 2005, 2006; Zelt et al., 2001) and onshore and offshore studies of deltaic deposits of the Fraser River Delta (Hunter et al., 1998).

AIR incorporates the geometry of the Georgia Basin into the AIR Earthquake Model for Canada by implementing high resolution depth information (0.2 km), as shown in Figure 42. The AIR model therefore takes full advantage of the capabilities of the NGA equations to capture basin effects. Notably, basin effects result in greater amplifications of longer-period ground motions, which resonate with the natural periods of tall, flexible buildings, making them more vulnerable.

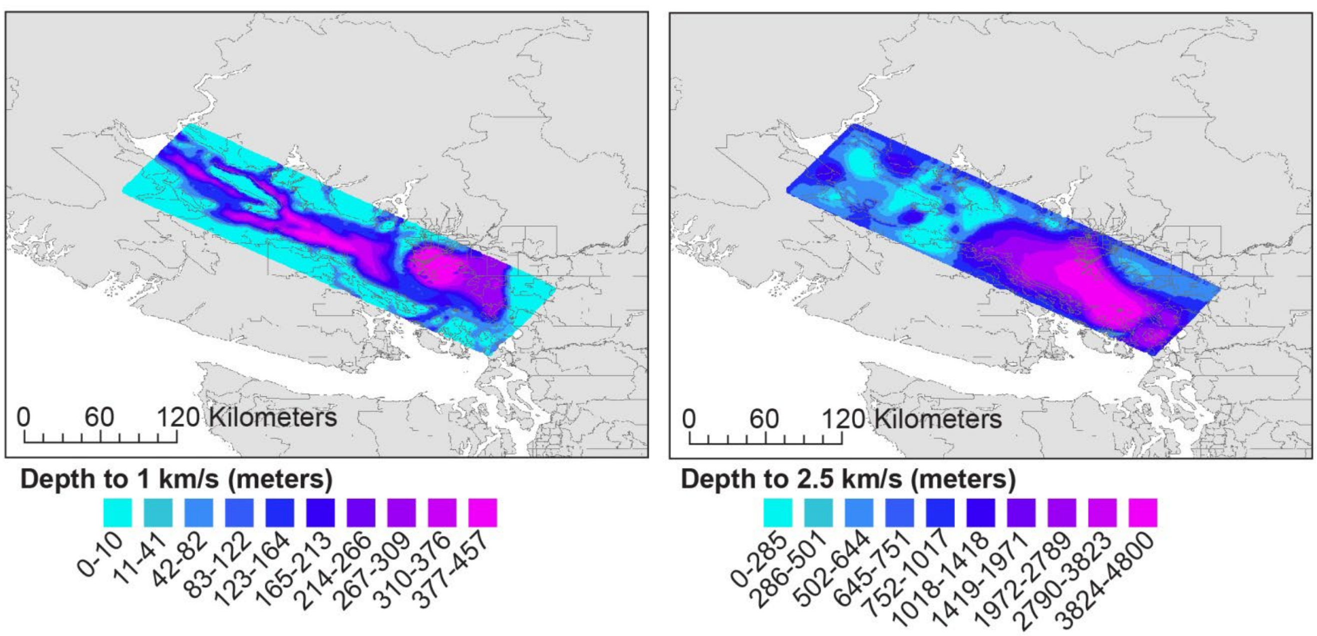

Figure 42. The geometry of the Georgia Basin is incorporated in the Canada model using the geometry of depths to the V_S = 1.0 km s^{-1} (left) and V_S = 2.5 km s^{-1} (right) isovelocity horizons on a 200 m resolution grid.

Validating Ground Shaking Intensity

To accurately estimate losses from earthquakes, a comprehensive risk analysis model must be calibrated against losses from historical events. An important component of the calibration process is the simulation of ground motion at exposure locations. Because the AIR earthquake model uses spectral accelerations to calculate damage ratios, robust validation for ground motion module should compare the modeled spectral accelerations with the observed spectral accelerations from historical earthquakes in Canada. Unfortunately, little strong motion observation data is available in Canada. In addition, only a few significant historical earthquakes have MMI intensity maps, which are rather qualitative because of the sparse population density in the regions affected by these earthquakes. Therefore, in the section below, we compare modeled MMI intensity footprint with the observed MMI seismic intensity maps for those few historical earthquakes as a way of indirect validation. Table 13 lists the selected historical earthquakes for which reported and modeled intensity are compared. (Note that these earthquakes are a subset of those released with the AIR software systems.) However, it is important to note that the reported damage from these events is limited due to their location in relatively remote or less populated areas of Canada.

Table 13. Historical significant earthquakes used for calibration

Event Location	Year	Magnitude (Mw)
Charlevoix-Kamouraska	1925	6.2
Saguenay	1988	5.9

1925 Charlevoix-Kamouraska, M6.2

Produced by slip within the Charlevoix-Kamouraska seismic zone, this earthquake caused localized damage due to its moderate magnitude and shallow depth (about 10 km). The widespread use of unreinforced masonry structures in the affected region also increased the damaging effects of this event. Figure 43 shows the observed ground shaking intensity (MMI) from this earthquake.

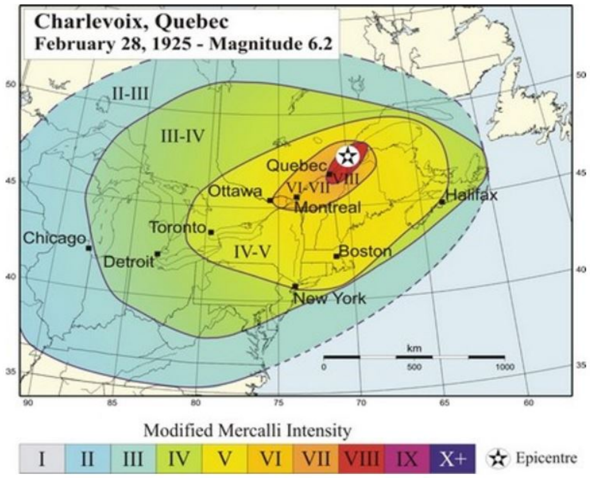

Figure 43. Reported intensity contour from the 1925 Charlevoix earthquake (Source: Geological Survey of Canada)

Figure 44 demonstrates the estimated ground motion footprints for the 1925 Charlevoix earthquake using *median ground motion* as predicted by ground motion prediction equations, and a more realistic *stochastic ground motion* simulation field. This stochastic ground motion simulation is just one of 100 ground-motion realizations; it considers the inter- and intra-event ground motion uncertainties (which include site correlations) and the observed intensity report as constraints while generating stochastic ground-motion fields. Note the good agreement between these two estimated ground motion footprints and the observed intensity contours for this event (shown in Figure 43).

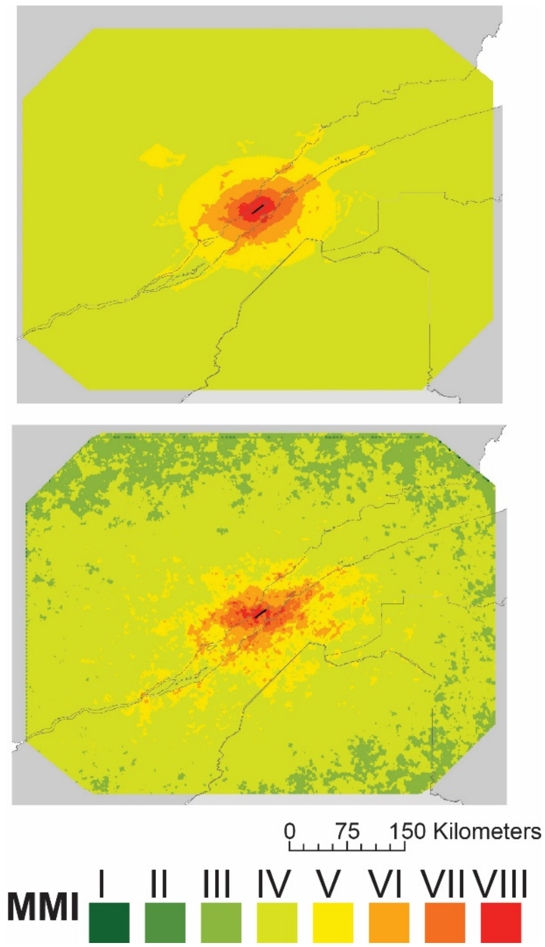

Figure 44. Median ground motion (top) and stochastic ground motion realization (bottom) with observed intensity constraints for the 1925 Charlevoix-Kamouraska earthquake

1988 Saguenay, M5.9

On November 25, 1988, Quebec and much of Eastern Canada was shaken by a M5.9 earthquake. Although the event produced widespread ground shaking, it caused only minor damage to buildings. The observed intensity footprint (MMI) for this event is shown in Figure 45.

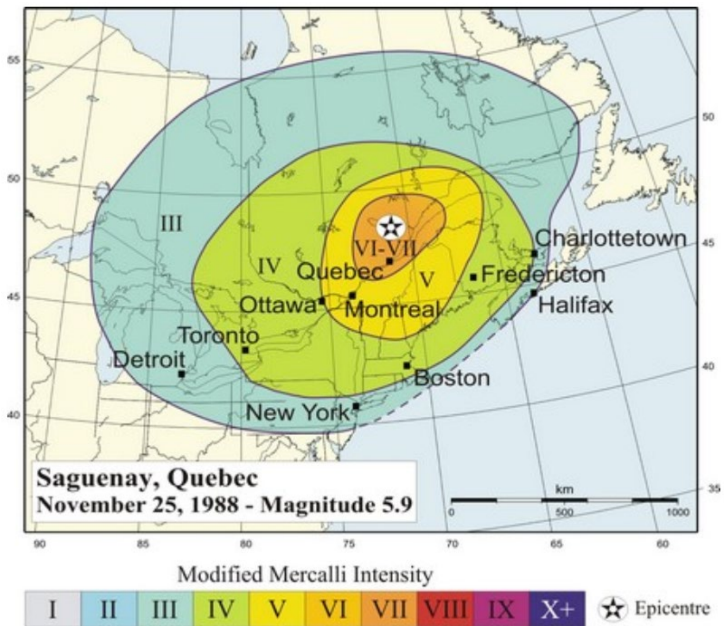

Figure 45. Reported intensity contour from the 1988 M5.9 Saguenay earthquake (Source: Geological Survey of Canada)

Figure 46 demonstrates the estimated ground motion footprints for the 1988 Saguenay earthquake using *median ground motion* as predicted by ground motion prediction equations, and a more realistic *stochastic ground motion* simulation field. This stochastic ground motion simulation is just one of 100 ground-motion realizations; it considers the inter- and intra-event ground motion uncertainties (which include site correlations) and the observed intensity report as constraints while generating stochastic ground-motion fields. Note the good agreement between these two estimated ground motion footprints and the observed intensity contours for this event in the epicentral area (shown in Figure 45).

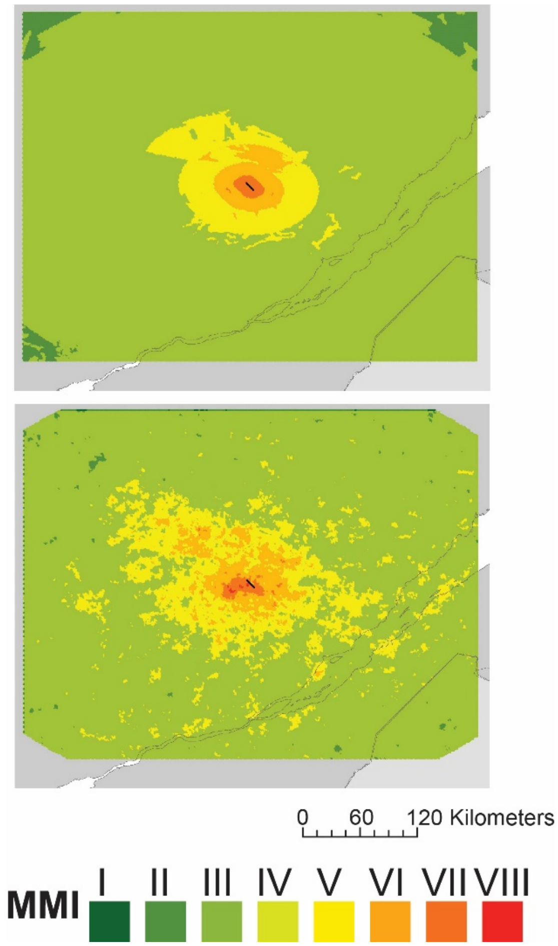

Figure 46. Median ground motion (top) and stochastic ground motion realization (bottom) with observed intensity constraints for the 1988 Saguenay earthquake

4.2 Liquefaction Intensity

When an earthquake strikes an area that is saturated with groundwater, the shaking can cause the soil to lose its stiffness due to increased pore water pressure, and behave like a heavy liquid. When this happens, the soil loses its capability to support structures. Buildings can suddenly tilt or even topple over as the ground beneath them becomes liquefied. Pipelines and ducts can surface, and as the liquefied soil shifts, it can break buried utility lines. If the saturated soil lies underneath a dry crust, the ground motion can crack the top dry soil allowing the liquefied sand to erupt through the cracks, creating sand boils. Sand boils can spread through utility openings into building, and damage the building or its electrical system.

Liquefaction is more likely in areas with loose coarse grained soils that have poor drainage and are saturated with water. An example would be loose sands, which are found along riverbeds, reclaimed lands, beaches, dunes, and other areas where sands have accumulated.

The AIR Earthquake Model for Canada includes a liquefaction component covering areas of highest exposure concentration in British Columbia, Ontario and Quebec. Input data for the liquefaction module include the depth of the groundwater table and surficial soil information. During the development of the liquefaction module, AIR collected or developed depth to groundwater table maps and surficial soil information for six regions. These six regions are the Lower Mainland, Metro Victoria area, Greater Toronto area, National Capital Region, Greater Montreal Areas, and Quebec City.

There are three minimum requirements for seismic induced liquefaction to occur at a site. These minimum requirements are as follows:

- The soil near the ground surface must contain a liquefiable layer (loose sand and silt).
- The liquefiable layer must be located below the groundwater table.
- The intensity of ground shaking must reach a certain critical level.

Thus, in addition to groundwater depth in the modeled region, the liquefaction module also incorporates the physical properties of the top soil layer (defined as the uppermost 20 meters). Further details of the liquefaction module are provided in the section that follows.

Groundwater Depth

Groundwater depth data were collected by AIR from several sources. The main data source was the Groundwater Information Network (GIN) water well data base. In addition to the water well data, AIR contacted local government agencies and acquired information regarding the groundwater depths.

An example of the water well data for Lower Mainland region can be seen in Figure 47. However, as can be seen in Figure 47, the distribution of these water wells is not uniform. For example, the Richmond and Delta areas have relatively few water wells in the database, while other regions have much denser coverage. Therefore, AIR contacted the engineering departments of the City of Richmond and the Corporation of Delta. Both engineering departments informed AIR that in the winter, the groundwater level can be within 1 meter of the surface, while in the summer it can be as low as 2 meters. Groundwater depth in the region also varies depending on location/proximity to bodies of water (e.g. the Fraser River, major drainage ditches, etc.) where the groundwater level can be high year round. This information is used in the development of groundwater depth maps.

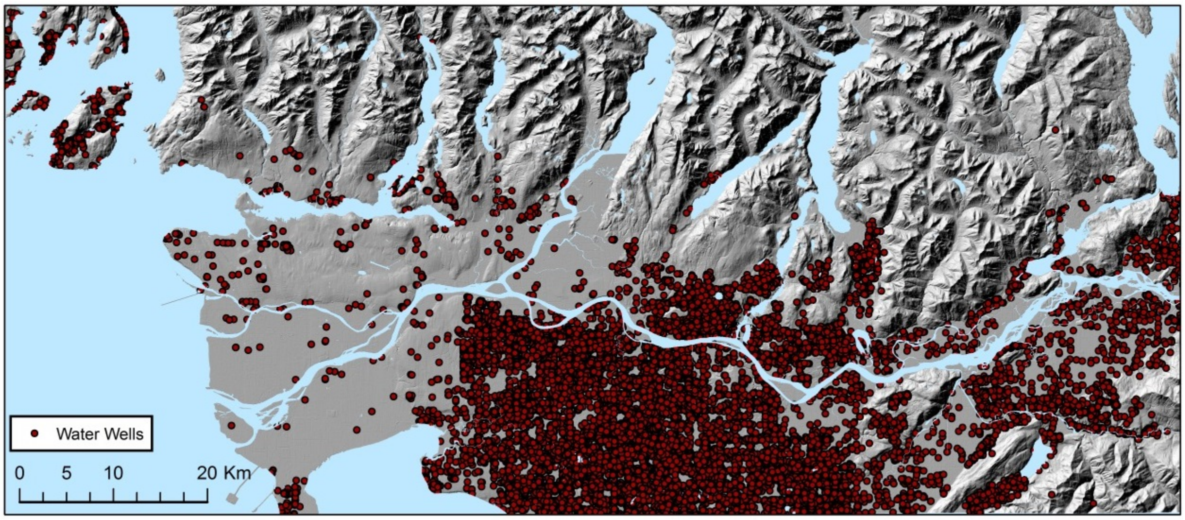

Figure 47. Water well data for Lower Mainland British Columbia

To estimate the groundwater depth at any given site, interpolation on the discrete data is needed to establish a continuous surface of the groundwater table in the region. The interpolation process used by AIR is outlined below.

To make a realistic estimate of the groundwater surface, a comprehensive hydrological model using detailed information on topography, precipitation, the regional water drainage system, and properties of aquifers and surface soils such as thickness, porosity, and conductivity had to be developed. Such a model requires extensive three-dimensional geological and hydrological data, in addition to groundwater well observations. Because liquefaction cannot occur in locations where the water table is deep (>20 meters), it is not necessary to infer deep groundwater depths to accurately calculate liquefaction potential. Therefore, a simplified yet effective method has been developed by AIR researchers to interpolate groundwater depth, especially for areas with a shallow groundwater table.

In the AIR groundwater interpolation process, surface bodies of water such as rivers, lakes and oceans were assigned a water table depth of zero. All surficial aquifers were assumed to be unconfined. A digital elevation model (DEM) was used to convert the depth to groundwater to groundwater elevation above sea level. The Natural Neighbor method was used to interpolate a continuous water elevation surface. This surface was then subtracted from the DEM to determine depth to groundwater for the entire study area. An example of interpolated groundwater depth for the Lower Mainland can be seen in Figure 48. Seasonal fluctuations in groundwater levels are also taken into consideration by analyzing groundwater observation well seasonal data.

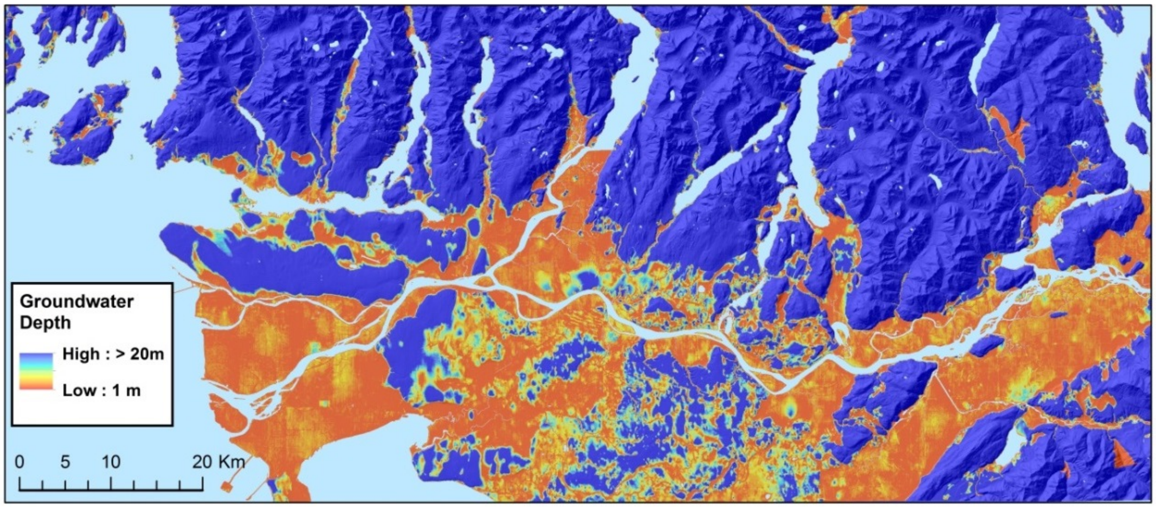

Figure 48. Interpolated depth to groundwater table in Lower Mainland British Columbia

Assessing Liquefaction Potential

Traditionally, geotechnical boreholes have been successfully used for site specific evaluation of liquefaction potential. However, for a regional liquefaction hazard analysis, using specific borehole locations would be impractical because this approach would require a large number of borehole data covering the entire region. To overcome this problem, researchers have long used surficial geological maps for regional mapping of liquefaction hazards (Holzer et al. 2011), as there is a strong correlation between liquefaction susceptibility and surficial geology.

In the development of the regional liquefaction module, published surficial geology maps are compiled from the most recent and best available sources. Then, liquefaction susceptibility maps are developed by characterizing the relative liquefaction susceptibility of each geological unit. This characterization is based on age, depositional environment, and material type of the surficial geological unit (Youd and Perkins, 1978). Each geological unit is assigned to one of five susceptibility classes. At this step, published liquefaction hazard maps are also incorporated into liquefaction susceptibility characterization. It is assumed that relative susceptibility is consistent within each map unit. An example of liquefaction susceptibility map developed for Lower Mainland region can be seen in Figure 49.

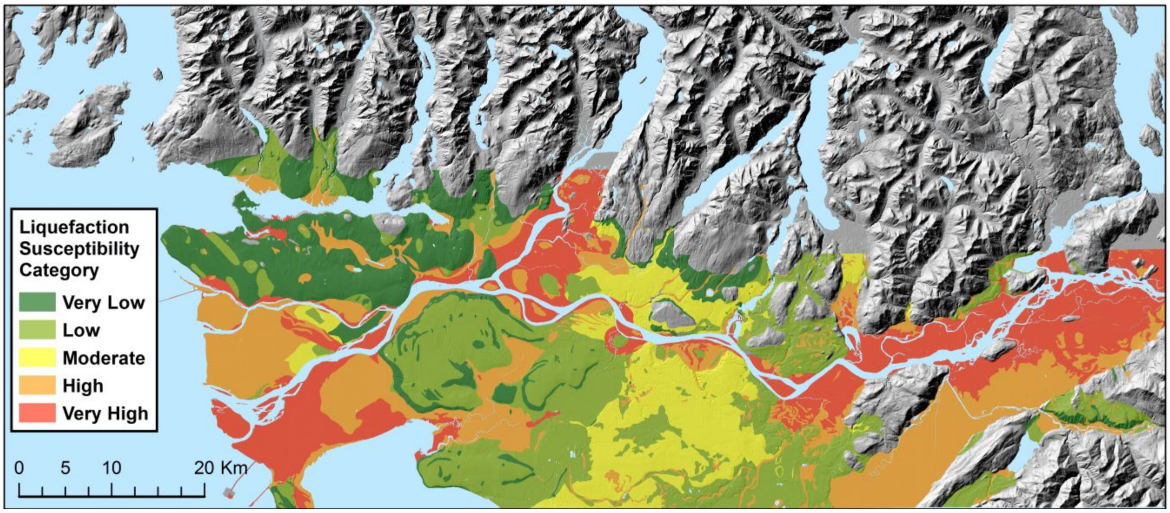

Figure 49. Liquefaction susceptibility in Lower Mainland British Columbia

In the liquefaction module of the AIR Earthquake Model for Canada, the shear-wave velocity of a soil is used as a measure of its physical properties, to calculate the cyclic stress resistance. After a rigorous investigation of all available shear wave velocity profile data from different sources (Hunter et al. 1998; Hunter el al. 2007), representative soil profiles are assigned to each susceptibility category for each region.

The liquefaction intensity estimation method used in the model, which compares liquefaction resistance to liquefaction demand, follows collective research summarized by Idriss and Boulanger (2008) and Andrus and Stokoe (2000). Liquefaction resistance is dominated by soil strength characterized by shear-wave velocity and groundwater depth, while liquefaction demand is a function of ground motion intensity.

For a discussion of how damage due to liquefaction is assessed in the model, see Section 5.6 of this document.

Validating Liquefaction Intensity

Due to the relatively short duration of the historical earthquake record for Canada, no compilations of historical liquefaction occurrence exist for this country. Therefore, no systematic comparison between observed and modeled liquefaction location and severity is possible for Canada. There are, however, some published reports of liquefaction associated with past earthquakes in the region. For example, in 1946, the M7.3 earthquake that shook Vancouver Island and the surrounding region caused extensive liquefaction damage to the wharf and cannery buildings in the community of Kildonan, located in southwest

Vancouver Island (Cassidy et al. 2010). In addition, geological structures indicative of liquefaction, including sand dykes and sand blows, have been observed in the Fraser River delta of Vancouver (Clague et al. 1997).

4.3 Landslide Intensity

Earthquake-triggered landslides can cause loss of life and the destruction of buildings, roads, power lines, and pipelines. Indeed, in some locations, the damage and fatalities caused by earthquake-triggered landslides sometimes exceed those directly inflicted by strong ground shaking and fault rupture (even though ground shaking often causes the majority of the damage attributed to an earthquake). It is therefore important to identify the regions most at risk of experiencing earthquake-triggered landslide hazards. The main objective of regional earthquake-triggered landslide hazard analysis is to evaluate the location of the areas where landslides can be triggered by future earthquakes. The susceptibility of an area to earthquake-triggered landslides can be assessed based on potential ground motion, and geological and topographical conditions.

In the literature, certain regions of Canada have been identified as particularly susceptible to landslides. For example, the Southern Coast Mountains of British Columbia (Blais-Stevens and Hungr, 2008), west central British Columbia (Geertsema et al., 2008) and northern British Columbia (Geertsema et al., 2006) are prone to landslides. As regards earthquake-induced landslides in Canada, historical data show that the 1985 Nahanni earthquakes triggered massive landslides in the Northwest Territories (Cassidy et al., 2010). In addition, historical data show that the 1946 Vancouver Island earthquake (M 7.3) triggered more than 300 landslides over an area of about 20,000 km^2 (Mathews, 1979). Therefore, in the event of a large earthquake, similar slope failures would be expected in the Southern Coast Mountains.

Vital infrastructure is located in these landslide-prone regions of Canada. The main highways, rail lines, and energy transmission lines in southwestern British Columbia pass through landslide susceptible areas, and probably would be blocked by landslides during a strong earthquake. Even though the Vancouver and Victoria urban areas might not be greatly affected by earthquake triggered landslide hazards because of the relatively low relief of these cities, numerous blockages to lifelines over a large area would disrupt economic activity and restrict access to Vancouver (Clague, 2002).

Although eastern Canada is less at risk from landslides than British Columbia, earthquake induced landslides have indeed occurred in eastern Canada (Aylsworth, 2000). For example, the Charlevoix earthquake of 1663 triggered large earthflows in sensitive clay over a wide region of the Saguenay Fjord basin. In addition, the 1988 Saguenay earthquake spawned several landslides as much as 180 km southwest of the epicenter (Ouellet, 2012).

The AIR Earthquake Model for Canada includes a landslide component covering the whole country. Input data for the landslide module includes Digital Elevation Model (DEM) data, surficial and bedrock geological maps, and seasonal precipitation data. DEM information is used to create slope maps, while surficial and bedrock geological maps are used to classify geological units based on their material strength. Precipitation data is used to estimate seasonal fluctuations in water saturation of soils which affects the stability of slopes. By combining the slope map with the geological maps, landslide susceptibility maps for wet and dry seasons can be produced.

Specifically, AIR uses a process-based earthquake-triggered landslide module that relies upon the mechanics of slope failure and employs models of seismic slope stability to assess the deformation of the slope following an earthquake. The infinite slope stability method coupled with Newmark's displacement method (Newmark, 1965) is the most popular process-based model for assessing the earthquake induced landslide susceptibility on a regional scale. The infinite slope model is a one dimensional process-based model which describes the stability of slopes with an infinitely long failure plane. In the Newmark displacement method, the landslide is modeled as a rigid-plastic frictional block resting on an inclined plane. The rigid block has a critical acceleration value which is defined as the minimum base acceleration that is required to overcome shear resistance and initiate sliding. Critical acceleration value depends on the steepness of the slope, the strength of the geological materials, and the groundwater conditions.

Each of these three key components used to determine the critical acceleration value – and hence the likelihood of landslide – are described below. The method used to calculate permanent ground displacement using the critical acceleration value is also described.

Slope Steepness

A key component in the landslide model is the determination of slope steepness. All else being equal, landslide occurrence is more likely on steeper slopes. Slope maps used for the model are derived from DEM data obtained from the Canadian Digital Elevation Data (CDED) and the Shuttle Radar Topography Mission (SRTM). CDED is provided by GeoBase. GeoBase is a federal, provincial and territorial government initiative that is overseen by the Canadian Council on Geomatics. The CDED is provided at scales of 1:50,000 and 1:250,000. Depending on the latitude of the CDED section, the grid resolution varies from 8 to 23 meters for the 1:50,000 National Topographic System (NTS) tiles, and from 32 to 93 meters for the 1:250,000 NTS tiles. SRTM is an international research effort that obtained DEM on a near-global scale from 56° S to 60° N. SRTM resolution for Canada is 3 arcsecond.

For six highly populated urban areas in Canada, CDED is used at 1:50,000 scale. These six regions are the Lower Mainland, Metro Victoria Area, Greater Toronto Area, National Capital Region, Greater Montreal Area, and Quebec City. For the rest of the country, SRTM data is used south of 60° N and CDED at a 1:250,000 scale is used north of 60° N. The slope is derived from DEM by calculating the maximum rate of change between each cell and its neighbors. Slope data is then grouped into eight slope classifications to be used in the slope map. An example of the slope map derived for the Lower Mainland region from CDED at 1:50,000 scale can be seen in Figure 50.

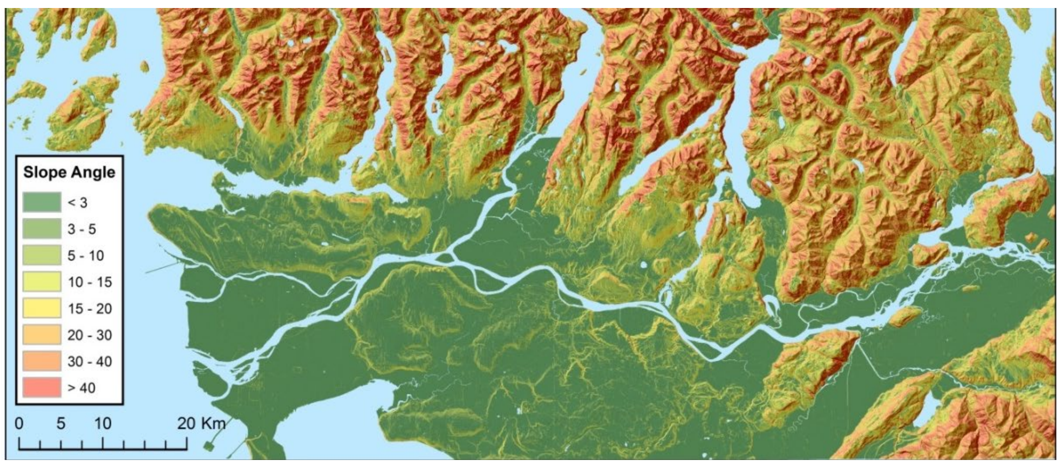

Figure 50. Slope Map for Lower Mainland derived from CDED (1:50,000)

Strength of Underlying Earth Material

In addition to the steepness of the slope, landslide occurrence is directly related to the strength of the earth material. AIR model uses the relationship proposed by Wilson and Keefer (1985) to categorize geological map units into one of the following three groups:

- **Geological Group A:** Strongly Cemented Rocks (crystalline rocks and well-cemented sandstones)
- **Geological Group B:** Weakly Cemented Rocks and Soils (sandy soils and poorly cemented sandstone);
- **Geological Group C:** Argillaceous Rocks (shales, clayey soil, existing landslides, poorly compacted fills).

After a careful analysis of all the available bedrock and surficial geological maps for Canada, AIR engineers assigned geological groups to each map unit. An example of the assigned geological groups for the Lower Mainland region can be seen in Figure 51.

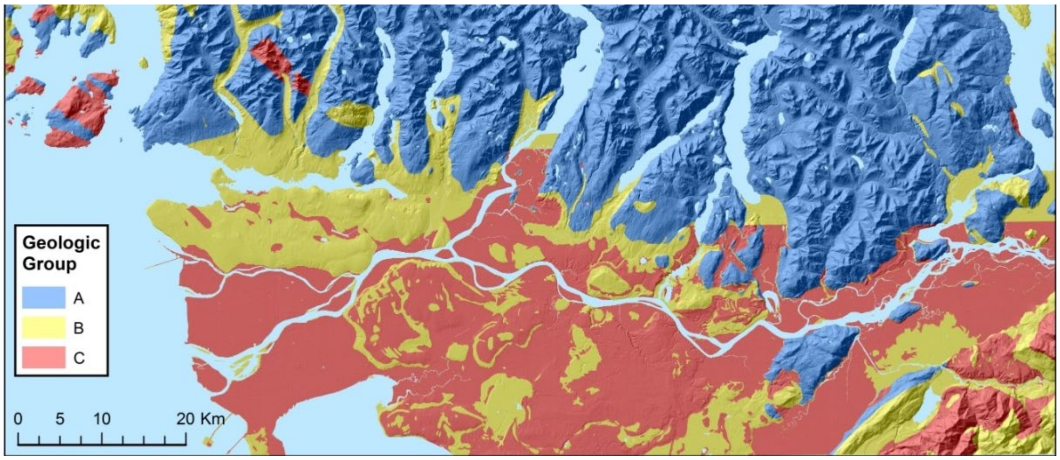

Figure 51. Geological Groups for Lower Mainland

Effect of Groundwater Conditions on Landslide Susceptibility

The geologic group map is then intersected with the slope map to create landslide susceptibility map according to the approach presented by Wilson and Keefer (1985). Wilson and Keefer (1985) defines ten landslide (I through X) susceptibility classes based on various combinations of eight slope category and three geologic groups. This approach also considers the dry and wet conditions because water saturation of soils affects the strength of the geological material.

Dry and wet conditions are defined as the conditions where the groundwater is below the level of sliding, and at the ground surface, respectively. Table 14 is used to assign the landslide susceptibility classes based on geological group and slope angle. An example of the landslide susceptibility maps for the Lower Mainland region for dry and wet conditions can be seen in Figure 52 and Figure 53. Comparison of Figure 52 and Figure 53 reveals that landslide susceptibility class is highly dependent on dry and wet conditions. In the AIR model, precipitation data obtained from a Canadian government website (http://climate.weather.gc.ca/) were used to estimate seasonal fluctuations in the water saturation of soils. Depending on the month of the year, landslide hazard is interpolated between the two extreme values corresponding to dry and wet conditions.

Table 14. Landslide susceptibility categories (modified from Solomon et al. 2004)

Geologic Group	Landslide Susceptibility Categories (Dry/Wet)							
	Slope Angle (°)							
	0-3	3-5	5-10	10-15	15-20	20-30	30-40	>40
A	None/None	None/None	None/None	None/III	I/VI	II/VII	IV/VIII	VI/VIII
B	None/None	None/None	None/V	II/VIII	IV/IX	V/IX	V/IX	VII/X
C	None/None	None/VII	V/VII	VI/IX	VI/X	IX/X	IX/X	IX/X

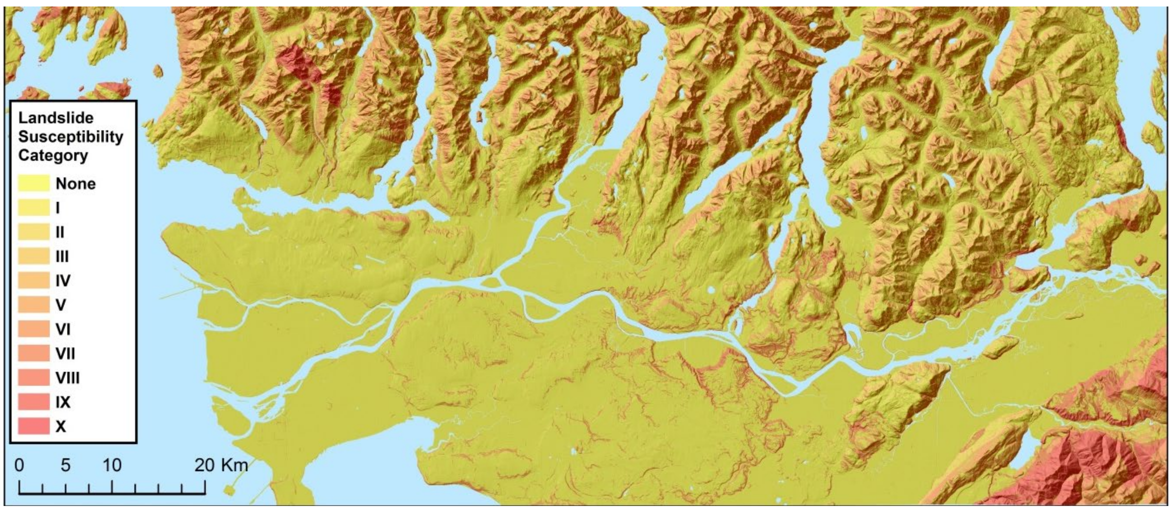

Figure 52. Landslide Susceptibility Map for Lower Mainland (Dry Conditions)

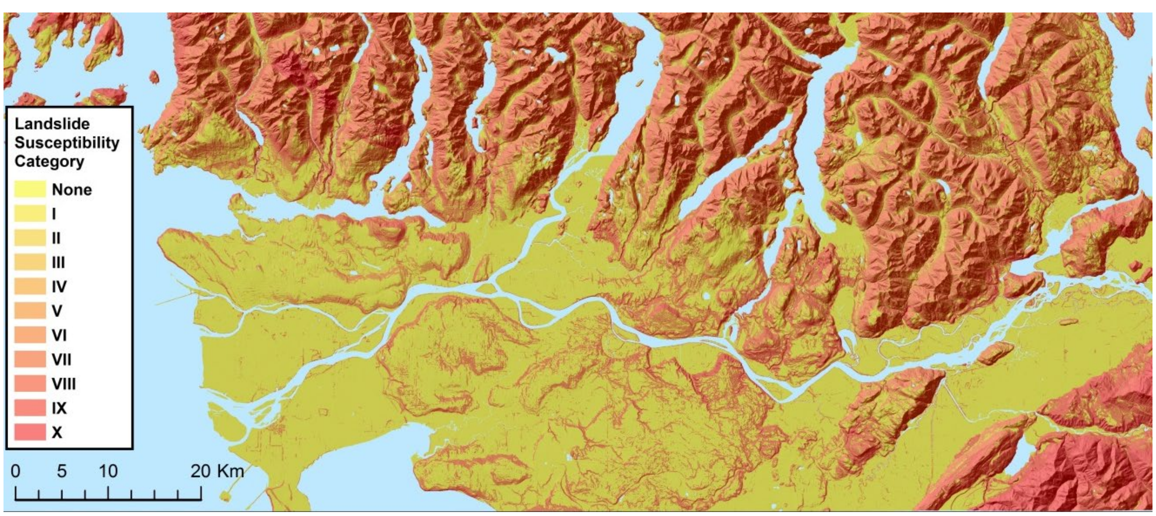

Figure 53. Landslide Susceptibility Map for Lower Mainland (Wet Conditions)

Table 15 relates each landslide susceptibility category to a critical acceleration value (i.e., the amount of ground acceleration needed to initiate downslope movement). Using the critical acceleration value and ground motion for a particular area, permanent ground displacements can be calculated.

Table 15. Critical acceleration values for different susceptibility classes

Susceptibility Category	None	I	II	III	IV	V	VI	VII	VIII	IX	X
Critical Acceleration (g)	None	0.60	0.50	0.40	0.35	0.30	0.25	0.20	0.15	0.10	0.05

Calculating Permanent Ground Displacement Due to Landslide

The permanent ground displacement due to landslides can be calculated using an approach developed by Newmark (1965). This method calculates the permanent displacement of a sliding block subjected to an earthquake acceleration time history. However, creating acceleration time histories for each location in a regional landslide hazard analysis is not feasible. Therefore, the AIR model uses an empirical relationship between critical acceleration values, Arias intensity and permanent displacement established by Jibson et al. (2000). Arias intensity is a measure of total shaking intensity developed by Arias (1970). The empirical equation is:

$$\log D_n = 1.521 \log I_a - 1.993 \log a_c - 1.546$$

where:

D_n = Newmark displacement in centimeters.

I_a = Arias intensity, in meters per second.

a_c = Critical acceleration, in g.

This equation requires values for critical acceleration and Arias intensity to calculate the permanent ground displacement. Critical acceleration values can be determined for each landslide susceptibility category using Table 15. Arias intensity is estimated using ground motion prediction equations defined by Wilson and Keefer (1985) and Jibson (1993). It is important to note that Newmark displacement is considered a relative index of slope performance, rather than an estimation of real-world deformation (Jibson et al. 1998).

It has been pointed out that relationships developed by Wilson and Keefer (1985) are conservative because they represent the most landslide-susceptible materials likely to be found in the geological unit (Wieczorek et al., 1985). Jibson and others (2000) estimate the probability of slope failure by comparing predicted Newmark displacements with an inventory of landslides triggered by the Northridge earthquake. The AIR model uses the equation of Jibson et al. (2000) to calculate the probability of landslide:

$$P(f) = 0.335[1 - \exp(-0.048 {D_n}^{1.565})]$$

where:

$P(f)$ = the proportion of grid cells occupied by landslide-source areas.

D_n = Newmark displacement in centimeters.

After calculating the permanent ground displacements, damage functions are used to calculate the damage to structures. For an overview of the damage functions used for the landslide module, see Section 5.8 in this document.

Validating Landslide Intensity

Due the relatively short duration of the Canadian historical earthquake record, and the sparse reports of damage inflicted by those earthquakes for which records do exist, there is no compilation of historical earthquake-induced landslides available for Canada. Therefore, a systematic comparison of the location and severity of modeled and observed earthquake-induced landslides is not possible for Canada. However, there are historical earthquakes known to have caused landslides in Canada. For example, the M6.6, M6.9, and M6.2 earthquakes of the Nahanni Range of the Northwest Territories – part of an unusual earthquake series that struck the region from 1985 to 1989 – are known to have triggered massive landslides (Cassidy et al., 2010). In addition, the M7.3 1946 Vancouver Island earthquake triggered more than 300 landslides over an area of about 20,000 km^2, according to historical records (Mathews, 1979).

4.4 Tsunami Intensity

The AIR Earthquake Model for Canada uses a modified version of TUNAMI[4] (Tohoku University's Numerical Analysis Model for Investigation of Near-field tsunamis) to perform tsunami simulations for modeled earthquakes that affect Canada. It is important to note that only stochastic events produced by seismic sources offshore of western North America – particularly the Cascadia subduction

[4] TUNAMI is a well-known numerical model that can simulate tsunamis within multiple high resolution domains. It is based on the Navier-Stokes equations, which describe the spatio-temporal motion of fluids.

zone and the Alaska-Aleutian subduction zone – are considered to pose tsunami risk to Canada in the AIR model. There is no modeled tsunami risk for eastern Canada.

The AIR model employs high resolution bathymetry, elevation, land use/land cover (LULC), and levee location and height data to estimate the intensity of tsunamis resulting from events of the stochastic catalog according to the following general procedure:

- An event of the stochastic catalog results in vertical displacement of the ocean floor and thus equal vertical displacement of the overlying water column, which initiates a tsunami;
- To determine how the tsunami wave propagates away from the epicenter, equations of motion for wave height and velocity are integrated forward in time on a high resolution grid using a numerical model;
- As the tsunami approaches the coast, high resolution bathymetry data are used to calculate how the tsunami characteristics change, e.g., its speed decreases, its height increases, and its wavelength decreases;
- As the tsunami washes onshore, friction (assessed using Manning coefficients), terrain elevation, and the shape of the coastline determine the tsunami's inundation extent and effective inundation depth (which captures both inundation depth and wave speed). The potential for levee failure and the influence of astronomical tides are included in these calculations as well.

In the AIR model, tsunami intensity is indicated by tsunami effective inundation depth. Details of the modeling procedure used to estimate tsunami intensity, and the data sources used in the model, are provided below. Text and exhibits are also provided that validate the modeled tsunami inundation heights.

Bathymetry, Elevation, and Friction

After an event of the stochastic catalog triggers a tsunami, the tsunami propagates outward through the ocean in all directions. In the deep ocean, friction has little effect on tsunami propagation; the model therefore uses linear dynamics to model the tsunami at this point.

As the tsunami wave approaches the coastline, the decreasing ocean depth and the increasing effects from friction along the ocean floor slow the speed of the wave, decreasing its wavelength and increasing its amplitude. As the wave travels inland, it passes over a variety of surfaces and hence its flow becomes even more complex. Therefore, to accurately model tsunami wave propagation and inundation, high-resolution bathymetry, elevation, and land use land cover (LULC) data are required.

In the AIR Earthquake Model for Canada, AIR researchers used four data sources to produce a comprehensive, high-resolution (250-meter grid) bathymetry dataset. These data sources are:

- National Geophysical Data Center (NGDC) ETOPO1[5], a 1 arc-minute global relief dataset;
- Southern Alaska Coastal Relief Model[6], a 24 arc-second dataset of relief data for the Gulf of Alaska, Bering Sea, and the Aleutian Islands;
- The NOAA Center for Tsunami Research digital elevation model for the Strait of Juan de Fuca[7], available on a 5 arc-second grid;
- The NOAA Center for Tsunami Research digital elevation model for Northern California[8], available on a 36 arc-second grid.

To capture bathymetry in the modeled region, these four datasets were merged by interpolating each to a 250-m grid. In geographic regions where these data sources overlap, only the highest-resolution values are used in the model.

A similar process was used to create a high resolution land elevation dataset, which is critically important for modeling tsunami inundation extent and depth. AIR researchers merged two datasets to produce a single high resolution (70-m grid) elevation dataset. Where more than one layer of elevation data is available, the AIR model uses only the highest-resolution data in the merged dataset. These two datasets were obtained from:

- United States Geological Survey (30-meter grid);
- GeoBase Canada (23-meter grid).

To determine the effects of friction as a simulated tsunami propagates, the AIR model uses the Manning coefficient n, where:

$$n = \sqrt{\frac{fD^{1/3}}{2g}}$$

Where D is the total depth and f is the friction coefficient defined as:

$$f = \frac{2gn^2}{D^{1/3}}$$

The friction coefficient is used to determine the effects of the ocean floor, or the ground, on the tsunami wave characteristics. As the tsunami enters shallower water (D decreases) the effects of the ocean floor become more pronounced (f

[5] Dataset and further information available at: http://www.ngdc.noaa.gov/mgg/global/global.html
[6] Dataset and further information available at: http://www.ngdc.noaa.gov/mgg/coastal/s_alaska.html
[7] Dataset and further information available at: http://www.ngdc.noaa.gov/dem/squareCellGrid/download/655
[8] Dataset and further information available at: http://www.ngdc.noaa.gov/dem/squareCellGrid/download/649

increases). As a result, both the wave amplitude and speed, and hence the inundation distance from the coast, are affected by *n*.

AIR researchers developed Manning coefficients using 150-meter resolution land use/land cover (LULC) data from the Commission for Environmental Cooperation North American Environmental Atlas (compiled in 2005)[9], along with Manning coefficients associated with these LULC types obtained from the published literature, such as Engman (1986) and Senarath et al. (2000). The Manning coefficients used in the AIR model are shown in Table 16. For each high resolution (125 m) tsunami grid cell of the model domain, the Manning coefficient was calculated as the mean of all of the Manning coefficients assigned to the 150-meter LULC cells within the tsunami grid cell.

Table 16. Manning coefficients used for selected LULC categories in the AIR model

LULC Category	Manning Coefficient
Mixed Forest	0.20
Wetland	0.05
Deciduous Forest	0.20
Grassland	0.05
Urban	0.05
Shrubland	0.05
Barren Land	0.025
Water	0.025
Moss	0.05
Snow and Ice	0.01
Needleleaf Forest	0.20
Cropland	0.05

An example of the LULC data in the Vancouver region, which shows the high level of detail available, is shown in Figure 54.

[9] Dataset and further information available at: http://www.cec.org/Page.asp?PageID=924&ContentID=2336

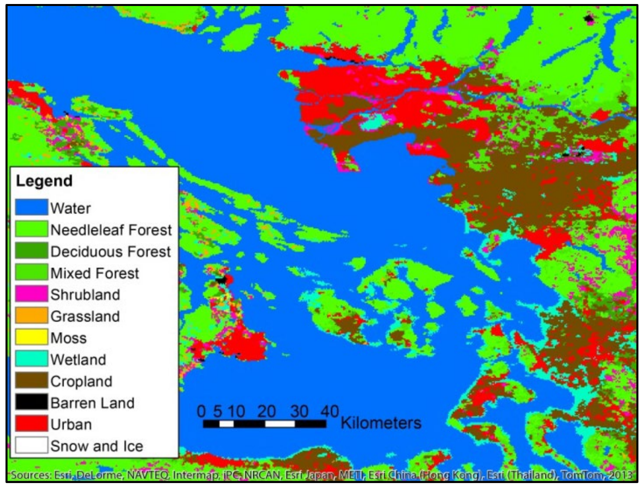

Figure 54. LULC categories in the Vancouver region

Effective Inundation Depth

When modeling tsunami damage and loss, AIR researchers account for the water's hydrostatic pressure and hydrodynamic force. In order to account for these effects, it was necessary for AIR researchers to account for both the depth of the tsunami wave once it is near-shore or on land as well as its speed. These two parameters can be combined into a single one called the effective inundation depth, d':

d'= d + $v^2/2g$

Where
d = depth
v = current speed
g = gravitational constant

In the AIR tsunami model, the effective inundation depth is tracked at every modeled time step, at every point on land as well as along adjacent waterways (e.g., harbors, channels, ports). The maximum effective inundation depth is used to estimate the damage and loss to exposures within the tsunami footprint.

Tsunami Flow Intensity and Water Depth

The shape of the coastline has a significant effect on inundation as the bays and inlets along a jagged coastline can amplify tsunami waves. At the same time however, the mountainous areas usually associated with jagged coastlines are associated with a sharper increase in elevation, which prevents inland extent of tsunamis.

The effect of elevation is significant; observations from several tsunamis show a sharp drop in tsunami damage with just a slight change in elevation. An example of the effect of elevation is shown in Figure 55, which shows the sharp drop in damage at elevations above the inundation height in a mountainous region after the Tohoku, Japan tsunami of March 2011.

Figure 55. Inundation height is indicated by the sudden decrease in damage at Taro, Miyako, Iwate Prefecture, from the 2011 Tohoku tsunami

The Effect of Astronomical Tides on Tsunami Inundation

A tsunami's inundation depth at a given location can be significantly affected by the phase of the astronomical tide at that location. Given that typical tidal amplitudes for British Columbia range from 1 meter to 3.5 meters, a high tide could potentially turn an otherwise 1 meter tsunami into a loss-causing event. The same tsunami at low tide, however, would probably not cause any damage.

To account for tides in the tsunami portion of the AIR Earthquake Model for Canada, AIR researchers specified a background tide value for each 125-meter resolution model domain along the coastline that depended on the Julian day and hour of the event. The specified values for a given event across adjacent domains reflect observed phase differences. (That is, it typically isn't high tide at exactly the same time for two locations that are hundreds of kilometers apart.) The background tide value was then subtracted from the grid cell's elevation, yielding a realistic "background ocean state" for each coastline grid cell. Therefore, the AIR model allows the background tide to influence tsunami extent as well as the tsunami inundation depth over inland exposure.

Modeling Levees and Levee Failure

The AIR tsunami model takes into account the presence of levees and the possibility of a breach or overtopping. Levee failure is modeled probabilistically as a function of the hydrodynamic force of the tsunami, and a randomness component that accounts for unknown information about each levee's construction. The data sources used to obtain levee locations, and further details about the probabilistic method used to model levee failure due to tsunamis, are provided below.

To determine the location of levees in the modeled region, AIR researchers digitized levee data provided by the British Columbia Ministry of Forests, Lands, and Natural Resource Operations. Aerial imagery from these sources, along with Google Streetview and observations from local neighborhood councils, were also used to identify and validate levee locations. For British Columbia, 718 kilometers of levees and seawalls were digitized. The location of these structures is shown in Figure 56 and Figure 57.

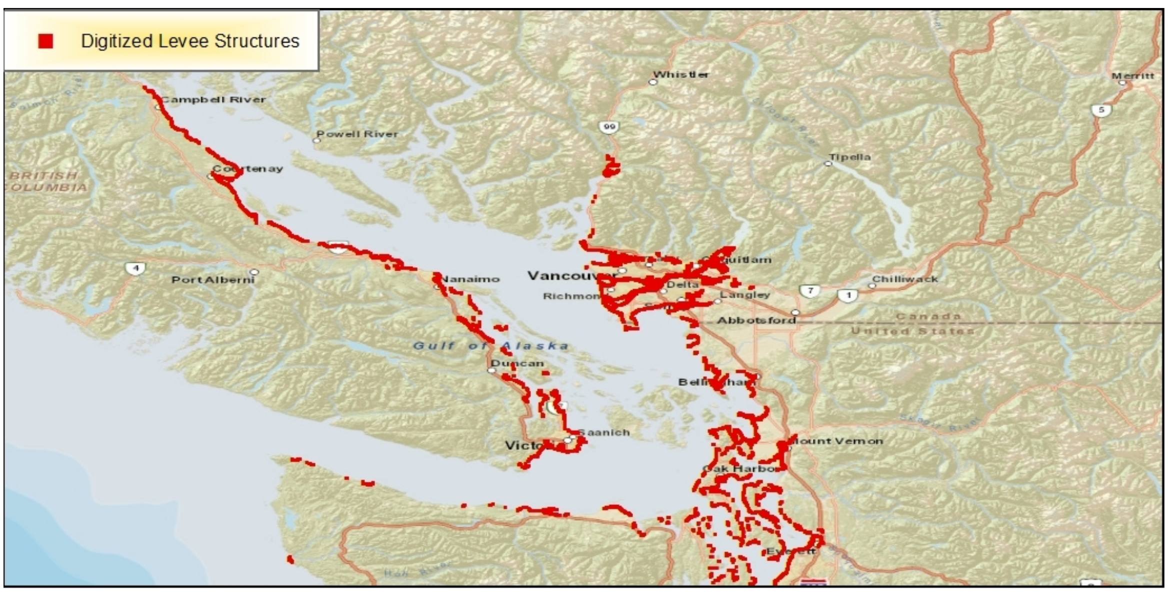

Figure 56. Location of digitized levee structures in the near Vancouver

Figure 57. Location of digitized levee structures zoomed in on Vancouver

However, site-specific levee height was not available. Therefore, AIR researchers assumed that all levee structures included in the model are 2 meters high relative to the land on which they are located. These assumed levee heights were then incorporated into the 125-meter coastal grid cells by adding 2 meters of elevation to the terrain in the cells where the levees are found.

Levee failure was then modeled probabilistically as a function of the hydrodynamic force of the tsunami and a randomness component that accounts for unknown information about each levee's construction. The hydrodynamic force, F, is a function of the drag and density of water, current velocity, and water depth:

$$F = 0.5 * C_p * \rho * v^2 * d / 1000$$

Where:

F is the hydrodynamic force (kN/m),
C_p is the drag coefficient (dimensionless) assumed to be equal to 1.0,
ρ is the sea water density (1025 kg/m^3),
v is the current velocity (m/s) normal to the levee, and
d is the water depth (m).

Using this equation, the model calculates the hydrodynamic force on each levee every two seconds and evaluates the probability of levee failure. This evaluation is achieved using modifications of published fragility curves (e.g. Suppasri et al. 2011) that relate the likelihood of levee failure to the hydrodynamic force experienced by the levee. An example of one of these fragility curves is shown in

Figure 58. Note that the published fragility curves were adjusted by AIR to reflect the fact that the tsunami produced by the Tohoku, Japan earthquake of 2011 destroyed 40-60% of the levees it impacted.

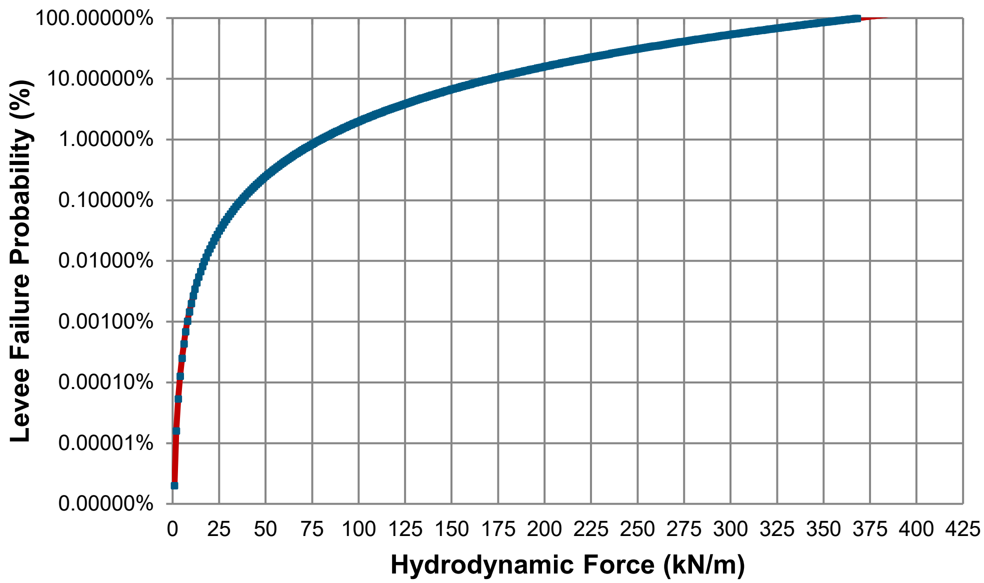

Figure 58. Hydrodynamic force versus levee failure probability

However, to account for unknown characteristics of the levee – such as levee height, construction material, and levee age – and ensure that each levee has a unique probability of failure when subjected to a given hydrodynamic force, the model uses a random draw process. If the random draw is less than the levee failure probability for a given hydrodynamic force (Figure 58), the levee will fail. Upon levee failure, the model subtracts two meters from the grid elevation, and flags the grid cell so that it cannot experience levee failure again for that particular simulated event. If the levee remains intact, no change is made to the grid cell elevation at that time in the simulation.

Validation of Tsunami Inundation Height

To validate the tsunami inundation heights produced by the AIR model, AIR researchers compare modeled maximum inundation heights[10] for historical tsunamis to actual observations of maximum tsunami inundation from these historical events. However, while large tsunamis are known to have occurred historically within the model domain (such as the M9.0 megathrust Cascadia subduction zone earthquake that occurred in 1700), written records of these

[10] Note that for tsunami hazard validation, effective inundation height is used rather than depth.

events and the damage they inflicted are sparse. In fact, just one historical event has produced a significant and damaging tsunami[11] in the model domain: the M9.2 Alaska earthquake of 1964. Therefore, the AIR method is validated by comparing the modeled and observed maximum tsunami inundation for the M9.2 Alaska event. However, it is important to recognize that the AIR tsunami model has also been extensively validated for the Japan region, where a wealth of tsunami observational data is available.

1964 M9.2 Alaska Earthquake and Tsunami

On March 27, 1964, the world's second largest earthquake of the twentieth century was produced by slip along the Alaska-Aleutian subduction zone. This event triggered a tsunami that caused widespread destruction and loss of life around the Pacific basin, particularly in Hawaii and Japan. Communities in coastal British Columbia were also affected by this event.

Figure 59 compares the modeled maximum inundation height (top) to observed maximum wave heights (bottom) in British Columbia from the tsunami produced by the M9.2 1964 Alaska earthquake. Note the good agreement between the modeled and observed wave heights (where observational data are available). For example, in Port Alberni, observed tsunami wave height from the 1964 earthquake was 2.6 meters (see bottom panel of the figure); the AIR tsunami model yields an estimated water elevation of 2.01-2.5 meters in this location (see top panel of the figure).

[11] The M9.5 Chile earthquake of 1960 produced a tsunami with a wave height of 1.26 meters in the British Columbia region, but this tsunami did not cause significant damage to exposures in Canada.

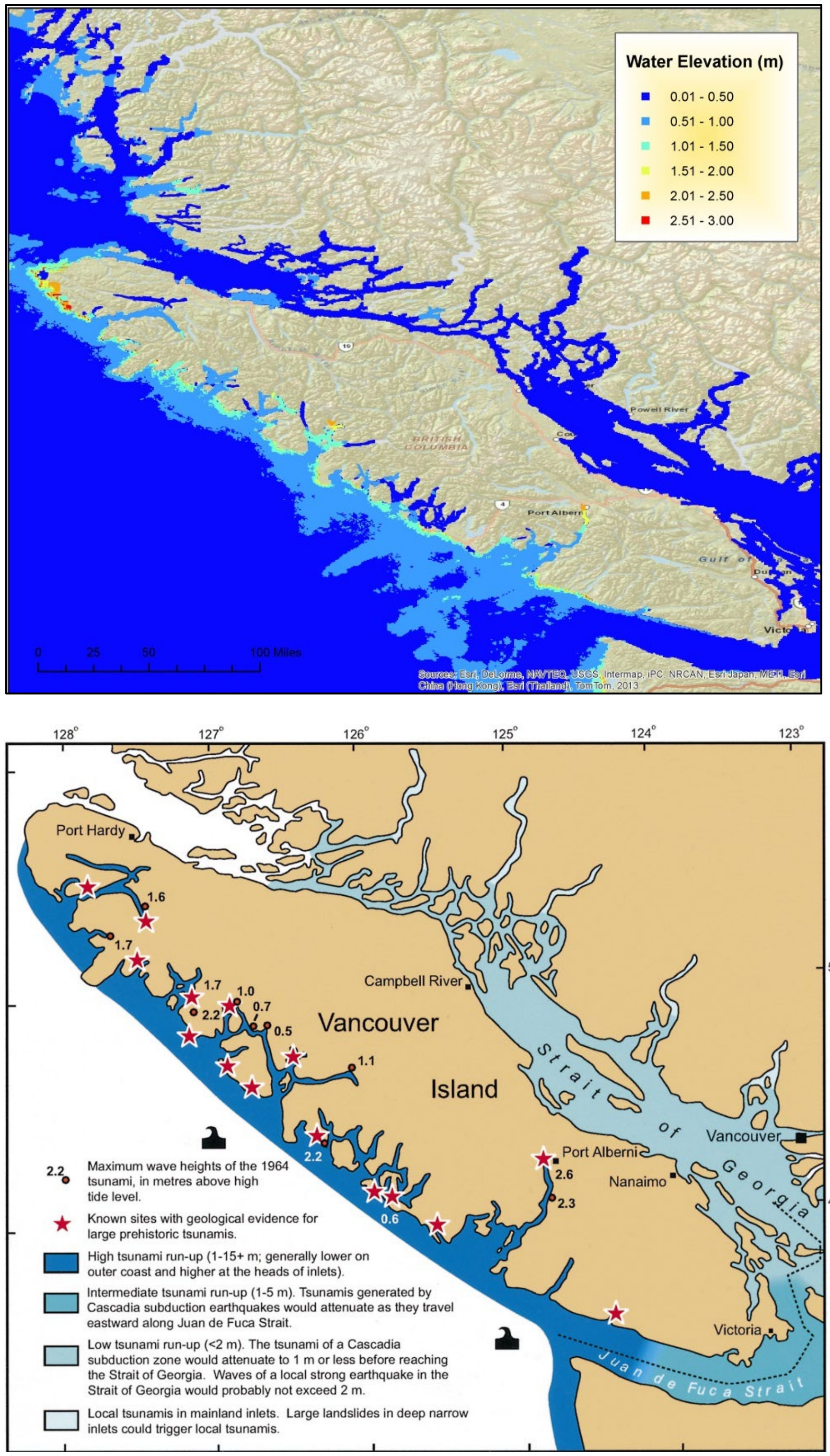

Figure 59. Modeled (top; in meters) and observed (bottom; observed tsunami heights are labeled [Source: Clague et al. 2000]) maximum tsunami inundation heights in British Columbia triggered by the 1964 M9.2 Alaska earthquake

5 Damage Estimation

The damage estimation component of the AIR Earthquake Model for Canada translates the intensity of each modeled peril – ground shaking, tsunami, liquefaction, landslides, and fire following earthquake – into expected damage. Once the intensity of each peril is determined at the site of the exposures, expected damage is estimated using damage functions appropriate for the exposure type[12]. A damage function is a statistical relationship between peril intensity and the mean damage ratio (where the damage ratio is defined as the fraction of the replacement cost of an asset needed to repair the damage).

The AIR Earthquake Model for Canada estimates damage to residential and commercial buildings, vehicles, infrastructure, and industrial facilities inflicted by earthquake ground shaking, fire following, liquefaction, landslides, and tsunamis. While an ideal vulnerability assessment would entail sophisticated structural analysis of individual buildings, such analysis is not feasible in regional loss estimation. Therefore, in the AIR model, damage estimation is achieved by grouping buildings based on their seismic behavior (which is characterized by construction materials, lateral force structural resisting systems, building height, and building age), and determining the seismic vulnerability of these groups rather than the vulnerability of individual structures.

The damage functions for the model were developed based on the study of buildings in Canada and their vulnerability, with adjustments made to reflect the evolution of building codes and construction quality. Therefore, the damage functions reflect local construction practices, the quality of construction materials, building height, and the year built of each property. (For buildings with "unknown" attributes, vulnerability is calculated as a weighted average of the vulnerability of buildings with known attributes.)

The following sections describe how damage estimation is accomplished for each exposure type using damage functions specific to each peril. These sections also provide background information about building types in Canada and their seismic resistance, as well as how building codes in Canada have been revised over time in response to perceived seismic risk.

[12] Exposure types included in the AIR model are buildings, contents, appurtenant structures, and business interruption.

5.1 Building Types in Canada and Their Seismic Resistance

Residential

Approximately 75% of residential buildings in Canada are of wood frame construction; the second most common residential structure type in Canada is masonry. However, there are regional differences in the frequency of these construction types across Canada. In general, wood frame homes make up a greater proportion of residential structures in Western Canada, compared to Eastern Canada, where masonry homes are not uncommon. For example, in British Columbia, over 90% of homes are wood frame and less than 10% are built of masonry or other materials. In contrast, nearly 40% of homes in Quebec are built of masonry.

A typical single family house of wood construction in Canada consists of a timber frame with horizontal wood plates forming the floors and vertical wood plates used as internal and external walls. The ground floor normally includes a platform of joists covered with plywood supported on a concrete foundation directly using anchor bolts or indirectly with cripple walls. The roof structure consists of prefabricated trusses covered with sheathing and roof tiles. According to Ventura and Kharrazi (2002), three distinct age groups can be identified for these buildings in Canada: pre-1940, 1940-1980, and post-1980. These age groups correspond to changes in wood production technology that affect the seismic performance of these buildings. For example, wood frame homes built between 1940 and 1980 reflect a shift in sheathing products from boards to panels such as plywood, with a resultant change in wall performance. Some popular construction styles that date from this time period are the post-and-beam homes of the 1950s, the "Vancouver Special"[13] of the late 1950s to the mid-1960s, and the "monster homes" of the 1980s.

In Canada, the majority of multi-unit residential buildings up to four stories are of wood construction. These buildings have numerous interior load-bearing walls, and their exterior walls are clad with wood, brick veneer, or metal. Prior to the late 1960s and early 1970s, these buildings were usually constructed without underground parking. After the 1970s, however, most of the multi-unit wood construction in Canada includes an underground concrete parking level.

[13] A "Vancouver Special" home is characterized by a low-pitched roof, an overall boxy shape, and a balcony across the front of the building.

Wood construction has historically performed well in earthquakes, due to its light weight and high material strength. Nail connections in wood frame construction allow flexibility, and thus permit wood structures to absorb large amounts of energy during earthquake shaking compared to other building types. Attachment of sheathing and finishes to wood joists and studs using numerous connections provides more redundancy in transferring earthquake forces to the building's base. Furthermore, the interaction of structural panels with the wood frame provides some shear wall-like effects and improves seismic resistance. According to the Canadian Wood Council, a typical shortcoming of wood construction is the existence of weak or soft first stories, often due to the use of first-floor space as a garage or storage area. Weak connections to the foundation, the use of cripple walls, and weak and/or heavy chimneys are other possible drawbacks associated with wood construction.

Commercial and Industrial

Most commercial and industrial buildings in Canada are constructed of masonry (36%), or wood (23%); however, reinforced concrete and steel are also used. A brief overview of the most common construction types in commercial and industrial structures in Canada is provided below.

While reinforced concrete moment resisting frames are not very common in Canada, concrete frames with infill walls and concrete frames with shear walls are common in commercial and industrial buildings. Concrete frames with masonry infill (for example, office buildings built before 1950) are not designed for seismic forces and do not perform well in earthquakes. In contrast, concrete frame buildings erected after 1985 generally behave well. However, these buildings often experience damage to cladding and other nonstructural damage when they are exposed to earthquake ground shaking.

Commercial and industrial masonry structures in Canada include unreinforced masonry (URM) and reinforced masonry. In general, commercial and industrial buildings of URM are common only in older Canadian cities such as Vancouver and Quebec City (however, many of these buildings have been seismically retrofitted). Specifically, prior to 1940, commercial buildings of four to six stories were often built of URM. In addition, URM was used for commercial and industrial buildings up to three stories in height until the early 1970s in Canada. URM buildings rely on masonry walls alone to resist both gravity and lateral loads, and have performed poorly in past earthquakes around the world. In fact, since 1973, the National Building Code of Canada (NBCC) has required that all masonry buildings in seismically active areas (such as most of British Columbia) be built with reinforcements.

Reinforced masonry is a very common construction type for industrial and commercial buildings in Canada. The seismic performance of reinforced masonry buildings is notably improved compared to URM. Although reinforced masonry walls can generally withstand ground shaking, the connection of the floors to the walls is usually a weak point, especially in pre-1985 buildings. Reinforced masonry buildings with storefront openings and and/or flexible diaphragms tend to be damaged due to torsional effects. Nonstructural and glazing (window) damage are examples of other common problems in these buildings.

Steel construction is also often used in industrial buildings in Canada. In particular, steel frames with concrete walls have frequently been used in low-rise industrial buildings after the 1970s, as well as in office towers. These types of buildings rely on both steel frames and concrete shear walls (mainly located around the elevator shafts, staircases, or along the building perimeter) to resist lateral loads, and thus perform well in earthquakes. Post-1985 buildings of this type perform well under ground shaking, especially if the walls are distributed. Seismic damage in these buildings is often caused by torsional effects.

Wood construction in the commercial and industrial sector often includes one or two story buildings with wood-frame exterior walls and cladding of wood or vinyl siding, plaster, brick veneer, or metal. Large buildings of this type are usually divided into segments by masonry fire walls (Ventura et al., 2005). Like residential wood structures, commercial and industrial wood construction tends to stand up well to ground shaking due to wood's light weight, flexibility, and high material strength.

Infrastructure

Assessing the seismic vulnerability of infrastructure is challenging because different types of infrastructure behave differently in an earthquake. For example, damage to roads and railroads is primarily related to ground failure; in contrast, damage to bridges is more complex and depends on the response of various structural elements. In addition, the seismic vulnerability of pipelines, which are major components of "lifeline" infrastructure, varies by how they are built. Specifically, a pipeline that is buried underground is highly sensitive to ground failure, while the vulnerability of an aboveground pipeline that is supported on trestles or pipe racks is a function of these structures' response to ground shaking.

Due to these differences, infrastructure is generally organized into three categories as regards seismic vulnerability: transportation systems such as highways, railroads, and mass transit; utility systems including electricity, communications, natural gas, and water lines; and high potential loss facilities such as dams and nuclear power plants.

In the AIR Earthquake Model for Canada, infrastructure of all three categories is included. For example, transportation systems and utility systems, such as bridges, railroads, highways, runways, tunnels, electrical transmission towers, telecommunication systems, and pipelines (both at-grade and underground) are included. While concrete and earthfill dams are also included in the model, nuclear power plants are not.

For further details about the types of infrastructure included in the model, refer to Section 8 of this document.

Industrial Facilities

The type of exposures that AIR classifies as industrial facilities include high-value[14] industrial sites such as large scale manufacturing, oil refining, metal smelting, and many others. Industrial facilities differ from the commercial and industrial buildings described above in that industrial facilities represent large-scale operations characterized by extensive machinery and a wide variety of distinct components.

It is important to recognize that the vulnerability of industrial facilities does not vary as much as the vulnerability of other buildings that comply with national standards. Two features of industrial facilities account for this fact. First, industrial facilities are better engineered that most other building types, as industrial facilities are constructed based on international, rather than national, standards. Second, the structural design of many industrial components is often governed by their function (i.e., the loads imposed by the processes the component facilitates), rather than their lateral resistance to earthquake loads. Thus, the vulnerability of industrial facilities is not as variable as that of other buildings constructed to national standards.

In order to model earthquake damage to industrial facilities in Canada, AIR employs modified versions of damage functions that were created for the AIR Earthquake Model for the United States. During development of the United States earthquake model, AIR formulated damage functions for industrial facilities using a component-based approach; specifically, AIR determined damage functions for a facility's individual components and then combined them to yield a single damage function for the whole facility. This approach accounts for more

[14] Industrial facilities have a replacement value of over USD 5 million, as defined by AIR.

than 550 primary components intrinsic to industrial facilities, as well as the interconnectivity between these components and their subcomponents. These components – which include generators, circuit breakers, pipelines, silos, transformers, and loading structures (cranes/conveyor systems), and many others – were selected from structural drawings, design specifications, and other sources.

In the AIR Earthquake Model for the United States, originally, three suites of damage functions were developed for different seismic zones. One suite of damage functions was used to estimate damage to industrial facilities in California, a second suite was used for facilities located in Oregon and Washington, and a third suite was used for facilities located in the rest of the contiguous United States. Through a study of the design and construction of large industrial facitlities, as well as insights obtained from contractors who build large industrial facilities around the globe, in the updated AIR Earthquake Model for the United States the number of zones for large industrial facilities has been increased from three zones to seven. These expanded zonation better reflect the spatial vartiation in vulnerability of the large industrial facilities. These zones represent six distinct seismic vulnerability class for the large industrial facilities. These seismic vulnerability classes are: 1- California, 2-Salt Lake City, 3-Pacific Northwest (Oregon and Washington), 4- Charleston, South Carolina and New Madrid Seismic Zone, 5-Northeastern US and 6- The rest of the USA.

To assess which of the damage functions developed for the AIR Earthquake Model for the United States would be most appropriate for the AIR Earthquake Model for Canada, AIR engineers studied the differences in the design base shear of industrial facilities in each of the seismic vulnerability zones of Canada (shown in Figure 60) and compared them with that in the United States. Based on this assessment, two suites of damage functions are needed to accurately estimate damage to industrial facilities in the AIR Earthquake Model for Canada.

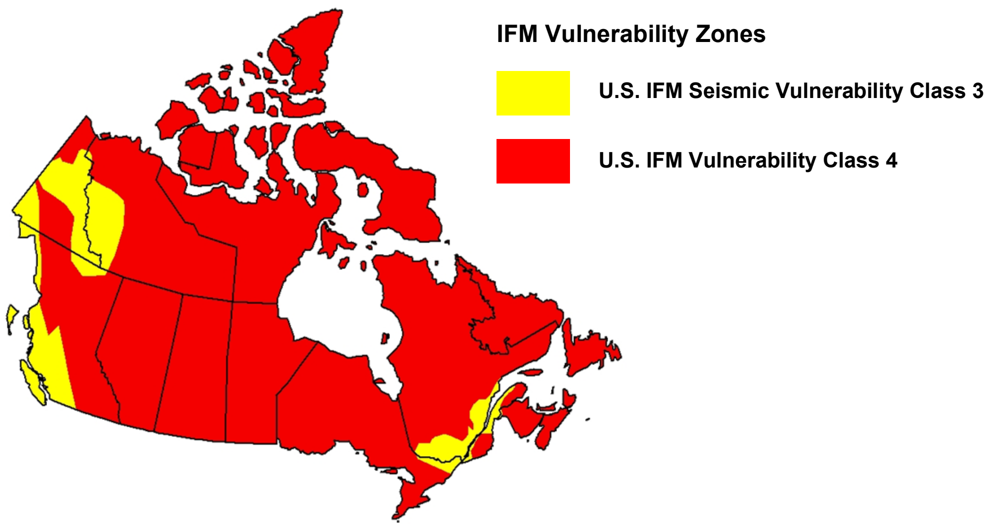

Figure 60. Seismic vulnerability zones used to estimate damage to industrial facilities in the AIR Earthquake Model for Canada

The suite of damage functions used for Northeastern United States (Seismsic vulnerability class 3) in the AIR Earthquake Model for the United States are applied to the vulnerability zones of Canada that exhibit higher seismic hazard compared to the rest of Canada (shown in yellow in Figure 60). Damage functions designed for the New Madrid Seismic Zone and Charleston South Carolina in the United States (Seismic vulnerability class 4) are used for all other zones in Canada, as shown in Figure 60 in red. It should be noted that the damage functions developed for California were not applicable to any vulnerability zone of Canada.

Further information about these industrial facility components, and examples of whole-facility damage functions used in the AIR Earthquake Model for Canada for the shake and tsunami perils, are provided in subsection "Industrial Facilities Damage Due to Ground Shaking" and subsection "Tsunami Damage Functions for Complex Industrial Facilities", respectively.

5.2 Evolution of Building Codes in Canada

Seismic design codes are usually established in the wake of devastating earthquakes, and evolve with the accumulation of new knowledge of hazards and building performance. Despite known seismic activity in certain regions of Canada, there has been little or no serious damage caused by historical earthquakes in that country. The advent and enhancement of seismic codes in Canada are mainly influenced by the observation of seismic destruction in other countries, and knowledge gained through research. Currently, the Canadian

Commission on Building and Fire Codes (CCBFC) is the main official body responsible for developing national standards of safety for buildings in Canada, which are collectively termed the National Building Code of Canada (NBCC). However, until the NBCC is adopted by local governments, it is not legally binding. When local (municipal or provincial) governments incorporate the NBCC code into their design regulations, the code becomes a legally binding document (Paz, 1994).

The first Canadian regulatory code for earthquake resistant buildings (NBCC 1941) was published in 1941. The code has periodically been revised to reflect the latest research findings, and some of these revisions have been quite significant. Design philosophy has also transformed from allowable stress design to ultimate strength design and ideas of performance based design. The NBCC 1941 code was based on the 1935 Uniform Building Code (UBC 1935). With no seismic regionalization, the code prescribed design forces between 0.02 and 0.05 times the building weight, depending on the bearing capacity of the soil.

The first seismic zonation map was introduced in the 1953 version of the NBCC code. The NBCC 1953 zoning map delineated four zones based on the locations of large historical events. Most of Canada was classified as Zone 0 (with no need for seismic consideration). The zone with the largest design forces (Zone 3) included regions such as southern and western parts of British Columbia in the west, and the St. Lawrence and the Ottawa River valleys in the east of Canada. Building design was based on working stress.

The code went through some updates in 1960 and 1965 to consider torsional effects and to add the "importance factor." However, the seismic zoning map of the NBCC 1953 was retained. The design philosophy underlying the NBCC 1965 was based on working stress design, but ultimate strength design was permitted for concrete structures as an alternative based on the American Concrete Institute (ACI) 1963.

The first fully probabilistic seismic zoning map was introduced in the 1970 version of the NBCC code. This zoning map was based on the peak ground acceleration with 100 year return period (exceedance probability of 0.01) and demonstrated four seismic zones with respect to design base shear calculations. NBCC 1970 introduced the period-dependent structural flexibility factor, and also considered higher mode effects through a concentrated force at the top of the structure. The NBCC 1970 is considered a major update in the code evolution.

The code was updated again in 1975, 1977 and 1980; however, the seismic zoning map was unchanged. In 1975 a foundation factor was introduced to account for soft soil effects. Moreover, dynamic analysis was presented as an alternative procedure. A change in the seismic response factor in NBCC 1980 resulted in some increase in the design forces for low- and mid-rise buildings while decreasing the design forces of taller buildings (period greater than 1.0 second).

A new seismic zoning map, generated based on the point source model, went into effect in the 1985 version of the NBCC code. This zoning map was developed based on the hazard with a 10% probability of exceedance in 50 years (475 year return period) and presented peak ground acceleration and peak ground velocity. Some refinements were also made in the design base shear formula. Load combination factors (for ultimate strength design) were the same as those in the 1975 version.

The next edition of the code, namely the NBCC 1990, used the same seismic zoning of NBCC 1985, but involved changes in the design base shear formula. In NBCC 1990 the construction type factor was replaced by the force modification factor to reflect the onset of yielding in structures. A calibration factor was also applied to maintain a similar level of design force with that of NBCC 1985. An update in 1995 offered additional force modification factors and a new formula for building period and torsional eccentricities. The zoning map of NBCC 1985 was still used in NBC 1995. Moreover, in the 1990 and 1995 versions of NBCC, the earthquake load factor in the design load combinations was taken as 1.0.

A milestone in the code evolution was set with introduction of the Uniform Hazard Spectrum (UHS) approach in the 2005 version of NBCC. In this approach, which was adopted from NEHRP 1997, design forces were calculated using site-specific response spectral acceleration with an exceedance probability of 2% in 50 years (2,475 year return period). The formula for determining design base shear was significantly modified in the NBCC 2005. The lower probability of exceedance was believed to provide a uniform margin against collapse across the country. The code also incorporated two types of force modification factor, one related to ductility (reflecting energy dissipation capability) and another related to overstrength (reserve strength beyond yielding).

The most recent version of the code, namely, the NBCC 2010, is essentially the same as NBCC 2005 except for a minor reduction in the low period hazard and a slight increase in the long period hazard in zones with low seismic activity such as Toronto. The minimum design base shear was also updated. A comparison of design factored base shear for various structures in Vancouver and Montreal shows an overall increasing trend from 1970 to 2005 (Mitchell et al., 2010).

It must be added that prior to 2000, the NBCC code had been adopted by Quebec government but since November 2000 the government enacted the "Code de construction de Quebec" which is a modified version of the NBCC codes. The seismic provisions in this code are the same as those in NBCC, but their evolution does not follow the timeline of the changes in the NBCC. For example, the seismic provisions in the 2000 version of the Quebec code were taken from the NBCC 1995 and those of the 2008 version of the Quebec code are taken from the NBCC 2005. In designation of the supported age band in the AIR model, this particular aspect of the seismic code updates in Canada has been taken into account.

Supported Age Bands

Examination of the code updates through the years allows one to define periods of time in which seismic design provisions had a particular degree of stringency. "Age bands" defined on the basis of the stringency of the design codes implicitly reflect the change in seismic vulnerability of structures built in these different eras. The building age bands used in the AIR Earthquake Model for Canada are: Pre-1955, 1955-1972, 1973-1987, 1988-1997, 1998-2007 and Post-2007. These age bands reflect the evolution of Canadian building regulations from a seismic design perspective. It must be noted that a 2-year time lag in implementation and enforcement of each code update is considered in defining these age bands.

5.3 Vulnerability Classification of Buildings

Recognizing the impact of seismic design regulations on building performance, some studies classify vulnerability with respect to the year buildings were designed. In this approach the years in which seismic design codes were effectively put in place, or went through substantial upgrades, are considered the milestones that define the changes in building vulnerability. Accordingly, the year buildings were built is manifested as a proxy of the vulnerability class (Erdik et al., 2003; Rota et al., 2008).

In the AIR Earthquake Model for Canada, building vulnerability is assessed using a combination of seismic design codes, implicit seismic resistance, and information on construction quality and standards. As a result, the damage estimation component of the AIR model appropriately reflects both spatial and temporal variation in Canadian building vulnerability.

Using Seismic Design Codes to Assess Building Vulnerability

Seismic design codes determine the minimum earthquake force that a building should be able to resist. For example, if two identical buildings are designed according to different codes, it is expected that the one designed to withstand smaller earthquake forces will be more vulnerable. The model classifies building vulnerability using seismic resistance, which is a reflection of the level of engineering attention paid to the design and construction of a building. This classification method is similar to the European Macroseismic Scale (EMS-98) (see EMS 1998), in which buildings are categorized into six vulnerability classes based on seismic design codes. The stringency of the seismic design codes in place when a building was designed and constructed provides an implicit measure of its seismic resistance. The AIR model includes five vulnerability classes based on seismic design code levels. For each primary class, sublevels are introduced to account for variation in vulnerability among different regions of Canada. A description of each of these vulnerability classes is provided in Table 17.

Table 17. Description of AIR's building vulnerability classes

Vulnerability Class (Seismic Design Code Level)	Vulnerability Class Sub-level	Vulnerability Class Description	Relevant Base Shear Coefficient
Pre-Code	-	Buildings are designed with no seismic considerations, such as non-engineered buildings	< 0.035
Low Code	I	Buildings are designed with minimum seismic considerations	0.035 – 0.09
	II		
Moderate Code	I	Buildings are designed with moderate seismic considerations	0.09 – 0.15
	II		
	III		
High Code	I	Buildings are designed with stringent seismic considerations	0.15 – 0.22
	II		
	III		
Special Code	I	Buildings are designed with very stringent seismic considerations	> 0.22
	II		
	III		
	IV		

Note that building vulnerability decreases with increasing code level—that is, a building classified as Low Code is more vulnerable than a building classified as High Code (see Table 17). AIR's classification system primarily follows the EMS-98 and HAZUS recommendations, with the exception of the Special Code class, which was added to accommodate the very stringent design criteria of some recent building codes.

5.4 Spatial and Temporal Variation in Building Vulnerability

Incorporating both seismic and wind design codes in the vulnerability module enables the model to capture concurrent spatial and temporal variations in vulnerability in Canada, as described in the remainder of this section.

Spatial Variation in Vulnerability

Seismic design codes divide a country into seismic zones based on hazard analysis, historical earthquakes and socioeconomic factors. In each zone, buildings must be designed to withstand a certain level of earthquake force. Accordingly, each seismic zone in the model domain is assigned an appropriate vulnerability class (see Table 17) based on design base shear requirements. This procedure allows the model to capture spatial variation in building vulnerability when specific seismic zonation schemes are in effect. Figure 61 shows an example of assigning vulnerability classes in various regions of Canada based on the

NBCC 1995 design provisions. Panel (a) shows the seismic zones of the NBCC 1985 code and Panel (b) shows the AIR vulnerability classification during the time period where this seismic zonation was in effect.

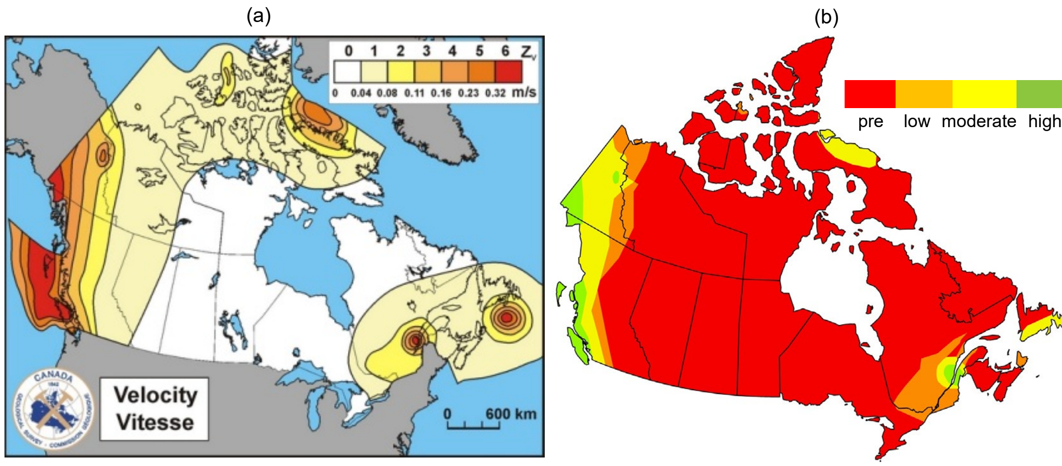

Figure 61. Example showing how seismic zonation data are used to determine building vulnerability; (a) Seismic zones of Canada (NBCC 1985); (b) AIR Vulnerability classification for Canada for 1986-1995

Temporal Variation in Vulnerability

Typically, seismic codes are developed in the aftermath of major earthquakes. Design provisions are enhanced over time in light of new engineering research and additional earthquake observations. For example, in early versions of the seismic codes in Canada, earthquake-resistant design was required only in geographic regions with a history of large earthquakes (that is, in some areas of British Columbia and Quebec). However, earthquake-resistant design was required more widely in subsequent revisions of the Canadian building code.

Because vulnerability classification is linked to seismic code provisions, incorporating changes in seismic zonation allows the vulnerability module to accurately represent changes in vulnerability over time (temporal variation). The AIR vulnerability module tracks the evolution of seismic codes and seismic zonation to effectively capture temporal variation in vulnerability. Figure 62 shows the AIR building vulnerability classifications in Canada for different periods of time, illustrating how vulnerability can vary by year-built and location within the model.

It must be noted that the resultant vulnerability classification shown in Figure 62 is independent of the exposure. That is, even if no major cities or centers of population currently exist in some areas in the north of Yukon and the Northern Territories, for the sake of completeness, the procedure assigns the appropriate vulnerability class to all regions of Canada, in accordance with the hazard parameters defined in the NBCC codes.

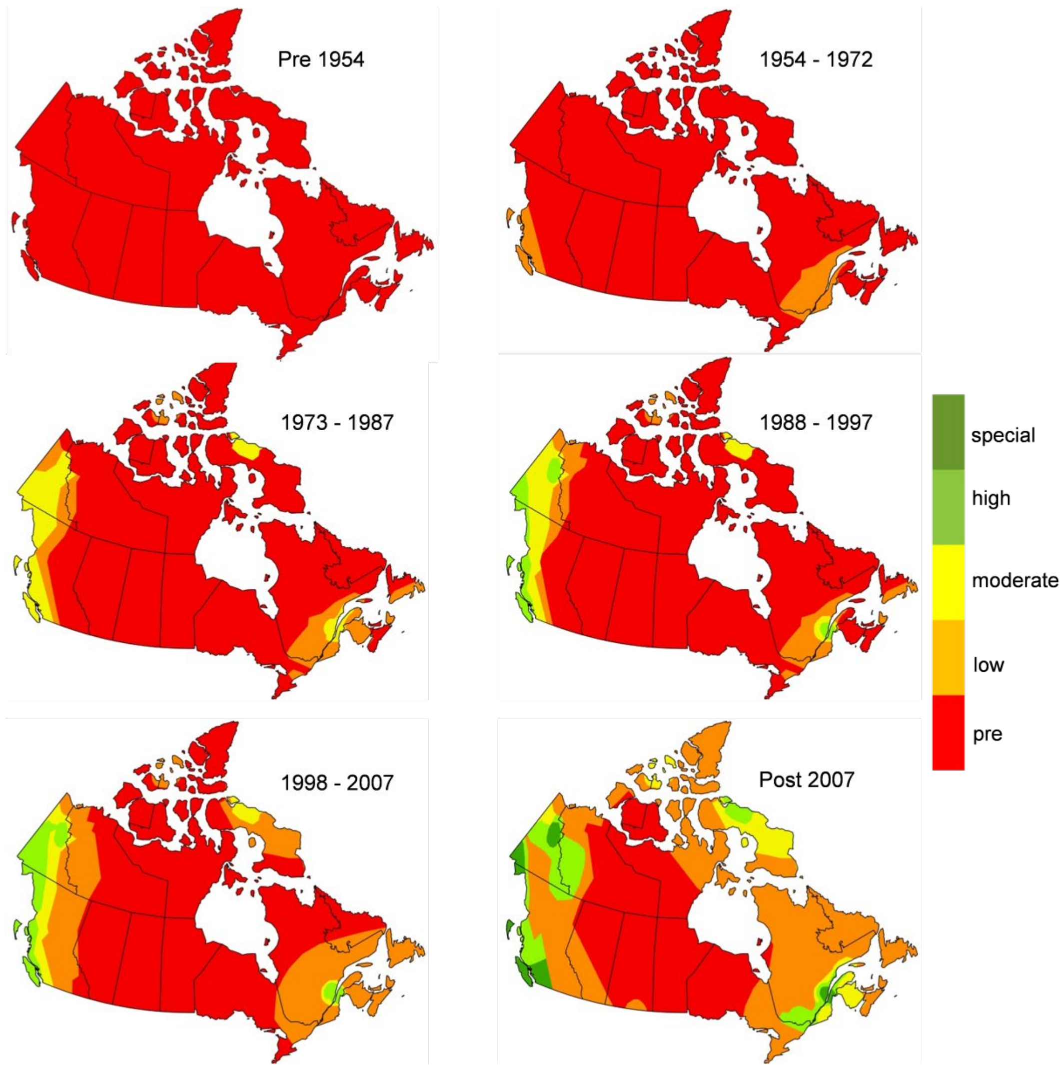

Figure 62. Spatial and temporal variation in vulnerability represented by code levels in Canada

5.5 Ground Shaking Damage

A building's response to ground motion is complex; it vibrates under coupled inertial forces imposed simultaneously by the movements of the ground and the building itself. These two inertial forces either combine with or cancel out one another, depending on their respective frequencies and phases. When the ground vibration contains a large component close to the natural frequency of the building, the forces combine; this amplifies the building response and causes greater structural damage. The ground motion characteristics that have the greatest impact on damage are the amplitude and frequency of the incoming seismic waves; these wave characteristics vary by location and depend on the local geological and geotechnical conditions along the path from the earthquake focus to the building site.

The damage estimation module of the AIR Earthquake Model for Canada correlates an appropriate measure of ground motion intensity to a building damage ratio (the ratio of the building's repair cost to its replacement value), yielding a damage function. If an infinite amount of damage and loss data – including ground motion recordings at each building location – was available for buildings of all construction classes and age bands, then deriving damage functions would be a relatively straightforward process. However, such large collections of damage and loss data are not available for several reasons. For example, even if all buildings were equipped to capture the necessary data, damaging earthquakes do not occur frequently enough to produce a reliable, extensive dataset. Therefore, in the absence of damage and loss data for all points of interest in a modeled region, damage functions are best derived using a combination of engineering and statistical tools.

The lack of damage data is particularly significant for Canada, as there has not been a damaging earthquake in that country in recent years. Therefore, in lieu of local damage data, vulnerability functions for the AIR Earthquake Model for Canada are developed using analytical studies and damage data from other countries with similar construction practices and building performance. To this end, AIR engineers have partnered with local researchers[15] to study the vulnerability of the building stock in Canada, and to compare the vulnerability of buildings in Canada and in the United States. Well-known similarities between American and Canadian design standards and construction practices make it possible to use data originally gathered during the development of the AIR Earthquake Model for the United States to derive damage functions for the Canada model. Moreover, the development of these damage functions is informed by local Canadian vulnerability studies (e.g., Ventura et al. 2005, Onur et al. 2005).

Estimating Building Damage Due to Ground Shaking

Damage functions are commonly developed based on expert opinion, observational data, analytical studies, or a combination of these (Rossetto and Elnashai, 2003). Observational method relies on statistical analysis of data from post-earthquake damage surveys, or insurance claim data. The approach is

[15] AIR has collaborated with professor Oh-Sung Kwon from University of Toronto, and with professor Marie-Jose Nollet from École de technologie supérieure (ETS) in Montreal as a peer reviewer.

realistic, but it is limited by the availability of data and by the ground motion parameters because building responses, which are better correlated with damage than ground motion intensity parameters, are usually not available. The data for statistical analysis can also be synthetized through simulation of analytical models. When data is available, AIR uses a hybrid approach in which claims or damage data supplements analytical research to generate and/or validate damage functions for various construction types.

Figure 63 shows a typical damage function. The parameter on the X-axis represents the ground motion parameter (GMP). The GMP reflects the shaking characteristics (frequency content, duration, etc.) and the building response.

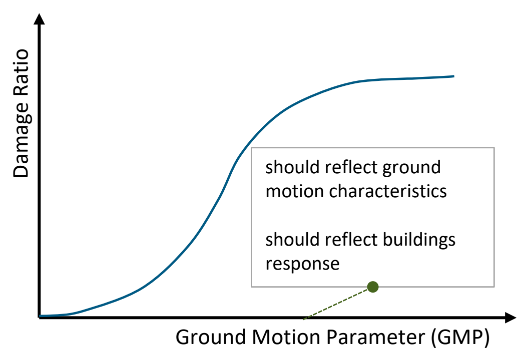

Figure 63. Typical damage function for buildings

Parameters such as Peak Ground Acceleration (PGA) and Modified Mercalli Intensity (MMI) have been frequently used in past studies (ATC-13, EMS-98, Ventura et al., 2005, etc.). However, experimental and analytical studies show that building damage is most accurately captured by building response parameters such as interstory drift (i.e. relative displacement between two successive stories). Accordingly, AIR considers drift ratio (Figure 64) as the primary determinant of damage.

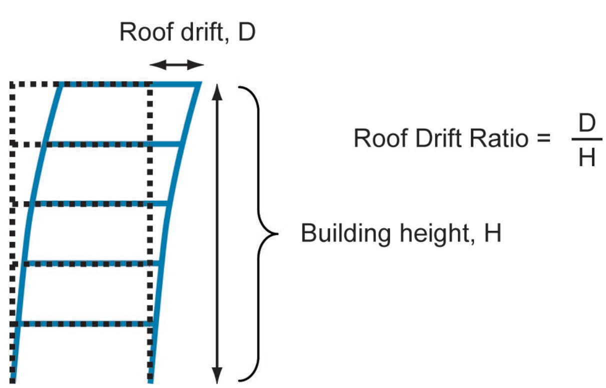

Figure 64. Definition of roof drift ratio

However, using drift ratio as the primary determinant of damage means that, in addition to determining ground motion intensity at each building location, it is also necessary to explicitly determine the seismic response of each building. This means that the model must calculate the drift ratio for each building, or the model must include relationships between ground motion parameters and structural responses that can be applied to each building. Both of these approaches have been used by AIR in the past. As regards the first approach, AIR has implemented a response calculation module using the well-known Capacity Spectrum Method (CSM). Regarding the second approach, AIR has identified relationships between ground motion parameters and roof drift ratio using a combination of the CSM and nonlinear dynamic analysis (NDA).

In the AIR Earthquake Model for Canada, AIR engineers employ the second approach described above, in which CSM and NDA are used to establish relationships between drift ratio and ground motion parameters. Damage functions are then developed in terms of ground motion parameters that have previously been correlated to the roof drift ratio. A description of this method, and further information about both CSM and NDA, are provided in the section that follows.

The Capacity Spectrum Method

To estimate a building's response to different levels of ground shaking, a computerized model of the building is subjected to a lateral load pattern that represents the force generated by the ground motion (see Figure 45). The lateral load pattern, or load vector, is chosen to have the same shape as the fundamental mode of the structure's vibration. The total load is then increased in successive steps to create a relationship between the intensity of the applied load (measured in terms of base shear) and the deformation of the building (measured in terms of roof drift). The analysis terminates when the building (virtually) collapses. This static nonlinear procedure is often called pushover analysis, and the force/deformation curve obtained is called a pushover curve.

When one is interested in predicting the response of a building to a specific ground motion, then an available analysis method is the Capacity Spectrum Method (CSM), in which the quantities in the full building pushover curve are transformed into response measurements of an equivalent single degree-of-freedom oscillator, such as the pendulum shown in Figure 65. The oscillator has the same natural frequency and degraded stiffness, after yielding, as that of the modeled building. More precisely, the applied load is translated into spectral acceleration, and the building deformation is translated into spectral displacement.[16] The pushover curve represented by these two parameters (which are related to the equivalent oscillator) is called the capacity curve. A building's capacity curve reflects various seismic characteristics of the building, such as its stiffness, its material brittleness or ductility, and its strength. This curve correlates the lateral deformation that a building is subjected to (in terms of spectral displacement) to a specific level of dynamic demand (expressed in terms of spectral acceleration).

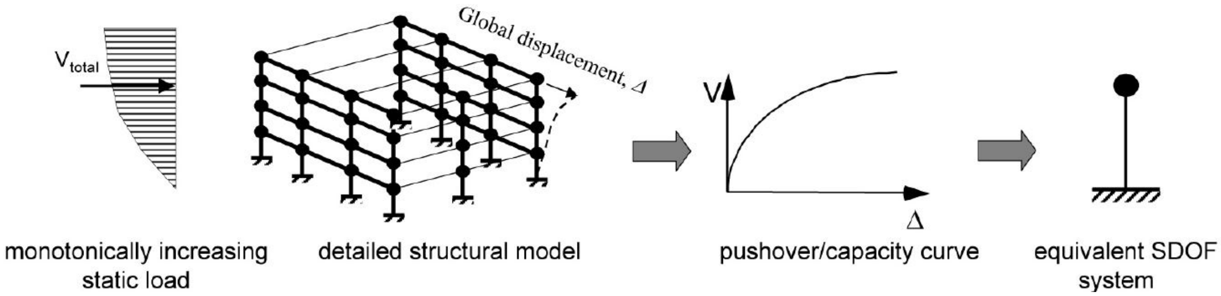

Figure 65. Schematic depiction of static pushover analysis used in the capacity spectrum method (Source: FEMA 440 [FEMA 2005])

Any anticipated ground motion that may affect a building can be approximately modeled through a response spectrum. In the response spectrum representation, which is convenient to use in the framework of the Capacity Spectrum Method, the demand on a building imposed by ground motion is represented by the maximum acceleration and displacement of a series of oscillators. The response of this collection of pendulums can be plotted as a curve of acceleration/displacement pairs known as the demand curve.

In Figure 66, a series of simple oscillators are subjected to ground shaking. The peak responses of the oscillators are plotted on the graph to the right, showing the spectral acceleration against the spectral displacement. The radial lines on the graph represent the periods of the oscillators.

[16] Spectral acceleration and spectral displacement are two response measures of oscillators with given vibration period and damping.

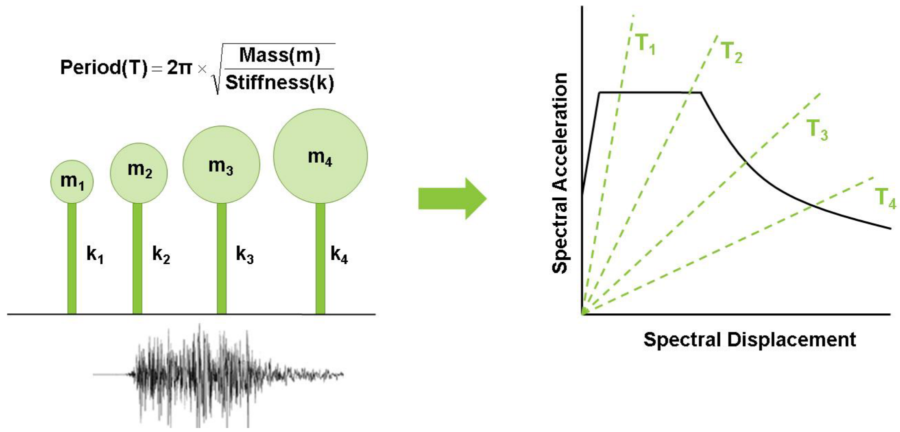

Figure 66. Maximum acceleration and displacement of a series of oscillators

The demand curve and the capacity curve are represented by the same parameters and can be plotted in the same figure. The intersection of the demand curve and the building capacity curve plotted on the spectral acceleration and spectral displacement plane corresponds, within a constant, to the maximum roof displacement of the building relative to the ground in response to that ground motion.

Figure 67 shows the intersection of the demand and capacity curves, which represents the peak response of the structure.

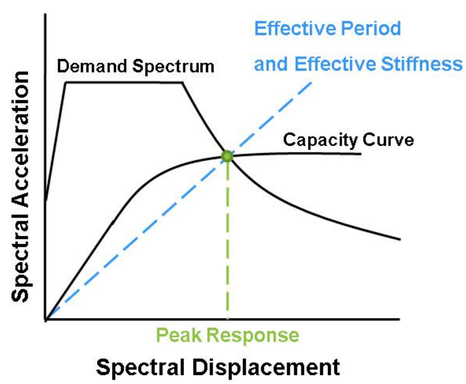

Figure 67. The peak response of a structure determined by its capacity curve

A capacity curve representing a single building of a certain construction class will have a unique intersection with different response spectra for different ground motion intensities. Similarly, different capacity curves representing different buildings of the same class will have unique intersections with the same response spectrum from a given ground motion intensity. These attributes provide the ability to distinguish between the responses of various building classes to different ground motion intensities.

During ground shaking, the amount of deformation incurred by the different stories of a building can be derived, given certain assumptions, from the deformation at the roof level. The story deformations can be related to the damage suffered by all types of components, both structural (e.g., columns and beams) and nonstructural (e.g., cladding, partitions, ceiling tiles, etc.) at each story and, therefore, to the repair strategies that are expected due to the predicted damage. The appropriate repair strategies for each damaged component can be priced and expressed in terms of a fraction of the replacement cost of the entire building.

Nonlinear Dynamic Analysis

To establish a correlation between ground motion and structural response, Nonlinear Dynamic Analysis (NDA) is carried out on computer models representing different construction classes subjected to a large suite of ground motion time histories. The refined computer models are able to demonstrate the post-elastic behavior of primary elements as they undergo damage.

The use of NDA allows an explicit consideration of the effects of earthquake duration on the cumulative damage of building components as well as capturing all the modes of failure. In each analysis, the forces and deformations occurring in all structural members as well as the global response measures such as maximum peak inter-story drifts and forces, roof displacement and peak story accelerations are evaluated (as shown schematically in Figure 68).

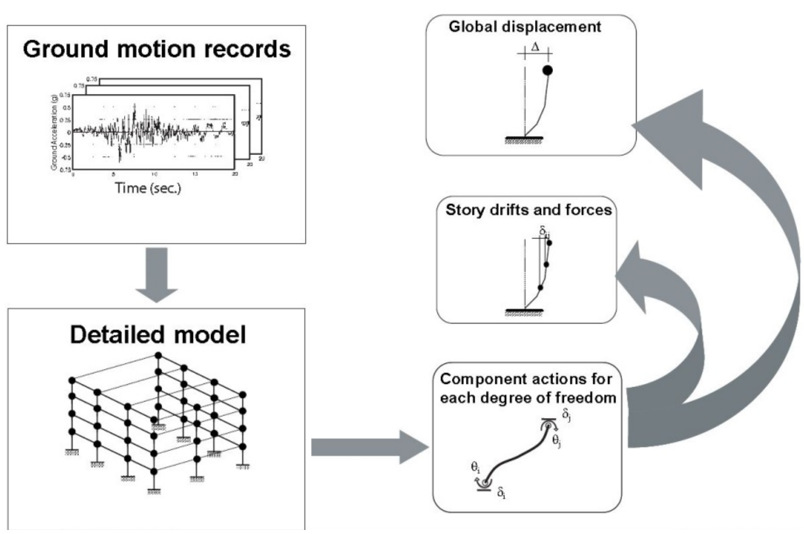

Figure 68. Flowchart showing the use of NDA to determine building response (Source: FEMA 440 [FEMA 2005])

The maximum peak inter-story drift (among all stories) is well correlated with the damage of structural elements (e.g., beams and columns) and of deformation-sensitive non-structural elements (e.g., wall partitions). Similarly, the maximum peak floor acceleration (along the entire height of the building) is well correlated with damage to acceleration-sensitive nonstructural components (e.g., suspended ceilings), and to contents. An example of the estimates of maximum peak inter-story drift and peak floor acceleration, obtained via NDA by applying ground motions from 100 earthquakes to a 10-story steel moment-resisting frame building, is shown in Figure 69.

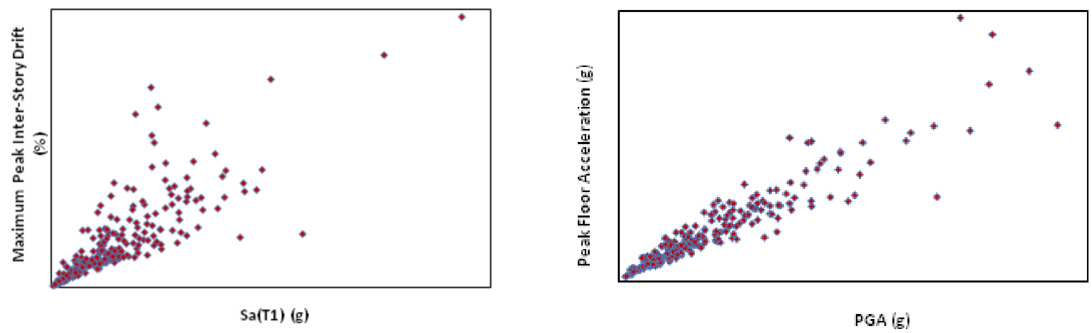

Figure 69. Maximum peak inter-story drift ratios (MIDR) and maximum peak floor accelerations (MPFA)

Regression analysis is performed on the results in Figure 69 to establish the best relationship between the ground motion intensity parameters (e.g. PGA or $Sa_{(T)}$) and the building's global response measurements (maximum peak inter-story drift and peak floor acceleration). The use of ground motions from multiple earthquakes allows the model both to obtain an estimate of the mean response given a certain level of ground shaking, and to account for the variability in the buildings' nonlinear response generated by different records of the same intensity.

Figure 70 shows the relationship between the global response parameters and the intensity of the ground motion, for the same 10-story steel moment-resisting frame, when the collapse cases are (correctly) considered (solid lines) or disregarded (dotted lines). The collapse cases must be considered because the building will not withstand indefinitely large deformation without failing.

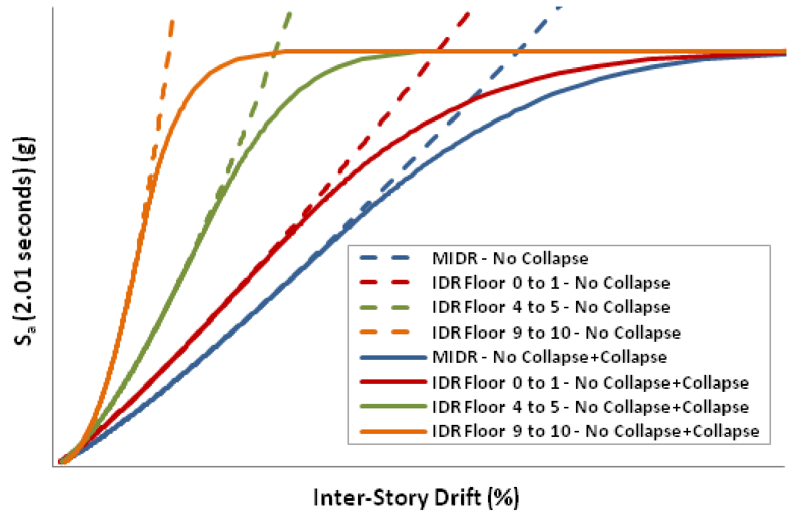

Figure 70. Relationship between spectral acceleration (Sa) at the fundamental period of a building and the induced MIDR and IDR

Developing Building Shake Damage Functions

In the AIR Earthquake Model for Canada, building shake damage functions are developed in terms of appropriate ground motion parameters, which have been correlated with structural response through the use of CSM and NDA (as described in the preceding subsection). These appropriate ground motion intensity parameters vary by construction type and height, as shown in Table 18.

Table 18. Independent ground motion parameters for different construction classes

Construction Class	Height	Independent Variable
Wood Frame	Low-Rise	Sa(0.3s)
Masonry Veneer	Low-Rise	Sa(0.3s)
Unreinforced Masonry – Bearing Wall and Frame	Low-Rise/Mid-Rise	Sa(0.3s)
Reinforced Masonry Shear Wall–With and Without MRF	Low-Rise/Mid-rise	Sa(0.3s)
	High Rise	Sa(1s)
Reinforced Concrete Shear Wall–With and without MRF; Reinforced Concrete MRF–Ductile and Non-Ductile; Tilt-Up and Pre-Cast Concrete	Low Rise	Sa(0.3s)
	Mid-Rise	Sa(1s)
	High Rise	Sa(3s)
Light Metal, Braced Steel Frame, Steel MRF–Perimeter and Distributed	Low-Rise/Mid-Rise	Sa(1s)
	High Rise	Sa(3s)
Long-Span	N/A	Sa(3s)
Mobile Homes, Industrial Facilities (400+ class) and other Construction Classes (200+)	N/A	PGA

Damage functions for different building construction classes are developed by AIR engineers using a combination of engineering analyses, evaluation of building codes, and damage and loss data. Engineering analyses are critical when empirical data are scarce. For the following types of buildings, engineering analysis (NDA) was used extensively:

- Low-rise, mid-rise, and high-rise brittle and ductile RC frame buildings
- Low-rise, mid-rise, and high-rise modern moment-resisting steel frame buildings

While NDA was also used in the development of damage functions for wood frame structures, this method was of lesser importance for this particular construction type. When NDA was required in damage function development, analyses were performed for multiple buildings within each class by both AIR engineers and other researchers, to explore variation in how similar buildings respond to similar ground shaking.

For single-family wood frame residential buildings, the AIR damage functions are based on engineering analyses, on claims data from the 1994 Northridge earthquake, and on damage and loss data from a number of historical events, including the 1989 Loma Prieta earthquake, the 2003 San Simeon earthquake, and the 2008 Chino Hills earthquake. The claims data for the Northridge earthquake include 450,000 policies filed with the California Department of Insurance (DOI) and another 27,000 policies from private insurers. The distribution of claims data from the private insurers is shown in Figure 71.

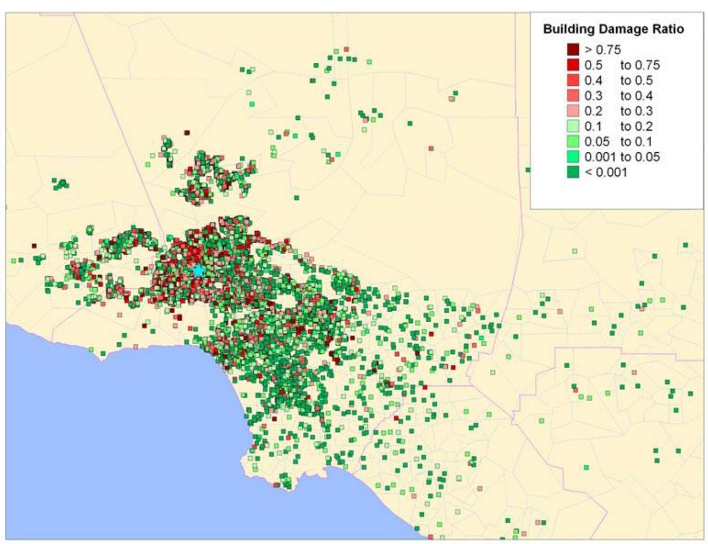

Figure 71. Claims data from the 1994 Northridge earthquake obtained from private insurers

At each location for which claims data are available, the damage ratio experienced by a structure at that location can be plotted against a selected ground motion intensity parameter. For example, Figure 72 shows the damage ratio experienced by wood frame homes (year built = 1976 – 1994) in the 1994 Northridge earthquake versus the ground motion intensity (specifically, 0.3s Sa). Note that plotting the mean damage ratio (blue circles) of the data grouped in spectral acceleration bins (pink diamonds) reveals the overall trend in the data. In addition, the average damage ratio (red squares) as calculated from data from the California Department of Insurance (DOI) is in good agreement with the average damage ratio calculated from private claims data.

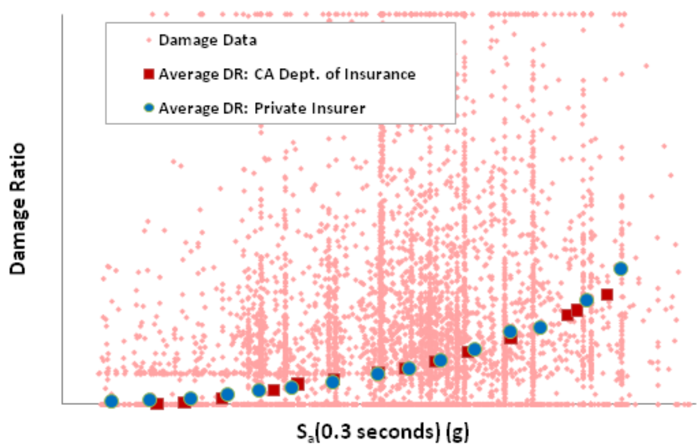

Figure 72. Damage data and average damage ratios from the 1994 Northridge earthquake for wood-frame houses built after 1976

Despite the availability of empirical data such as these, engineering analyses are still a vital part of damage function development. This is because claims data do not identify all features of a building – such as foundation type or number of stories -- that influence that building's vulnerability. NDA analyses can readily determine the effects of these features on damage ratios. Therefore, using both claims data and engineering analysis yields the most scientifically realistic damage functions.

Figure 73 exhibits the results of NDA analysis for wood frame homes of similar vintage (year built = 1980). In the figure, each green dot represents the result of non-linear dynamic analysis under a single ground motion record. The green dots near the top of the plot represent analyses that caused the structure to collapse. Note that the damping ratio (ζ) in all of these analyses is 5% of critical damping.

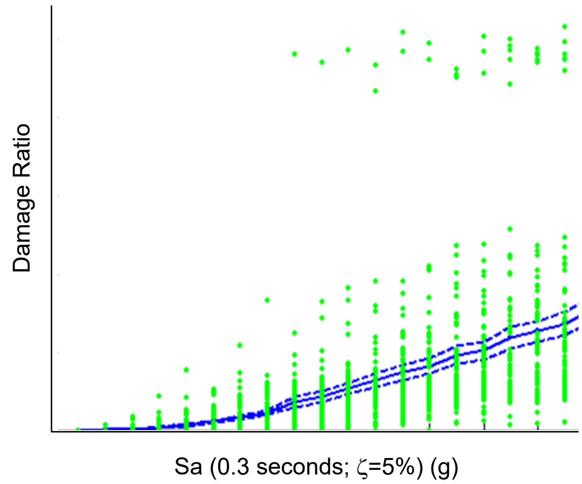

Figure 73. Damage ratio versus spectral acceleration (Sa=0.3s) for wood frame homes built around 1980

Unfortunately, extensive claims data are not available for construction classes other than wood frame homes. There are, however, historical damage data for several construction classes that provide detailed descriptions of the damage experienced by a building at a given location. These damage data can then be used to estimate the repair cost and, after normalization to the replacement cost of the building, the damage ratio. Extensive damage datasets are available for the following construction types:

- Concrete tilt-up buildings
- Unreinforced masonry buildings
- Steel moment-resisting frame buildings
- Concrete moment-resisting frame buildings

For unreinforced masonry buildings, most of the historical damage data used by AIR to develop damage functions for this construction type were collected by the Office of Emergency Services (OES) in California, after the 1989 Loma Prieta earthquake and the 1994 Northridge earthquake. This dataset comprises damage data for 850 URM buildings damaged by the Loma Prieta earthquake, and 3,500 URM buildings damaged by the Northridge earthquake. The locations of these damaged buildings are shown in Panels a) and b) of Figure 74.

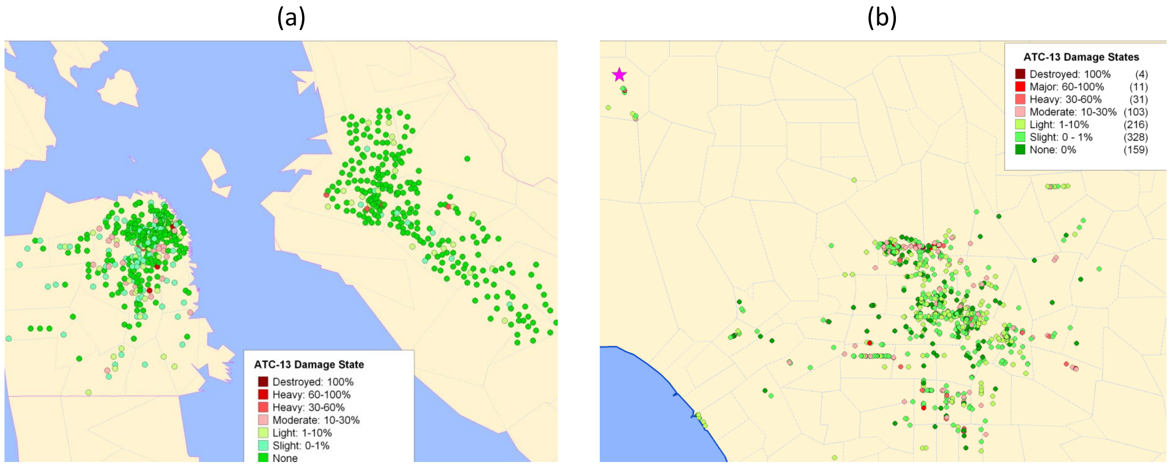

Figure 74. Damage distribution for URM buildings from historical earthquakes: a) 1989 Loma Prieta earthquake, and b) 1994 Northridge earthquake

The inferred damage ratios for these URM buildings versus the ground motion intensity they experienced in the Loma Prieta (light pink circles) and North Ridge (light blue squares) earthquakes are plotted in Figure 75. In addition, the figure shows the average URM damage ratio (for different spectral acceleration bins) for the Loma Prieta earthquake (dark red circles), the Northridge earthquake (blue triangles), and several earthquakes in Italy (dark blue squares). The average damage ratios for Italy were determined from a very large set of URM damage data collected by the Italian Department of Civil Protection, which include damage information from earthquakes in Italy since 1975. In spite of differences in the details of URM construction between Italy and the U.S., the overall trends exhibited by the Italy data and the U.S. data in Figure 75 are notably similar.

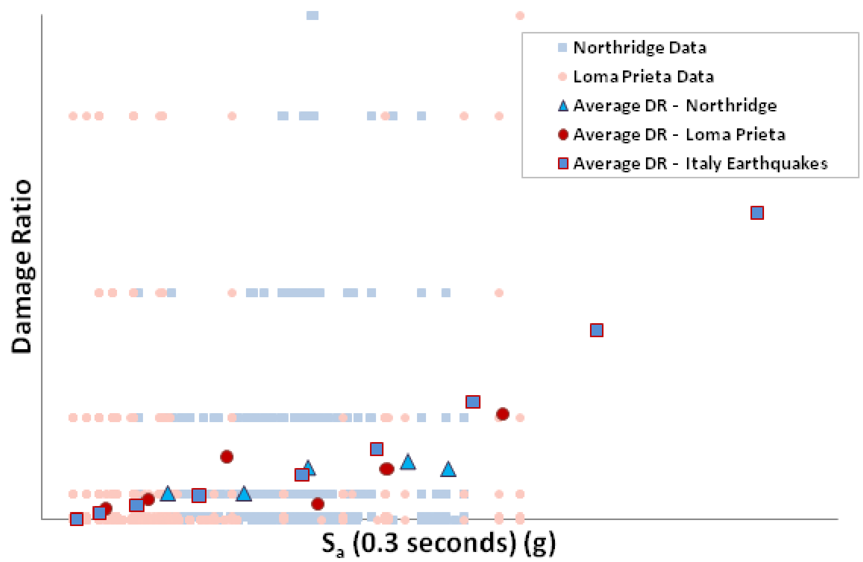

Figure 75. Damage ratios for URM buildings for earthquakes in California and Italy

The finalized damage functions used in the AIR model for several construction types – including URM – are shown in Figure 76.

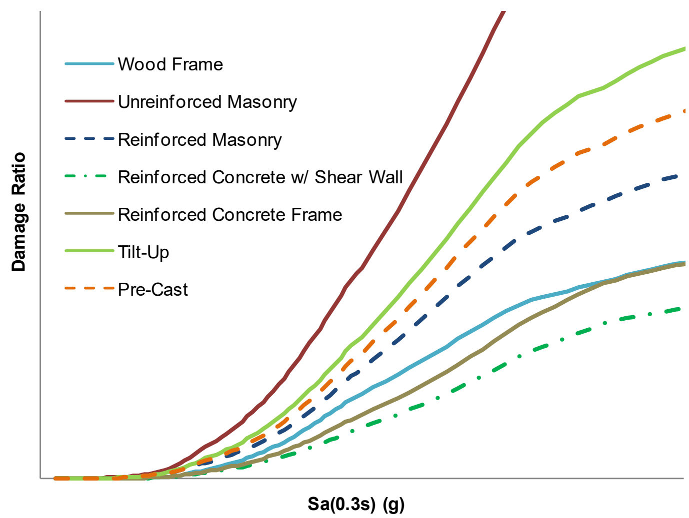

Figure 76. Damage functions for various construction types in California

The preceding material has described the development of damage functions for construction classes in regions such as California in the United States, which are considered "special code" according to the AIR vulnerability assessment framework (see Section 5.3). To develop damage functions for structures of other vulnerability classes in Canada, AIR has modified damage functions for corresponding buildings in California, accounting for differences in design loads and construction practices between the U.S. and Canada. Relative vulnerabilities obtained from local vulnerability studies, and from vulnerability studies conducted by AIR for other regions, were used to adjust these modified damage functions as necessary. Note that studies of building vulnerability in the central and eastern United States, such as those conducted by the Mid-America Earthquake Center (MAE) (e.g., see Ellingwood et al. 2007), were also used to inform the modification of these damage functions. Finally, data from HAZUS, as well as studies by Ventura et al. (2005) and Onur et al. (2005), were also used. The resulting damage functions for low-rise reinforced concrete (RC) buildings for different vulnerability classes (code levels) are shown in Figure 77.

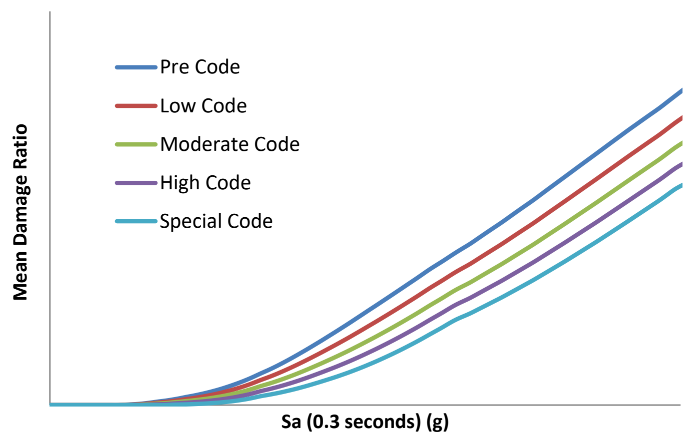

Figure 77. Damage functions for low-rise reinforced concrete frame buildings

The Distribution of Damage: Uncertainty in Damage Estimation

The model's damage functions provide estimates of the mean, or expected, damage ratio corresponding to median ground motion at each affected site. However, as is commonly seen in the course of damage surveys in the aftermath of an earthquake, similar structures at the same location may experience different levels of damage. This variation in building damage can arise due to the inherent randomness in building response or to differences in building characteristics, construction materials or workmanship.

To capture this uncertainty in damage, the AIR model constructs distributions around the mean damage ratio as illustrated in the schematic of the damage function shown in Figure 78. AIR engineers found that a bimodal-Beta distribution best represents this damage pattern in the AIR Earthquake Model for Canada.

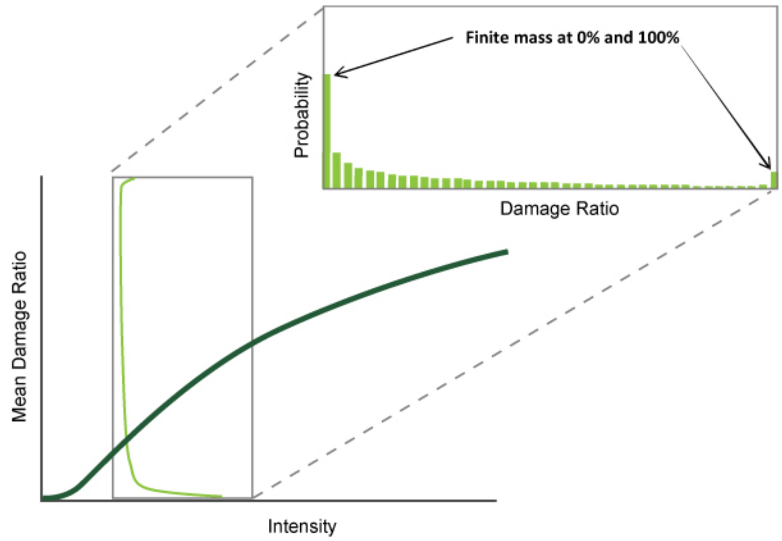

Figure 78. Schematic damage function and distribution around the mean damage ratio

Integrated Damage Functions That Include Ground Motion Uncertainty

It is important to recognize that the damage functions discussed so far in this document are in fact *mean* damage functions; that is, damage functions that have been developed using fixed ground motion intensities (that is, median ground motion). Mean damage functions are appropriate tools for damage assessment when there is little uncertainty in the estimated ground motion intensity. For example, mean damage functions can be used to accurately assess damage from historical earthquakes experienced by buildings located close to recording stations (which limits the uncertainty associated with ground motion intensity at the buildings' sites).

However, there is generally significant variation in the estimation of ground motion intensity at any site during an earthquake. Acknowledging this fact, AIR uses *integrated damage functions* – damage functions that have been modified to account for ground motion uncertainties – to estimate damage for events in the stochastic catalog, as well as for historical events with little or no instrumentally recorded data. An example of an integrated damage function is provided in Figure 79. (Note that this integrated damage function accounts for intra-event uncertainty in ground motion estimates, as well as the non-linear shape of damage functions in general.)

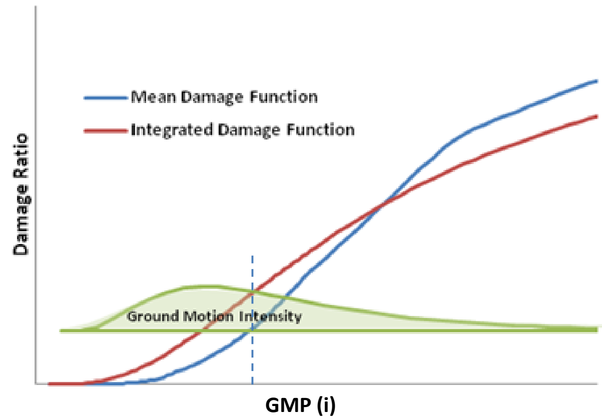

Figure 79. Schematic of an integrated damage function, which accounts for intra-event uncertainty in ground motion estimation

The mean damage function (the solid blue line in Figure 79) gives the mean damage ratio DR (i) at each level of intensity, Sa(i). The value of Sa(i) is, however, the mean value of a distribution of possible ground motion intensities (shown by the green line) that can be generated at a site by an event of a given magnitude. Each level of ground motion in that distribution, if it were to occur, would generate a damage ratio that is generally different from DR(i).

The value of the integrated damage function at Sa(i) is simply the weighted average of all the damage ratios generated by all possible ground motion levels in the green distribution. The weights are equal to the likelihood of the occurrence of each ground motion level as calculated from the green distribution. By taking the variability of ground motion into account, the integrated damage function is less steep than the original damage function, as can be seen in the figure.

Damage Functions for Buildings of Unknown Attributes

When estimating losses for a given portfolio, information about construction type, occupancy type, or height is often not available for a number of buildings in the portfolio. In the AIR Earthquake Model for Canada, damage functions for unknown construction, occupancy, and height classes are exposure-weighted averages of the damage functions corresponding to all known classes, with weights determined by the relative share of the total insurable value of each class. Different damage functions are used depending on how many variables, and which specific variables, are unknown. The AIR model appropriately accounts for the combination of known and unknown attributes shown in Table 19.

Table 19. Combination of known and unknown attributes in the AIR model (0=Unknown; 1=Known)

Combination	Construction	Occupancy	Height	Year Built
1	1	1	1	1
2	1	1	1	0
3	1	1	0	1
4	1	1	0	0
5	1	0	1	1
6	1	0	1	0
7	1	0	0	1
8	1	0	0	0
9	0	1	1	1
10	0	1	1	0
11	0	1	0	1
12	0	1	0	0
13	0	0	1	1
14	0	0	1	0
15	0	0	0	1
16	0	0	0	0

Unknown Construction, Occupancy, or Height

For buildings of unknown construction, occupancy, or height (or any combination of these three unknown attributes), damage functions are determined as a weighted average of damage functions for known attributes. The weighting factors are calculated using the relative share of the total insurable value of each class in the AIR industry exposure database (IED). For example, the damage function for a particular exposure of known occupancy and height class, but unknown construction, would be a weighted average of the damage functions for exposures of the same occupancy and height class in all construction classes.

Figure 80 shows an example of a damage function for unknown construction taken as a weighted average of those of known construction for low-rise residential buildings. Because damage functions for different height classes may not use the same intensity measure (i.e. low-rise is based on Sa 0.3s, whereas mid-rise is based on Sa 1s), the damage function for unknown height is not taken as the weighted average. Instead, the loss is taken as the weighted average of the losses for the known height class. The weights for each construction class are calculated from the IED.

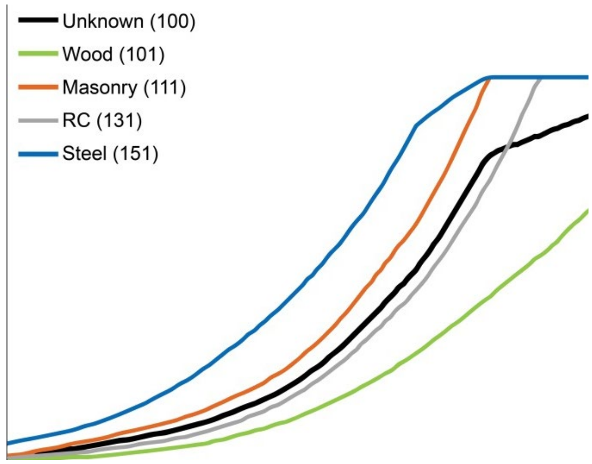

Figure 80. Damage function for unknown construction (low-rise, residential)

Unknown Year Built

As discussed in Section 5.3, the vulnerability of buildings of a given construction class, occupancy class, and height is further split into five levels (see Table 17) based on expected seismic performance, as approximated by the stringency of relevant design codes. This means that each region of Canada is assigned a vulnerability class (code level). When the year built is known, the assignment of these vulnerability classes must account for the age band (year built) of the buildings in the region and the design codes relevant for buildings of that vintage.

When the year built is unknown, the vulnerability class (code level) must be determined using the age distribution of buildings in the region. However, because vulnerability class (code level) is a discrete index, the code level of buildings of unknown age cannot be calculated as the weighted average of code levels of buildings of known age. Instead, the vulnerability class for an unknown age band in any region of Canada is assigned the same vulnerability class as the dominant age band in that region. However, it should be noted that AIR applies adjustment factors to the damage functions for buildings of unknown year built, to account for the vulnerability class (code level) of age bands other than the dominant age band. This adjustment factor, which reflects the age distribution of buildings in Canada as well as the relative vulnerability of all code levels, is shown in Table 20.

Table 20. Relativity by code level (vulnerability class) normalized to pre-code

Code Level	Relative Vulnerability
Pre-Code	1.000
Low Code	0.874
Moderate Code	0.682
High Code	0.553
Special Code	0.424

To identify the dominant age band of buildings in a region, AIR used building distributions obtained from the 2007 Survey of Household Energy Use (OEE 2007) published by the Office of Energy Efficiency, a division of Natural Resources Canada. The building distribution for each province of Canada is shown in Figure 81. Note that, for most of Canada, 1971-1985 is the dominant age band.

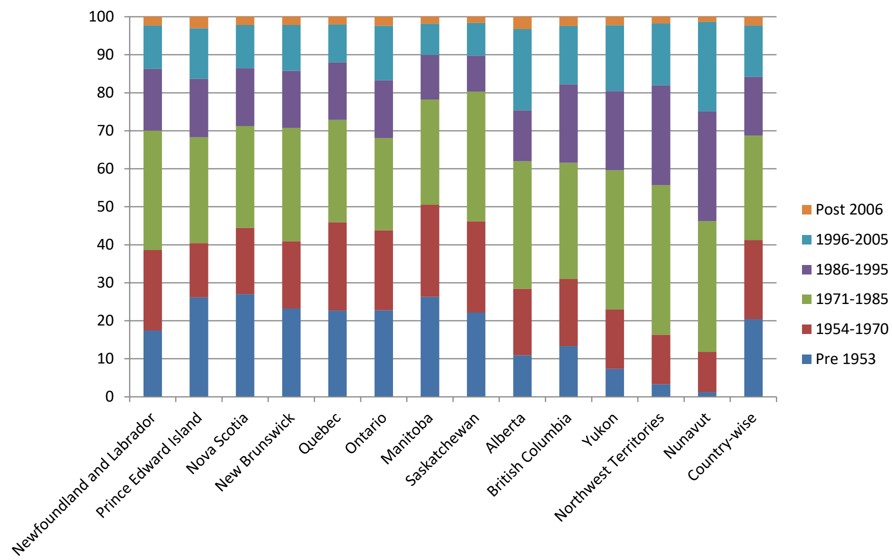

Figure 81. Building inventory of Canada (by province) by year built (data obtained from OEE 2007)

Contents Damage Due to Ground Shaking

Damage to contents constitutes a substantial portion of the total loss in an earthquake event. The mechanism by which contents of a building are damaged depends on the type of the content and the ground motion. While some contents are sensitive to acceleration (e.g. shelves, TV stands, etc.), other are sensitive to displacement (decorative walls, windows, etc.).

At low levels of shaking, the primary determinant of contents damage is floor acceleration, which imposes inertial lateral forces proportional to the product of the contents mass and the floor acceleration. At higher levels of shaking, contents damage depends on both inertial forces and building damage. For example, contents may be damaged due to the collapse of both structural and nonstructural components, including ceilings, beams and columns.

In the AIR Earthquake Model for Canada, contents damageability is a function of building damage and occupancy class. Occupancy provides information on the contents likely to be present and their potential vulnerability. As with building damage, shake damage ratios for contents are calculated using the median values for ground motion.

Automobile Damage Due to Ground Shaking

The AIR model provides damage estimates for both commercial and personal vehicles. These include passenger cars, buses, and trucks, and other types of commercial vehicles.

Automobile damage during an earthquake occurs primarily as a result of debris falling from damaged buildings. Therefore, damage to automobiles is modeled as a function of building damage.

Industrial Facilities Damage Due to Ground Shaking

To assess the damage and loss potential to a large industrial facility as a whole, AIR employed a component-based approach, which allows the damage functions to account for the many primary components intrinsic to this type of facility. AIR obtained the value breakdown of a facility according to its components, and combined this information with the component damage functions to derive the damage function for an entire industrial facility. The primary components are categorized into classes and subclasses based on their function in the manufacturing process. AIR engineers developed damage functions for more than 400 components. Several examples of primary components of large industrial facilities are shown in Figure 82. The primary categories of components are listed in Table 21.

Figure 82. Industrial facility components used in the AIR Earthquake Model for Canada

Table 21. Selected industrial facility components used in the AIR Earthquake Model for Canada

Industrial Facility Components		
Air Handling Units	Distribution Panels	Open-Frame Structures
Baffles	Electric Power Backup	Paddles
Basins	Electric Transmission Towers	Pipe Racks
Battery Chargers	Elevated Pipes	Pipes and Pipelines
Battery Racks	Engine Generators	Potential Transformers
Boiler/Pressure Vessels	Equipment	Pressurized Reactors
Boilers	Fans	Process Towers
Buildings	Filter Gallery	Pumps
Chillers	Flares	Scrapers
Chlorination Equipment	Generators	Sediment Flocculation Equipment
Circuit Breakers	Highways/Runways/Railroads	Silos
Commercial Backup Power	Large Horizontal Vessels	Stacks/Chimneys
Compressors	Large Motor-Operated Valves	Switch Gears
Control Panels	Large Vertical Vessels with Formed Head	Tanks
Cooling Towers	Lightning Arrestors	Transformers
Coupling Capacitors	Loading Structures (Cranes/Cargo Handling/Conveyor Systems)	Tunnels

Industrial Facility Components		
Current Transformers	Motor Control Centers	Wells
Dams	Large Motor-Operated Valves	Valves
Disconnect Switches	Motor-Driven Pumps	

To predict the response of an industrial facility exposed to ground shaking, the AIR model uses peak ground acceleration (PGA). Since the components are parts of a larger facility, only a single ground motion parameter has been used to estimate the response of all of the components. Using PGA as the ground motion parameter for assessing the vulnerability of industrial facility components is advantageous for four reasons:

- Majority of components (e.g., machinery and equipment) in industrial plants are anchored and fairly rigid, and therefore PGA correlates well with their seismic performance.
- As discussed later in this section, the damage functions for an entire industrial facility are obtained by combining the weighted average of component damage functions. This process is streamlined by using the same ground motion parameter for all components without adding uncertainties in the process due to aggregation of different ground motion intensities.
- The majority of the component fragility functions developed by other researchers are PGA-based and therefore using PGA facilitates the consideration of damage functions already available.
- Historical damage data for industrial plants is often available along with an estimate of the PGA at the site. Estimates of other ground motion parameters are generally not reported.

Some components' damage functions are leveraged from the infrastructure module. For example, pipelines and tanks are typical components of many large industrial facilities. For many other industrial components (e.g., chimneys, cooling towers, flare towers, open-frame structures, pipes, pipe racks, process towers, and silos), there is insufficient damage data or studies in the literature to derive damage functions accurately. In these cases, AIR used engineering analyses—primarily nonlinear static pushover analyses. Most industrial facility components are simple structures and vibrate in essentially one mode, which makes static pushover analysis appropriate. All analyses were carried out in accordance with state-of-the-art, performance-based provisions, taking into account the complexity of each component and its characteristic response to shaking.

Structural models were subjected to a progressively increasing lateral force (corresponding to increasing levels of ground motion) to evaluate the trigger of key limit states, ranging from the onset of inelastic response to complete structural collapse. The response of each structure was quantified in terms of a functional relationship between the ground motion intensity (PGA) and the key limit states of the structure (e.g., first yield, buckling, ultimate strength of anchor bolts, instability, etc.). The damage ratio associated with each limit state was derived in accordance with ATC-13 guidelines.

Figure 83 shows pushover analysis results for an open-frame plant structure being displaced in two orthogonal directions. As the figure indicates, under the action of transverse lateral loads, the first limit state is the buckling of a knee brace (shown by the red dot in the left figure in the left panel), and is associated with a sharp drop in the lateral strength. As the lateral load increases, an additional brace buckles, resulting in another drop in the lateral strength.

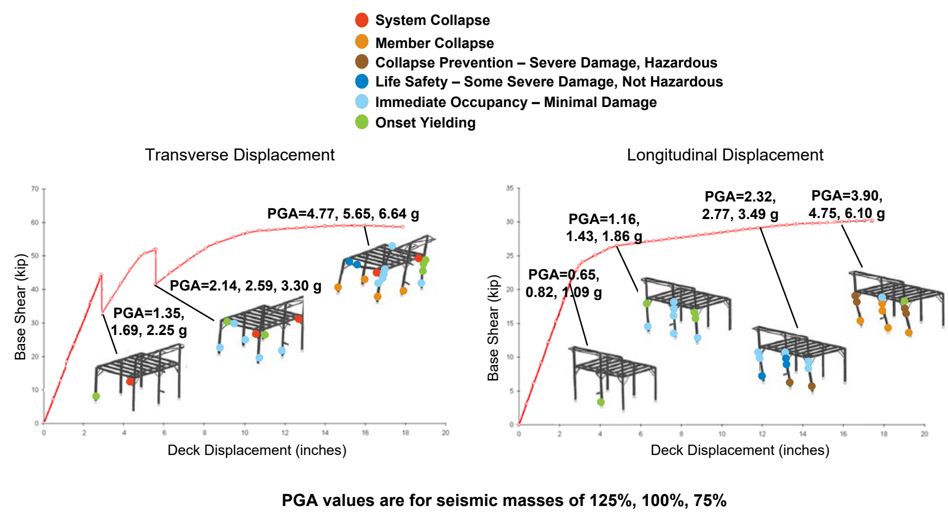

Figure 83. Pushover analysis results for an open-frame structure showing PGA values at several limit states

Additional stress in the legs and braces results in more deformation and eventual collapse. With increasing lateral loads in the longitudinal direction, the first plastic hinge forms at the base of a leg, followed by more plastic hinges at the leg bases and braces.

Each engineering analysis takes into account three different loading conditions: light, moderate, and heavy. This is done to take into account the variability in the live load, which affects the performance of structures in earthquakes. The transverse displacement has three limit states, while the longitudinal displacement shows four limit states. These correspond to live loads (seismic loads) equal to 75%, 100%, and 125%, respectively, of the dead load of the structure itself. The dead load includes the self-weight of the structure and appurtenances, plus any equipment that it supports. The three PGA values close to each illustration represent the average ground motion level that brings that structure to the specified level of deformation, for each of the three loading conditions.

With a lighter load, a higher level of PGA is needed to bring the structure to the onset of a specific limit state. For example, at the first longitudinal displacement, a PGA value of 0.65 g is needed to bring this open frame structure with heavy load conditions (i.e., live loads equal to 125% of dead load) to the onset of minor damage. However with moderate loading on the same structure, a higher PGA (0.82 g) is needed, on average, to reach the same level of damage.

The following two figures show damage functions for open-frame structures with different load conditions derived from pushover analysis. Figure 84 shows the damage functions for an open-frame steel plant structure. Figure 85 shows the damage functions for an open-frame steel dock, which has a narrow frame supporting pipes and equipment.

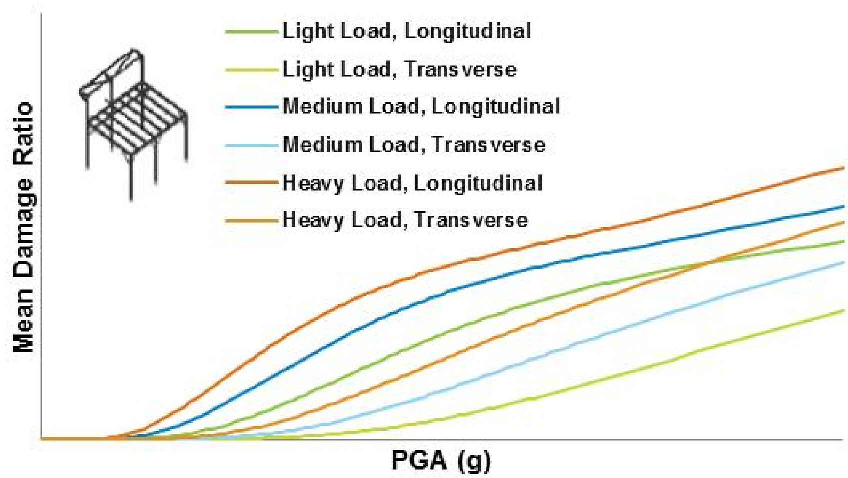

Figure 84. Damage functions for an open-frame steel plant structure

For each type of industrial facility, the aggregated damage functions were developed based on the damage functions for the component classes (e.g., tanks) and subcomponent classes (e.g., fully anchored tanks). The damage functions for each component and subcomponent were assigned a weight equal to the ratio between the replacement value of the class to the replacement value of the industrial facility.

The weights for different industrial facilities were derived from three major sources: studies performed by AIR for private industrial corporations (e.g., petrochemical and chemical facilities); ATC-13 1985 (for industrial classes such as heavy and light fabrication and assembly, food and drug, chemicals, metals, high technology, construction, and mining); and HAZUS (hydro- and thermo-power systems, potable and waste water, and gas processing plants). Each source provided, for each seismic region, a distribution of components for each type of facility.

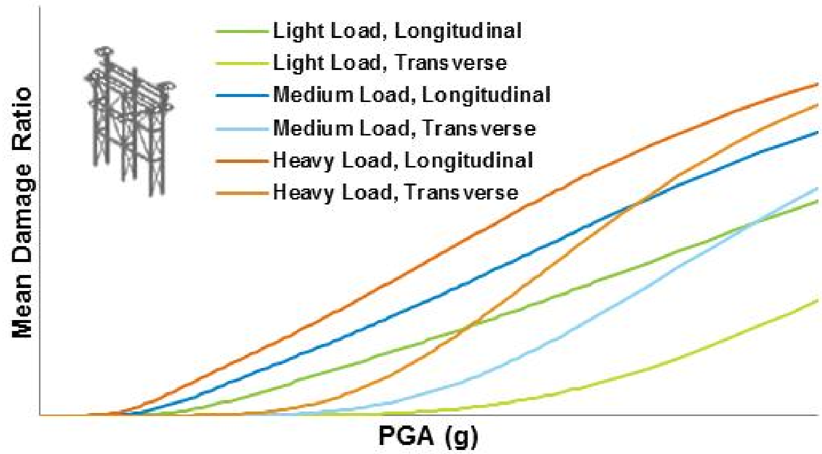

Figure 85. Damage functions for an open-frame steel dock structure

Based on consulting studies, some reasonable assumptions were made about the typical characteristics and weight of individual sub-components in an industrial facility to develop the damage functions for different components. For example, AIR assumed different percentages of anchored and unanchored tanks; and tanks with different filling levels and aspect ratios within a facility.

Once damage functions for components are developed, damage functions for facilities are constructed as a weighted average of the facility's primary components. Regional variation is then applied to facility-level damage functions, accounting for regional variation in seismic design and construction. Six seismic vulnerability classes are defined to reflect the regional variation in vulnerability of large industrial facilities. These classes are defined with respect to the seismic design requirements and construction practice in various regions in United States. Table 22shows the six vulnerability classes and the regions that they represent in the AIR Earthquake Model for the USA in the increasing order of vulnerability. That is, Seismic Vulnerability Class 1 assigned to California represents the least vulnerable facilities whereas Class 6 assigned to the rest of the USA represents the most vulnerable facilities.

Table 22. Seismic Vulnerability Classification for large industrial facilities in increasing order of vulnerability

Seismic Vulnerability Class	Region
IFM Seismic Vul Class 1	California
IFM Seismic Vul Class 2	Salt Lake City
IFM Seismic Vul Class 3	Pacific Northwest (Washington and Oregon)
IFM Seismic Vul Class 4	Charleston South Carolina and the New Madrid Seismic Zone
IFM Seismic Vul Class 5	Northeastern United States
IFM Seismic Vul Class 6	The rest of the USA

As discussed in section 5.1, reginal vulnerability variation for large industrial facilities in Canada is determined by assigning appropriate seismic vulnerability classes in Table 22. Areas with elevated seismic risk in British Colombia and Quebec provinces are assigned Seismic Vulnerability Class 3 (Washington and Oregon) and other regions in Canada are assigned Seismic Vulnerability Class 4.

For example, an oil refinery in highly seismic zones is expected to be less vulnerable to earthquakes than a similar facility located in non-seismic zone. Figure 86 shows vulnerability differences between facilities located in these two regions in Canada.

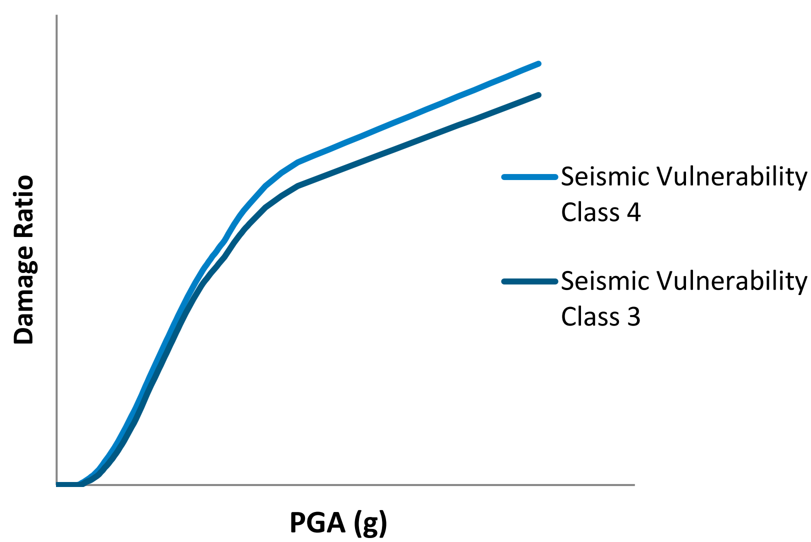

Figure 86 Comparison of damage functions for two oil refineries at two locations

For unknown facility types, the damage functions for different regions are obtained by performing the same weighted averaging of the damage functions for different industrial facility types in each area.

Table 23 lists all large industrial facility occupancy codes supported in the AIR Earthquake Model for the United States, which are grouped into 13 classes. Each class includes one or more sub-classes, which share similar primary components and manufacturing procedures. For example, the "Chemical, Oil and Gas Processing" class includes both gas processing plants (482), oil refinery systems (475), and specific chemical plants. From the top to the bottom of Table 23, the earthquake vulnerability among the 13 classes follows a decreasing order. Electric substations are the most earthquake vulnerable types of facilities and power plants are the least vulnerable. Within each class, the vulnerability of sub-classes has limited variation.

Table 23. Notes on vulnerability of main components of supported large industrial facility classes and sub-classes

Facility Type	Notes
Electric Substations	
479-Electric Substation	A majority of substations were designed and constructed without proper seismic provisions.
Chemical, Oil and Gas Processing	
438-General chemical processing	Primary facility components include pipes, tanks (raw material and finished product storage), distillation towers (cracking units), heat exchangers, condensers and similar components, pipe connections that are prone to failure when subjected to ground shaking.
439-Chlorine plants	
440-Vinyl plants	
441-Light hydrocarbon or aromatics plant	
442-Plastics plants	
443-Chlorohydrin plants	
444-Fertilizer plants	
446-Other chemical and allied products	
475-Oil Refinery Systems	
482-Gas Processing Systems	
Food, Tobacco and Beverage	
429-General food and drug processing	Primary facility components include tanks, pipes, packaging and conveyer systems. The structure is not necessarily built to high standards with connections like pipes and the structure itself prone to failure when subjected to ground shaking.
430-Food and kindred products	
431-Tobacco products	
434-Wineries	

Retail, Wholesale and Miscellaneous	
402-Automotive manufacturer	Usually warehouses with automated systems (assembly and conveyers). They can be repurposed old factory/buildings or built for a specific purpose (not necessarily for an extended period of time).
407-Textile mill products	
409-Stone/clay/glass/ceramics products	
414-General light fabrication and assembly	
415-Furniture and fixtures	
416-Apparel and other finished products made from fabrics and similar materials	
417-Printing/ publishing and allied industries	
418-Rubber and miscellaneous plastics products	
419-Leather and Leather products	
424-Miscellaneous manufacturing industries	
425-Tire manufacturers	
Consumer Electronics - Product and Equipment	
420-Electronic and other electrical equipment (except computer equipment)	Primary components include high level of climate control, clean rooms (to an extent, not as sophisticated as semiconductors), a significant amount of manual labor in terms of assembly, high technology that are paid some attention with the goal of mitigating damage.
421-Measuring analyzing and controlling instruments	
422-Photographic medical and optical goods	
423-Watches and clocks	
457-Electronic computer devices	
460-Printed circuit boards	
Heavy Fabrication and Assembly	
401-General heavy fabrication and assembly	Primary components include various types of cranes (e.g. aerospace industry), rails, furnaces, and robots.
404-Industrial and commercial machinery and equipment	
405-Transportation equipment	
403-Fabricated metal products	
Raw Material Manufacturing	
406-Pulp/Paper and allied products	Primary components include chimneys, conveyer systems, furnaces, tanks, and storage constructions.
445-Cement plants/ Cement Mills	
449-General metal and mineral processing	
450-Primary metal industry	
451-Steel Mills	
452-Smelters	

Water Treatment	
480-Potable water Systems	Primary components include pumping stations, tunnels, pipes, and tanks.
481-Waste water treatment Systems	
Laboratory and High Technology Pdts	
432-Pharmaceutical plants	Specialized facilities that are generally built to high standards due to the sensitive nature of the manufacturing process. Components include clean rooms, climate control and possible vibration isolation. These facilities include expensive high precision machinery and are monitored / maintained to mitigate damage.
433-Biological Products (except diagnostic) Medicinal/Botanicals/Biomedical	
455-General high technology	
456-Semi-conductor and related devices	
458-Computer storage devices	
459-Electron tubes	
Lumber and Wood Products	
408-Lumber and wood products (except furniture)	These facilities usually have external operations with components that are highly durable (e.g. saws).
Construction	
463-General building/ construction contractors	These facilities usually include construction equipment such as cranes, excavators, trucks among others that are prone to damage.
464-Heavy constructions	
465-Construction special trade contractors	
Mining	
470-General mining	These generally include underground/large quarries, with few complex operations. Not much to damage. Note: Vulnerable parts would be initial product processing, and/or some machines.
471-Mining operations	
472-Metal mining	
473-Coal mining	
474-Mining / quarrying - Non-metallic mineral (except fuels)	
Power Plants	
476-Hydro-Electric Power Systems	Large structures built to high standards. Robust components with minimal damage potential (e.g. turbines, dams) (excludes nuclear)
477-Thermo-Electric Power Systems	

Content Damage in Industrial Facilities

For large industrial facilities, raw materials, products on production lines, and final products are modeled as contents in AIR's IFM module. In addition, a distinction is made between the modeling of solid and fluid (liquid or gas) raw materials and finished products. Solid raw materials are typically stored in warehouses or in stock yards. Given their rough nature, they are fairly robust and can be salvaged if they topple from shelves. Similarly, solid finished products are usually stored with some type of protective packaging. While they may be jostled by ground shaking, their packaging will likely provide protection, allowing the finished product to be salvaged.

Unlike solid raw materials or finished products, fluids are generally stored in tanks or pipes. Past earthquakes have demonstrated that tanks or pipes containing fluid are typically some of the most vulnerable components of an industrial facility. Therefore, when a tank or pipe is subject to damage, the fluid inside is prone to spillage or contamination. The expected consequence of spilled, escaped, or contaminated fluid (raw materials or finished products) is greater than that of solid raw materials and finished products.

Figure 87 presents shake damage functions for Coverage C for large industrial facilities.

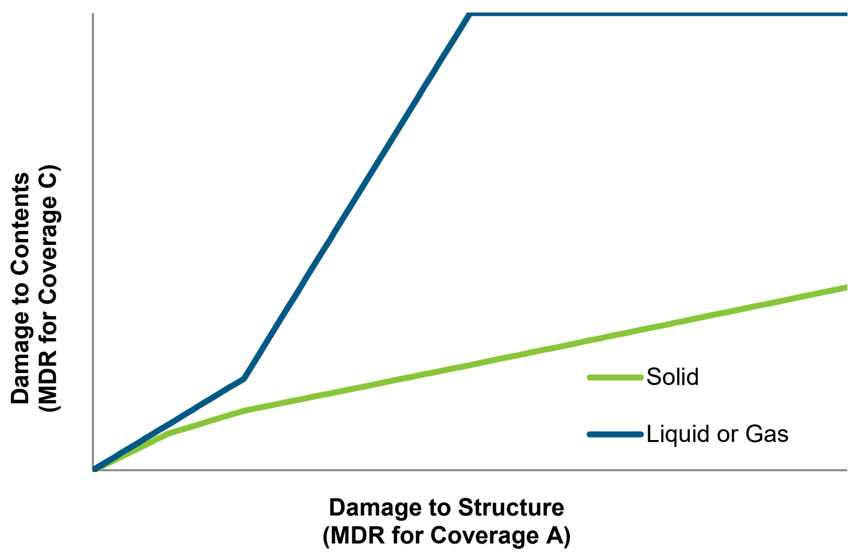

Figure 87. Content damage functions (for ground shaking) for large industrial facilities

Some industrial facilities produce fragile solid products while some products are robust. For example, computer storage device manufactures' product are sensitive and can be easily damaged. In the February 2016 Taiwan earthquake, TSMC (2016) reported damage to many silicon wafers that were in the process of being manufactured, although no structural damage was reported to their facilities. The damaged wafers caused delivery delay of 5 to 20 days.

Some industrial facilities use or produce hazardous products, such as vinyl plants, fertilizer plants, and other chemical product manufactures. Spill, leakage, or any kind of damage to the hazardous materials or products could cause serious environmental problems. Therefore, at the same level of ground motion intensity, hazardous contents can cause larger losses than non-hazardous ones.

5.6 Validating Shake Damage Functions

At AIR, damage functions are commonly validated by comparing them with damage functions developed by other researchers, as well as with actual damage data when these data are available. Due to lack of seismic damage observation in Canada, data from other countries – particularly the Unites States – have been used for developing damage functions in the AIR Earthquake Model for Canada. Because these damage data were directly used in generating the damage functions for many construction types, re-use of the same data for validation would not be appropriate. Thus, the AIR damage functions developed for the Canada earthquake model are validated using information from local vulnerability studies.

Validating Building Shake Damage Functions

In one of the few comprehensive vulnerability studies in Canada, Ventura et al. (2005) developed damage functions for some common construction types in British Columbia based on expert opinion. The study is similar to the well-known ATC-13 (1985) publication that presents a damage probability matrix for various construction types as a function of Modified Mercalli Intensity (MMI). Although AIR damage functions do not use MMI intensity, here we infer MMI-based damage functions from the output of AIR's model and compare them with those from Ventura et al. (2005) and ATC-13 (1985), for validation purposes.

For any simulated event, the AIR model determines ground motion parameters (PGA and SA) at all exposure locations. Using empirical relationships (e.g. Wald et al., 1999; Atkinson and Kaka, 2007), AIR then converts these parameters to an equivalent MMI intensity. Finally, when the modeled damage ratios are plotted against the converted intensities, the result is AIR damage functions (originally created in terms of PGA or SA) converted to MMI-based damage functions. Figure 88 compares the AIR converted damage functions to the damage functions reported in Ventura et al. (2005) and ATC-13 (1985), for the low-rise wood frame buildings.

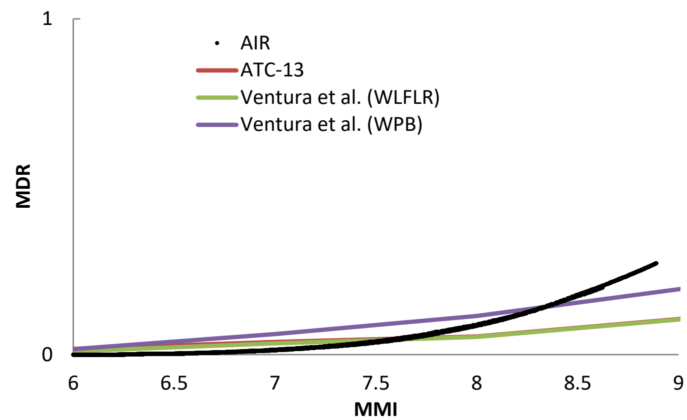

Figure 88. Damage function comparison for low-rise wood frame construction

It must be noted that a perfect match between the AIR damage functions and those of other studies, such as Ventura et al. (2005) and ATC-13 (1985), is not expected. This inevitable discrepancy stems from the fundamental difference in how these damage functions are generated. While the Ventura et al. (2005) and ATC (1985) studies are essentially expert opinion-driven, the AIR damage functions are developed through a hybrid analytical/observational approach.

Information deduced from published vulnerability studies – such as relative vulnerability among various building types – provides another means of validating the AIR damage functions. Comparisons of relative vulnerabilities obtained from the AIR model and those inferred from the literature are particularly valuable when they are based on local vulnerability studies. Relative vulnerabilities from Ventura et al. (2005) are therefore used for this validation step as well. Although the MMI-based damage functions from Ventura et al. (2005) are not directly applicable to AIR's model, the relativity inferred from this study indicates what local experts anticipate about the seismic performance of Canadian construction types.

Figure 89 compares the relative vulnerabilities, normalized to wood frame, from AIR's model with those inferred from Ventura et al. (2005) and with those from ATC-13 (1985). Note that the relative vulnerability here is approximated as the ratio of the area under the damage functions. As can be seen in the figure, relativity among different construction types in the AIR model is in reasonable agreement with those from other studies.

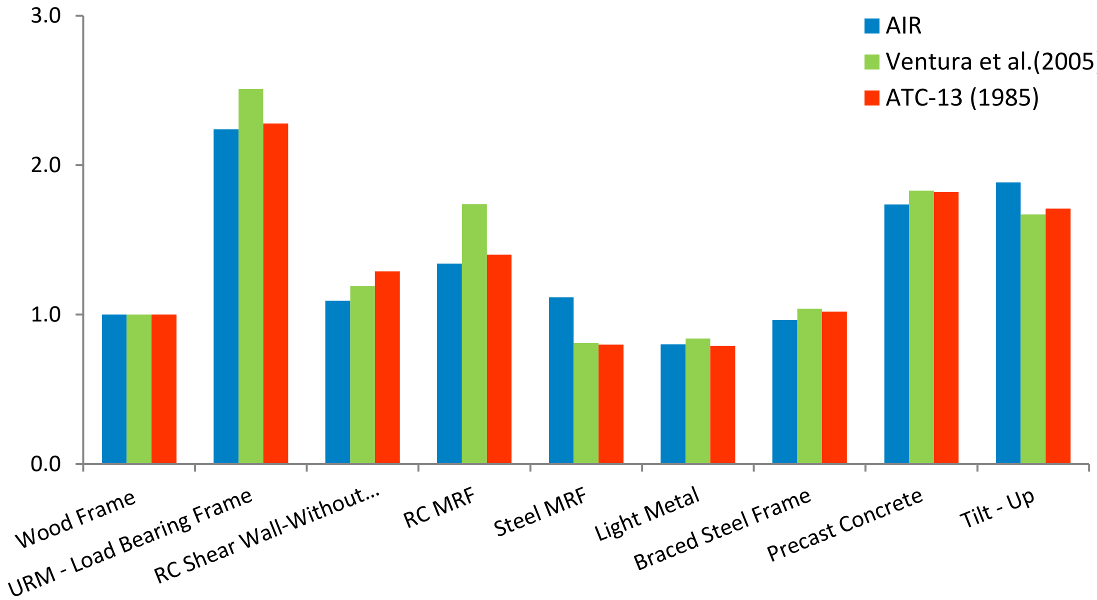

Figure 89. Relativity by construction type (normalized to wood frame) from AIR, Ventura et al. (2005), and ATC-13 damage functions

Validating Contents Shake Damage Functions

As discussed in Section 5.5, contents damage is a function of spectral acceleration and occupancy in the AIR model. Figure 90 compares the residential contents damage function in the model to contents claims data from the 1994 Northridge earthquake. Note the good agreement between the AIR contents damage function and the contents claims data.

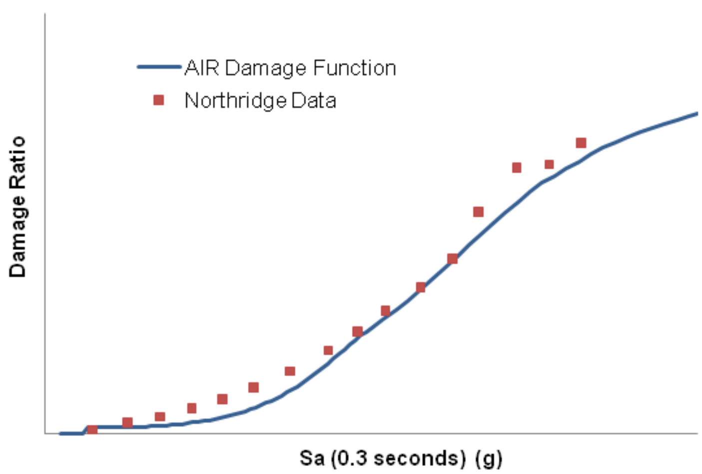

Figure 90. Northridge earthquake claims data and the AIR damage function for residential building contents

Validating Additional Living Expenses (ALE) Damage Functions

Additional Living Expenses, or ALE, loss – which is related to business interruption – is a function of the mean building damage, as discussed in Section 5.11. Figure 91 compares the AIR damage function for residential ALE to ALE claims from the 1994 Northridge earthquake.

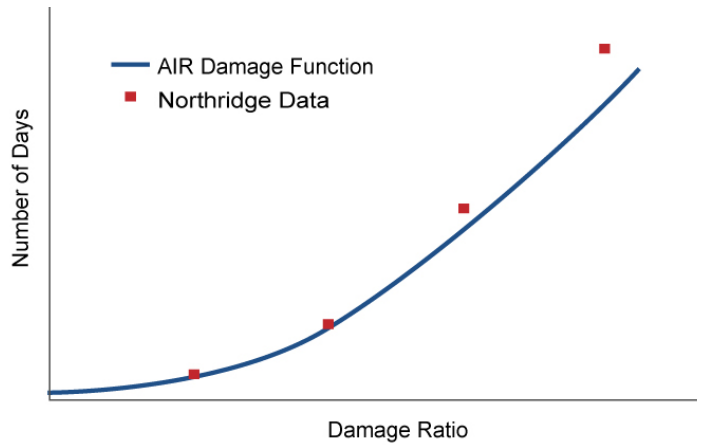

Figure 91. Northridge earthquake claims data and the AIR damage function for residential additional living expenses (ALE)

Validating Damage Functions for Industrial Facilities

To validate the damage functions (at both the component and facility level), observational damage data to industrial facilities was collected from damage reconnaissance reports after historical earthquakes. Table 24 lists 40 historical earthquakes from which damage data was collected for validating the damage functions for industrial facilities.

Table 24. Historical earthquakes used for industrial facility and component damage function validation

Earthquake	Year	Earthquake	Year
Gediz, Turkey	1970	Dinar, Turkey	1995
San Fernando, California	1971	(Hyogo-Ken Nanbu) Kobe, Japan	1995
Imperial Valley, California	1979	Lijiang, Yunnan Province, China	1996
Borah Peak, Idaho	1983	Adana-Cayhan, Turkey	1998
Coalinga, California	1983	El Quindio, Colombia	1999
Morgan Hill, California	1984	Chichi (Jiji), Taiwan	1999
Chile	1985	Kocaeli, Turkey	1999
Michoacan, Mexico	1985	Duzce, Turkey	1999
San Salvador, El Salvador	1986	Nisqually, Washington	2001
Palm Springs, California	1987	Bhuj, India	2001
Whittier Narrows, California	1987	Southern Peru	2001
Tejon Ranch, California	1988	Molise, Italy	2002
Armenia	1988	Denali, Alaska	2002
Loma Prieta, CA	1989	Boumerdes, Algeria	2003
Philippines	1990	San Simeon, CA	2003
Costa Rica	1991	Bam, Iran	2003
Erzincan, Turkey	1992	Tecoman, Mexico	2003
Hokkaido-Nansei-Oki, Japan	1993	Nigata Ken Chuetsu, Japan	2004
Guam	1993	Sumatra, Indonesia	2004
Northridge, CA	1994	Hawaii	2006

Figure 92, Figure 93, and Figure 94 show facility-level damage functions plotted against observational data from some historical earthquakes.

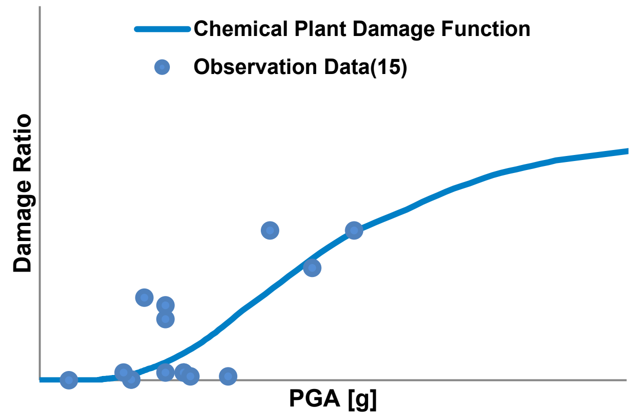

Figure 92. Damage functions and observed damage data for chemical processing plants in a high seismicity area

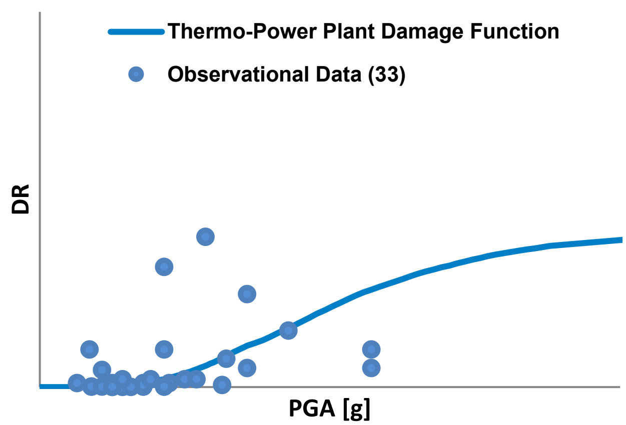

Figure 93. Damage functions and observed damage data for a thermo-power plant in a high seismicity area

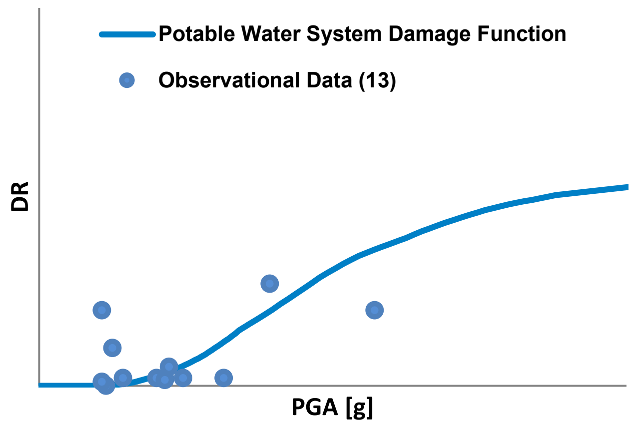

Figure 94. Damage functions and observed damage data for potable water systems in a high seismicity area

Validating Damage Functions for Large Industrial Facility Contents

To validate IFM Coverage C damage functions, AIR collected observational damage data from post-event reconnaissance reports. Figure 95 provides a comparison of observed and modeled mean damage ratios (MDRs) for contents at different types of large industrial facilities.

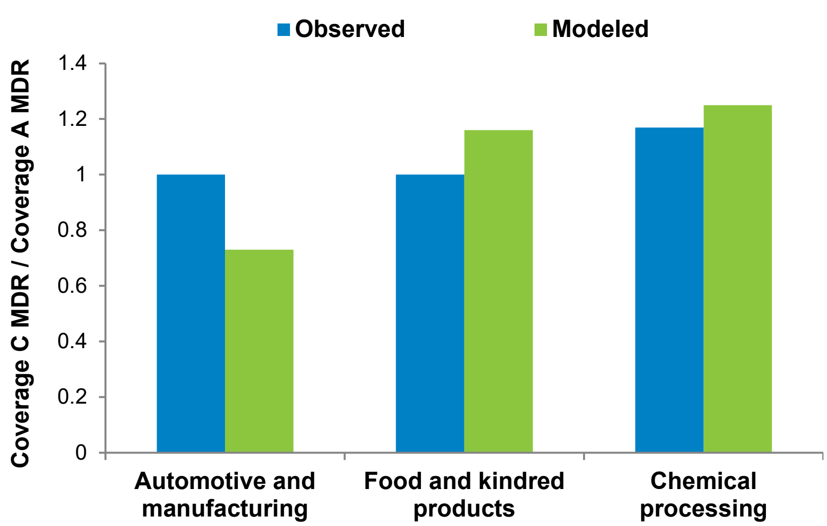

Figure 95. Mean damage ratios for observed and modeled IFM coverage C for different types of large industrial facilities

Validating the Distribution of Damage

As discussed in Section 5.5, similar structures at a given location may experience different levels of damage. To capture this uncertainty in damage, the AIR model constructs distributions around the mean damage ratio. Although beta distributions are commonly used, they do not accurately reflect the variation in damage. Following an extensive analysis of claims data, AIR engineers found that a combination of two beta distributions (referred to here as a bimodal-beta distribution) better represents the uncertainty. This point is illustrated in Figure 96, which compares the modeled and observed damage distributions at mean damage ratios of 0.026 and 0.17. The observed and modeled damage distributions are notably consistent.

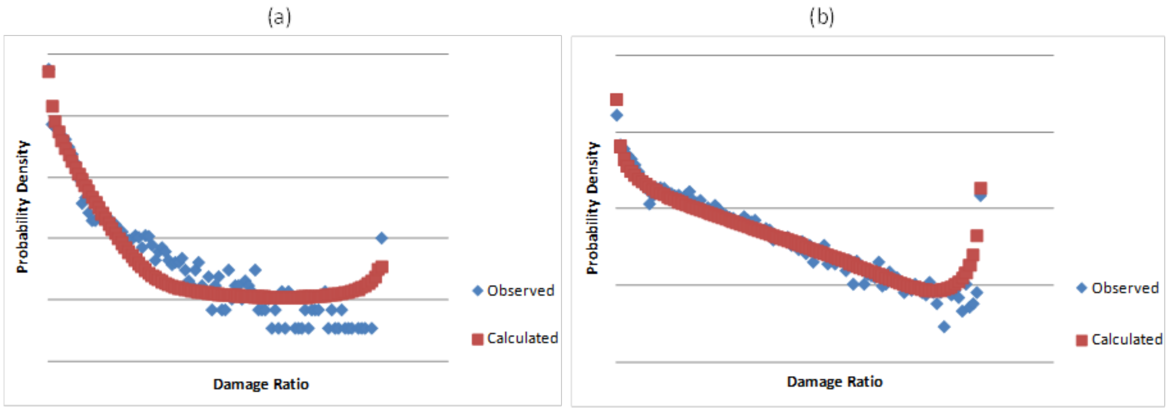

Figure 96. Modeled and observed probability distributions of damage where: a) mean damage ratio is 0.026; and b) mean damage ratio is 0.17

5.7 Liquefaction Damage

In the AIR model, building damage resulting from liquefaction is modeled as a function of permanent ground displacement (PGD), which causes damage when the building becomes vertically displaced due to post-liquefaction reconsolidation settlement. To determine vertical ground displacement, the AIR method uses the relationship between factor of safety and volumetric strain proposed by Ishihara and Yoshimine (1992). The Liquefaction Potential Index (LPI) is also calculated by integrating the factor of safety along soil profile. Liquefaction Potential Index values are used to calculate correction factors which represent the percentage of map unit subject to liquefaction for each grid.

Specifically, to develop damage functions for liquefaction, AIR engineers incorporated a process published by HAZUS (FEMA 2012) to determine the probability of damage due to permanent ground displacement (PGD). This information was combined with damage functions that AIR created using a combination of empirically and statistically derived functions based on earthquake-induced liquefaction damage in New Zealand and Japan.

AIR made extensive use of observational data from two major liquefaction events in 2011: those of March 11 offshore of Tohoku, and February 22 in Christchurch, New Zealand. Both of these events provided valuable claims data and observational data on liquefaction damage and the Christchurch earthquake also provided important insight into liquefaction effects. While shaking intensity was moderate and weaker than the September 4, 2010 earthquake in the same region, it was very shallow and ground shaking affected sediments prone to liquefaction, directly under the city of Christchurch.

For the Christchurch liquefaction data, AIR engineers studied the change in the ground surface elevation and resulting building damage using data from the Earthquake Commission (EQC) of New Zealand. Similar data from the Tohoku event was obtained from the Japan Government. The amount of damage was categorized based on ground settlement. Figure 97 shows an example liquefaction damage function developed based on observational liquefaction damage from the two events.

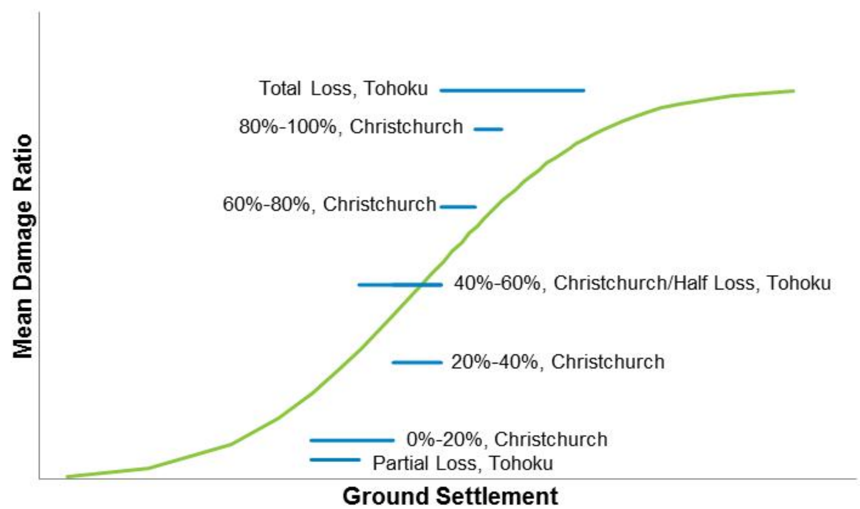

Figure 97. Example of a liquefaction damage function

Note that contents damage due to liquefaction is not included in the AIR model. This is because the vertical displacement associated with liquefaction has been shown to result in negligible damage to contents.

Automobile damage during an earthquake may occur due to liquefaction-induced ground failure. Therefore, damage to automobiles inflicted by liquefaction, as a function of permanent ground displacement, is included in the AIR model.

It is important to recognize that the AIR liquefaction module relies on surficial geological maps, and the limited soil profile data that is available, for evaluating liquefaction hazard. This approach yields reasonable estimates of liquefaction damage on a *regional* scale; however, predicting site specific liquefaction damage requires additional input, such as detailed geotechnical data and building foundation characteristics. It is also important to recognize that the AIR model does not account for efforts to mitigate liquefaction at specific sites.

Finally, note that liquefaction losses will not be separable from shake losses in the AIR software.

5.8 Landslide Damage

To develop the damage functions for landslide, AIR engineers incorporated a process published by HAZUS (FEMA 2012) to determine the probability of damage due to permanent ground displacement (PGD). In the model, landslide damage ratios are calculated at the resolution of the underlying DEM (about 30 m x 30 m in urban areas). In this calculation, the exposure is assumed to be uniformly distributed inside each 1 km^2 grid cell.

In the AIR model, landslide damage to buildings, contents, and automobiles is assessed. Automobile damage during an earthquake may occur due to landslide-induced ground failure. Therefore, damage to automobiles inflicted by landslide, as a function of permanent ground displacement, is included in the AIR model.

A sample damage function for landslide damage to buildings is shown in Figure 98.

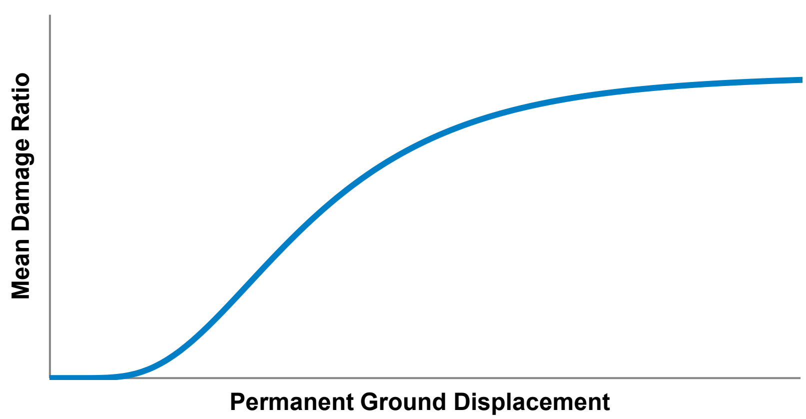

Figure 98. Sample damage function used in the AIR model to estimate landslide damage to buildings

Areas that are underlain by sensitive marine sediments in the Ottawa and St. Lawrence River valleys are highly vulnerable to earthquake-triggered landslides. Leda clay, a sensitive marine clayey silt, loses its strength and becomes liquefied upon disturbance. Once movement is initiated, the unique properties of the Leda clay allow it to flow quite rapidly, even in areas with relatively low topographic relief (Aylsworth et al., 2000). Traditional regional earthquake-triggered landslide analysis does not consider earth flows in sensitive sediments. One of the reasons for this exclusion is that identification of areas where sensitive sediments may be present requires extensive site-specific surveys (Calvert and Hyde, 2002). Therefore, AIR does not model Leda clay landslides because there is not sufficient information on the location and extent of these sensitive sediments.

It is also important to note that the AIR model uses a generalized approach that provides reasonable estimates of landslide damage at a regional scale, but the model does not provide site specific slope stability analysis. Site-specific evaluations require more detailed slope profile and geotechnical information; therefore, it is not practical to perform site-specific evaluations at the regional level.

5.9 Tsunami Damage

The AIR Earthquake Model for Canada provides explicit tsunami damage estimates for all lines of business. To achieve this goal, AIR derived tsunami damage functions using empirical relationships among observed damage, tsunami effective depth, the velocity of the water, and debris collision. Additional sources of damage such as soaking, scouring, contamination, and sedimentation are implicitly accounted for in the damage estimates, as the data used to develop the damage functions include the losses due to these sources.

Details of how the damage functions for tsunami were developed are provided below. Examples of tsunami damage functions for buildings, contents, automobiles, and complex industrial facilities are also provided.

Development of the Tsunami Damage Functions

There are a number of processes that can be used to estimate building damage and loss due to tsunamis. These include the use of vulnerability indexes, tsunami loading, and fragility curves. Vulnerability indexes are suitable for regional tsunami hazard analysis but lack damage analysis and are therefore not useful for tsunami loss estimates. Tsunami loading does not provide a complete relationship between tsunami forces and property damage. Fragility curves, which provide a relationship between the water depth (or velocity), and the amount of damage that can result based on the construction and occupancy classes of the structures being analyzed, were therefore selected by AIR engineers as the more appropriate method for estimating building damage and loss due to tsunamis.

Fragility Curves

The tsunami damage functions of the AIR Earthquake Model for Canada employ fragility curves that were developed using extensive data from the 1993 Hokkaido, 2004 Indian Ocean, and 2011 Tohoku tsunamis. In addition, studies from Japan's Ministry of Land, Infrastructure, Transport and Tourism (MLIT, 2012), and a study by Witter et al. (2008) on the Oregon tsunami of 1700, were used to determine relationships between tsunami flow and velocity, which were in turn used to develop the tsunami damage functions.

Figure 99 shows examples of fragility curves. In the curve on the right, the current velocity refers to the water current, which affects the forward velocity of the tsunami wave front. A structure may be completely destroyed when the tsunami intensity (inundation depth or water current velocity) exceeds a certain level.

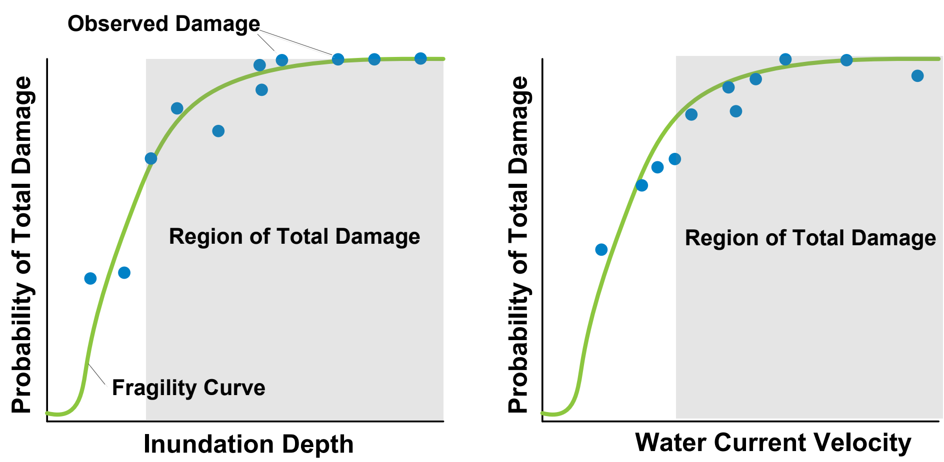

Figure 99. Examples of fragility curves used for determining likely tsunami damage based on inundation depth (left panel) and current velocity (right panel).

Damage States

A key component of tsunami damage function development is determining a relationship between each damage state and the expected damage ratio for different levels of tsunami inundation. To do this, AIR researchers compared damage states from several studies of empirically-derived vulnerability functions.[17] Following this method, AIR was able to derive realistic damage ratios that corresponded with these damage states. Damage states used in developing the fragility curves, which are shown in Table 25, were adapted from MLIT report (2011a).

[17] These studies include several from HAZUS (1999), ATC-13, and RISK-UE, as well as Rossetto and Elnashai (2003).

Table 25. Damage states used in developing fragility curves

Damage State	Description
D0	No damage.
D1	Light damage. Basement is inundated but not the first floor. Mud removal is necessary for occupancy.
D2	Minor damage. Inundation less than 1m. Some repair is necessary for occupancy.
D3	Moderate damage. Inundation is at least 1m but does not top the first story of the building. Significant repairs are necessary for occupancy.
D4	Major damage. Inundation is above the first floor. Major repairs are necessary for occupancy.
D5	Total damage. Building is completely submerged or washed away.

Incorporating Topography in Tsunami Damage Functions

As described in Section 4.4, the shape of the coastline has a significant effect on inundation as the bays and inlets along a jagged coastline can amplify tsunami waves. The inland extent is also greatly affected by elevation. At the same time however, the mountainous areas usually associated with jagged coastlines cause a sharper increase in elevation, which prevents in inland extent of tsunamis. The effect of elevation is significant; observations after several tsunamis show a sharp drop in tsunami damage with just a slight change in elevation.

Studies from Japan's Ministry of Land, Infrastructure, Transport, and Tourism (MLIT) provide a great deal of data on the effects of the tsunami flow velocity in these areas, taking into account the existence of levees. AIR engineers used these studies and observations from the Tohoku tsunami, the Indonesia tsunami of 2004, and the study by Witter et al. (2008) of the Oregon tsunami of 1700 to develop relationships between the tsunami flow and velocity to use in the damage functions.

Calculating the Mean Damage Ratio for Tsunami Damage

As described earlier in this section, and in Section 4.4, tsunami damage is highly sensitive to inundation depth, which is affected greatly by the local elevation. It was therefore necessary to account for the uncertainty in the digital elevation model when determining the mean damage ratio for tsunami damage. A recent study conducted by the National Aeronautics and Space Administration (NASA) shows uncertainty is inherent even in very high resolution digital elevation models (Tachikawa et al., 2011).

Therefore, in order to obtain the most reliable damage estimate possible, AIR engineers explicitly accounted for the uncertainty in the digital elevation data used by the model. To do this, they developed a two-step process to determine the mean damage ratio for tsunami damage.

As described in Section 3.8, the lifetime of a tsunami is modeled using a series of nested computational grids, with the finest, innermost grid having a resolution of 125 meters. For the first step in the calculation of the mean damage ratio, the effective inundation depth is determined for each 125-m grid cell, as described in Section 4.4. For the second step, the mean damage ratio is determined for each 125-m grid cell, and then averaged over the 1-km grid containing the exposure.

Let N_{land} be the number of 125-m grid cells that include land inside a given 1-km grid cell. Out of the N_{land} land grid cells, there are $M_{inundated}$ grid cells that are inundated (i.e., have positive effective inundation depth). The damage ratio for this 1-km grid cell can then be calculated as:

$$Mean\ Damage\ Ratio = \frac{\sum_{i=1}^{M_{inundated}} DamageRatio(i)}{N_{land}}$$

where $DamageRatio(i)$ is calculated for the i^{th} 125-m resolution land grid cell using the corresponding effective inundation depth. In Figure 100, a 1-km grid is illustrated by the red rectangle, which includes smaller light gray squares that indicate the 125-m cells.

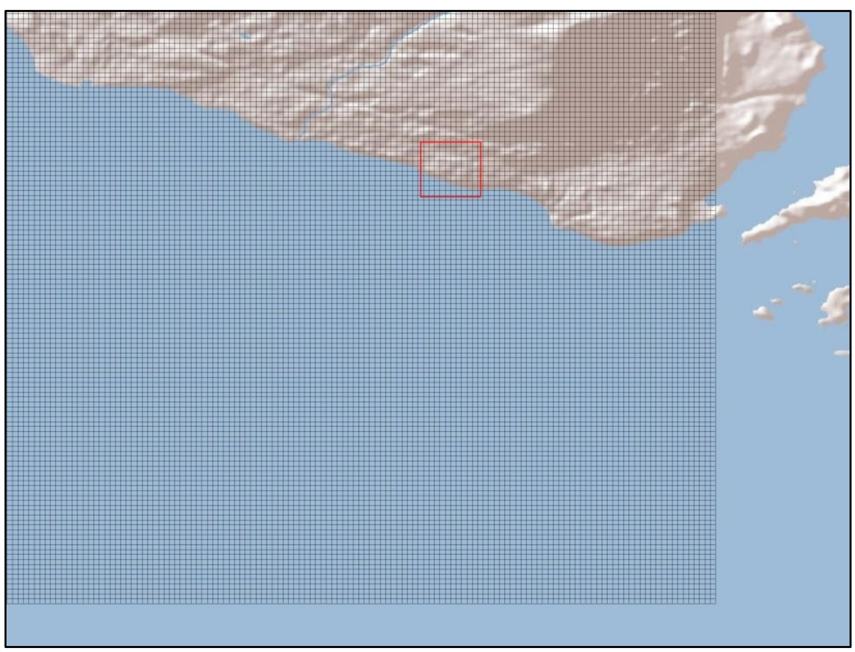

Figure 100. The mean damage ratio is determined for each 125-m grid cell (black) and then averaged over the 1-km grid (red square) containing the exposure

Using a method similar to that used for shake damage, the model constructs probability distributions around the mean damage ratio. These distributions account for the uncertainty in the building's resistance to tsunami damage. See "The Distribution of Damage: Uncertainty in Damage Estimation" in Section 5.5.

Tsunami Damage Functions for Buildings

In the AIR Earthquake Model for Canada, tsunami damage to buildings is influenced by several factors, including building construction class, building height, and the presence of debris. The effects of these three factors, and example damage functions for each, are provided below.

Effect of Construction Class

According to an analysis conducted by MLIT (2011b), wooden structures experienced much heavier damage from the 2011 Tohoku tsunami than other construction classes (see Figure 101).

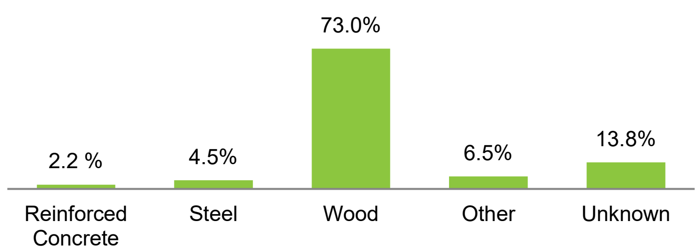

Figure 101. Percentage of construction classes damaged by the 2011 Tohoku tsunami (MLIT, 2011b)

Further analysis of survey and claims data was performed to determine the performance of different construction types. Virtually all of the data indicated that timber was significantly more vulnerable to tsunami inundation, with masonry being less vulnerable than timber but more vulnerable than steel or reinforced concrete buildings.

Wood buildings are far more susceptible to tsunami damage than steel or concrete ones. This is due not only to the materials, which are weaker in the face of moving water, and more vulnerable to buoyant force, but also to the fact that wood buildings are usually residential and no higher than three stories, and therefore not well-engineered and more susceptible to flood damage.

Both steel and reinforced concrete buildings are generally used for commercial purposes and have a higher degree of engineering than wood or masonry residential buildings. The material itself is also less vulnerable to tsunami damage. According to many studies, including those from AIR, steel is more vulnerable than concrete for a number of reasons. Steel is lighter than concrete and therefore more vulnerable to buoyant force, and is also susceptible to erosion from seawater. Steel buildings located in coastal areas can show a higher vulnerability if enough erosion has occurred to make them more easily damageable if a tsunami strikes.

Figure 102 shows the damage functions for different effective inundation depths for different construction types.

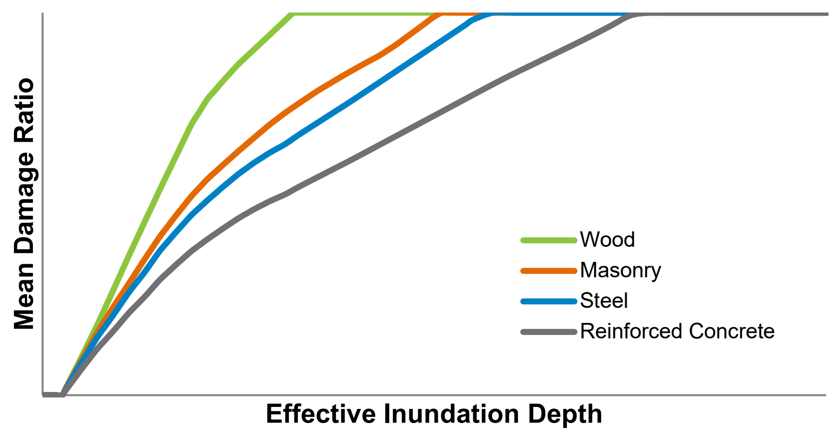

Figure 102. Tsunami damage functions for different construction classes

Effect of Building Height

The height of a building, which is largely determined by its occupancy class, is an important factor for determining tsunami vulnerability. For example, high-rise buildings receive a higher degree of engineering and are usually constructed of steel or reinforced concrete, rendering them less vulnerable to tsunami damage. In addition, a larger portion of the building stands above the inundation depth, so a lower percentage of the building is damaged. Even though higher buildings may have more fittings and fixtures on the lower floors, perhaps entire shops or apartments, the fact that they are engineered, and generally have better flood control systems, makes a significant difference in the amount of damage. Figure 103 shows the effect of height on the damage ratio for a reinforced concrete building. As shown in the figure, the mean damage ratio for buildings of all heights increases with increasing inundation depth, with damage to low-rise buildings (1-3 stories) rising dramatically. However, the effect levels off at higher inundation depths (after total damage is reached).

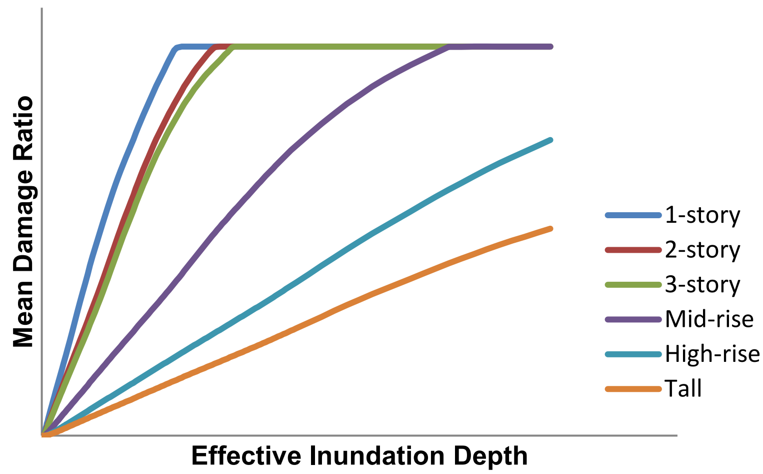

Figure 103. Tsunami damage functions for reinforced concrete buildings of different heights

Figure 104 compares observational claims data from a major insurer in Japan with modeled tsunami damage for a low-rise steel building. (Data for Japan are shown here by way of comparison, because similar data for Canada are not available.)

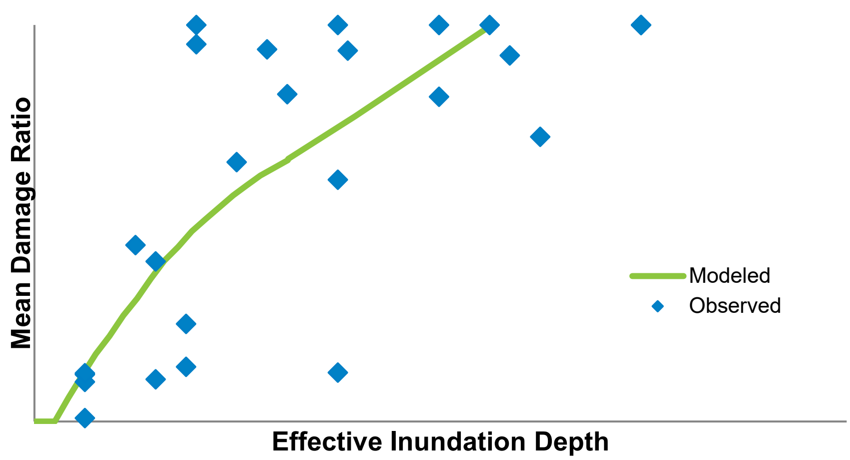

Figure 104. Observed tsunami damage and modeled damage function for low-rise steel buildings

Effect of Debris on Building Vulnerability

Debris is any item that is dislodged from its original position by a tsunami, and is buoyant enough to be carried along with the waves. If the tsunami is large enough, this can include large structures such as marine craft, crates, vehicles, or any item located in or near the coast. As witnessed during the Tohoku tsunami, the damage caused by debris impact can be immense (see Figure 105).

Figure 105. Any object dislodged by a tsunami becomes potentially damaging debris, Kesennuma, Miyagi Prefecture, 2011 Tohoku tsunami

In the AIR Earthquake Model for Canada, three debris zones – light debris, moderate debris, and heavy debris – are developed for tsunami-prone areas. Figure 106 shows the debris zones in the Vancouver region. Each debris zone is assigned an empirically-developed debris function. At very shallow depths (<0.5 m), no debris is created; hence, there is no debris effect. As the inundation increases, the buoyancy forces increase and debris generation becomes possible. The debris effect increases with inundation to a point; it then tapers off at higher inundation levels where the building is already damaged and the debris does not further increase the damage.

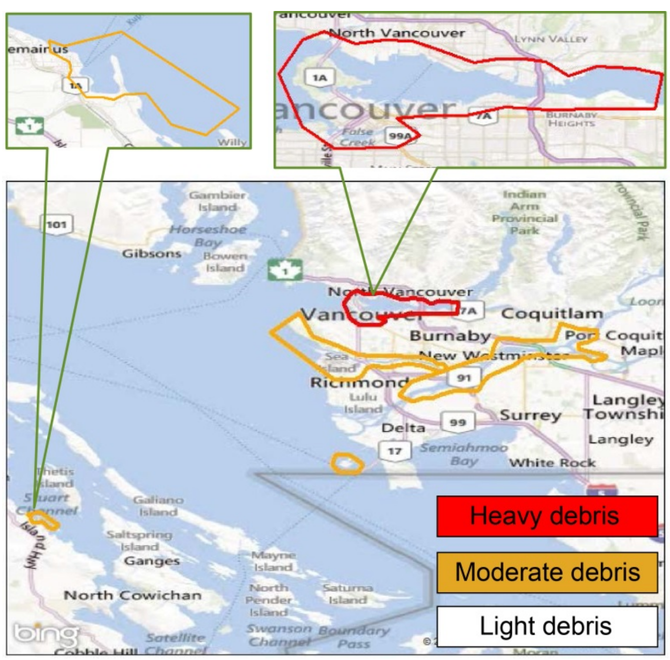

Figure 106. Tsunami debris zones in the Vancouver region

Figure 107 and Figure 108 show tsunami damage functions for low-rise buildings of different construction types for light and heavy debris, respectively. For wood frame buildings, which are nearly always low-rise residential buildings, the impact of heavy debris results in complete destruction at a relatively low inundation depth. Other buildings fare much better when impacted by heavy debris due to their construction materials.

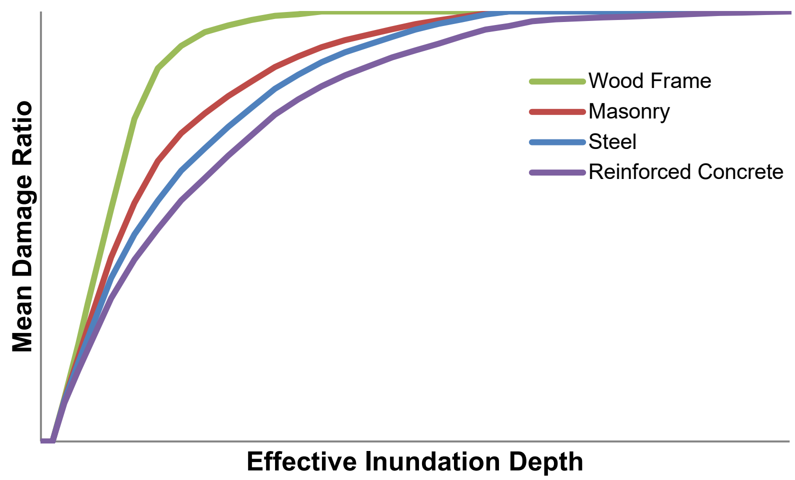

Figure 107. Tsunami damage functions for low-rise buildings of different construction types, with light debris

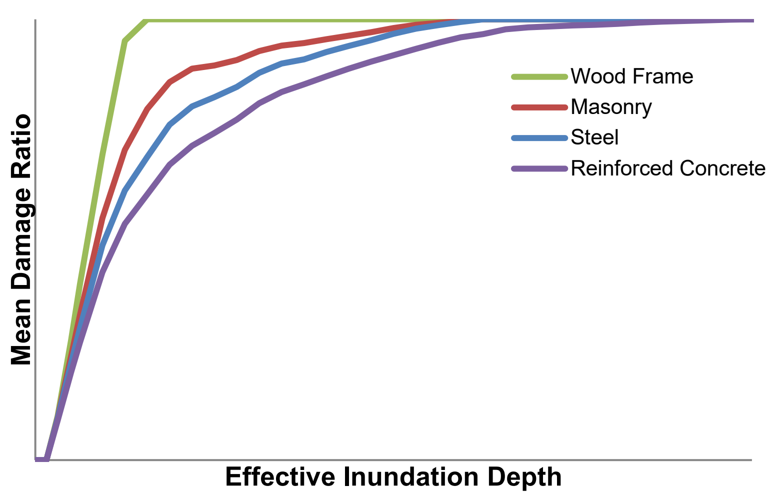

Figure 108. Tsunami damage functions for low-rise buildings of different construction types, with heavy debris

Figure 109 shows damage functions for each of the three types of debris for a low-rise wood frame residential building. The light debris damage function was calibrated against studies from Koshimura et al. (2009), and from a 2011 study of damage from the Tohoku tsunami conducted by MLIT.

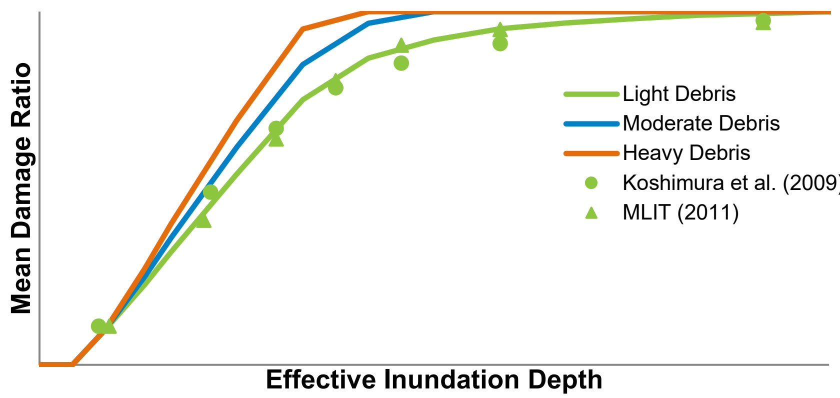

Figure 109. Effect of light, moderate, and heavy debris on damage ratio for a low-rise wood frame residential building

AIR engineers developed damage functions that capture the effect of different debris levels on each construction type in a similar manner. Figure 110 shows damage functions for a low-rise steel building, based on three levels of debris. The light debris damage function was calibrated against studies from Reese et al. (2011), and the 2011 study of damage from the Tohoku tsunami conducted by MLIT. Note that although the building is still low-rise, damage is mitigated due to the less vulnerable nature of steel as opposed to wood frame.

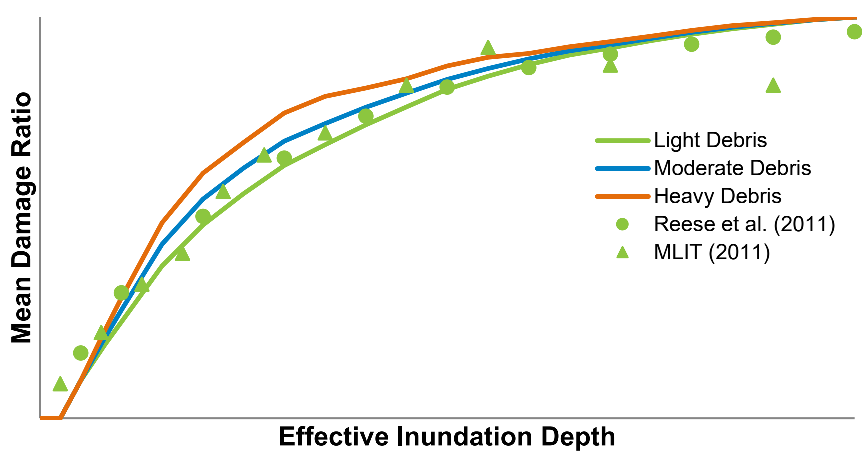

Figure 110. Effect of light, moderate, and heavy debris to damage for a low-rise steel commercial building

By analyzing the vulnerability of different construction classes to the effective inundation depth, and factoring in different amounts of debris, AIR engineers were able to develop damage functions for the building classes that are common in Canada.

Tsunami Damage Functions for Building Contents

When developing damage functions for building contents, AIR engineers assumed that contents are equally distributed across all of a building's stories. Therefore, at a given inundation depth, a low-rise building would experience a much higher damage ratio than a mid-rise or high-rise building. (No contents damage occurs in stories above the effective inundation depth.) For low-rise buildings, there is also a higher probability of the entire building being destroyed, in which case it is assumed that all of the contents are destroyed.

For taller buildings, not only will the buildings withstand higher effective inundation depths, but many of the contents can be moved to the upper floors to prevent damage. Figure 111 shows the damage functions for buildings of different heights. As expected, the mean damage ratio increases more quickly for shorter buildings.

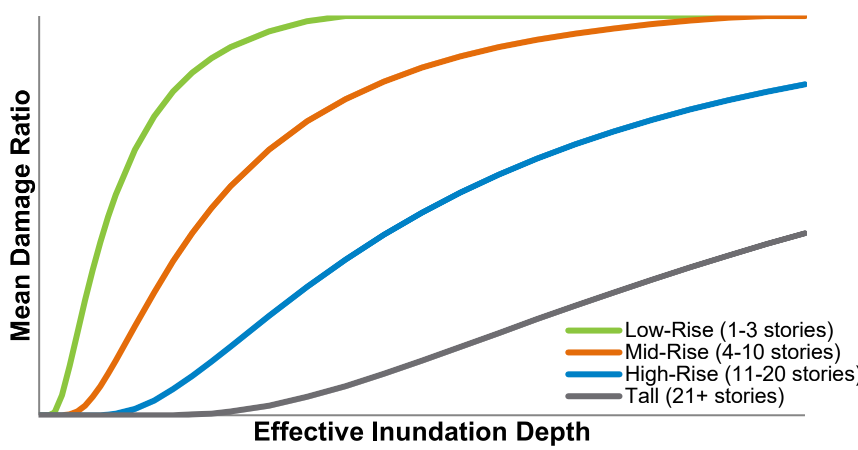

Figure 111. Tsunami damage functions for contents housed in buildings of different heights

Tsunami Damage Functions for Automobiles

Observations of automobile damage from tsunamis[18] indicate that the damage depends on the height of the exhaust pipe from the ground. Saltwater entering the exhaust pipe can be significantly damaging.

Automobile vulnerability to tsunamis is affected by the fact that the automobiles may be driven to a safe location when a tsunami warning occurs. AIR engineers assumed a 20% evacuation rate for automobiles. A sample tsunami damage function for automobiles is shown in Figure 112.

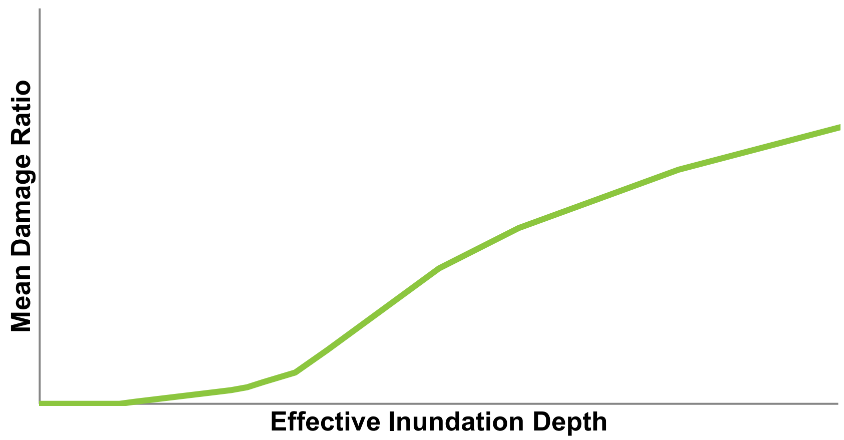

Figure 112. Tsunami damage function for automobiles

Tsunami Damage Functions for Complex Industrial Facilities

The damaging effects of tsunamis on industrial facilities have not been widely studied, due largely to the lack of historical data. Tsunamis that are damaging enough to significantly affect a facility are perceived as being relatively rare. Most established structural design codes provide little guidance to account for the effects of loads induced by tsunami inundation (Grundy, 2007). The design codes that do cover tsunami resistance are not comprehensive and are based on empirical rather than on physical relationships (Yeh, 2007; Cruz 2010; and FEMA P646, 2008). Further, impact forces from significant water-borne debris such as marine vessels and cargo containers cannot be accurately predicted and are not considered in current code provisions (Yim, 2006).

[18] Note that tsunami damage to the auto risk is significantly different from the tsunami damage to carpool risks. Carpools refer to autos that are parked at a port awaiting shipment, and cannot be evacuated.

However, observations show that the damaging characteristics of tsunamis have many similarities with those of tropical cyclone storm surges; in fact, many of the design codes that do exist for tsunami loading are based on storm surge design. While the generation mechanisms of the perils are entirely different, the physical characteristics of their wave propagation (in deep water), the nonlinear transformation (in shallow water), and inundation depth are identical (Yim, 2006). Observations of storm surge damage (e.g., structural damage, debris impact and uplift failures due to the surge from Hurricane Katrina) are consistent with those from past tsunami events (FEMA P646, 2008).

AIR has therefore been able to use the extensive research and analysis on storm surge vulnerability of industrial facilities when developing estimates of the vulnerability of industrial facilities to tsunamis. In developing these however, they did carefully consider the key differences between the perils; in particular, the higher flow velocities of tsunamis, which result in higher velocity-related loads on structures. A recent study (Koshimura, 2009) developed fragility curves in terms of inundation depth, current velocity, and hydrodynamic force due to tsunamis and determined that the best application of these functions was that regarding inundation depth. Even in state-of-the-art modeling of computational fluid dynamics, it is extremely challenging to estimate local tsunami current velocity as it is affected by many factors, particularly the inundation flow among densely populated areas.

Therefore, given the empirical nature of the relationships for tsunami load estimation, and the uncertainties associated with flow velocity estimation, AIR's analysis of tsunami vulnerability of industrial facilities is defined in terms of inundation depth, which can be observed and measured after all tsunami events and is therefore more reliable.

Tsunami Damage Functions for Industrial Facility Components

Because information on tsunami damage is limited, AIR researchers developed damage functions for industrial facility components using damage data or available research on storm surges. In these cases, information from many sources, including historical damage data, scientific literature, site-specific measurements, and structural analyses was incorporated to assign mean damage ratios over a range of inundation heights. All analysis took into account the complexity of each component and its characteristic response to water depth.

Figure 113 shows the damage functions for selected industrial facility components for tsunami, based on water depth.

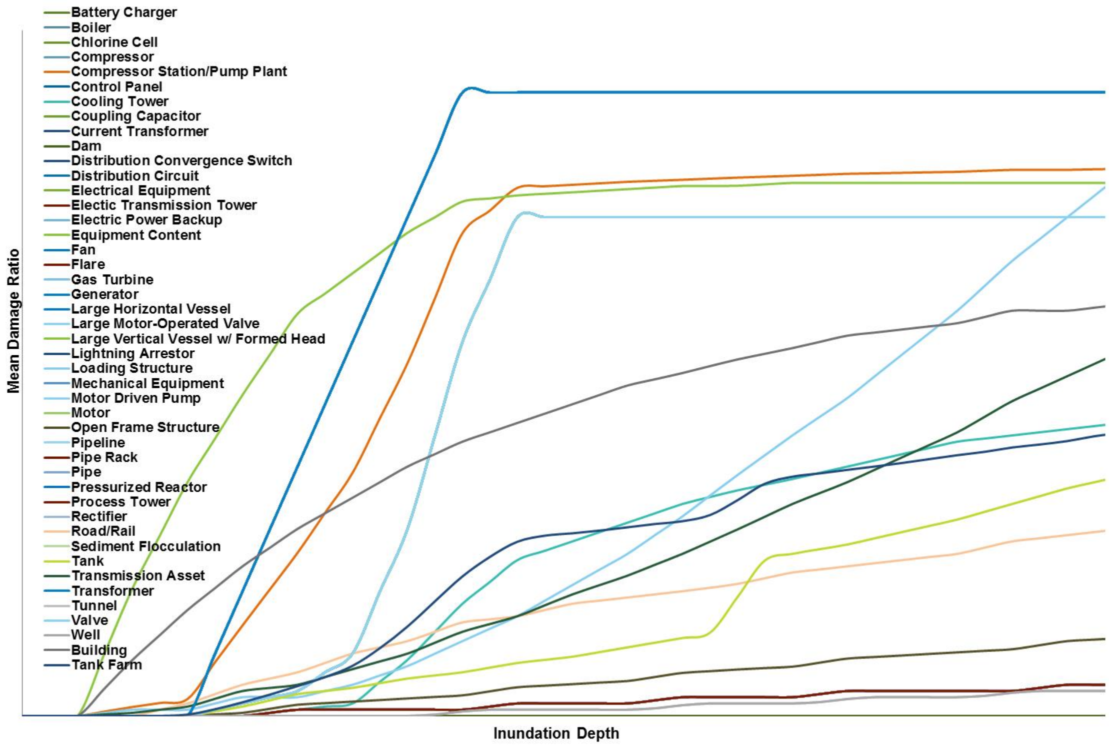

Figure 113. Tsunami damage functions for selected industrial facility components

Tsunami Damage Functions for Industrial Facilities

As with shake damage, AIR developed aggregated tsunami damage functions for each type of industrial facility, based on the damage functions for the components and subcomponents associated with that type of facility. The damage functions for each component and subcomponent were assigned a weighting factor equal to the ratio between the replacement value of the class and the total replacement value of the industrial facility. The facility-level damage function is a weighted average of the damage functions of the individual components.

Figure 114 shows the tsunami damage functions for selected industrial facilities, based on inundation depth. Damage functions for the unknown (general) facility type, indicated with a dotted black line, are based on the weighted average of the damage functions.

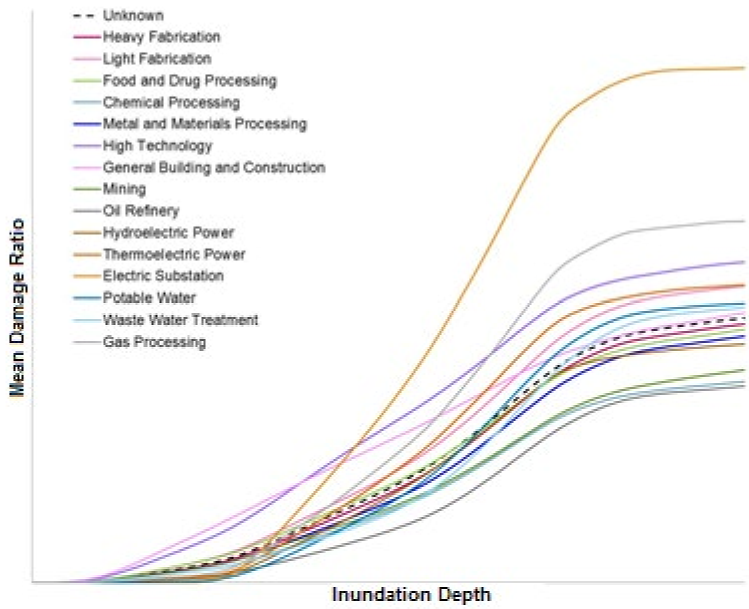

Figure 114. Tsunami damage functions for selected industrial facilities

Business Interruption to Industrial Facilities due to Tsunami Damage

As described for shake damage, business interruption damage functions at the facility level are derived from component distribution information and the individual component and subcomponent downtime functions.

Figure 115 shows the time element functions for selected industrial facilities due to tsunami damage.

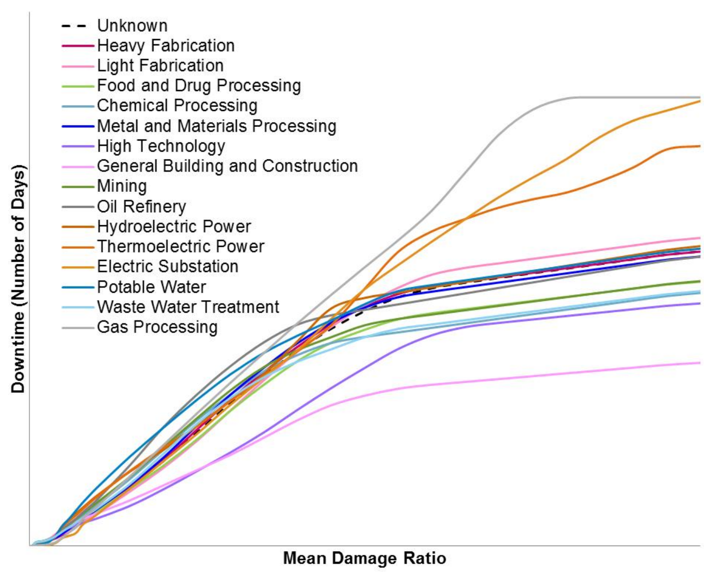

Figure 115. Business interruption tsunami damage functions for selected industrial facilities

5.10 Fire Following Earthquake

The risk of fire outbreaks following an earthquake is largely contingent on the ground shaking intensity at a given location. If the local shaking is strong enough to damage a building and its contents, it can also damage gas lines and electrical wiring, overturn heating elements, or cause chemical spills, all of which can cause a fire to ignite.[19] The subsequent spread of the fire depends on the extent of the shake damage, the prevalence of flammable materials in the vicinity, the integrity of suppression systems, weather conditions, building density and building construction materials.

To simulate fire following earthquakes, the AIR Earthquake Model for Canada models fire occurrences using a dynamic simulation of the fire in the local built environment. The behavior of a fire is simulated for its entire lifespan: from ignition and spread to burnout or suppression. The model incorporates a multi-level approach within a high-resolution (1 km) grid. The multi-level design allows the fire spread to be modeled first within the block where it originates, and then to adjacent blocks using data that accounts for the variable factors that affect fire spread. These data include wind speed and direction, width of roads (which can function as firebreaks), and building types.

Data from several sources was used in the fire following model for Canada. Specifically, land use data for the fire following model was obtained from Agriculture and Agri-Food Canada, and the National Geophysical Data Centre. Detailed building data came from Natural Resources Canada and from Geografx Digital Mapping Services. Wind speed and direction data are from the National Climatic Data Centre. Fire station location data were obtained from Natural Resources Canada, municipal fire departments, and population based station modeling.

Figure 116 provides a high-level illustration of the fire following model. The green components in the figure represent the dynamic model in which fire simulations are run, within a 1 km grid at a regional level, for each earthquake event. The simulation incorporates data on fire behavior at the city block level, which is calculated using a cellular automata model shown among the blue components in the upper left. The cellular automata model was developed by AIR based on several existing fire following models, including those developed by Cousins et

[19] Observations from many earthquake-generated fires indicate that roughly one-third of fire outbreaks after an earthquake are caused by damage to electrical systems, one-third are gas related, and the remaining one-third are due to other causes.

al. (2002, 2003, 2004), Heron et al. (2003), Himoto and Tanaka (2010), and Zhao (2011).

The other blue components in the upper left of Figure 116 represent the raw land use and building distribution data, the characteristic city blocks (discussed in one of the following sections), and the regional building distribution algorithm that the model uses to assign characteristic blocks to each 1 km grid cell. The blue components in the lower part of the diagram represent additional data used in the dynamic regional simulation.

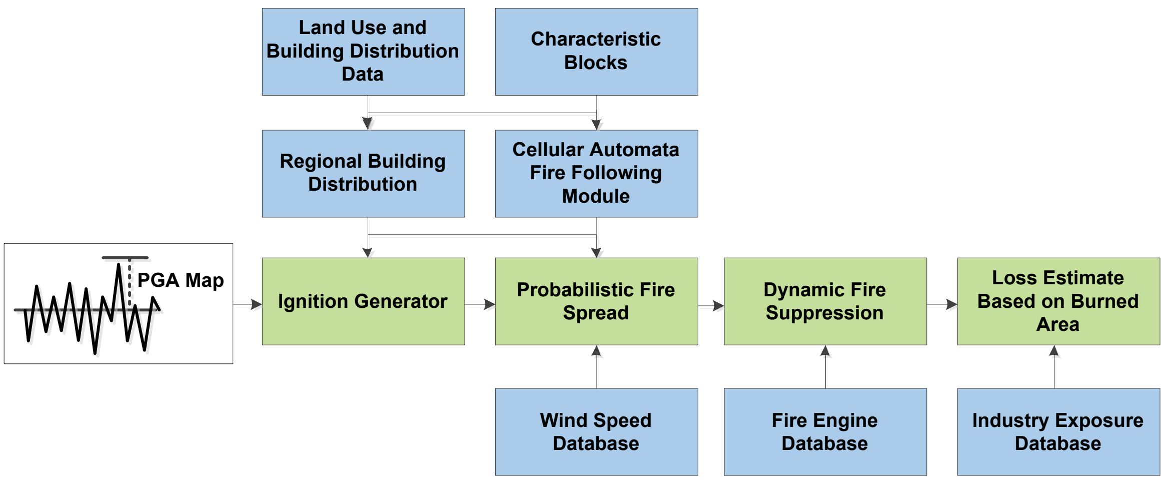

Figure 116. Primary components of the fire following earthquake model

Using Characteristic Blocks to Simulate the Built Environment

To accurately simulate the built environment of any location in Canada, AIR researchers developed 20 characteristic city blocks based on actual city blocks in Canada, which were digitized using satellite imagery[20]. These 20 blocks represent different configurations of building density and occupancy classes that include single family homes, apartments, commercial buildings, and mobile homes. The 20 blocks include single occupancy and mixed occupancy blocks, and one open area block without buildings that is used to represent open spaces such as parks and water bodies (which act as firebreaks).

Each characteristic block is rectangular, with an area of about 17,500 m² (± 2,500 m²), which reflects the block sizes typically found in Canada. The layout and

[20] The satellite imagery used to develop characteristic blocks came from the Bing Maps data available with the GIS mapping software from ESRI (Environmental Systems Research Institute).

building distribution on each block is a realistic representation of its block type in Canada. Buildings mapped on each block were each assigned a height, construction, occupancy type, combustibility for the cladding, and roof combustibility.

Each 1 km grid cell in the model contains 30 city blocks which are a combination of the 20 characteristic block types. The particular block types present in each grid cell is determined based on high resolution land use and building data. Specifically, the distribution of characteristic blocks within each grid cell is based on probabilities of building types, such as high-density commercial or medium-density mixed use. An example of the characteristic blocks assigned within a grid cell is shown in Figure 117.

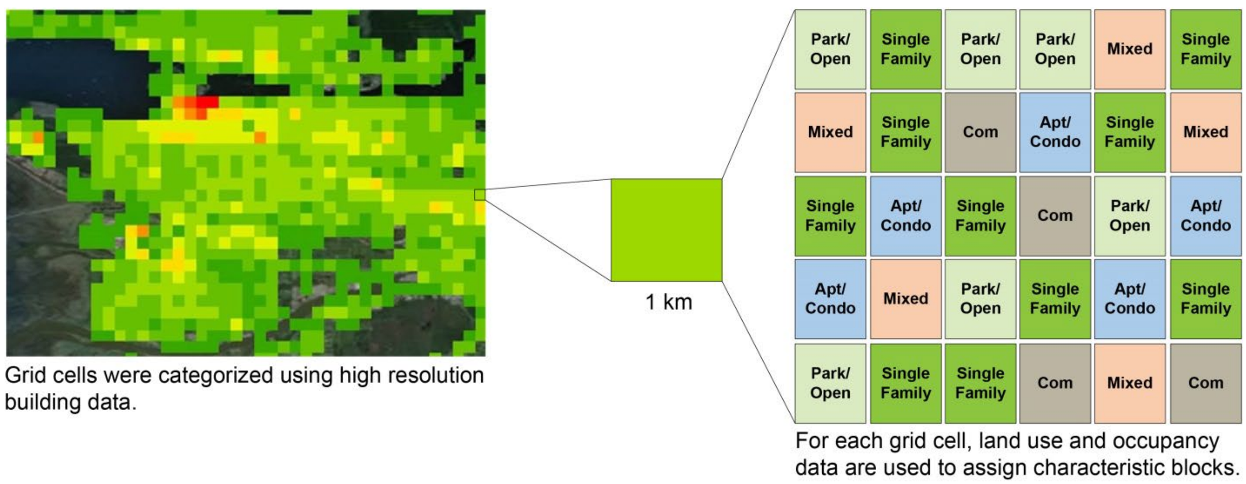

Figure 117. Example of the characteristic blocks assigned within a grid cell

In the model, multiple ignitions can occur within a single grid cell. These ignitions can occur in any of the 30 city blocks in the grid cell, provided that the city blocks contain buildings. The distribution of event-wide ignitions is modeled on a grid cell by grid cell basis, in which grid cells with more floor area and higher PGA levels experience more ignitions.

Building Combustibility

Fire following earthquake risk is determined largely by building type and distribution; therefore, an accurate simulation requires detailed information on the types of buildings involved, including their occupancy, combustibility, and urban setting. Each characteristic block captures a version of typical combustibility distributions seen throughout Canada.

To accurately model building combustibility, several substitute versions of the 20 characteristic blocks, with identical structural footprints and varying combustibility levels, are used to populate a grid cell based on the level of combustible buildings observed in that area. To capture the combustibility of each supported construction/occupancy class combination, the fire following module assigns one of seven combustibility classifications to each, which are shown in Table 26.

Table 26. Building combustibility classifications used in the AIR model

Residential Combustible	Commercial Combustible	Apartment Combustible
Residential Noncombustible	Commercial Noncombustible	Apartment Noncombustible
Mobile Home Combustible		

Note that the residential combustible category includes wood frame buildings with a brick veneer or exterior. The fire spread risk for these buildings is considered equal to those with combustible siding due to the high rates of failure of brick veneer as a result of ground shaking.

The behavior of fire spread is different when spreading into combustible buildings versus non-combustible buildings. While fire spread into buildings with a non-combustible exterior is certainly possible, the methods are different and the likelihood of this happening is decreased when compared to fire spread into combustible buildings. (For example, fire may spread into non-combustible buildings via ignition of the combustible contents inside the building, through a window.) For more details on fire spread in different building types, see *Fire Spread and the Cellular Automata Model* below.

Modeling Fire Ignitions at the Regional Level

The AIR model uses an ignition rate model based on a function developed by Scawthorn (2009) for events in California. In the AIR model, the Scawthorn (2009) function has been modified to account for the expected ignition risk in Canada. Specifically, the ignition rate for Canada was set to 1.5 times the ignition rate of Scawthorn (2009). The Scawthorn (2009) ignition function and the AIR ignition function are shown in Figure 118.

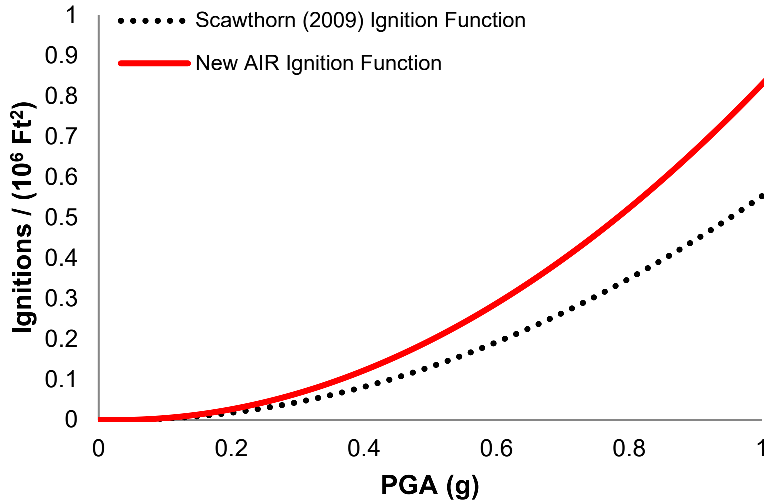

Figure 118. Fire following earthquake ignition rate published by Scawthorn (2009) and the modification of the Scawthorn function used in the AIR model

The Scawthorn (2009) function was chosen because it incorporates the latest research for modeling ignitions. This function was also selected due to the general similarity of building codes and building stock between the U.S. and Canada. However, the Scawthorn (2009) function was modified to produce higher ignition rates for Canada (as described in the preceding paragraph) because the building codes of California have led to the construction of more shake-resistant buildings than in Canada, which will likely reduce the number of ignitions. In addition, over the past century, several earthquakes in California have destroyed older buildings that would likely be more subject to ignition; in Canada, however, comparable buildings are still standing.

Note that, in the AIR model, modeled ignitions are limited to those that result in a fire large enough to warrant a fire engine response. The ignition rate for downtown Vancouver and Toronto are higher than the surrounding areas to account for the overhead power lines which are not typically observed in a central business district of a major city.

For each simulated earthquake event, the fire following model assesses the peak ground acceleration (PGA) and building floor area within each 1 km grid cell to determine the number of ignitions in that grid cell. The model accounts for the uncertainty in the ignition rate for a given region in an event by allowing a significant amount of variability in the ignition rate used for each grid cell. For example, two grid cells with identical PGA values and building floor areas, in the same event, might be assigned different ignition rates, accounting for the highly variable nature of fire ignitions following an earthquake. The ignition rate for each of the two grid cells is drawn from a log-normal distribution corresponding to the mean ignition rate for the PGA value. The ignitions are distributed temporally throughout the two days following the earthquake based on post-earthquake ignition research by Scawthorn (2009) and Zhao et al. (2006b).

Fire Spread and the Cellular Automata Model

Each post-earthquake ignition within a grid cell is assigned to a random city block within that grid cell. For each type of city block, the growth of a fire within the block is simulated using the results of the cellular automata model. This model calculates the fire behavior within a given block type based on the type and configuration of buildings in the block.

The cellular automata model uses a grid consisting of 3 m wide cells to model fire spread on each characteristic block, as shown in Figure 119. The fine resolution allows a realistic determination of the fire's spread rate, spread pattern, and duration.

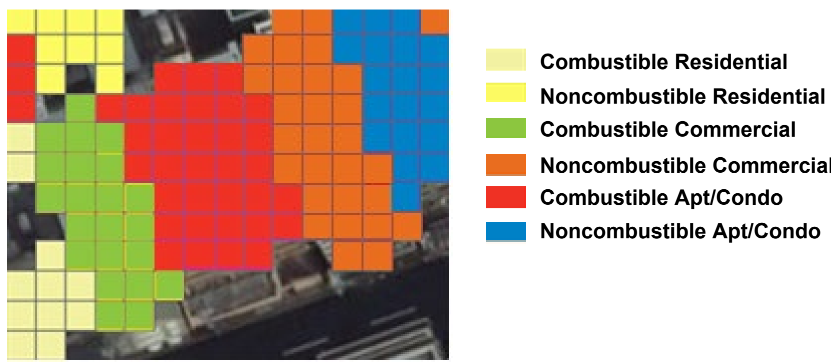

Figure 119. Each characteristic block is run on a 3-m resolution grid in the cellular automata model

During each time step of the simulations, each cell that represents part of a building is assigned one of five states: no ignition, ignition, fires in full burn, fires diminishing, and fires completely burned out. The life cycle of each fire follows fire growth and spread behaviors based on research by Cousins et al. (2002) and Heron et al. (2003).

Using discrete time steps of 2.5 minutes, the cellular automata model analyzes the state of each cell at each time step. If a cell reaches the ignition state, the fire grows until the cell reaches the full burn state. This transition from ignition to the burning of all combustible objects in a given space is known as flashover. Flashover is the result of room temperature increasing considerably, which allows fire to spread to other cells. The duration of the fire on the city block depends on the built environment and the building heights.

Fire spread in the cellular automata model can occur by direct flame contact, spontaneous ignition, spark-based piloted ignition, and branding. Fires can only spread during the full burn stage, as they are too weak in the ignition and diminishing stages to spread. The probabilities of spark-based and flying brand ignition depend on the wind speed and direction, and building spacing. Building spacing and window placement are also accounted for in the model as a fire may have a strong chance of spreading into a non-combustible building through windows.

Modeled fires can spread to combustible buildings through many methods including direct flame contact, spontaneous ignition, piloted ignition and wind-borne firebrands. Non-combustible buildings have exteriors that resist fire; however, they can still ignite if the interior is subjected to significant radiation through the windows, or if the building has a combustible roof.

For noncombustible buildings, the model accounts for the spacing between buildings, data on the number and sizes of windows and their positioning and the materials within the buildings. This information was obtained from local fire codes, which restrict the size and number of openings on sides of a building that face another building, and validated using street level imagery. The source of the fire is also taken into consideration since it affects the heat flux that is radiated. Fires inside noncombustible buildings will only radiate from the windows; hence emit less heat to nearby objects.

For each characteristic block type, the cellular automata model is run 1,000 times with varying ignition locations within the block. Wind speed and wind direction are also varied. Indirect mechanisms of fire spread are stochastically controlled, which allows the rate of indirect spread to vary among simulations. This large number of simulations captures the variability of fire behavior within each block type. The results of the simulations are captured as functions which describe the fire behavior, including a mean burn function that specifies the burned floor area as a function of time for a particular characteristic block, and the standard deviation of the burned floor area at each time step.

Figure 120 shows damage functions for characteristic blocks of different densities and building types. The undulations in the functions are due to the effect of the cellular automata model running in discrete time and space (2.5 minutes, 9 m^2 cells) rather than continuous time and space. As shown in the figure, high density blocks of apartments or commercial buildings have a much larger burn area with time, even though they have the same spatial footprint (17,500 m^2). This is due to the fact that these blocks contain skyscrapers, large buildings, or apartment complexes; therefore, the modeled fires will spread through many stories of the building.

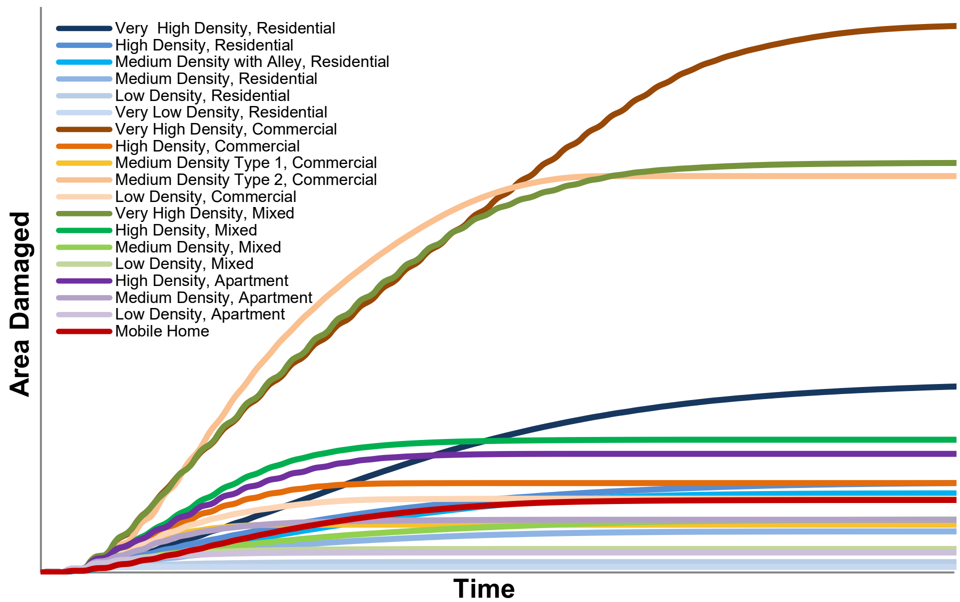

Figure 120. Fire following damage functions from the cellular automata model for blocks of different densities and occupancy types

Validation of the Cellular Automata Model

Due to a lack of fire following earthquake data for Canada, the cellular automata model cannot be validated using Canada-specific information. However, validation data are available for Japan. Therefore, the AIR cellular automata model employed in the fire following component of the AIR Earthquake Model for Canada was validated by comparing its performance to that of a full physical fire-following model developed for Japan by Himoto and Tanaka (2008). Details of this validation process are provided below.

The AIR cellular automata fire spread model was validated by comparing results of the model with that of a physical model from Himoto and Tanaka (2008) and with the empirical Hamada model run for a specific test. This test used a 25 x 100 array of uniformly spaced buildings, each 3 cells x 3 cells (81 m²), with one cell-width of space between each building. The building type distribution reflects the one used by the Himoto and Tanaka model with 20% wood, 40% wood/stucco, and 40% noncombustible buildings (Note: This test was designed based on Japanese building parameters, and included a characteristic Japanese construction type of wood-frame/stucco houses. The AIR cellular automata model for Japan is nearly identical to that for Canada, but accounts for the unique fire risk posed by this Japan specific construction type. The validation results shown below were generated using the AIR cellular automata model for fire spread in Japan).

Different wind speeds were used during the test to verify the fire spread rate would adjust accordingly. Figure 121 shows the results of the AIR cellular automata model and the model by Himoto and Tanaka, for a wind speed of 5 m/s, showing good agreement between the two models.

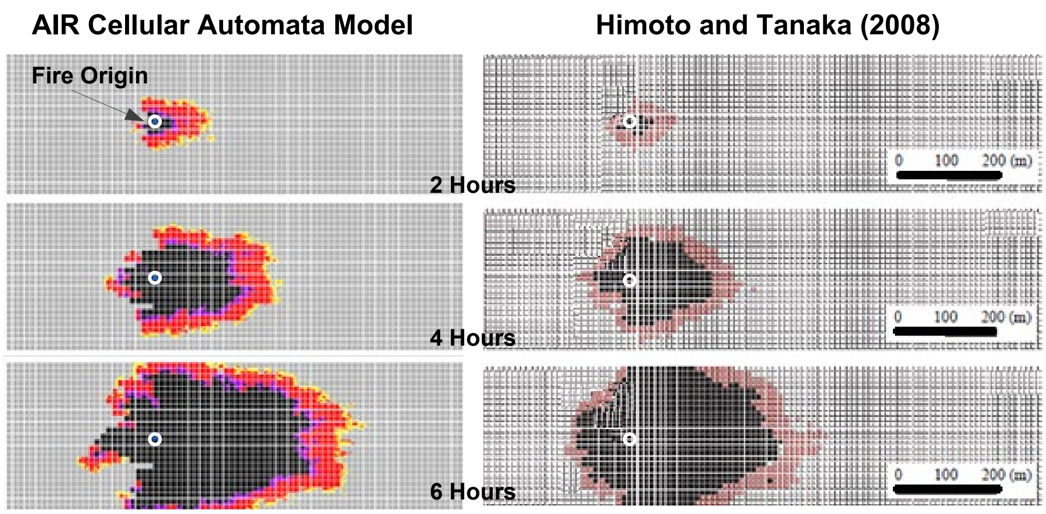

Figure 121. Comparison of fire spread from the AIR cellular automata model (left) and from Himoto and Tanaka (2008) (right), with wind speed of 5 m/s

Table 27 compares the fire spread rates in the AIR cellular automata model and the models by Himoto and Tanaka (2008) and Hamada, showing good agreement between the models. (Note that the Hamada model assumes the fire spreads at a constant rate.)

Table 27. Comparison of fire spread rates in the AIR cellular automata model and published studies

	AIR	Himoto and Tanaka (2008)	Hamada
2 hours	1.025 m/min	0.90 m/min	1.194 m/min
4 hours	1.163 m/min	1.15 m/min	
6 hours	1.208 m/min	1.20 m/min	

Firebreaks

The AIR model accounts for the probabilities of a fire spreading across streets or alleys to adjacent blocks of buildings. The probability of spread across firebreaks depends on wind speed, wind direction, fire suppression, and firebreak width. The timing of firebreak crossing is dependent on the burn rate, with higher burn rates associated with more firebreak crossings that can occur sooner after the time of ignition.

Note that the firebreak width is larger than the street width, as it is measured from the face of one building to the face of another. Firebreak widths are determined from a detailed, Canada-wide survey of street widths and setback distances.

Fire Suppression

The model determines the effectiveness of fire suppression based the amount of time that elapses before fire suppression efforts begin, the presence and number of fire engines, and the water supply system. It also accounts for the possibility of infrastructure disruptions including lack of communications, impassable roads, and damage to water pipelines. In cases of inadequate suppression, fires will continue to spread until all fuels are spent, or the fires reach an effective firebreak.

Once a fire ignites, the amount of time until the fire has been reported is stochastically assigned. For some fires, the model assumes disruption in communications during the reporting efforts, with a small percentage (10%) relying on alarms and on the fire being noticed from outside the building. Once the fire is reported, the nearest available engine is dispatched. The number of fire engines in each area is modeled using data that show the number of fire engines per capita, published by the National Fire Protection Association (NFPA) of Canada. These engines are then distributed to fire station locations using data from Canada's municipal fire departments and the Natural Resources Canada CanVec dataset. Where data for fire engine station locations are lacking, fire engine numbers and locations are modeled using the population based model. The AIR model distributes a total of 4,836 fire engines throughout Canada. The speeds at which fire engines can travel under post-earthquake conditions are based on published studies (e.g., Scawthorn et al., 2005), and vary due to ground motion intensity. Areas with stronger ground shaking are more likely to experience damaged roads, or debris within the roads which may inhibit fire engine travel.

Once suppression efforts begin, the size of the burning area and whether the fire has passed the flashover point for the originating room determines if additional water from a hydrant is needed. The model assumes that small, pre-flashover fires can be controlled with only the water onboard the fire engine. For larger fires, suppression effectiveness is calculated using a method similar to that in the HAZUS fire following model (FEMA 1997)[21]. Under partial, or inadequate, levels of suppression, a fire may continue to grow at a reduced rate compared to an unsuppressed fire, as illustrated in Figure 122.

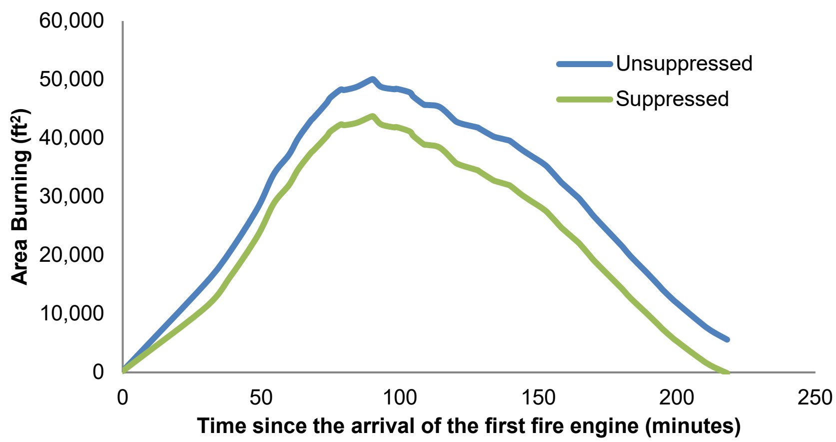

Figure 122. Impact of incomplete fire suppression on burn area

Suppression efforts are affected by the integrity of the water supply system. Damage to water systems is captured by a factor applied to the measure of suppression effectiveness based on water system shortcomings. The model uses pipeline fragility functions recommended by American Lifelines Alliance (Eidinger et al., 2001) to predict the rate of damage to pipes (which can occur from ground shaking or liquefaction).

In Vancouver, the fire following earthquake model explicitly accounts for the presence of the Dedicated Fire Protection System (DFPS). Within grid cells covered by the DFPS, water availability is increased by a factor to account for the redundant water supply pipelines in the region. It should be noted that these pipelines have been designed to withstand significant earthquake ground shaking.

[21] HAZUS (Hazards-United States) is a GIS-based loss estimation software package for natural hazards developed by the U.S. Federal Emergency Management Agency (FEMA). In the HAZUS model, fire suppression effectiveness is calculated using the ratio of fire engines available to the number that are needed, as well as the ratio of water flow available to the water flow needed. The amount needed is based on the size of the fire.

Fire Following Earthquake Damage Calculation

Once all fires in the model have burned out completely, the final burned floor area in each fire class in each grid cell is obtained by summing the burned floor areas on the blocks within the grid cell. The total burned floor areas are then divided by the total floor areas in the grid cell to determine the mean damage ratios for each fire class in the grid cell. For a given earthquake, the fire following model is typically run 50 times, and the final mean damage ratios output by the model are obtained by averaging the results over the multiple simulations. The resulting mean fire damage ratios can then be applied to exposure portfolios to get the corresponding fire following losses for each fire class within each grid cell. The loss from all grid cells is combined to calculate the total event loss.

Damage to Residential and Commercial/Industrial Buildings from Fires Following Earthquakes

As with shake damage, similar structures at the same location may experience different levels of fire damage. Therefore, to apply policy conditions, the model incorporates fire damage distributions around the mean damage ratio. The assumed damage distributions are based on both the observed fire damage distribution in areas that were extensively damaged by fires following historical earthquakes, and estimates of the fire damage distribution in the surrounding areas that were not as heavily damaged. For purposes of comparison, damage distributions corresponding to two mean damage ratios—0.10 and 0.74—are illustrated in Figure 123.

In areas affected by earthquakes, there is a tendency for buildings to be either totally undamaged or completely damaged by fire, with a lower percentage being partially damaged. As Figure 123 suggests, at lower mean fire damage ratios, the spike at zero damage is more prominent than the spike at 100% damage, and most buildings escape fire damage altogether.

At higher mean fire damage ratios, the spike at 100% damage becomes more prominent. Ignition frequency increases at these levels making fire suppression more difficult and many buildings are left to burn. In general, then, as the mean fire damage ratio increases, the probability of zero damage decreases while that of greater-than-zero damage increases. As the mean damage ratio gets larger, the probability of total damage increases while the probability of partial damage decreases.

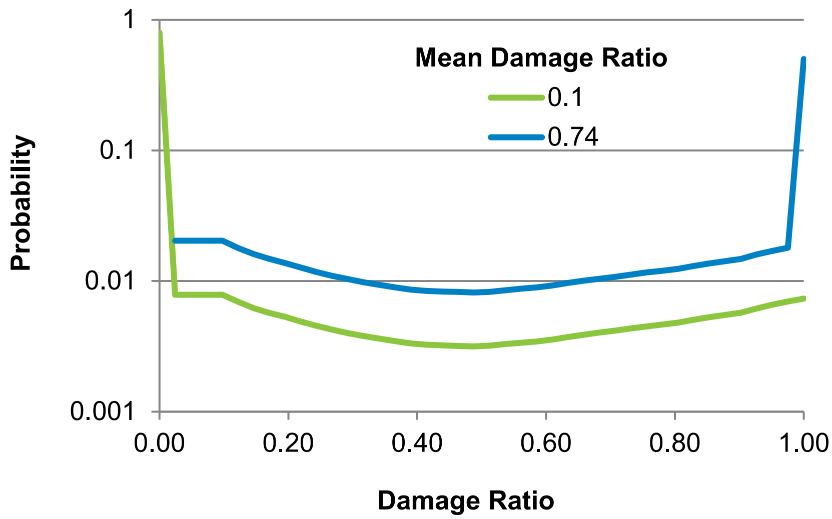

Figure 123. Fire damage distributions used for two mean fire damage ratios

Damage to Automobiles from Fires Following Earthquakes

In the AIR model, the fire damage ratios for automobiles are based on the building fire damage ratios in the same grid cell. However, the location of automobiles in the modeled region can, of course, vary. For any fire event, automobiles may be driving on the roads, parked in a garage attached to a residential building or a commercial building, or located in a detached garage or parking lot. The model estimates the time-averaged probabilities of these possible situations and calculates the resulting mean damage ratio.

To estimate time-averaged probabilities that an automobile within a grid cell is parked at home, parked away from home, or actively being driven, AIR researchers used data regarding the age distribution of the population throughout Canada and the driving habits of each age group, and their daily schedules. The categories of days considered in the model are: Mondays through Thursdays, Fridays, Saturdays, and Sundays/Holidays. Age distribution data provided the number of drivers who were students, working adults, nonworking adults, or retired, and the typical driving habits of each age group.

Then, automobiles are assigned the same mean damage ratio as the associated building fire class if they are parked in an attached garage, and half the mean damage ratio of the building fire class if they are located in detached parking. (Industry exposure data is used to estimate the probability that, if parked, an automobile is parked in attached garage or detached parking, and if the associated building is combustible or noncombustible.) The automobiles in each grid cell that are being driven are assigned one quarter of the mean damage ratio for different building fire classes within that cell, weighted by the exposure value of each fire class.

Damage to Industrial Facilities from Fires Following Earthquakes

The nature of fire following damage to industrial facilities varies considerably from standard fire following damage to other lines of business. The industrial facility components and specialized equipment require an approach that accounts for ignition probabilities, fire spread, and construction types that are unique to these large facilities.

To develop fire following damage functions for individual components and for the facilities as a whole, AIR researchers incorporated data on fire following for several historical earthquakes. The key events they used are listed in Table 28.

Table 28. Key historical earthquakes used for fire following analysis

Earthquake	Year	Earthquake	Year
Taisho-Kanto	1923	Miyagi-ken-oki	1978
Long Beach, California	1933	Nihonkai-Chubu	1983
Vrancea, Romania	1940	Kobe	1995
Fukui	1948	Kocaeili (Izmit), Turkey	1999
Kern County, California	1952	Tokachi-oki	2003
Anchorage, Alaska	1964	Niigata-ken-Chuentsu-oki	2007
Niigata	1964	Maule, Chile	2010
Mudurnu Valley, Turkey	1967	Tohoku-oki	2011

Fire Following Damage Function for Refineries

Historical data and research studies (Cooper, 1997; Chang and Lin, 2006) indicate that within complex industrial facilities, fires following earthquakes occur most often in refineries. Fires that break out in refineries due to ground shaking usually affect the storage tanks (however, fires at refineries have historically damaged other industrial components such as pipes, cooling towers, and electrical wiring). The most common causes of these fires are explosions, ignition of leaks, and sloshing of storage materials within tanks that have floating roofs. In some cases, tanks can be dislodged or even overturned by heavy ground shaking or a tsunami, which can lead to fires. While recorded data on fire damage varies in the amount of detail included, the number of damaged tanks is consistently available.

By using the storage tank damage data available, AIR researchers developed a fire following damage function for storage tanks, and for an entire refinery, shown in

Figure 124. At low PGA values, no damage is incurred. In addition, as damage to storage tanks increases, it affects a higher percentage of the refinery as a whole.

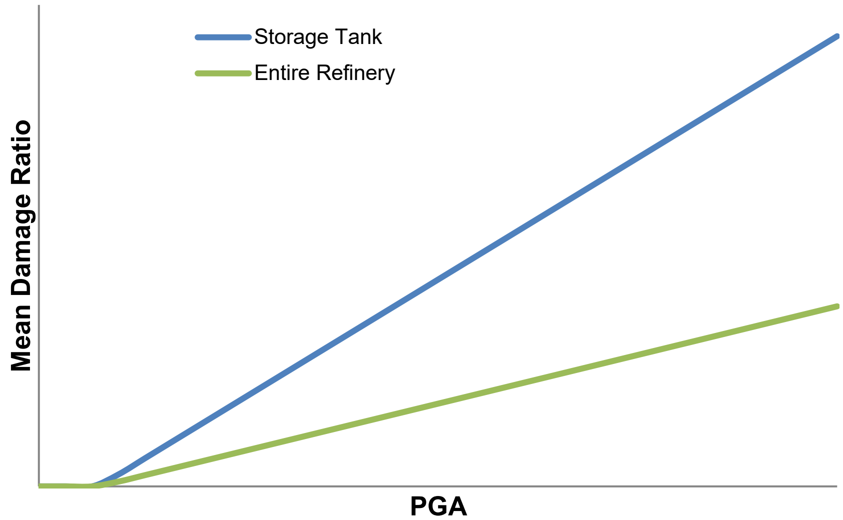

Figure 124. Fire following damage function for tanks and entire refineries

Damage Functions for Industrial Facilities at Different Risk Levels

The risk of fire following ignitions at an industrial facility varies depending on the materials, equipment, and contents of the facility. To develop damage functions for different types of industrial facilities, AIR researchers evaluated the level of risk at each facility type. Using historical data along with studies of facility components and processes, they identified five levels of risk with the highest level corresponding to the risk seen at petroleum refineries.

The damage function developed for the highest risk level utilizes the empirically-derived petroleum refinery damage function. For each subsequent lower risk tier, the damage function is reduced by 20% relative to the refinery damage function. For example, a level 4 risk facility's damage function is 80% of that of the refinery damage function, while a level 3 risk facility's damage function is 60% of the refinery damage function. Industrial facilities with risk level 1 have a fire following risk level similar to standard commercial properties. The full set of industrial facilities damage functions is shown in Figure 125.

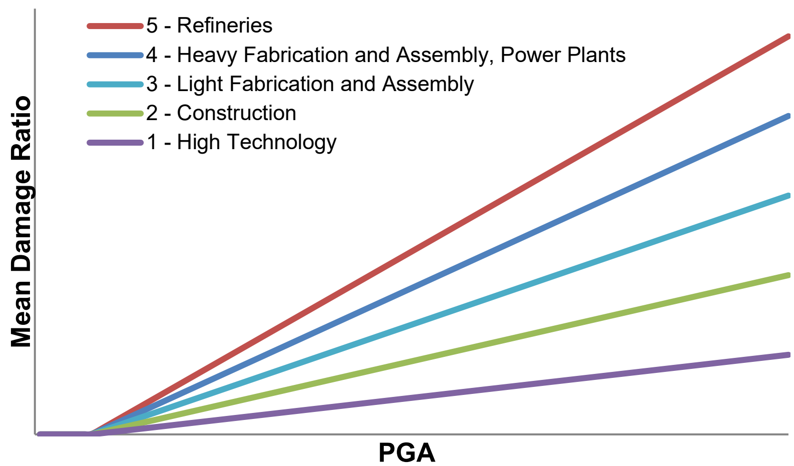

Figure 125. Fire following damage functions for different levels of risk associated with different types of facilities

Fire Damage Compared with Shake Damage to Industrial Facilities

Fire following damage is generally low when compared to shake damage. There are several factors responsible for this difference. First, ground shaking affects an entire industrial facility, while fires affect only the parts of the facility that are flammable or contain flammable materials. In addition, even if an industrial facility that contains flammable components experiences shake damage, if a fire is never sparked the facility will escape fire following damage. Finally, fire mitigation systems will limit the fire spread (although they would have no impact on shake damage). For example, facility design components, such as barriers separating storage tanks, and the strategic placement of storage tanks within a facility, will generally limit the extent to which a fire can impact a facility.

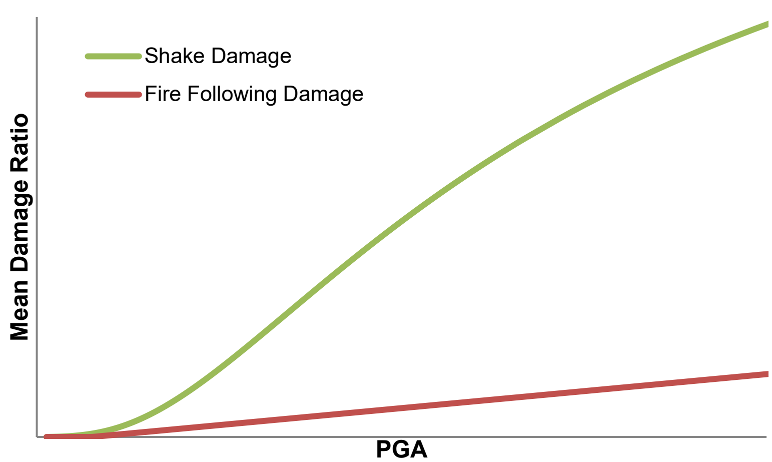

Figure 126. Damage functions for shake and fire following, for a refinery

5.11 Combining Damage from Multiple Perils

With the explicit modeling of five individual perils (ground shaking, fire following, tsunami, landslide, and liquefaction), damage and loss estimates due to each peril are performed separately. While this provides greater accuracy in the effects of each individual peril, the estimates need to correctly account for damage due to multiple perils. Many structures sustain damage from a combination of perils, particularly if the damage is severe. For example, during the 2011 Tohoku, Japan earthquake many buildings were initially damaged from ground shaking, and were then damaged further due to fire outbreaks and the tsunami. Many buildings incurred damage from liquefaction as well.

Determining the Probability of Damage Overlap due to Multiple Perils

When determining the damage and loss to a structure due to a particular peril, it is necessary to account for damage that is already sustained from other perils. Essentially, any particular aspect of damage must not be attributed to more than one peril as this type of "double counting" would increase the damage and loss estimation, potentially resulting in a total mean damage ratio that exceeds 100%.

AIR engineers have therefore developed a methodology that accounts for any damage overlap, which occurs when more than one peril causes damage to a building. This methodology uses a sigmoid function that estimates the probability that at least part of the building has damage from more than one peril, such as a wall that is both cracked from ground shaking and burned by a fire. The methodology guarantees that the total mean damage ratio does not exceed 100%.

The sigmoid function developed by AIR is illustrated in Figure 127. As shown, it describes the relationship between the total mean damage ratio sustained by a building and the probability of damage overlap occurring on the building due to multiple perils. The two circles in the figure represent the calculated mean damage ratio for two separate perils (MDR_i) while the intersection of these circles (MDR_c) represents the mean damage ratio caused by a combination of the two perils. The total mean damage ratio can be expressed as:

$$MDR_{total} = \sum_{i=1}^{n} MDR_i$$

where n represents the number of perils.

As shown in Figure 127, the probability of damage overlap is negligible when the total mean damage ratio from the expression above is small, and this probability increases as the total mean damage ratio increases. The sigmoid function developed by AIR determines this probability using the total mean damage ratio as an independent variable.

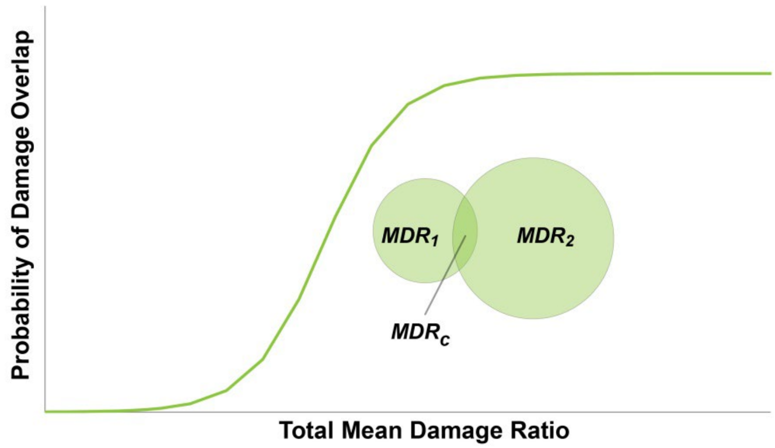

Figure 127. The probability of damage overlap on a building increases as the total mean damage ratio increases

Removing Damage Overlap from the Total Mean Damage Ratio

By removing any damage overlap, the total mean damage ratio will not include any double counting of damage due to multiple perils affecting a building. To do this, the expected amount of damage overlap on a building is determined using the following expression:

$$P_c * DR_c = P_c * [\min(MDR_c) + \max(MDR_c)]/\ 2$$

where, P_c is the probability of damage overlap, as illustrated in Figure 127. The minimum and maximum amount of overlapped damage (MDR_c) is calculated as:

$$\min(MDR_c) = \sum_{\mathrm{i=1}}^{\mathrm{n}} MDR_i - 1 \geq 0$$

$$\max(MDR_c) = \sum_{i=1}^{n} DR_i - \max\,(MDR_i)$$

Once the expected amount of damage overlap is determined, it is subtracted from the total mean damage ratio. Subsequently, the mean damage ratio for a given peril (MDR_i) can be calculated as

$$MDR_i' = w_i * \left(\sum_{i=1}^{n} MDR_i - P_c * MDR_c\right)$$

where w_i is the proportion of damage from the peril that is incurred out of the total mean damage ratio, before accounting for the damage overlap.

5.12 Additional Living Expenses

Damage functions are also included for time element, or additional living expenses, for residential structures. The AIR ALE damage functions take into account the time that people may need to stay in a hotel or elsewhere while their home is repaired. It also takes into consideration any necessary time taken off work due to the inability to get to their place of employment, or necessary time spent with contractors.

ALE loss is a function of the mean building damage due to all perils, which in turn is used to estimate the number of days required to repair or rebuild the structure, and an estimate of per diem ALE costs.

5.13 Business Interruption

Downtime, or the number of days before a business can return to full operation, is the primary parameter in estimating business interruption (BI) losses. The AIR BI estimation (Figure 128), which utilizes an event tree approach, incorporates the latest research and an extensive analysis of claims data. For each damage state, a probability is assigned to two possible outcomes: continued operations or cessation of operations at the location. If operations cannot continue at the location, a probability is assigned to the possibility of relocation. These probabilities vary by occupancy. For example, while relocation is feasible for an office, it is not for a hotel. Thus the two will take different paths to recovery, and hence will have different downtimes in the event of business interruption.

Downtime is calculated for each stage of the damage assessment and recovery process. The first stage is the time before repairs can get underway (pre-repair). The damage must be assessed, the repair cost negotiated with contractors, and the building permit obtained. The next stage is the repair time. Some businesses choose to relocate rather than wait for repairs, but relocation takes time as well. Once repairs are completed, revenues may not resume at the pre-disaster level; it may take some time to regain market share, or to rebuild a labor force that may have been dislocated.

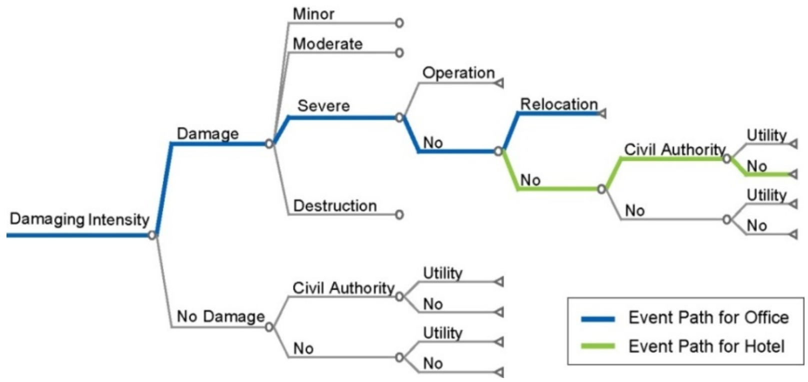

Figure 128. Hypothetical event tree of BI estimation for an office and a hotel

In the AIR model, the estimated number of days needed to restore the business to full operation depends on a number of key factors, including the level of damage sustained, the size of the building (as approximated by building height) and its architectural complexity (as approximated by occupancy class).

For a given damage ratio, a 2,500 square meter hotel will take significantly longer to repair than a 450 square meter professional office. Since square footage info is not available, building height is used as approximation. For a given floor area, buildings with significant architectural complexity will also take more time to repair. Warehouses can be quite large, but repairs are likely to take place quickly because of their architectural simplicity. Interior finishes must also be taken into account. Hotels are not only typically larger than offices, but can take more time to repair due to higher quality of interior finishing.

Some types of businesses—such as hospitals—are more resilient than others and may be able to restart operations before repairs are complete, or they may have had disaster management plans in place that allow them to relocate quickly. For other businesses—such as hotels—location is important and relocation is not an option. As many parameters critical to determining business interruption, including building size, complexity, and business resiliency, are generally not available for input into the model, occupancy class is used as a proxy to measure these parameters.

Based on the observation that BI downtime days, or the number of days before a business can return to full operation following a disaster, are correlated with building damage, the BI damage distribution is assumed to be similar to the building damage distribution. Occupancy is also used to estimate the probability that there may be business interruption at a dependent building within the damage footprint—such as the supplier of a necessary manufacturing input—that will exacerbate BI losses at the principal building. Estimation of the impact of the dependent building damage on the principal building requires knowledge of the location and degree of interdependency between dependent and principal buildings. Since this level of detail information is generally unavailable, logical assumptions are made to estimate the impact of the dependent building on the principal building downtime.

The methodology for estimating BI losses relies in part on loss experience data and in part on expert judgment in the face of limited available exposure information.

5.14 Validating the Model's Damage Functions Against Historical Damage

Comparison of modeled results with historical observations (when these data are available) provides another layer of validation for the overall performance of the model. However, this level of validation is only possible to the extent that thorough data from past earthquakes are abundant and readily available. In general, damage observations are obtained from post-event damage surveys completed by engineers at AIR, or from reports by other researchers and organizations. In this model, reports by Natural Resources Canada (NRCan) are used. Because damaging earthquakes are not very common in Canada, we have used descriptive reports of damage and intensity to validate the model's results.

One of the few events in the history of seismic activity in Canada that is associated with reported damage is the November 25, 1988, M5.9 Saguenay earthquake, which occurred about 35 km south of Chicoutimi, Quebec, and 75 km north of the Charlevoix-Kamouraska earthquake zone at a focal depth of about 29 km. The Saguenay event was characterized by a single foreshock, relatively minor aftershock activity, and a large amount of high frequency energy. Here, we compare AIR's simulated intensity and damage footprints for this event with the descriptive intensity and damage reports for this event obtained from NRCan and other publications, as an additional layer of validation for the AIR model.

The Geological Survey of Canada used information from a survey of felt intensity supplemented with data collected by the National Earthquake Information Service in the United States to produce an isoseismal (intensity) map of the 1988 Saguenay event (Cajka and Drysdale, 1996). The intensity map reported by NRCan is shown in Figure 129.

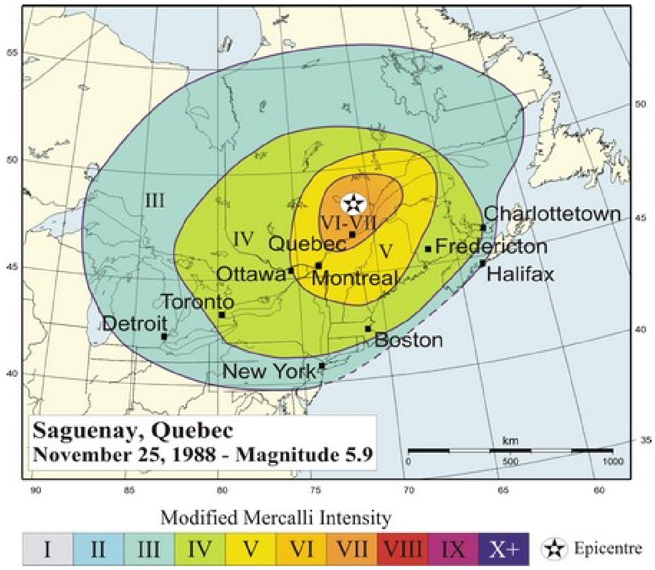

Figure 129. Isoseismal map for the Saguenay 1988 earthquake (MMI) (Source: Geological Survey of Canada)

The earthquake was felt with a maximum intensity of MMI VIII, but more typically MMI VII, in the Chicoutimi-Jonquière-La Baie area. Ground shaking was felt strongly in areas within 500 km of the epicenter. Overall, shaking was felt as far as 1000 km away from the epicenter.

Figure 130 shows the simulated intensity footprint generated by the AIR model. The model accurately predicts some areas with intensity VI and VII close to the epicenter. Farther from the epicenter, the overall modeled intensity map is reasonably consistent with the reported intensity.

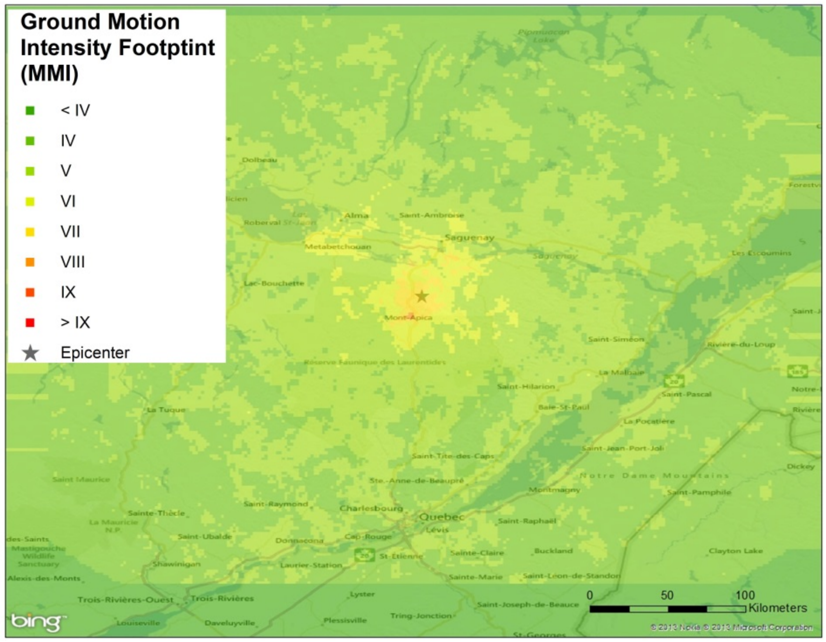

Figure 130. Intensity footprint (MMI) for the 1988 Saguenay earthquake generated by the AIR model

According to NRCan reports, damage in the sparsely populated epicentral area was modest, and was limited to cracked or fallen unreinforced masonry walls and a few minor landslides. In Chicoutimi (about 40 km from the epicenter), damage consisting of fallen masonry blocks from unreinforced masonry walls was reported. Indeed, the NRCan report in general pointed out the poor performance of unreinforced masonry in this event (Mitchell et al., 1989). Statistical analysis of 1850 claims submitted to a government organized compensation program indicates minor damage, with a maximum of 15%, to small buildings near the epicenter (Paultre et al., 1993). Figure 131 shows footprints of damage in URM constructions obtained from AIR's model (using a uniform exposure consisting of low rise URM at 1 km grid). The damage ratio is generally low, estimated at about 10-30% in the vicinity of the epicenter, and less than 10% just outside the epicentral area. These values, consistent with the definition of MMI intensity, correspond well to the NRCan reported intensity maps. Although no map of reported damage is available, the model's result is consistent with the descriptive damage observations reported by NRCan and with the statistical data from Paultre et al. (1993).

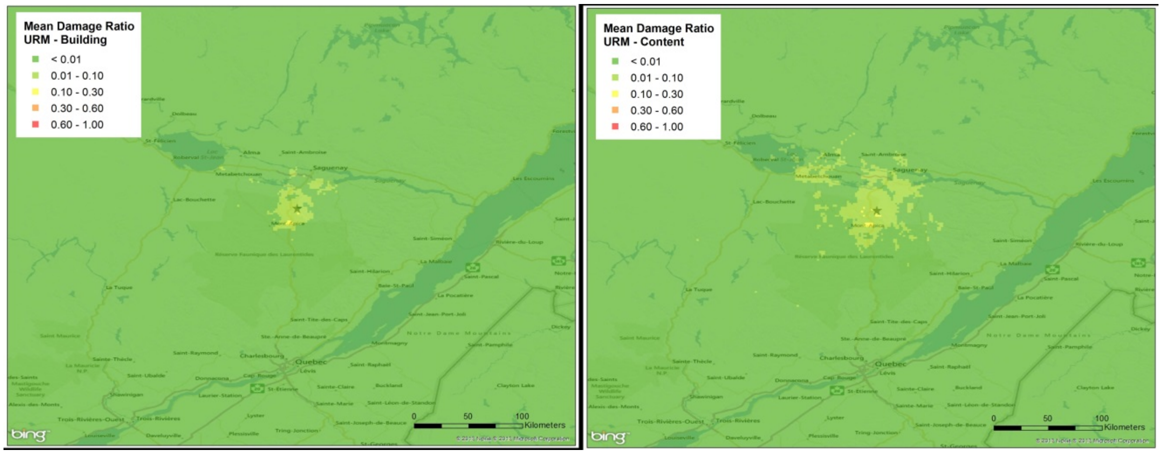

Figure 131. Footprint of the modeled mean damage ratio for URM buildings in the 1988 Saguenay earthquake

6 Insured Loss Calculation

In this component of the AIR Earthquake Model for Canada, ground-up damage is translated into financial loss. Insured losses are calculated by applying policy conditions to the total damage estimates resulting from the damage estimation module. A wide variety of policy conditions are supported in this model, including franchise deductibles, coverage limits, loss triggers and risk-specific reinsurance terms.

6.1 Aggregating Losses Probabilistically

Post-disaster surveys and actual claims data reveal an inherent variability in the damage that results from a given intensity of a peril (e.g., ground shaking intensity, tsunami inundation depth). Loss estimates generated by the AIR Earthquake Model for Canada capture this variability in intensity by accounting for both primary and secondary uncertainty. Primary uncertainty derives from the uncertainty associated with the event generation process (i.e., the stochastic catalog), while secondary uncertainty describes the uncertainty in damage resulting from a given event. This secondary uncertainty captures the uncertainty in damage and in the local intensity estimation. The uncertainty in building damage arises due to inherent randomness in the response of buildings of similar construction to a given intensity, as well as from variability in building characteristics, construction materials, workmanship, etc. The uncertainty in local intensity of the hazard can be attributed to unmodeled phenomena and local site factors. Secondary uncertainty is modeled through a probabilistic distribution around the calculated mean damage.

As was discussed in Section 5, losses are calculated by damage functions that provide, for a given level of intensity, a mean damage ratio (MDR) and a probability distribution around the mean that captures the secondary uncertainty in damage. For the AIR Earthquake Model for Canada, a bimodal-Beta distribution combined with empirically derived probabilities of 0% and 100% damage levels are used to model the secondary uncertainty.

The damage functions are used to produce, for each event, a distribution of ground-up loss by location and coverage. Limits, deductibles and reinsurance are applied in the financial module to the ground-up loss distribution to produce gross and net loss estimates. Note that insured losses can accumulate even if the mean loss is below the deductible, because some structures are damaged above the mean loss and the deductible. The distributions are applicable to the analysis of a single exposure and usually have a high degree of uncertainty. The individual distributions are combined to obtain the portfolio distribution, where the uncertainty relative to the mean is lower than that for a single exposure.

In the financial module there clearly is a need for aggregating losses probabilistically, at various levels. Specifically, computational techniques are developed for statistically aggregating nonparametric distributions.[22] That is, even though the ground-up, coverage level damage distributions typically use parametric distributions, after the application of location and policy terms the distributions cannot be represented in a parametric way. Further aggregations of such loss distributions are achieved using numerical algorithms.

The financial module within AIR's software applications allows for application of a wide variety of location, policy and reinsurance conditions. Location terms may be specified to include limits and deductibles by site or by coverage. Supported policy terms include blanket and excess layers, minimum and maximum deductibles, and sublimits. For more information on the policy conditions, see Section 8.7.

6.2 Demand Surge

Market forces generally ensure that the availability of materials and labor in any particular geographical area is sufficient to accommodate a normal level of demand without affecting price. However, demand can increase sharply and unexpectedly after a catastrophe such as a significant hurricane or earthquake. The resulting widespread property damage can cause a sharp increase in the need for building materials and labor, which in turn can cause prices to inflate temporarily. Demand for related services and resources such as transportation, equipment, and storage also might escalate in the affected area.

Scarce resources can also result in an increase in the time required to repair and rebuild damaged property, which may cause greater business interruption losses and additional living expenses. Infrastructure damage, delayed building permit processes, and a shortage of available building inspectors also increase time element loss. These factors can lead to insured losses exceeding expectations for a particular event and portfolio, a phenomenon known as demand surge. The greater and more widespread the damage from an event, the greater the resulting demand surge and insured losses will be.

[22] Nonparametric statistical methods do not rely on the estimation of parameters, such as the mean or the standard deviation, to describe the distribution of the variable of interest. They also do not rely on assumptions that the data are drawn from a given probability distribution. Parametric methods assume that the variable fits a probability distribution in order to make predictions regarding how that variable may behave in repeated samples.

Note that the current default AIR demand surge function was developed using economic principles and validated based on U.S. loss levels and component cost analyses as described in *The AIR Demand Surge Function*, which is available on the AIR website. Because demand surge is a phenomenon seen only with especially large catastrophes, there are relatively few events with which to validate demand surge functions outside of the U.S. This scarcity of data is further complicated by the relative paucity of cost indices and detailed data.

For countries other than the U.S., clients may choose to apply the U.S. demand surge function or a user-defined demand surge function, at their discretion. Clients are also encouraged to perform sensitivity testing to better understand the scale of impact and uncertainty inherent in applying demand surge to non-U.S. models and perils.

6.3 Validating Modeled Losses

Event losses account for ground motion, vulnerability, and industry inventory data. Validating event losses ensures a model's overall performance, and comparing historical and modeled loss data is a critical component of model validation. A comparison of modeled losses for historical earthquakes with the actual reported losses for that event, after these losses have been normalized (projected) to the current year, provides insight into the overall performance of the model. Total event losses are the result of interaction among all model components – including exposure, hazard, and vulnerability – and can be used to validate the model as a whole, when compared to the reported losses.

It must be noted, however, that due to large variations in earthquake insurance take-up rates and policy conditions over time, and to the fact that the AIR model contains only the most up-to-date policy conditions and take-up rates, reported insured losses are not used to validate modeled losses. Rather, ground-up losses are used instead.

As has been noted at several points in this document, the development and validation of the AIR Earthquake Model for Canada has had to meet the challenge posed by the lack of observational data for earthquakes in Canada. AIR addresses this issue for validation by using the most reliable and thorough loss estimates for earthquakes in Canada that are available from the fairly sparse historical record; namely, loss estimates for the 1988 M5.9 Saguenay earthquake and the 1964 M9.2 Alaska earthquake reported by NRCan and NOAA. (While the NRCan report also includes losses from a small tsunami generated by the 1929 Grand Banks earthquake, this value is not used to validate the losses estimated by the AIR model.) According to these reporting sources, losses in Canada associated with the 1964 Alaska earthquake were caused only by tsunami; there are no reports of losses due to ground shaking. In addition, it should be noted that that total loss reported for this event is subject to uncertainty and therefore less reliable for model validation. With these points in mind, AIR uses the range of losses from the 1988 Saguenay and the 1964 Alaska earthquakes in the following figure to evaluate overall model performance.

A scatterplot comparing the modeled and reported losses for selected events provides another indication of model performance (Figure 132). If the modeled and reported losses were equal, they would define a 45 degree diagonal line on the scatterplot (that is, y = x). In reality, however, it is not possible for modeled and reported losses to be identical for each event. Rather, a model is considered to be reasonable and unbiased if its losses are close to the reported values, and the modeled losses are not consistently smaller or larger than the reported values. Figure 87 indicates that the model is able to reasonably reproduce historical event losses and that there is no bias in the modeled loss estimates.

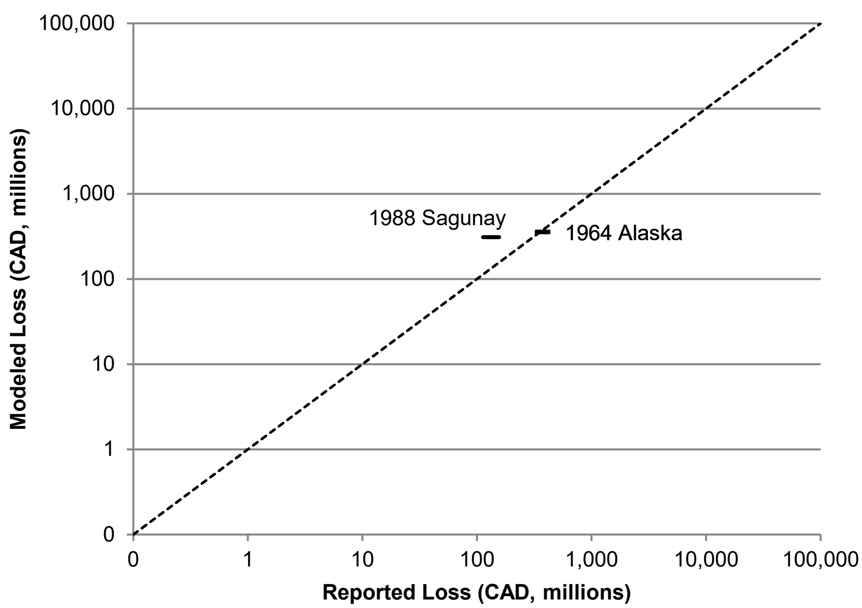

Figure 132. Modeled versus reported ground-up losses (CAD millions) for the 1988 Saguenay and the 1964 Alaska earthquake

7 AIR Earthquake Model for Canada in CATRADER

7.1 Available Catalogs

CATRADER supports two 10,000-year stochastic catalogs of simulated earthquake events: a time-dependent catalog and a time-independent catalog. These stochastic catalogs are seamlessly integrated with the corresponding 10,000-year stochastic catalogs available in the AIR Earthquake Model for the United States.

A historical event set containing the 33 events listed in Table 29 is also available in CATRADER for the AIR Earthquake Model for Canada. Note that this historical event set has also been integrated with the event set provided with the AIR Earthquake Model for the United States. To accommodate the observed uncertainty in source parameters for the historical earthquakes of 1663 and 1732 listed in the table, AIR provides three alternate scenarios for both of these events in CATRADER. The rationale for this decision is discussed more fully in Section 3.7.

Table 29. Historical event set available in CATRADER

Event ID	Year	Event Name	M_w
1	1663	Charlevoix-Kamouraska, QC—Scenario 1	7
2	1663	Charlevoix-Kamouraska, QC—Scenario 2	6.8
3	1663	Charlevoix-Kamouraska, QC—Scenario 3	7.2
4	1700	Cascadia Subduction Zone, Offshore of BC	9
5	1732	Montreal region, QC—Scenario 1	6.3
6	1732	Montreal region, QC—Scenario 2	6.05
7	1732	Montreal region, QC—Scenario 3	5.8
11	1791	Charlevoix-Kamouraska region, QC	5.5
20	1860	Charlevoix-Kamouraska region, QC	6
23	1870	Charlevoix-Kamouraska region,QC	6.6
30	1899	Yakutat Bay, AK	8.1
31	1904	Passamaquoddy Bay, NB	5.7
37	1918	Vancouver Island, BC	6.9
38	1920	Gulf Islands,BC	5.5
39	1925	Charlevoix-Kamouraska region, QC	6.2
43	1929	Laurentian slope, offshore NS and NL	7.1
45	1933	Baffin Bay, NU	7.4

Event ID	Year	Event Name	M_w
46	1988	Saguenay Region, QC	5.9
47	1935	Témiscaming region, QC	6.1
52	1944	Between Massena, NY, and Cornwall, ON	5.5
54	1946	Vancouver Island, BC	7.3
56	1949	Offshore of Haida Gwaii/Queen Charlotte Islands, BC	8.1
64	1958	Lituya Bay, AK	7.95
67	1964	Prince William Sound, AK	9.2
70	1970	Offshore of Haida Gwaii/Queen Charlotte Island, BC	7.4
76	1979	Southern Yukon region, YT	7.5
84	1982	Miramichi Highlands, NB	5.6
88	1985	North Nahanni River, NT	6.9
106	2001	Nisqually, WA	6.8
107	2002	Denali, AK	7.9
114	2010	Val-des-Bois, QC	5
116	2011	Vancouver Island, BC	6.5
117	2012	Haida Gwaii/Queen Charlotte Islands, BC	7.7

Table 30 lists the world scenario events (RDS and EDS) available in CATRADER for the AIR Earthquake Model for Canada. Descriptions of these events are available in Section 3.5 of this document. Modeled losses to exposures in Canada from these events are also provided in the table; if the events also cause loss to U.S. exposures this is indicated in the table (but insured loss estimates to U.S. exposures are not provided in the table).

Table 30. World scenario events available in CATRADER

Event ID	Event Name	Modeled Insured Loss (CAD Millions)*	Causes Loss to U.S. Exposures?
4	RDS ERRO British Columbia Earthquake 100 Year	2,067	Y
5	RDS ERRO British Columbia Earthquake 250 Year	9,389	Y
6	RDS ERRO British Columbia Earthquake 500 Year	17,895	Y
7	RDS ERRO Quebec Earthquake 100 Year	1,105	Y
8	RDS ERRO Quebec Earthquake 250 Year	5,163	Y
9	RDS ERRO Quebec Earthquake 500 Year	16,460	Y
10	EDS Montreal Earthquake	212,738	Y
11	EDS Ottawa Earthquake	34,559	Y
12	EDS Toronto Earthquake	289,176	Y
13	EDS Quebec City Earthquake	37,114	Y
14	EDS British Columbia Earthquake	42,102	Y
15	IBC Western Scenario	18,073	Y
16	IBC Eastern Scenario	11,895	Y
23	EDS Pacific Northwest Earthquake	179,800	Y
28	EDS New Hampshire Earthquake	17	Y
41	EDS Michigan Earthquake	14,656	Y
43	EDS Maine Earthquake	68	Y
44	EDS Ohio Earthquake	273	Y
59	EDS Vermont Earthquake	18,398	Y

**These estimates include insured loss to exposures in Canada only.*

7.2 Resolution of Analysis Results

In CATRADER, modeled loss estimates are reported at the country, province, and FSA levels.

7.3 AIR Industry Exposure Database

The Industry Exposure Database (IED) is an integral and highly valuable component of CATRADER. This database contains estimates of insured and insurable property exposures at a high degree of resolution, including the number of risks, their replacement values broken down by line of business (LOB), by coverage, by occupancy, and by construction type, building attributes, and information regarding standard policy terms and conditions.

AIR uses a variety of public and private sources to estimate industry exposures, including government data, commercially available demographic information, and other industry data. AIR's industry exposure database is extensively validated via comparison against values obtained from various insurance industry and governmental sources. For more information about the IED for this model, see the document *The AIR Industry Exposure Database for Canada*, which provides further details about the IED for this region and peril, including:

- Details regarding how the IED was developed
- Data sources used to develop the IED
- Maps detailing the total exposure for the modeled region
- Share of Industry Exposure by LOB
- Construction Splits by LOB
- Coverage Splits by LOB
- Height Band Splits by LOB
- Assumed Take-up Rates
- Policy Condition Assumptions

7.4 Supported Lines of Business for Reporting Modeled Losses

CATRADER supports the following lines of business for reporting modeled losses (the components of each line of business are also indicated below):

- Residential Building : Building, Contents, and Time
- Mobile Home: Building, Contents, and Time
- Commercial : Building, Contents, and Time
- Automobile: Personal and Commercial

8 AIR Earthquake Model for Canada in Touchstone

8.1 Available Catalogs

Touchstone supports two 10,000-year stochastic catalogs of simulated earthquake events for the AIR Earthquake Model for Canada: a time-dependent catalog and a time-independent catalog. These stochastic catalogs are seamlessly integrated with the corresponding 10,000-year stochastic catalogs available in the AIR Earthquake Model for the United States.

A historical event set of the 33 earthquakes listed in Table 31 is also available in Touchstone. To accommodate the observed uncertainty in source parameters for the historical earthquakes of 1663 and 1732 listed in the table, AIR provides three alternate scenarios for both of these events in Touchstone. The rationale for this decision is discussed more fully in Section 3.7.

Table 31. Historical event set available in Touchstone

Event ID	Year	Event Name	M_w
1	1663	Charlevoix-Kamouraska, QC—Scenario 1	7
2	1663	Charlevoix-Kamouraska, QC—Scenario 2	6.8
3	1663	Charlevoix-Kamouraska, QC—Scenario 3	7.2
4	1700	Cascadia Subduction Zone, Offshore of BC	9
5	1732	Montreal region, QC—Scenario 1	6.3
6	1732	Montreal region, QC—Scenario 2	6.05
7	1732	Montreal region, QC—Scenario 3	5.8
11	1791	Charlevoix-Kamouraska region, QC	5.5
20	1860	Charlevoix-Kamouraska region, QC	6
23	1870	Charlevoix-Kamouraska region,QC	6.6
30	1899	Yakutat Bay, AK	8.1
31	1904	Passamaquoddy Bay, NB	5.7
37	1918	Vancouver Island, BC	6.9
38	1920	Gulf Islands,BC	5.5
39	1925	Charlevoix-Kamouraska region, QC	6.2
43	1929	Laurentian slope, offshore NS and NL	7.1
45	1933	Baffin Bay, NU	7.4
46	1988	Saguenay Region, QC	5.9
47	1935	Témiscaming region, QC	6.1
52	1944	Between Massena, NY, and Cornwall, ON	5.5
54	1946	Vancouver Island, BC	7.3

Event ID	Year	Event Name	M_w
56	1949	Offshore of Haida Gwaii/Queen Charlotte Islands, BC	8.1
64	1958	Lituya Bay, AK	7.95
67	1964	Prince William Sound, AK	9.2
70	1970	Offshore of Haida Gwaii/Queen Charlotte Island, BC	7.4
76	1979	Southern Yukon region, YT	7.5
84	1982	Miramichi Highlands, NB	5.6
88	1985	North Nahanni River, NT	6.9
106	2001	Nisqually, WA	6.8
107	2002	Denali, AK	7.9
114	2010	Val-des-Bois, QC	5
116	2011	Vancouver Island, BC	6.5
117	2012	Haida Gwaii/Queen Charlotte Islands, BC	7.7

Table 32. World scenario events available in Touchstone lists the world scenario events (RDS and EDS) available in Touchstone for the AIR Earthquake Model for Canada. Descriptions of these events are available in Section 3.5 of this document. Modeled losses to exposures in Canada from these events are also provided in the table; if the events also cause loss to U.S. exposures this is indicated in the table.

Table 32. World scenario events available in Touchstone

Event ID	Event Name	Modeled Insured Loss (CAD Millions)*	Causes Loss to U.S. Exposures?
4	RDS ERRO British Columbia Earthquake 100 Year	2,067	Y
5	RDS ERRO British Columbia Earthquake 250 Year	9,389	Y
6	RDS ERRO British Columbia Earthquake 500 Year	17,895	Y
7	RDS ERRO Quebec Earthquake 100 Year	1,105	Y
8	RDS ERRO Quebec Earthquake 250 Year	5,163	Y
9	RDS ERRO Quebec Earthquake 500 Year	16,460	Y
10	EDS Montreal Earthquake	212,738	Y
11	EDS Ottawa Earthquake	34,559	Y
12	EDS Toronto Earthquake	289,176	Y
13	EDS Quebec City Earthquake	37,114	Y
14	EDS British Columbia Earthquake	42,102	Y
15	IBC Western Scenario	18,073	Y
16	IBC Eastern Scenario	11,895	Y
23	EDS Pacific Northwest Earthquake	179,800	Y
28	EDS New Hampshire Earthquake	17	Y
41	EDS Michigan Earthquake	14,656	Y
43	EDS Maine Earthquake	68	Y
44	EDS Ohio Earthquake	273	Y
59	EDS Vermont Earthquake	18,398	Y

**These estimates include insured loss to exposures in Canada only.*

8.2 Supported Geographic Resolutions

The following geographic resolutions are supported for the AIR Earthquake Model for Canada in Touchstone:

- CRESTA
- FSA
- Postal code (LDU)
- Street address (when Trillium is licensed)

8.3 Modeling Aggregate Data

During analysis, aggregate CRESTA exposures and aggregate FSA exposures are automatically disaggregated to a 1-km grid, based on industry exposure weights, by line of business.

8.4 Modeled Coverages

The modeled coverages in the AIR Earthquake Model for Canada in Touchstone are as follows:

Coverage A: Buildings

Coverage B: Other Structures

Coverage C: Contents

Coverage D: Business Interruption (Time Element)

8.5 Supported Construction and Occupancy Classes, Age and Height Bands, and Relative Vulnerabilities

As discussed in Section 5 of this document, the vulnerability of a structure depends on its construction and occupancy class combination as well as its age and height. With the goal of enabling clients to code their exposure data as specifically as possible, the AIR Earthquake Model for Canada in Touchstone supports 75 construction classes and 110 occupancy classes. Of the 110 occupancy classes, 62 are classes for industrial facilities.[23] The model also supports 7 age bands and 4 height bands.

AIR has compiled all of this supported building information along with relative building vulnerabilities into a Microsoft Excel workbook. This file is available at the following link:

AIR Earthquake Model for Canada Supplement

Specifically, this workbook contains the following information:

- Complete lists of supported construction and occupancy classes
- Supported construction/occupancy class combinations
- Supported age and height bands
- Relative vulnerabilities for all supported construction and occupancy class combinations for the shake peril (Coverage A)

Note that detailed descriptions of the supported construction classes and the supported occupancy classes are available in the UNICEDE/px Preparer's Guide, which can be accessed at: http://www.unicede.com.

[23] The industrial facilities set of occupancy classes refers to the 400-series, which include structures that are very different from the 300-series as they represent large, complex facilities composed of many components and can be differentiated as facilities with a replacement value of over USD 5 million. Small facilities (those with replacement values of USD 5 million or less) consist of mostly buildings and some machinery.

8.6 Supported Individual Risk Characteristics (Secondary Modifiers)

AIR's individual risk methodology follows a structured, logical approach that groups building characteristics according to their function to reflect the contribution of each characteristic to overall building performance. This knowledge-based methodology relies on simulations using the latest seismological engineering models as well as damage observations from post-disaster surveys. A modification function is applied to the base damage function, resulting in a modified damage function that reflects the impact of one or more selected building characteristics. Weighting factors are used to combine the effects of features whose interaction is complex and not necessarily additive. These are introduced to evaluate features that modify the performance of the system.

The individual risk characteristics supported by the model include earthquake-resistant systems, equipment bracing, short columns, soft stories, wall materials, and several other building attributes that affect a building's response to ground shaking. Older structures in particular may lack earthquake-resistant engineering or materials that withstand ground-shaking. They may have short columns, whose height is restricted by beams or infill walls increasing the likelihood of collapse or damage. Other characteristics of buildings such as the type of materials used for the external walls or internal partitions, soft stories, exterior ornamentation, the type of foundation, etc. have an effect on a building's ability to resist damage from ground shaking. Retrofitting is also included as an individual risk characteristic to accommodate older buildings that have been modified to make them more earthquake-resistant.

Table 41 describes the individual risk characteristics that are supported in the AIR Earthquake Model for Canada. The table also includes relative importance factors for these characteristics in order to provide a general sense of how they might impact the loss results. These factors were determined by examining each risk characteristic's impact on the vulnerability of a building, assuming moderate ground shaking and average modifier values.

It is important to note that the actual influence of any of these characteristics during a specific analysis may be quite different, since the impact of each depends heavily on the ground shaking conditions and the structural characteristics of the building, such as height and year built. Some characteristics have a greater impact under moderate ground shaking conditions, but under severe shaking conditions they may assume a different level of importance. Therefore, the relative importance factors are provided as ranges rather than a single value. It is also important to note that the building class itself has a strong influence on these importance factors. For example, the relative importance of Earthquake-Resistant Systems are typically not used for wood frame buildings and therefore have little or no relative importance for buildings of this construction class.

Table 33. Individual risk characteristics for buildings in Canada

Individual Risk Characteristic	Description
Relative Importance ≥ 30%	
Building Foundation	Single-family dwellings are often built on basements or shallow foundations. Most mid-rise buildings are built on mat foundations. High-rise buildings tend to be supported on pile-foundations, which generally perform better during earthquakes.
Building Shape (Footprint)	In general simple regular forms such as square and circular buildings perform better than L-shaped and T-shaped buildings.
Earthquake-Resistant Systems	Some new commercial buildings have special devices or design elements, such as base isolation, that resist earthquake loads.
Soft Story	A structural weakness on any floor (usually the first) in buildings with two or more stories. The lateral load-resisting capacity of the floor is weak and can result in total collapse of the floor (pancaking).
Structural Irregularity	Irregular floor plans, structural components, uneven weight distribution, etc makes a structure more vulnerable to damage. If the columns in concrete structures, such as parking facilities, are restricted by spandrel beams or infill walls, the effective length of the columns is reduced and they can no longer bear the loads for which they were originally designed.
Relative Importance 20–30%	
Building Condition and Quality	The building's overall general condition, based on a visual inspection, is provided here. The condition of the building is estimated based on the external appearance of cladding and maintenance.
Equipment Bracing	Anchoring mechanical and electrical equipment, particularly heavy or large pieces, to the floor, or bracing them against structural elements can resist damage. Vibration isolators (springs) are not as effective. Also, piping should be braced to restrain the movement.
Proximity to the Nearest Structure (Pounding)	If the gap between adjacent high-rise buildings is not adequate, there is a danger of "pounding" or collision of the two buildings during an earthquake.
Tall One-Story	Single-story buildings that are taller than usual (e.g., churches, gymnasiums, concert halls, etc.) may be more susceptible to damage from ground shaking. The roofs of such buildings are higher than usual from the ground, which means the lateral forces are higher and can cause these buildings to experience larger overturning forces. In addition, taller one-story buildings require taller columns or walls for support. These elements are likely to span large lengths without being braced out of plane, which can make the supporting columns or walls more susceptible to buckling.
Wall Siding	The materials used for weather protection of walls. Brick veneer and stone panels are more susceptible to falling off in an earthquake. Wood frame houses usually fare better.

Relative Importance 10–20%	
Building Exterior Opening	A shear wall with many openings for windows and doors has less resistance to earthquake loads. Buildings whose walls are more than 50% open are evaluated as having less seismic resistance than they would otherwise.
Exterior Ornamentation	Decorative and attached items such as entryway roofs can fall off during an earthquake. Falling ornaments can cause additional damage to anything they fall onto, especially roofs or other surfaces exposed directly to the falling objects.
Internal Partitions	The type of partition wall (e.g., masonry or gypsum board) is indicative of damage susceptibility during earthquakes. Masonry internal walls usually result in higher-than-average building damage.
Retrofit Measure	Proper retrofitting can make even a weak structure resistant to earthquakes. This may include no cripple walls, bracing for parapet walls and soft stories, bolting of older structures to foundations, glass/window strengthening, anchoring of tilt-up structures, bracing and anchoring of URM walls.
Short Columns	This applies to old concrete structures in which the full height of some columns has been restricted by spandrel beams or infill walls. If some of the columns along the perimeter are shorter than the adjacent columns, there is high chance that the shorter column can no longer bear the loads for which they were originally designed.
Torsion	In wedge-shaped and corner buildings, the lateral load-resisting components are placed asymmetrically. This induces torsional forces when the building is shaken, which can lead to significant damage.
Wall Type	The material used for the external walls. Unreinforced masonry walls increase the likelihood of a building being damaged during shaking; however these materials are used extensively in some regions because of their fire resistant properties. Pre-cast concrete panels or reinforced masonry walls are prone to damage. Plywood and OSB sheathing have similar shear strength and damageability.
Relative Importance < 10%	
Brick Veneer	Brick veneer masonry is usually unreinforced, and is therefore prone to cracking or loosening during ground shaking. If pieces of the veneer are dislodged, they may fall and damage other parts of the building. This modifier covers direct damage to the brick veneer itself and any subsequent indirect damage to other building components.
Building Foundation Connection	The connection between the structure and its foundation. Loss of anchorage between a building and its foundation has been a common type of failure in California earthquakes. Generally structures with anchor bolts or structurally connected foundation will have much less damage compared to the structures with gravity or friction connection.
Chimney	Masonry chimneys are heavy, rigid, and usually brittle, and therefore particularly vulnerable to earthquakes.
Redundancy	Multiple lateral load-resisting elements (frames or shear walls) in a building provide additional reinforcement.
Roof Deck	The material and construction type of the roof deck. Roof decks transfer the roof loads to the underlying joists and purlins. A heavy roof can cause relatively higher damage from earthquakes.
Tanks on Adjoining Higher Buildings	Rooftop tanks on adjoining, higher buildings are a falling hazard during earthquakes.
Water Heaters (Residential Structures)	If the water heater in a residential building is not properly secured, there is a good chance that it will topple during earthquakes and cause damage, both to itself and any part of the structure underneath it.

8.7 Damage Functions for Unknown Construction/Occupancy Classes

In the AIR Earthquake Model for Canada, building and contents damage functions are available for unknown construction, occupancy, and height classes.

Touchstone uses composite damage functions based on AIR's industry exposure database. The damage functions for unknown construction, occupancy, and height classes are exposure-weighted averages of the damage functions corresponding to all values of the unknown parameters, with weights determined by the relative share of the total insurable value of each class. Different damage functions are used depending on how many variables, and which ones, are unknown. For further details about how AIR has developed these damage functions, see Section 5.5, subsection "Damage Functions for Buildings of Unknown Attributes" in this document.

8.8 Supported Take-Up Rates and Policy Conditions

The financial module in Touchstone allows for the application of a wide variety of location, policy, and reinsurance conditions. Location terms may be specified to include limits and deductibles by site or by coverage. Supported policy terms include blanket and excess layers, minimum and maximum deductibles, and sublimits. Reinsurance terms include facultative certificates and various types of risk-specific and aggregate treaties with occurrence and aggregate limits.

For more information about policy terms, see the AIR publication *Industry Deductible Assumptions* for the appropriate year. Take-up rate information can be found in the AIR publication *Industry Take-Up Rates* for the appropriate year. Both of these publications are available through the Client Portal of the AIR website.

9 Selected References

Selected references used in the development of the AIR Earthquake Model for Canada are listed below:

Abrahamson, N. 2012, "Summary of the B.C. Hydro GMPE for Subduction Earthquakes," United States Geological Survey Pacific Northwest Workshop for the Update of the National Seismic Hazard Maps, March 21-22, 2012. Available at: http://earthquake.usgs.gov/hazards/about/workshops/PacNWworkshoptalks/2012workshop/Abrahamson2012_BCHydroGMPE.pdf

Abrahamson, N. A., and W. J. Silva 2008, "Summary of the Abrahamson & Silva NGA Ground Motion Relations," *Earthquake Spectra*, 24, 67–97.

Adams, J. 2011, "Seismic Hazard Maps for the National Building Code of Canada," CSCE 2011 General Conference, Jagmohan Humar Symposium, June 14-17, 2011, Ottawa, Ontario.

Adams, J. and S. Halchuk, 2003, "Fourth generation seismic hazard maps of Canada: Values for over 650 Canadian localities intended for the 2005 National Building Code of Canada," Geological Survey of Canada Open File Report 4459.

Andrus, R. D., and K. H. Stokoe II 2000, "Liquefaction resistance of soils from shear wave velocity," *Journal of Geotechnical and Geoenvironmental Engineering*, 126, 1015–1025.

Applied Technology Council (ATC) 1985, "Earthquake Damage Evaluation Data for California," ATC Series Report 13 (ATC-13). Redwood, CA: Applied Technology Council. Available at: https://www.atcouncil.org/pdfs/atc13.pdf

Arias, A. 1970, "A measure of earthquake intensity," in Hansen, R.J., editor, *Seismic Design For Nuclear Power Plants.* Cambridge, Massachusetts Institute of Technology Press, p. 438-483.

Atkinson, G. M. 2008, "Ground-Motion Prediction Equations for Eastern North America from a Referenced Empirical Approach: Implications for Epistemic Uncertainty," *Bulletin of Seismological Society of America*, 98, 1304–1318.

Atkinson, G. M. 2012, "Latest results on subduction zone GMPEs," United States Geological Survey Pacific Northwest Workshop for the Update of the National Seismic Hazard Maps, March 21-22, 2012. Available at: http://earthquake.usgs.gov/hazards/about/workshops/PacNWworkshoptalks/2012workshop/Atkinson2012SubductionGMPEs.pdf

Atkinson, G. M., and D. M. Boore 2011, "Modification to Existing Ground-Motion Prediction Equations in Light of New Data," *Bulletin of Seismological Society of America*, 101, 1121–1135.

Atkinson, G. M., and D. M. Boore 2006, "Earthquake Ground Motion Prediction Equations for Eastern North America," *Bulletin of the Seismological Society of America*, 96, 2181–2205.

Atkinson, G. M., and D. M. Boore 2003, "Empirical Ground Motion Relations for Subduction-Zone Earthquakes and their Application to Cascadia and Other Regions," *Bulletin of Seismological Society of America*, 93, 1703–1729.

Atkinson, G. M., and K. Goda 2011, "Effect of Seismicity Models and New Ground-Motion Prediction Equations on Seismic Hazard Assessment for Four Canadian Cities," *Bulletin of Seismological Society of America*,101, 176–189.

Atkinson, G. M. and S. Kaka 2007, "Relationships between felt intensity and instrumental ground motions for earthquakes in the central United States and California," *Bulletin of the Seismological Society of America*, 97, 497-510.

Atkinson, G. M., and M. Macias 2009, "Predicted Ground Motions for Great Interface Earthquakes in the Cascadia Subduction Zone," *Bulletin of Seismological Society of America*, 99, 1552–1578.

Atkinson, G. M. and S. N. Martens 2007, "Seismic hazard estimates for sites in the stable Canadian craton," *Canadian Journal of Civil Engineering*, 34, 1299-1311.

Aylsworth, J.M., D. E. Lawrence, J. Guertin 2000, "Did two massive earthquakes in the Holocene induce widespread landsliding and near-surface deformation in part of the Ottawa Valley, Canada?" *Geology,* 28, 903-906.

Barrie, J. V., P. R. Hill, K. W. Conway, K. Iwanowska, and K. Picard 2005, "Georgia Basin: seabed features and marine geohazards," *Geoscience Canada*, 32, 145-156.

Bazzurro, P., and J. Park 2007, "The Effects of Portfolio Manipulation on Earthquake Portfolio Loss Estimates," Proceedings of the 10th International Conference on Applications of Statistics and Probability in Civil Engineering, Tokyo, Japan, July 31-August 4, 2007.

Bazzurro, P., J. Park, P. Tothong, and N. Jayaram 2008, "Effects of Spatial Correlation of Ground Motion Parameters for Multi-Site Seismic Risk Assessment," Collaborative Research with J. Baker of Stanford University and AIR Worldwide, Report December, 2008. Available at: http://earthquake.usgs.gov/research/external/reports/07HQGR0032.pdf.

Blais-Stevens, A., O. Hungr 2008, "Landslide Hazards and Mitigation Along the Sea to Sky Corridor, British Columbia," Proceedings of the 4th Canadian Conference on Geohazards : From Causes to Management. Presse de l'Université Laval, Quebec

Boore, D. M., and G. M. Atkinson 2008, "Ground-Motion Prediction Equations for the Average Horizontal Component of PGA, PGV, and 5%-damped PSA at Spectral Periods between 0.01 s and 10.0 s," *Earthquake Spectra*, 24, 99–138.

Boore, D. M., J. F. Gibbs, W. B. Joyner, J. C. Tinsley, and D. J. Ponti 2003, "Estimated ground motion from the 1994 Northridge, California, earthquake at the site of the interstate 10 and La Cienega Boulevard bridge collapse, west Los Angeles, California," *Bulletin of the Seismological Society of America*, 93, 2737-2751.

Borcherdt, R. D., 1994, "Estimates of Site-Dependent Response Spectra for Design (Methodology and Justification)," *Earthquake Spectra*, 10, 617–653.

Braunmiller, J., and J. Nábělek 2002, "Seismotectonics of the Explorer Region," *Journal of Geophysical Research*, 107, 2208, doi:10.1029/2001JB000220.

Burgette, R.J., R.J. Weldon, and D.A. Schmidt 2009, "Interseismic uplift rates for western Oregon and along-strike variation in locking on the Cascadia subduction zone," *Journal of Geophysical Research*, 114, B01408, doi:10.1029/2008JB005679.

Cajka, M. G. and J. A. Drysdale 1996, "Intensity report of the November 25, 1988 Saguenay, Quebec, earthquake," Geological Survey of Canada Open File Report 327.

Calvert, H.T., and S. B. Hyde 2002, "Assessing Landslide Hazards In The Ottawa Valley Using Electrical And Electromagnetic Methods," 15th EEGS Symposium on the Application of Geophysics to Engineering and Environmental Problems.

Campbell, K. W. 2003, "Prediction of Strong Ground Motion using the Hybrid Empirical Method and its use in the Development of Ground-Motion (Attenuation) Relations in Eastern North America," *Bulletin of the Seismological Society of America*, 93, 1012–1033.

Campbell K. W., and Y. Bozorgnia 2007 "Campbell-Bozorgnia NGA Ground Motion Relations for the Geometric Mean Horizontal Component of Peak and Spectral Ground Motion Parameters," PEER Report 2007/02, Berkeley, California: Pacific Earthquake Engineering Research Center.

Campbell K. W., and Y. Bozorgnia 2008, "NGA Ground Motion Model for the Geometric Mean Horizontal Component of PGA, PGV, PGD and 5% Damped

Linear Elastic Response Spectra for Periods Ranging from 0.01 to 10s," *Earthquake Spectra*, 24, 139–171.

Cassidy, J.F., G. C. Rogers, M. Lamontagne, S. Halchuk, J. Adams 2010, "Canada's Earthquakes: 'The good, the bad, and the ugly'," *Geoscience Canada*, 37, 1-16.

Chiou, B. S. J., and R. R. Youngs 2008, "Chiou-Youngs NGA Ground Motion Relations for the Geometric Mean Horizontal Component of Peak and Spectral Ground Motion Parameters," Earthquake Spectra, 24, 173–215.

Chouinard, L. and P. Rosset 2007, "Seismic site effects and seismic risk in the Montreal area – the influence of marine clays," 9th Canadian Conference on Earthquake Engineering, Ottawa, Ontario, Canada, June 2007.

Chouinard, L. and P. Rosset 2011, "Microzonation of Montreal, variability in soil classification," 4th IASPEI/IAEE International Symposium, August 2011.

Clague, J. J. 2002, "The Earthquake Threat in Southwestern British Columbia: A Geologic Perspective," *Natural Hazards* 26: 7–34

Clague, J. J., P. T. Bobrowsky and I. Hutchinson, 2000, "A review of geological records of large tsunamis at Vancouver Island, British Columbia, and implications for hazard," *Quaternary Science Reviews*, 19, 849-863.

Clague, J. J., E. Naesgaard, and A. R. Nelson 1997, "Age and significance of earthquake-induced liquefaction near Vancouver, British Columbia, Canada," *Canadian Geotechnical Journal*, 34, 53-62.

Cooper, T. W. 1997, "A Study of the Performance of Petroleum Storage Tanks During Earthquakes, 1933-1995," National Institute of Standards and Technology, NIST GCR 97-720, Gaithersburg, Maryland.

Cousins, J., D. Heron, S. Mazzoni, G. Thomas, and D. Lloydd 2002, "Estimating Risks from Fire Following Earthquake," Institute of Geological and Nuclear Sciences Client Report 2002/60, Prepared for New Zealand Fire Service Commission.

Cousins, J., D. Heron, S. Mazzoni, G. Thomas, and D. Lloydd 2003, "Modelling the spread of post-earthquake fire," Proceedings of the 2003 Pacific Conference on Earthquake Engineering, February 13-15, 2003, Christchurch, New Zealand.

Cousins, J. and D. Smith 2004, "Estimated Losses due to Post-Earthquake Fire in Three New Zealand Cities," Technical Paper No. 28, Proceedings of the 2004 Conference of the New Zealand Society for Earthquake Engineering, March 19-21, Rotorua, New Zealand.

Craymer, M. R., J. A. Henton, M. Piraszewksi, E. Lapelle 2011, "An Updated GPS Velocity Field for Canada", American Geophysical Union, San Francisco, CA, December 5-9, 2011, Abstract #G12A-0793.

Cruz, A. M., E. Krausmann, and G. Franchello 2011, "Analysis of Tsunami Impact Scenarios at an Oil Refinery," *Natural Hazards* 58, 141–162.

Dao, M. H. and P. Tkalich 2007, "Tsunami propagation modelling – a sensitivity study," *Natural Hazards and Earth System Sciences*, 7, 741–754.

Dragert, H., R. D. Hyndman, G. C. Rogers, and K. Wang 1994, "Current deformation and the width of the seismogenic zone of the northern Cascadia subducted thrust," *Journal of Geophysical Research*, 99, 635-668.

Dziak, R. P. 2006, "Explorer deformation zone: Evidence of a large shear zone and reorganization of the Pacific–Juan de Fuca–North American triple junction," *Geology*, 34, 213-216.

Eidinger, J. M., E. A. Avila, D. Ballantyne, L. Cheng, A. der Kiureghian, B. F. Maison, T. D. O'Rourke, and M. Power 2001, "Seismic Fragility Formulations for Water Systems, Part 1 – Guideline," Report of the American Lifelines Alliance, a public-private partnership between the American Society of Civil Engineers (ASCE) and the Federal Emergency Management Agency (FEMA). Available at: http://nisee.berkeley.edu/library/seismicfragilitywatersystems.pdf

Elliott, J. L., C. F. Larsen, J. T. Freymueller, and R. J. Motyka 2010, "Tectonic block motion and glacial isostatic adjustment in southeast Alaska and adjacent Canada constrained by GPS measurements," *Journal of Geophysical Research*, 115, B09407, doi:10.1029/2009JB007139.

Ellingwood, B. R., O. C. Celik, and K. Kinali 2007, "Fragility assessment of building structural systems in Mid-America," *Earthquake Engineering and Structural Dynamics*, 36, 1935-1952.

EMS 1998, *The European Macroseismic Scale EMS-98*. G. Grünthal (ed), Luxembourg: European Seismological Commission (ESC). Available at: http://media.gfz-potsdam.de/gfz/sec26/resources/documents/PDF/EMS-98_Original_englisch.pdf

Engman, E. T. 1986, "Roughness coefficients for routing surface runoff," *Journal of Irrigation and Drainage Engineering*, 112, 39-53.

Federal Emergency Management Agency (FEMA) 2012, *HAZUS – MH 2.1 Technical Manual, Earthquake Model*, Washington, D.C.: Department of Homeland Security, FEMA Mitigation Division.

Federal Emergency Management Agency (FEMA) 2008, *Earthquake Loss Estimation Methodology HAZUS-MH MR3 (HAZUS)*. Washington, D.C.: National Institute of Building Sciences.

Federal Emergency Management Agency (FEMA) 2005, *Improvement of Nonlinear Static Seismic Analysis Procedures (FEMA 440)*. Washington, D.C.: Department of Homeland Security, Federal Emergency Management Agency.

Federal Emergency Management Agency (FEMA) 2003, *Multi-hazard loss estimation methodology: HAZUS MR4 technical manual*. National Institute of Building Sciences, Washington D.C.: Department of Homeland Security, Federal Emergency Management Agency.

Federal Emergency Management Agency (FEMA) 1997, *NEHRP Guidelines for the Seismic Rehabilitation of Buildings (FEMA 273)*. Washington, D.C.: Federal Emergency Management Agency.

Fenton, C., J. Adams, and S. Halchuk 2006. "Seismic hazards assessment for radioactive disposal sites in regions of low seismicity," *Geotechnical and Geological Engineering*, 24, 579-592.

Frankel, A., C. Mueller, T. Barnhard, D. Perkins, E. Leyendecker, N. Dickman, S. Hanson, and M. Hopper 1996, "National Seismic Hazard Maps—Documentation June 1996," U.S. Geological Survey Open-File Report 96–532, 110.

Fulton, R.J. (compiler), 1996, "Surficial materials of Canada," Geological Survey of Canada, Map 1880A.

Geertsema, M., J. W. Schwab, and A. Blais-Stevens 2008, "Landslide and Linear Infrastructure in West-Central British Columbia," in Proceedings of the 4th Canadian Conference on Geohazards: From Causes to Management, Quebec City, Canada, May 20-24, 2008.

Geertsema, M., J. J. Clague, J. W. Schwab and S. G. Evans 2006, "An overview of recent large catastrophic landslides in northern British Columbia, Canada," *Engineering Geology*, 83, 120-143.

Goda K. and G. M. Atkinson 2009, "Probabilistic Characterization of Spatially Correlated Response Spectra for Earthquakes in Japan", *Bulletin of Seismological Society of America*, 99, 3003–3020.

Goto, C., Ogawa, Y., Shuto, N., and Imamura, F. *Numerical method of tsunami simulation with the leap-frog scheme*. IUGG/IOC Time Project, IOC Manuals and Guides No. 35, UNESCO 1997. Available at: http://ftp.jodc.go.jp/info/ioc_doc/Manual/122367eb.pdf

Gregor, N. J., W. J. Silva, I. G. Wong, and R. R. Youngs 2002, "Ground motion attenuation relationships for Cascadia subduction zone megathrust earthquakes based on a stochastic finite-fault model," *Bulletin of the Seismological Society of America*, 92, 1923–1932.

Grundy, P., A. Thurairaja, and G. Walker, 2005 "Some Reflections on the Structural Engineering Aspects of Tsunami Damage," *Proceedings of The Australian Earthquake Engineering Society Conference*, 2005.

Halchuk, S., Allen, T.I., Adams, J., and Rogers, G.C., 2014. "Fifth Generation Seismic Hazard Model Input Files as Proposed to Produce Values for the 2015 National Building Code of Canada," Geological Survey of Canada, Open File 7576. doi:10.4095/293907.

Heron, D., J. Cousins, B. Lukovic, G. Thomas, and R. Schmid 2003, "Modeling Fire-Spread in and around Urban Centers," *Institute of Geological and Nuclear Sciences Client Report*, 2003/96.

Himoto, K., and T. Tanaka 2000, "A Preliminary Model for Urban Fire Spread: Building Fire Behavior Under the Influence of External Heat and Wind," U.S./Japan Government Cooperative Program on Natural Resources (UJNR), Fire Research and Safety, 15th Joint Panel Meeting Proceedings, V. 2.

Himoto, K., and T. Tanaka 2008, "Development and Validation of a Physics-Based Urban Fire Spread Model," *Fire Safety Journal*, 43, 477–494.

Himoto, K. and T. Tanaka 2010, "Physics-based Modeling of Fire Spread in Densely-built Urban Area and its Application to Risk Assessment," *Monografias de la Real Academia de Ciencias de Zaragoza*, 34, 87-104.

Holzer T., T. Noce, M. Bennett 2011, "Liquefaction Probability Curves for Surficial Geologic Deposits," *Environmental and Engineering Geoscience*, 27, 1–21.

Hong H. P., and K. Goda 2007, "Orientation-Dependent Ground-Motion Measure for Seismic-Hazard Assessment", *Bulletin of Seismological Society of America*, 97, 1525–1538.

Hunter, J. A., R. A. Burns, R. L. Good, and C. F. Pelletier 1998, "A compilation shear wave velocities and borehole geophysical logs in unconsolidated sediments of the Fraser River delta", Open File Report 3622, Geological Survey of Canada, Ottawa, Canada.

Hunter, J. A., R. A. Burns, R. L. Good, J. M. Aylsworth, S. E. Pullan, D. Perret, and M. Douma 2007, "Borehole shear wave velocity measurements of Champlain Sea sediments in the Ottawa–Montreal region," Open File Report 5345, Geological Survey of Canada, Ottawa, Canada.

Hunter, J. A., H. L. Crow, G. Brooks, M. Pyne, D. Motazedian, M. Lamontagne, A. J.-M. Pugin, S. E. Pullan, T. Cartwright, M. Douma, R. A. Burns, R. L. Good, K. Kaheshi-Banab, R. Caron, M. Kolaj, I. Folahan, L. Dixon, K. Dion, A. Duxbury, A. Landriault, V. Ter-Emmanuil, A. Jones, G. Plastow, and D. Muir 2010, "Seismic site classification and site period mapping in the Ottawa area using geophysical methods," Geological Survey of Canada, Open File Report 6273.

Hyndman, R.D., G. C. Rogers, H. Dragert, K. Wang, D. Oleskevich, J. Henton, J. J. Clague, J. Adams, P. T. Bobrowsky 2008, "Giant earthquakes beneath Canada's West coast," Publication of the Geological Survey of Canada. Available at: http://www.nrcan.gc.ca/earth-sciences/energy-mineral/geology/geodynamics/earthquake-processes/8595

Hyndman, R. D., S. Mazzotti, D. Weichert, and G. C. Rogers 2003, "Frequency of large crustal earthquakes in Puget Sound–Southern Georgia Strait predicted from geodetic and geological deformation rates," *Journal of Geophysical Research*, 108, 2033-2045, doi:10.1029/2001JB001710.

Hyndman, R. D., R. P. Riddihough, and R. Herzer 1979, "The Nootka fault zone—A new plate boundary off western Canada," *Geophysical Journal of the Royal Astronomical Society*, 58, 667-683.

Idriss, I. M. and R. W. Boulanger 2008, "Soil liquefaction during earthquakes," Monograph MNO-12, Earthquake Engineering Research Institute, Oakland, California.

Ishihara, K. and M. Yoshimine 1992, "Evaluation of settlements in sand deposits following liquefaction during earthquakes," *Soils and Foundations*, 32, 173–188.

Jibson, R. W. 1993, "Predicting earthquake-induced landslide displacements using Newmark's sliding block analysis," *Transportation Research Record*, 1411, 9-17.

Jibson, R.W., E. L. Harp, and J. A. Michael 1998, "A Method for Producing Digital Probabilistic Seismic Landslide Hazard Maps: An Example from the Los Angeles, California area," U.S. Geological Survey Open-File Report 98-113. Available at: http://pubs.usgs.gov/of/1998/ofr-98-113/

Jibson, R.W., E. L. Harp, and J. A. Michael 2000, "A method for producing digital probabilistic seismic landslide hazard maps," *Engineering Geology*, 58, 271-289.

Klassen, R.A., S. Paradis, A. M. Bolduc, and R. D. Thomas 1992, "Glacial landforms and deposits, Labrador, Newfoundland and eastern Québec," Geological Survey of Canada, Map 1814A.

Koehler, R. D., R-E. Farrell, P. A. C. Burns, and R. A. Combellick 2012, "Quaternary Faults and Folds in Alaska: A Digital Database," Alaska Division of Geological and Geophysical Surveys, Miscellaneous Publication 141.

Kostrov, B. V. 1974, "Seismic moment and energy of earthquakes, and seismic flow of rocks," *Izvestiya Akademii Nauk SSSR, Fizika Zemli* [*Bulletin of the Academy of Sciences of the USSR, Physics of the Solid Earth*], 1, 23-44.

Kovacs, P. 2010, *Reducing the Risk of Earthquake Damage in Canada: Lessons from Haiti and Chile*. Research Paper No. 49, Institute for Catastrophic Loss Reduction (ICCLR).

Kovacs, P., and H. Kunreuther 2001, "Managing Catastrophic Risk: Lessons from Canada," Presentation at ICCLR/IBC Earthquake Conference, Vancouver, Canada, March 23, 2001.

Lanphere, M. A. 1978, "Displacement history of the Denali fault system, Alaska and Canada," *Canadian Journal of Earth Sciences*, 15, 817-822.

Larsen, C. F., R. J. Motyka, J. T. Freymueller, K. A. Echelmeyer, E. R. Ivins 2005, "Rapid viscoelastic uplift in southeast Alaska caused by post-Little Ice Age glacial retreat," *Earth and Planetary Science Letters*, 237, 548-560.

Leonard, L. J., R. D. Hyndman, S. Mazzotti, L. Nykolaishen, M. Schmidt, and S. Hippchen 2007, "Current deformation in the northern Canadian Cordillera inferred from GPS measurements," *Journal of Geophysical Research*, 112, B11401, doi:10.1029/2007JB005061.

Leonard, L. J., S. Mazzotti, and R. D. Hyndman 2008, "Deformation rates estimated from earthquakes in the northern Cordillera of Canada and eastern Alaska," *Journal of Geophysical Research*, 113, B08406, doi:10.1029/2007JB005456.

Lewis, T. J., C. Lowe, and T. S. Hamilton 1997, "Continental signature of a ridge-trench-triple junction: Northern Vancouver Island," *Journal of Geophysical Research*, 102: 7767-7781.

Liu, P. L.-F. , S-B. Woo, and Y-S Cho 1998, "Computer programs for tsunami propagation and inundation," Technical report, Cornell University, 1998.

Lowe C., S. A. Dehler, and B.C. Zelt 2003, "Basin architecture and density structure beneath the Strait of Georgia, British Columbia," *Canadian Journal of Earth Sciences*, 40, 965–981.

Mahdyiar, M., B. Dodov, B. Shen-Tu, K. Shabestari, J. Guin, and Y. Rong 2010, "Stochastic Simulation of Earthquake Ground Motion Footprints Constrained by Recorded Data and MMI Intensity Maps," Proceedings of the 9th U.S. National and 10th Canadian National Conference on Earthquake Engineering, Toronto, Canada.

Manshinha, L. and D. E. Smylie 1971, "The displacement fields of inclined faults," *Bulletin of the Seismological Society of America*, 61, 1433–1440.

Mathews, W.H. 1979, "Landslides of central Vancouver Island and the 1946 earthquake," *Bulletin of the Seismological Society of America*, 69, 445–450.

Matthews, M. V., W. L. Ellsworth, and P. A. Reasenberg 2002, "A Brownian model for recurrent earthquakes," *Bulletin of the Seismological Society of America*, 92, 2233–2250.

Mazzotti, S., H. Dragert, J. Henton, M. Schmidt, R. Hyndman, T. James, Y. Lu, and M. Craymer 2003, "Current tectonics of northern Cascadia from a decade of GPS measurements," *Journal of Geophysical Research* 198, DOI: 10.1029/2003JB002653.

Mazzotti, A., T. S. James, and J. Henton 2005, "GPS crustal strain, postglacial rebound, and seismic hazard in eastern North America: The Saint Lawrence valley example," *Journal of Geophysical Research* 110, B11301, doi:10.1029/2004JB003590

Mazzotti, S., A. Lambert, N. Courtier, L. Nykolaishen, and H. Dragert 2007, "Crustal uplift and sea level rise in northern Cascadia from GPS, absolute gravity and tide gauge data," *Geophysical Research Letters*, 34, L15306, doi:10.1029/2007GL030283.

Mazzotti, S., L. J. Leonard, J. F. Cassidy, G. C. Rogers, and S. Halchuk 2011, "Seismic hazard in western Canada from GPS strain rates versus earthquake catalog," *Journal of Geophysical Research*, 116, B12310, doi:10.1029/2011JB008213.

McCaffrey, R., A. I. Qamar, R. W. King, R. Wells, G. Khazaradze, C. A. Williams, C. W. Stevens, J. J. Vollick, and P. C. Zwick, 2007, "Fault locking, block rotation and crustal deformation in the Pacific Northwest," *Geophysical Journal International*, 169, 1315–1340.

McCaffrey, R., R. W. King, S. J. Payne, and M. Lancaster 2013, "Active Tectonics of Northwestern U.S. inferred from GPS-derived Surface Velocities," *Journal of Geophysical Research*, 118, 709-723.

McCrory, P. A., J. L. Blair, D. H. Oppenheimer and S. R. Walter 2003, "Depth to the Juan de Fuca slab beneath the Cascadia subduction margin: A 3-D model for sorting earthquakes," U.S. Geological Survey Digital Data Series, 1 CD-ROM.

McCrory, P. A., J. L. Blair, D. H. Oppenheimer and S. R. Walter 2006, "Depth to the Juan de Fuca slab beneath the Cascadia subduction margin--A 3-D model sorting earthquakes," U.S. Geological Survey Data for Series 91, v.1.2 (CD-ROM and available on the World Wide Web at http://pubs.usgs.gov/ds/91).

Mitchell, C. E., P, Vincent, R. J. Weldon, and M. A. Richards 1994, "Present day vertical deformation of the Cascadia margin, Pacific Northwest, United States," *Journal of Geophysical Research*, 99, 12257-12277.

Mitchell, D., P. Paultre, R. Tinawi, M. Saatcioglu, R. Tremblay, K. Elwood, J. Adams, and R. DeVall 2010, "Evolution of seismic design provisions in the national building code of Canada," *Canadian Journal of Civil Engineering*, 9, 1157–1170.

MLIT 2011, "Great East Japan Earthquake," Japanese Government, Ministry of Land, Infrastructure, Transport, and Tourism (in Japanese)

MLIT 2011a, "Status Survey Results of the Great East Japan Earthquake (1st Report)," Japanese Government, Ministry of Land, Infrastructure, Transport, and Tourism (in Japanese)

MLIT 2011b, "Status Survey of the Great East Japan Earthquake and Tsunami (2nd Report)," Japanese Government, Ministry of Land, Infrastructure, Transport, and Tourism (in Japanese)

Monahan, V. M., P. H. Levson, and A. Sy 2000, "Relative Amplification of Ground Motion Hazard Map of Greater Victoria," scale 1:25,000, Geological Survey Branch, British Columbia Ministry of Energy and Mines, Geoscience Map 2000-3b.

Motazedian D, J. A. Hunter, A. Pugin, and H. Crow 2011, "Development of a Vs30 (NEHRP) Map for the City of Ottawa, Ontario, Canada," *Canadian Geotechnical Journal*, 48, 458–472.

Newmark, N.M., 1965, "Effects of earthquakes on dams and embankments," *Géotechnique*, 15, 139-160.

Office of Energy Efficiency (OEE) 2007, *2007 Survey of Household Energy Use (SHEU-2007)*, Ottawa: Natural Resources Canada.

Onur, T., C. E. Ventura, W. D. L. Finn 2005, "Regional seismic risk in British Columbia – damage and loss distribution in Victoria and Vancouver", *Canadian Journal of Civil Engineering*, 32, 361–371.

Ouellet, M. 2012, “Lake sediments and Holocene seismic hazard assessment within the St. Lawrence Valley, Quebec,” *Geological Society of America Bulletin* 1997, 109, 631-642.

Park, J., P. Bazzurro, and J. W. Baker 2007, “Modeling Spatial Correlation of Ground Motion Intensity Measures for Regional Seismic Hazard and Portfolio Loss Estimation,” Proceedings of the 10th International Conference on Application of Statistic and Probability in Civil Engineering , Tokyo, Japan, July 31–August 4, 2007.

Paultre, P., Lefebvre, G., Devic, J.-P. and Côté, G. (1993): “Statistical analyses of Damages to Buildings in the 1988 Saguenay Earthquake", Can. J. of Civ. Eng., 20(6), 988-998.

Paz, M. 1994, *International Handbook of Earthquake Engineering: Codes, Programs, and Examples*. New York, New York: Chapman and Hall, Inc.

Petersen, M. D., A. D. Frankel, S. C. Harmsen, C. S. Mueller, K. M. Haller, R. L. Wheeler, R. L. Wesson, Y. Zeng, O. S. Boyd, D. M. Perkins, N. Luco, E. H. Field, C. J. Wills and K. S. Rukstales 2008, “Documentation for the 2008 Update of the United States National Seismic Hazard Maps,” United States Geological Survey Open-File Report 2008-1128.

Peterson, M. D., M. P. Moschetti, P. M. Powers, C. S. Mueller, K. M. Haller, A. D. Frankel, Y. Zeng, S. Rezaeian, S. C. Harmsen, O. S. Boyd, N. Field, R. Chen, K. S. Rukstales, N. Luco, R. L. Wheeler, R. A. Williams, and A. H. Olsen, 2015,The 2014 United States National Seismic Hazard Model, Earthquake Spectra, Volume 31, No. S1, pages S1–S30.

Plafker, G., T. Hudson, T. Bruns, and M. Rubin 1978, “Late Quaternary offsets along the Fairweather fault and crustal plate interactions in southern Alaska,” *Canadian Journal of Earth Sciences*, 15, 805-816.

Power, M., B. Chiou, N. Abrahamson, Y. Bozorgnia, T. Shantz, and C. Roblee 2008, “An Overview of the NGA Project,” *Earthquake Spectra*, 24, 3-21.

Prest, V. K., and J. Hode-Keyser 1975, “Surficial Geology, Montreal Island, Quebec/Géologie des dépôts meubles, Île de Montréal, Québec,” Geological Survey of Canada “A” Series Map 1426A.

Ramachandran K., S. E. Dosso, C.A. Zelt, G. D. Spence, R. D. Hyndman, and T. M. Brocher 2004, “Upper crustal structure of southwestern British Columbia from the 1998 Seismic Hazards Investigation in Puget Sound,” *Journal of Geophysical Research*, 109, B09303.

Ramachandran, K., S. E. Dosso, C. A. Zelt, G. D. Spence, R. D. Hyndman, and T. M. Brocher 2005, "Forearc structure beneath southwestern British Columbia: A 3-D tomography velocity model," *Journal of Geophysical Research*, 110, B02303.

Ramachandran, K., R. D. Hyndman, and T. M. Brocher 2006, "Regional P wave velocity structure of the northern Cascadia subduction zone," *Journal of Geophysical Research*, 111, doi:10.1029/2005JB004108.

Reese, S., B. A. Bradley, J. Bind, G. Smart, W. Power, and J. Sturman. 2011, "Empirical building fragilities from observed damage in the 2009 South Pacific tsunami," *Earth Science Reviews*, 107, 156-173.

Rossetto, T., and A. Elnashai 2003, "Derivation of vulnerability functions for European–type RC structures based on observational data," *Engineering Structures*, 25, 1241–1263.

Rota, M., Penna, A., Strobbia, C. L. 2008, "Processing Italian Damage Data to Derive Typological Fragility Curves," *Journal of Soil Dynamics and Earthquake Engineering*, 28, 933-947.

Savage, J. C., and M. Lisowski 1991, "Strain measurements and potential for a great subduction earthquake off Oregon and Washington," *Science*, 252, 101-103.

Scawthorn, C., J. M. Eidinger, and A. J. Schiff 2005, "Fire Following Earthquake," Technical Council on Lifeline Earthquake Engineering Monograph No. 26.

Scawthorn, C. 2009, "Enhancements in HAZUS-MH," SPA Risk Project # 10010-01-07-01.

Senarath, S. U. S., F. L. Ogden, C. W. Downer, and H. O. Sharif 2000, "On the calibration and verification of two-dimensional, distributed, Hortonian, continuous watershed models," *Water Resources Research*, 36, 1495-1510.

Silva, W., N. Gregor, and R. Darragh 2002, "Development of Hard Rock Attenuation Relations for Central and Eastern North America," Internal Report from Pacific Engineering, November 2002. Available at: http://www.pacificengineering.org/CEUS/Development%20of%20Regional%20Hard_ABC.pdf

Solomon, B. J., N. Storey, I. Wong, W. Silva, N. Gregor, D. Wright, and G. McDonald 2004, "Earthquake-Hazards Scenario for a M 7 Earthquake on the Salt Lake City Segment of the Wasatch Fault Zone, Utah," Utah Geological Survey, Special Study 111 DM.

Somerville, P., N. Collins, N. Abrahamson, R. Graves, and C. Saikia 2001, "Ground Motion Attenuation Relations for the Central and Eastern United

States—Final report, June 30, 2001," Report to the United States Geological Survey for Award 99HQGR0098, 38.

Suppasri, A., S. Koshimura, and F. Imamura 2011, "Developing tsunami fragility curves based on the satellite remote sensing and the numerical modeling of the 2004 Indian Ocean tsunami in Thailand," *Natural Hazards and Earth System Sciences*, 11, 173–189.

Tachikawa, T., M. Kaku, A. Iwasaki, D. Gesch, M. Oimoen, Z. Zhang, J. Danielson, T. Krieger, B. Curtis, J. Haase, M. Abrams, R. Crippen, C. Carabajal 2011. *ASTER Global Digital Elevation Model Version 2 – Summary of Validation Results*. Compiled by D. Meyer on behalf of the NASA Land Processes Distributed Active Archive Center and the Joint Japan-U.S. ASTER Science Team.

Tavakoli, B., and S. Pezeshk 2005, "Empirical-Stochastic Ground-Motion Prediction for Eastern North America," *Bulletin of the Seismological Society of America*, 95, 2283–2296.

Toro, G. R. 2002, "Modification of the Toro et al. (1997) Attenuation Equations for Large Magnitudes and Short Distances," Technical report by Risk Engineering, Inc. Available at: http://www.riskeng.com/downloads/attenuation_equations

Ventura, C. and M. H. K. Kharrazi 2002, "Single-family wood frame house," *World Housing Encyclopedia*, Report 82. Joint project of the Earthquake Engineering Research Institute (EERI) and the International Association for Earthquake Engineering (IAEE). Available at: http://www.world-housing.net/category/north-america/canada

Ventura, C. E., W. D. L. Finn, T. Onur, A. Blanquera, and M. Rezai 2005, "Regional seismic risk in British Columbia — classification of buildings and development of damage probability functions", *Canadian Journal of Civil Engineering*, 32, 372–387.

Ventura, C. E., T. Onur, and K.X-S. Hao 2004, "Site period estimations in the Fraser River delta using microtremor measurements – experimental and analytical studies," Natural Resources Canada, Earth Sciences sector, General Information Product 23.

United States Geological Survey 1999, "Earthquake Probabilities in the San Francisco Bay Region: 2000 to 2030 – A Summary of Findings." USGS Open-File Report 99-517.

Wald, D. J., V. Quitoriano, T. H. Heaton, and H. Kanamori 1999, "Relationship between Peak Ground Acceleration, Peak Ground Velocity, and Modified Mercalli Intensity for Earthquakes in California," *Earthquake Spectra*, 15, 557-564.

Walling, M., W. Silva, and N. Abrahamson 2008, "Nonlinear Site Amplification Factors for Constraining the NGA Models," *Earthquake Spectra*, 24, 243–255.

Wang, K., R. Wells, S. Mazzotti, R. D. Hyndman, and T. Sagiya 2003, "A revised dislocation model of interseismic deformation of the Cascadia subduction zone," *Journal of Geophysical Research*, 108, 2026.

Weichert, D. H. 1980, "Estimation of the earthquake recurrence parameters for unequal observation periods for different magnitudes," *Bulletin of the Seismological Society of America*, 70, 1337-1346.

Wesson, L. R, O. S. Boyd, C. S. Mueller, C. G. Bufe, A. D. Frankel, and M. D. Petersen 2007, "Revision of time-independent probabilistic seismic hazard maps for Alaska", USGS Open-File Report 2007-1043.

Wieczorek, G. F., Wilson, R. C., and Harp, E. L. 1985, "Map of slope stability during earthquakes in San Mateo County, California," U.S. Geological Survey Miscellaneous Investigations Map I-1257-E, scale 1:62,500.

Wilson, R. C., and Keefer D. K., 1985," Predicting Areal Limits of Earthquake Induced Landsliding, Evaluating Earthquake Hazards in the Los Angeles Region," U. S. Geological Survey Professional Paper, Ziony, J. I., Editor, p. 317-493.

Witter, R.C., Y. Chang, and G. R. Priest 2008 , "Reconstructing Hydrodynamic Flow Parameters of the 1700 Tsunami at Ecola Creek, Cannon Beach, Oregon," *Natural Hazards* 63, 223–240.

Yeh, H. 2007, "Design Tsunami Forces for Onshore Structures," *Journal of Disaster Research*, 2, 531–539.

Yim, S. C. 2005, "Modeling and Simulation of Tsunami and Storm Surge Hydrodynamic Loads on Coastal Bridge Structures," 21st U.S. Japan Bridge Engineering Workshop, Tsukuba, Japan and McLean, VA.

Youd, T. L., and Perkins, D. M., 1978, "Mapping liquefaction-induced ground failure potential," *Journal of the Geotechnical Engineering Division*, 104, 433-446.

Youngs, R. R., S.-J. Chiou, W. J. Silva, and J. R. Humphrey 1997, "Strong ground motion attenuation relationships for subduction zone earthquakes," *Seismological Research Letters*, 68, 58–73.

Zelt, B. C., R. M. Ellis, C. A. Zelt, R. D. Hyndman, C. Lowe, G. D. Spence, and M. A. Fisher 2001, "Three-dimensional crustal velocity structure beneath the Strait of Georgia, British Columbia," *Geophysical Journal International* 144, 695-712.

Zhao, S. J. 2011, “Simulation of Mass Fire-Spread in Urban Densely Built Areas Based on Irregular Coarse Cellular Automata,” *Fire Technology*, 47, 721-749.

Zhao, J. X., and H. Xu 2012, “Magnitude-scaling rate in ground-motion prediction equations for response spectra from large subduction interface earthquakes in Japan,” *Bulletin of the Seismological Society of America*, 102, 222-235.

Zhao J. X., J. Zhang, A. Asano, Y. Ohno, T. Oouchi, T. Takahashi, H. Ogawa, K. Irikura, H. Thio, P. Somerville, and Y Fukushima 2006a, “Attenuation Relations of Strong Ground Motion in Japan Using Site Classification Based on Predominant Period,” *Bulletin of the Seismological Society of America*, 96, 898–913.

Zhao, S. J., L. Y. Xiong, and A. Z. Ren 2006b, “A Spatial-Temporal Stochastic Simulation of Fire Outbreaks Following Earthquake Based on GIS,” *Journal of Fire Science* 24, 313-340.

10 About AIR Worldwide

AIR Worldwide (AIR) provides catastrophe risk modeling solutions that make individuals, businesses, and society more resilient. AIR founded the catastrophe modeling industry in 1987, and today models the risk from natural catastrophes, terrorism, cyber attacks, and pandemics globally. Insurance, reinsurance, financial, corporate, and government clients rely on AIR's advanced science, software, and consulting services for catastrophe risk management, insurance-linked securities, site-specific engineering analyses, and agricultural risk management. AIR Worldwide, a Verisk Analytics (Nasdaq:VRSK) business, is headquartered in Boston with additional offices in North America, Europe, and Asia. For more information, please visit www.air-worldwide.com.